



HAL
open science

Analysis of head domain-mediated oligomerization of the focal adhesion protein vinculin induced by the *Shigella* effector IpaA

Benjamin Cocom Chan

► **To cite this version:**

Benjamin Cocom Chan. Analysis of head domain-mediated oligomerization of the focal adhesion protein vinculin induced by the *Shigella* effector IpaA. Microbiology and Parasitology. Université Paris Cité, 2023. English. NNT : 2023UNIP5011 . tel-04687135

HAL Id: tel-04687135

<https://theses.hal.science/tel-04687135v1>

Submitted on 4 Sep 2024

HAL is a multi-disciplinary open access archive for the deposit and dissemination of scientific research documents, whether they are published or not. The documents may come from teaching and research institutions in France or abroad, or from public or private research centers.

L'archive ouverte pluridisciplinaire **HAL**, est destinée au dépôt et à la diffusion de documents scientifiques de niveau recherche, publiés ou non, émanant des établissements d'enseignement et de recherche français ou étrangers, des laboratoires publics ou privés.

Université Paris Cité

École doctorale Bio Sorbonne Paris Cité (BioSPC, ED562)

Equipe Signalisation Calcique et Infections Microbiennes
Institut de Biologie Intégrative de la Cellule
(I2BC, UMR 9198, USC 1425)

**Analysis of head domain-mediated oligomerization of
the focal adhesion protein vinculin induced by the
Shigella effector IpaA**

Par Benjamin COCOM CHAN

Thèse de doctorat de Microbiologie

Dirigée par Guy TRAN VAN NHIEU

Présentée et soutenue publiquement le 26 Janvier 2023

Devant un jury composé de :

Jacqueline CHERFILS, DR, Université Paris-Saclay, rapportrice
Stéphane MÉRESSE, DR, Aix-Marseille Université, rapporteur.
Christophe LE CLAINCHE, DR, Université Paris-Saclay, examinateur
Amel METTOUCHI, DR, Université Paris Cité, examinatrice.
Jost ENNINGA, Group leader, Université Paris Cité, examinateur.
Guy TRAN VAN NHIEU, DR, Inserm.

Analyse de l'oligomérisation médiée par le domaine de la tête de la protéine d'adhésion focale vinculine induite par l'effecteur *Shigella* IpaA

Résumé :

La vinculine est une protéine associée au renforcement des structures d'adhérence dépendantes des intégrines des cellules à la matrice extracellulaire (ECM). L'organisation structurelle de la vinculine permet à cette protéine d'interagir avec d'autres partenaires tels que la taline à travers des hélices amphipathiques spécifiques, appelés sites de liaison à la vinculine ou VBS et de se lier à la F-actine lors de son activation. Des modèles structurels récents et des données biochimiques suggèrent que l'interaction structure-fonction spécifique de la vinculine dépend aussi de la capacité de la vinculine à répondre à la tension mécanique exercée sur la molécule elle-même. *Shigella*, l'agent causal de la dysenterie injecte diverses protéines effectrices dans le cytoplasme de sa cellule hôte dans le cadre de son processus infectieux. Nos résultats montrent que la protéine effectrice IpaA de *Shigella* induit des changements conformationnels de la vinculine, qui n'ont pas été rapportés pour d'autres ligands, pour déclencher l'internalisation bactérienne. Ces changements conformationnels, que nous appelons « supra-activation » de la vinculine, conduisent à l'oligomérisation de la vinculine par son domaine « tête ». Nos résultats suggèrent que la supra-activation de la vinculine se produit également lorsque soumise aux forces mécaniques durant la mécanotransduction requise pour la maturation des structures d'adhérence cellulaires. Mon travail est consacré à la caractérisation du rôle de résidus dans les sous-domaines D1 et D2 de la tête de la vinculine, impliqués dans l'interaction avec IpaA-VBS3 responsable de la supra-activation. Les effets *in vitro* et *in vivo* des substitutions de résidus dans les domaines D1 et D2 suggèrent un rôle lors des changements conformationnels de la vinculine associés à la tension mécanique lors de la maturation de l'adhésion cellulaire. La relation entre IpaA-VBS3 et la vinculine pourrait conduire à l'identification d'autres activateurs endogènes potentiels.

Mots clés : *Shigella*, IpaA, vinculine, oligomérisation, adhésions cellulaires

Analysis of head domain-mediated oligomerization of the focal adhesion protein vinculin induced by the *Shigella* effector IpaA

Abstract

Vinculin is a protein associated with the reinforcement of integrin-dependent adhesion structures of cells to the extracellular matrix (ECM). The structural organization of vinculin allows this protein to interact with other partners such as talin through specific amphipathic helices, called vinculin binding sites or VBS and to bind to F-actin during of its activation. Recent structural models and biochemical data suggest that the specific structure-function interaction of vinculin also depends on the ability of vinculin to respond to mechanical stress exerted on the molecule itself. *Shigella*, the causative agent of dysentery injects various effector proteins into the cytoplasm of its host cell as part of its infectious process. Our results show that the effector protein IpaA from *Shigella* induces conformational changes in vinculin, which have not been reported for other ligands, to trigger bacterial internalization. These conformational changes, which we call "supra-activation" of vinculin, lead to the oligomerization of vinculin by its "head" domain. Our results suggest that supra-activation of vinculin also occurs when subjected to mechanical forces during the mechanotransduction required for the maturation of cell adhesion structures. My work is devoted to the characterization of the role of residues in the D1 and D2 subdomains of the vinculin head, involved in the interaction with IpaA-VBS3 responsible for supra-activation. The *in vitro* and *in vivo* effects of residue substitutions in the D1 and D2 domains suggest a role in conformational changes of vinculin associated with mechanical tension during cell adhesion maturation. The relationship between IpaA VBS3 and vinculin could lead to the identification of other potential endogenous activators.

Keywords: *Shigella*, IpaA, vinculin, oligomerization, cell adhesions

ACKNOWLEDGEMENTS

TABLE OF CONTENT

I. INTRODUCTION

1. ***Shigella* spp. the causative agent of bacillary dysentery**
 - Generalities
 - The *Shigella* infection cycle
 - Type III Secretion System
 - *Shigella* invasion of epithelial cells

2. **Integrin-mediated adhesions receptors.....**
 - Generalities, the extracellular matrix
 - Integrins: structural and biological aspects
 - Integrin activation: outside-in and inside-out signaling

3. **Integrin-dependent adhesion complexes (IDACs)**
 - Integrin organization in adhesions and elementary clusters
 - Focal Adhesions' composition and organization
 - Focal Adhesion signaling
 - Mechanosensing, mechanotransduction and Focal Adhesion maturation
 - Talin structure and mechanotransduction

4. **Vinculin**
 - *Vinculin tructure and evolutionary aspects*
 - Vinculin functions
 - Vinculin Binding Sites (VBSs) and vinculin activation
 - Vinculin allosteric changes: the input of modeling.
 - Vinculin oligomerization.

5. **IpaA VBSs interaction with vinculin and talin**

6. **Thesis rationale**

II. RESULTS

- **Article 1.**

“*Shigella* IpaA mediates actin bundling through diffusible vinculin oligomers with activation imprint”.

Authors: Cesar Valencia-Gallardo, Daniel-Isui Aguilar-Salvador, Hamed Khakzad, Benjamin Cocom-Chan, Charles Bou-Nader, Christophe Velours, Yosra Zarrouk, Christophe Le Clainche, Christian Malosse, Diogo Borges Lima, Nicole Quenech’Du, Bilal Mazhar, Sami Essid, Marc Fontecave, Atef Asnacios, Julia Chamot-Rooke, Lars Malmström, Guy Tran Van Nhieu

- **Article 2.**

“Polar interactions determine head domain-mediated vinculin oligomerization induced by *Shigella* IpaA”

Authors: Benjamin Cocom-Chan, Hamed Khakzad, Cesar Valencia-Gallardo, Yosra Zarrouk, Guy Tran Van Nhieu

- **Supplementary results**

“A key role for IpaA K499 in vinculin supra-activation”

Authors: Benjamin Cocom-Chan, Guy Tran Van Nhieu

III. DISCUSSION

IV. BIBLIOGRAPHY

I. INTRODUCTION

Bacterial pathogens need to adhere or invade to host cells tissues to promote diseases. Adhesion may occur through direct binding of a ligand of the bacterial surface termed adhesin to host cell receptors or, indirectly, through the association between the adhesin and a component of the extracellular matrix. Invasion may also also result from the association of so called bacterial “invasins” with adhesion receptors such as integrins or cadherins to promote uptake in a “zippering” mode, where the host cell plasma membranes wrap around the surface of the invading bacterium, leading to its engulfment in a tight vacuole. Alternatively, invasion may result from the injection of bacterial effectors into the host cell cytosol by means of a specialized type III secretion apparatus, resulting in localized membrane rufflings and internalization in a so called “trigger” mode (Sansonetti, 2002; Ribet and Cossart, 2016).

Both zippering and triggering modes requires actin polymerization, however, the “triggered” invasion implicates an important but local reorganization of the actin cytoskeletal through the concerted action of multiple bacterial type III effectors. The precise coordination and regulation of the action of these effectors, some with opposite functions, is still incompletely understood.

During my thesis, I focused on studied a newly reported mode of activation of the focal adhesion protein by IpaA, a *Shigella* type III effector. While our laboratory’s prime interest lies in the mechanism of bacterial invasion of host cells, deciphering this new mode of vinculin activation by IpaA led me to study the effects of vinculin mutations in in vitro and cellular systems.

1. *Shigella* spp. the causative agent of bacillary dysentery

- **Generalities**

Shigella is the causative agent of bacillary dysentery, a diarrheal disease prevalent in developing countries. *Shigella* is a Gram-negative bacterial pathogen that can be considered as an *E. coli* subspecies adapted to growth inside host cells. The genus *Shigella* contains 4 species, with *Shigella dysenteriae* and *Shigella flexneri* being responsible for the epidemic and endemic form of shigellosis. Cases related to *Shigella boydii* infections are rare and limited to the southern part of India. *Shigella sonnei* is responsible for less severe diarrhea and is prevalent in developed countries.

Shigella is held responsible for ca 1.5 million cases and 250 000 deaths annually and worldwide, the majority of casualties being children under the age of 5 in developing countries. Following ingestion, *Shigella* reaches and invades the colonic mucosa where it induces an intense inflammatory reaction leading to its destruction and the emission of muco-purulent stools associated with the dysenteric syndrome.

- ***The Shigella cell infection cycle***

As opposed to other enteroinvasive pathogens, such as *Salmonella* or *Listeria*, *Shigella* does not disseminate in other tissues and shows a tropism for intestinal epithelial cells. After invading cells, *Shigella* rapidly lyses the phagocytic vacuole to replicate freely in the cell cytosol (Schnupf and Sansonetti, 2019). During this intracellular replication phase, *Shigella* can polymerize actin at one bacterial pole to move inside cells. At the levels of cell-cell contact, *Shigella* actin-based motility results in the formation of bacteria-containing protrusions that push in adjacent cells. Following lysis of protrusion double-membrane, *Shigella* can resume bacterial intracellular replication in adjacent cells and the infectious cell cycle (Schnupf and Sansonetti, 2019). The ability of *Shigella* to invade and disseminate inside epithelial cells is key to its virulence and allows the bacteria to colonize the intestinal mucosa hidden from host immune responses. Both invasion and dissemination properties of *Shigella* are determined by the activity of a bacterial type III secretion apparatus (T3SS) (Muthuramalingam et al. 2021).

- ***The Type III Secretion System***

T3SSs also called injectisomes are secretion systems expressed in a variety of Gram-negative bacterial that are pathogen to mammals, fish and plants. While constituents of the Type 3 secretion apparatus (T3SA) show a large diversity in their primary sequences, T3SA show a structural and functional conservation. All T3SSs are inactive at the basal state and get activated upon contact with host cells, to allow the delivery of bacterial effectors, or type III effectors into host cells (Muthuramalingam et al. 2021). T3SSs are related to the bacterial flagellum, with a basal body composed of rings spanning the bacterial inner and outer membranes connected by a hollow hinge region. The basal body is prolonged by a so called hollow “needle” formed by the polymerization of a major “pilin” protruding from the bacterial surface. The T3SS needle is capped by a “tip complex” composed of one or two hydrophobic proteins connected to the needle by a hydrophilic protein (Dey et al. 2021; Muthuramalingam et al. 2021).

Assembly of the basal body depends on the Sec general secretory pathway, while secretion of the needle and tip complex proteins depend on a specific T3SS ATPase related to the flagellar ATPase. At the basal state, following assembly of the tip complex, the T3SA is inactive. Upon contact with host cell membranes, the hydrophobic components of the tip complex insert into the host cell membranes to form a so-called translocon believed to form a continuum between the T3SS needle and allowing the delivery of type III effectors directly from the bacterial to host cell cytosol (Dey et al. 2021; Muthuramalingam et al. 2021). 3D reconstruction of single particles analyzed by electron microscopy has provided with exquisite insights into the structures of various T3SA. The inner diameter of the translocon matches that of the needle and ranges from 2 to 4 nm depending on the system (Dey et al. 2021; Muthuramalingam et al. 2021). This diameter is not compatible with the secretion of fully folded proteins and type III effectors are presumed to be channeled into the T3SA under an unfolded or partially folded state. Elegant studies have shown that the T3SS ATPase is involved in the recognition of T3SS substrates and their unfolding during secretion (Akeda and Galan, 2005). Once delivered into host cells, type III effectors may divert diverse host cell functions, including cytoskeletal, trafficking or inflammatory processes (Mattock and Blocker, 2017).

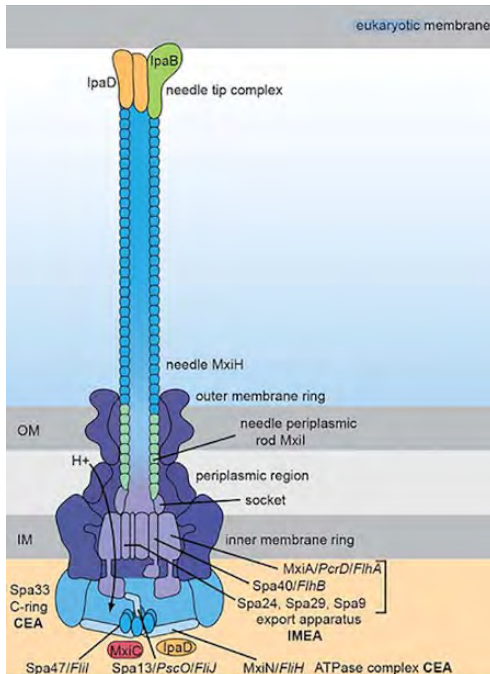


Figure 1. Scheme of the *Shigella* T3SA (Shen et al., 2016). The *Shigella* T3SA basal body spans the bacterial inner and outer membranes and is prolonged by the MxiH needle. The tip complex composed of IpaB and IpaD is shown contacting host cell membranes.

A scheme of the *Shigella* T3SA is depicted in **Figure 1**. The *Shigella* T3SS determinants are mostly encoded by a large virulence plasmid. These include components of the T3SA as well as 27 type III effectors that have been divided in two main categories: i, type III effectors that are constitutively expressed, including the invasion effectors; ii, type III effectors that are up-regulated following bacterial invasion of host cells. The functions of the first wave of type III effectors are well characterized and include those associated with cytoskeletal reorganization during bacterial invasion (Mattock and Blocker, 2017). More recent studies have highlighted functions for type III effectors of the “second wave” involved in the dampening of inflammatory responses, diversion of trafficking processes or cell death / survival pathways.

- ***Shigella* invasion of epithelial cells**

Shigella invasion occurs with little constitutive bacterial adhesion to epithelial (Valencia-Gallardo et al. 2015). Bacteria transiently interact with cells and are captured by thin cell extensions, called filopodia, in a seemingly stochastic manner. Upon

contact, most often occurring between one bacterial pole and the filopodial tip, filopodia retract to bring bacteria to the cell cortex where invasion proceeds. *Shigella* invasion is characterized by the formation of actin-rich membrane ruffles that surround the invading bacteria and engulf them in a large vacuole (Valencia-Gallardo et al. 2015). During the cytoskeletal reorganization associated with *Shigella* invasion, bacteria anchors to the cell plasma membrane by forming a pseudo-focal adhesion structure enabling its pulling within the cell body. Bacterial capture by filopodia and cell invasion depend on the *Shigella* T3SS (Valencia-Gallardo et al. 2015).

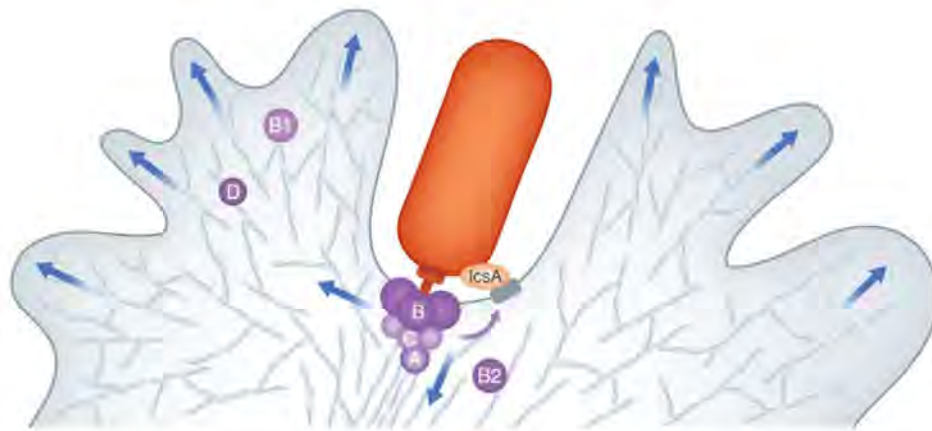


Figure 2. *Shigella* invasion of epithelial cells by mediated by the T3SS. Purple: B, IpaAB. The type III effectors of invasion: A, IpaA; B1, IpgB1; B2, IpgB2; C, IpaC; D, IpgD. IcsA promotes actin-based motility and also acts as a transient adhesin. The arrow represent actin-based forces leading to membrane ruffling or pulling the bacteria inside the cell (Valencia-Gallardo et al. 2015).

The five type III effectors of invasion have been identified and show activities that must act in a regulated manner to coordinate the actin remodeling required for bacterial uptake (**Figure 2**; Mattock and Blocker, 2017). IpaB and IpaC are the hydrophobic proteins forming the translocon required for the injection of type III effectors (Dey et al. 2021; Muthuramalingam et al. 2021). In addition to its role in translocon formation, however, IpaC also directly contribute to *Shigella* invasion by activating the Src tyrosine kinase that amplifies actin polymerization at invasion sites, through the phosphorylation of cortactin, a cytoskeletal protein involved in actin polymerization dependent on the Arp2/3 complex (Valencia-Gallardo et al. 2015). IpgD is a phosphatidyl (4, 5) bisphosphate (PIP₂) 4-phosphatase (Tran Van Nhieu et al. 2022). IpgD is a multifaceted enzyme that was proposed to facilitate invasion through PIP₂ hydrolysis, leading to the

disassembly of cortical actin, favoring de novo actin polymerization at bacterial invasion sites. PI5P, produced by IpgD-mediated PIP₂ hydrolysis, was also shown to stimulate the activity of Tiam-1, a GEF for the small GTPase Rac. IpgD, through its phosphatase activity, stimulates the recruitment of ARNO, a GEF for the small GTPase Arf6, thereby leading to Arf6 activation, likely contributing to actin remodeling by stimulating the small GTPase Rac (Tran Van Nhieu et al. 2022). Finally, by depleting cells for PIP₂, IpgD also reduces the levels of Inositol (1, 4, 5) triphosphate (InsP₃), the main second messenger involved in the release of Ca²⁺ from intracellular pools. Reduced InsP₃ levels mediated by IpgD contribute to the formation of atypical long lasting Ca²⁺ microdomains at invasion sites required for *Shigella* invasion (Tran Van Nhieu et al. 2022). Of interest, during bacterial intracellular replication, IpgD virtually inhibits Ca²⁺ cytosolic increase linked to Ca²⁺ release and thereby prevents the disassembly of focal adhesions otherwise triggered by the activation of the Ca²⁺-dependent protease calpain. IpgB1 is a GEF for Rac, that stimulates actin-ruffle formation in a Rac and Arp2/3 dependent manner. IpgB2 is a GEF for the small GTPase Rho, stimulating acto-myosin contraction. While the Rac-dependent actin polymerization and Rho-dependent actomyosin contraction are often antagonistic processes during cell adhesion, IpgB1 and IpgB2 were both shown to be required for *Shigella* invasion of polarized intestinal epithelial cells, indicating a concerted action of these two type III effectors (Valencia-Gallardo et al. 2015).

IpaA is required for filopodial capture and bacterial transient adhesion during *Shigella* invasion by targeting the cytoskeletal linkers talin and vinculin, key players in integrin adhesion structures that will be developed in the next section (Valencia-Gallardo et al. 2019).

2. Integrin-mediated adhesions

- **Generalities, the Extracellular Matrix**

Cells can establish adhesion with the extracellular matrix or with other cells through various adhesion receptors that are classically divided into four major groups: integrins,

selectins, cadherins and the immunoglobulin superfamily of adhesion molecules. Cell adhesion to the extracellular matrix is mainly conferred by integrin receptors, while cell-cell adhesion is mediated by the other groups of adhesion molecules. The reinforcement of adhesion implicates linkage between the actin cytoskeleton and adhesion receptors, that have been particularly studied for integrins and cadherins. These receptors form dynamic macromolecular complexes determining adhesion and acting as signaling hubs controlling various cell processes including transcriptional programs. In the last decade, it has become clear that cells adjust the strength of adhesion in response to mechanical stimulation, in a process called “mechanotransduction” that will be developed further.

The ECM (ECM) represents a key evolutionary feature that accompanied the emergence of metazoans. From sponges to whales, tissues are made of cellular and non-cellular components. This non-cellular component (mostly proteins and polysaccharides) provides a physical support that allows resident cells to organize, hold together and interact with each other. The ECM is dynamic in nature, as it can be remodeled by degradation or synthesis.

Noteworthy, the ECM cannot be considered as a passive tissue component. Physically, by changing its topography, ligand spacing or stiffness, the ECM can influence the intracellular response derived from its interaction with different extracellular receptors. At the biological level, cells need to be attached (or not) to this network in order to regulate different aspects that include survival, growth, migration, shape or differentiation, for example. The ECM can influence a cell's fate and behavior by acting as a reservoir of a variety of signaling molecules like growth factors or cytokines (Walma and Yamada 2020; Vogel 2018). Therefore, the ECM acts both as a physical and a signaling scaffold for cells.

By acting as organizing centers, ECM proteins can be assembled according to different requirements and tuning its composition, mechanical or signaling demands. Regarding their counterpart, there are a variety of cell receptors able to interact with the ECM,

however, this work is focused on the cell-network adhesions mediated by integrins.

- **The integrins: structural and biochemical aspects.**

Cells interact in a bidirectional manner with the ECM via cellular adhesions localized at specific sites. Integrins are evolutionary conserved receptors present in animals. The integrin family is composed of 24 α - β heterodimeric and conformationally flexible cell surface receptors that mediate dynamic connections between ECM molecules and the intracellular actin cytoskeleton. Overall, the shape of the crystallized conformer is that of a composed “head” on two “legs”. There are four distinguishable domains (**Figure 3**): the N-termini of both subunits forming the head; connected to their corresponding flexible legs; continuing into single transmembrane helices that end in short cytoplasmic domains at the C-termini. Both integrin subunits are non-covalently associated (M. J. Humphries 2002; Cormier et al. 2018).

Most of the receptor dimer is extracellular, but the short cytoplasmic domains are responsible to initiate the assembly of large signaling complexes, and thereby bridge the ECM to the intracellular adaptors and the cytoskeleton (Campbell and Humphries 2011).

subset of integrins (8 out of 24) recognizes the RGD sequences in native ligands (Moreno-Layseca et al. 2019). In some ECM molecules, such as collagen and some laminin isoforms, the RGD sequences are only accessible after denaturation or proteolytic cleavage (Barczyk, Carracedo, and Gullberg 2010; Campbell and Humphries 2011).

The binding sites for the ECM ligands either comprise epitopes from both α and β subunits or reside on a specific domain of the α -subunit, as the case of the RGD motif found in fibronectin and vitronectin. As integrins bind to its ligands, the ECM fibers can transmit the mechanical tension of the substrate, thus altering binding kinetics and promoting global conformational transitions between bent, extended-closed and extended-open forms of integrins (Yunfeng Chen et al. 2017), the later conformational form associated with higher receptor affinity and the separation of the α and β cytoplasmic tails. This mechanism implying ligand recognition/binding and conformational changes corresponds to integrin activation leading to outside-in signaling (Kechagia, Ivaska, and Roca-Cusachs 2019). In this sense, integrins can be considered as mechanical sensors probing the ECM properties like stiffness.

- **Integrin activation: outside-in and inside-out signaling**

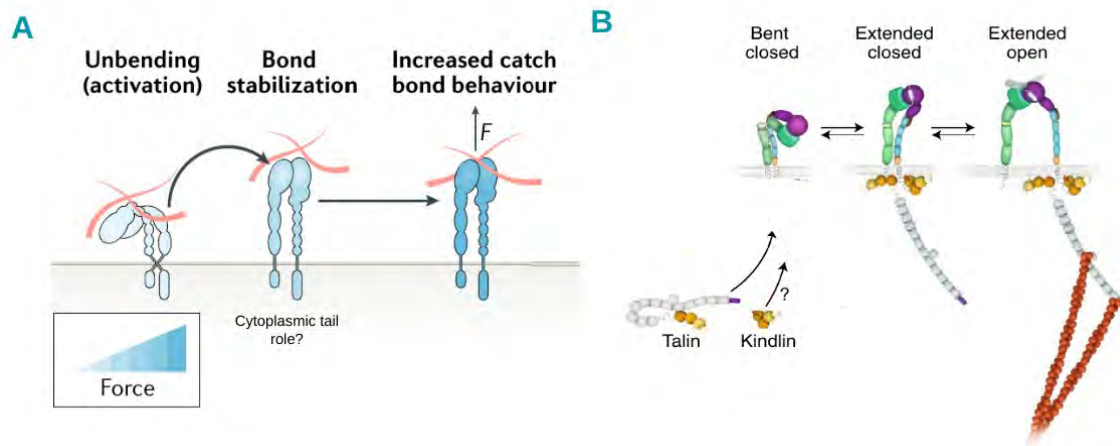


Figure 4. Models of integrin receptor activation. (A) Outside-in model of integrin activation: upon ligand recognition, integrin receptors can increase its affinity in a catch-bond dependent manner. Stabilizing this interaction as the pulling force of the ECM ligands is exerted on the receptors, induces integrin activation. (B) On the other hand, talin or kindlin binding to the cytoplasmic tail from the β subunit are also considered receptor activators, as they can

promote conformational changes and increased ligand binding. The relative contribution of each activation mode remains to be determined. [Adapted from Kechagia, Ivaska & Roca-Cusachs, 2019; Moreno-Layseca et al., 2019].

Integrin activation may also occur from “inside-out” signaling following ligand binding to the cytoplasmic tail of the integrin beta subunit. As integrins are non-enzymatic proteins, signaling relies on the assembly of intracellular complexes. Protein-protein interactions within the cytoplasmic tail domain can also regulate the integrin conformational changes leading to its active form and subsequent signaling responses. Among the intracellular adaptor proteins, talin and kindlin are recognized as the most important integrin activators (**Figure 4**). Talin (which will be addressed in detail in the following sections) is a major adaptor protein found in integrin-dependent cell adhesion. After recruitment, talin directly or indirectly link integrins to the actin cytoskeleton. The mechanism(s) of talin recruitment to integrins are still not well understood. However, structural studies have determined that the F3 module of talin’s FERM domain binds to the cytoplasmic (membrane proximal) NPXY motif of integrin’s β tail domain in order to start the integrin activation cascade (Z. Sun, Costell, and Fässler 2019; Moser et al. 2009). Noteworthy, at the distant C-termini domain, talin possess a dimerization domain able to bridge integrins.

Kindlin is another major effector of inside-out integrin activation and signaling. Kindlin also harbors a FERM domain, however the interaction with the integrin tail depends on the membrane distal NxxY motif. Unlike talin, which bridges integrins with the actin cytoskeleton, kindlins scaffold kinases or phosphatases and adaptors (i.e. paxillin, RAC1 or the Arp2/3 complex) (Z. Sun, Costell, and Fässler 2019; Campbell and Humphries 2011).

4. Integrin-dependent adhesion Complexes (IDACs)

IDACs comprehend a family of heterogeneous macromolecular structures such as nascent adhesions, focal complexes, focal adhesions, fibrillar adhesions that allow cells to connect with the ECM. IDACs mediate stable and force-dependent matrix adhesions (Revach, Grosheva, and Geiger 2020). We will not review invasive IDACs such as podosomes and invadopodia.

- **Integrin organization in adhesions and elementary clusters**

With the advent of Super Resolution Microscopy techniques, it became possible to study in detail the localization and dynamics of proteins in the context of supramolecular structures, such as integrins when cells form adhesions with the ECM. For instance, tracking single molecule dynamics on integrin adhesions, challenged the view of cell matrix adhesions as homogeneous molecular assemblies (**Figure 5**). In the Shibata et al. study, the authors measured the residence time of single integrin $\beta 3$ receptors inside relative to outside integrin-dependent adhesions (Shibata et al. 2012; Rossier et al. 2012). They compared the “classical homogeneous model” with high residence time, very low diffusion: the “*Venetian canal model*” where macroscopic diffusion is restricted to the “*Archipelago model*” with scattered spots residing in highly fluid membranes. The latter model was more favored by the data (Shibata et al. 2012), as integrin receptors lasted between 0.1-0.6 seconds inside the adhesion area with frequent arresting events in nanometer-sized areas but comparable diffusion between outside and inside adhesions.

Another study also supported the *Archipelago model* architecture and showed that the arresting events into adhesion sites depended on the activation of the receptors, as suggested by constitutively active and inactive controls. The residence time inside adhesions seems to be also dependent on the heterodimer under study. As suggested by a lower arresting time of $\beta 1$ compared to $\beta 3$ (Rossier et al. 2012). Another feature of $\beta 1$ receptors is the particular linear or stripes pattern inside adhesion sites relative to the scattered clustering characteristic for $\beta 3$ adhesions (Spiess et al. 2018).

Importantly, those integrin nanoclusters were detectable to form also in cells deposited

on highly fluid-low stiffness substrates, such as supported lipid bilayers functionalized with RGD peptides, compared to RGD on glass. Nanocluster formation is robust independent of stiffness or ligand fluidity (both ~100 nm in size with ~50 molecules) (**Figure 5C**). In practice, this kind of adhesion structures resemble nascent adhesions (NAs). However, the main difference is that cells spreading on stiff substrates can reach micrometer size adhesions, characteristic of mature cell-matrix adhesions, during a maturation process linked to mechanotransduction (Changede et al. 2015). Changede *et al.* tested different patterns and spacing of printed RGD-matrix fibers, and determined a minimal spacing of ~100 nm between thin fibers (≤ 30 nm) to form stable adhesions and spread. A bigger spacing did not allowed cells to assemble more integrin nano-clusters to further increase adhesions in size or mature (Changede et al. 2019).

The assembly of these integrin NAs has been suggested be determined by lipid domains or rafts in the cell membranes, the oligomerization of intracellular partners (i.e. talin) or the clustering by exclusion of the glycocalyx and other extracellular components (Changede and Sheetz 2017).

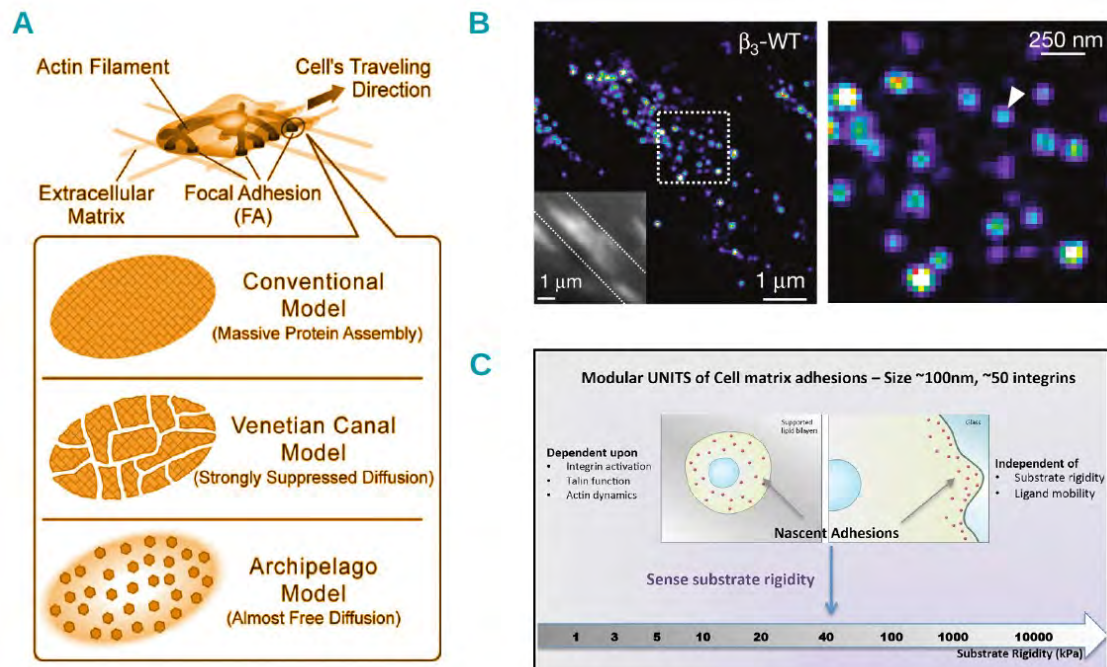


Figure 4. Models of integrin-ECM adhesions assembly, dynamics and response to stiffness. (A) The spatial organization and residence of integrins into adhesion structures evolved as novel microscopy methods allowed to detect single receptors: from single

homogeneous protein assemblies to nanometer-size clusters residing into restricted micrometer-size areas in fluid membranes. Panel **(B)** represents a zoom in of what at first sight appears to be homogeneous patches of proteins (small insert down left) results in scattered regular size clusters ~100 nm confined in bigger adhesion areas that connect with the actin cytoskeleton. **(C)** The integrin nano-clusters can also form under low stiffness and fluidity. Nonetheless, a minimum spacing and highly stiff substrates are required for adhesions in order to increase in size, further mature, connect to the cytoskeleton and allow cell spreading. [Adapted from Shibata et al., 2012; Rossier et al., 2012; Changede et al., 2015].

- **Focal Adhesions' composition and organization**

On stiff substrates, cells form large adhesion structures called Focal Adhesions (FAs). FAs have been analyzed in details in studies using biochemical, mass spectrometry and various microscopy approaches (Winograd-Katz et al. 2014; Horton et al. 2015; Han and de Rooij 2016; Humphries et al. 2019; Kanchanawong et al. 2010).

The collective set of (~230) proteins that mediate the interaction between integrins and the actin cytoskeleton is referred to as the **integrin 'adhesome'** (Winograd-Katz et al. 2014). Two major functions are recognized for the adhesome: **i)** a *physical scaffold* coupling the mechanical interaction between the ECM and the cytoskeleton (i.e. adaptor proteins, actin, actin-associated proteins); and **ii)** *signaling hubs* that translate the external the mechanical input into biochemical responses, thus affecting downstream signaling targets locally, as well as multiple cellular functions (i.e. kinases, phosphatases, G proteins, transcription regulators). Both physical and signaling functions contribute to regulating certain cell physiology aspects like the cell shape, their mechanical properties, tissue morphogenesis, ECM remodeling, cell migration, differentiation or invasion.

Among the adhesome components, there seems to exist a core of ~60 proteins identified, termed as the *consensus adhesome*, mostly studied in cells attached to FN via the $\alpha 5\beta_1$ and $\alpha V\beta_3$. We will focus on some components playing a role in mechanical sensing, regulation of FA formation, maturation and disassembly. Accordingly, I will base my description according to the model of vertical organization previously described in the literature (**Figure 6**; Horton et al. 2015; Han and de Rooij 2016). Three

major protein-protein interaction hubs have been described: 1, the ILK-kindlin and the FAK-paxillin at the integrin regulatory layer; 2, the talin-vinculin axis at the force transduction layer; 3, the alpha-actinin-zyxin-VASP at the actin regulatory layer (J. D. Humphries et al. 2019; Kanchanawong et al. 2010). One may consider the extracellular matrix itself as a different layer in terms of its mechanobiological properties. Analysis of the protein-protein interaction network of the consensus adhesome also provides support for this distinction of these three layers (**Figure 6**; Horton et al. 2015; Han and de Rooij 2016; Humphries et al 2019).

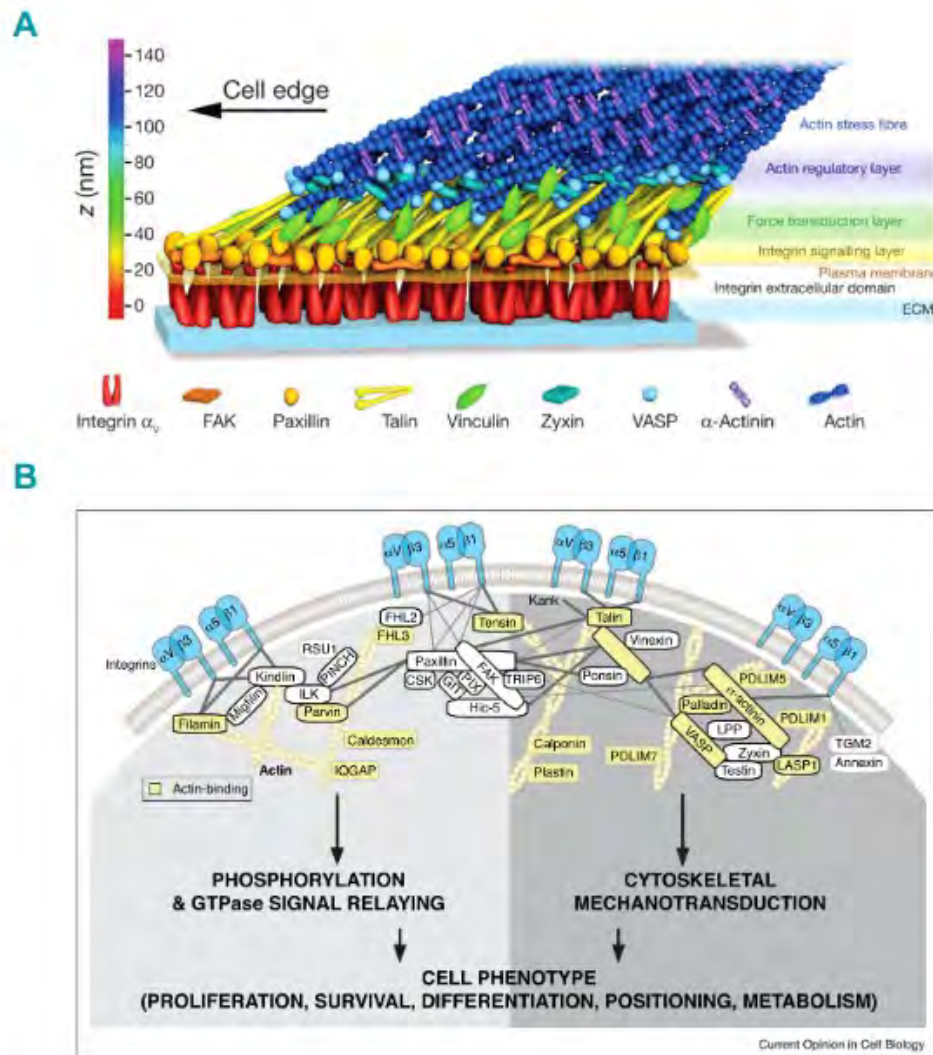


Figure 6. Structural organization and signaling pathways converging at the integrin-dependent adhesion structures. **A)** The organization of Focal adhesions is represented considering the z-axis: the ECM layer, the integrin signaling, the force transduction and the F-actin regulatory layers are depicted. **B)** In terms of cellular phenotypes, the signaling response to mechanical signals from the extracellular environment can be subdivided in two branches, one regulating the mechanosignaling aspects of mechanotransduction, and the other corresponds to cytoskeletal regulators regulating the mechanosensing aspects of this cellular structures. Examples of the proteins described to participate on each branch are indicated (Humphries et al. 2019).

- **Integrin-mediated adhesions' signaling**

Integrin-mediated adhesions mediates a plethora of signaling pathways regulating actin dynamics as well as diverse cellular processes regulating for example cell survival and differentiation (Jansen et al. 2015).

Downstream integrin signaling is particularly involves the Focal Adhesion Kinase, a non-receptor tyrosine kinase. FAK has an N-terminal FERM domain, a mid-kinase domain and a C-term focal adhesion targeting (FAT) sequence. FAK has multiple phosphorylation sites, as well as docking sites to other cell adhesion components (Zhao and Guan 2011). FAK has also been shown to participate in cell proliferation and differentiation, and acts in synergy with RTKs to regulate the entry to the S phase in the cell cycle progression. Consequently, FAK signaling deregulation can have a role in the appearance of transformed cells (Walker, Fournier, and Assoian 2005). Among downstream effector molecules, FAK activates the Phosphoinositide 3-Kinase (PI3K). PI3K, in turn, activates Rac, a member of the Rho family of GTPases, that in turn induces Arp2/3-dependent actin polymerization at the cortex of migrating cells (Zhao and Guan 2011).

The upstream signaling events that recruit FAK to the integrin adhesion structures may depend indirectly on the response of cells to mechanical stimuli and the presence of phosphatidylinositol (4,5)-bisphosphate (PIP₂). As we will discuss later, talin acts as a mechanosensor, and its conformational status influences the local recruitment and interaction with other proteins. This is the case for the enzyme phosphatidylinositol-4-phosphate-5-kinase (PIP₅K γ) that synthesizes PIP₂ and is recruited by talin at FAs

during mechanotransduction. Upon binding of PIP₂ molecules, FAK undergoes a conformational change that exposes its kinase domain (**Figure 7**; Tapial Martínez, López Navajas, and Lietha 2020). Importantly, the binding of talin to PIP₂ is occluded in its “closed” or non-extended conformation (as mentioned in the following sections), which suggests that this interaction depends mostly on the response of talin to mechanical signals.

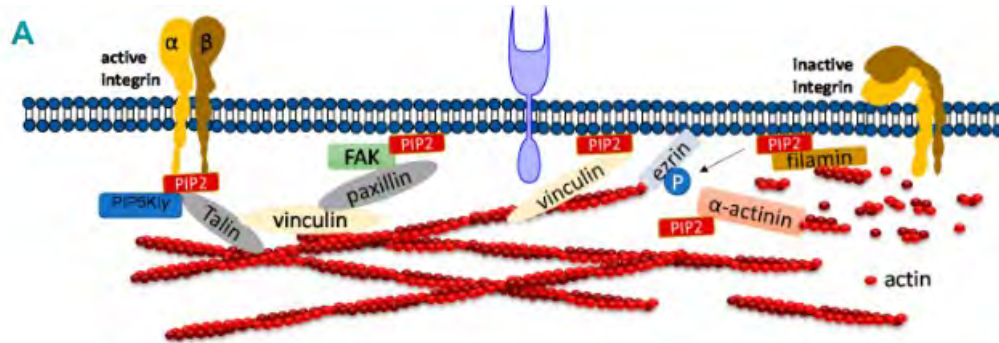


Figure 7. PIP₂ regulates the localization of cell adhesion components at adhesion sites and contribute to the regulation of the actin cytoskeleton. PIP₂ interact directly with integrins, talin, vinculin, FAK and actin bundling proteins like filamin or alpha-actinin to regulate the organization of the actin cytoskeleton (Tapial Martínez, López Navajas, and Lietha 2020).

Paxillin is another important adaptor protein and signaling hub integrating cell adhesion and growth factor signaling responses. Paxillin recruits a diversity of proteins through several protein-protein interaction motifs such (LD motifs, LIM domains, SH domains) that allow the recruitment of cytoskeletal regulators, kinases and GEFs permitting cells to form stable adhesions required for cell spreading (Schaller 2001; Turner 2000).

Talin, FAK, paxillin and vinculin, that will developed further, are recruited early in integrin adhesion structures and are also present in nascent adhesions and focal complexes, where they appear to regulate their dynamics of formation and disassembly (Deakin and Turner, 2008). Other components are recruited at maturing FAs during mechanotransduction.

For example, Tensin is a phosphoprotein marker related to integrin dependent adhesions that have reached a certain maturation state. The 220 kDa protein contains (as an

analogy to talin) multiple binding sites to actin filaments and an integrin binding domain. Tensin participates in the disassembly of focal adhesions by recruitment of tyrosine-phosphorylated proteins recruited through its SH2 domain (Lo, 2004). Also, multiple phosphatases and kinases downstream of FAK have been involved along with the microtubule network asymmetry, in focal adhesion disassembly. FAK is an important regulator of FA turnover. Local Ca^{2+} increase augments FAK residency in cell adhesions, further contributing to the disassembly signaling events by reducing myosin contractility (Broussard, Webb, and Kaverina 2008).

- **Mechanosensing, mechanotransduction and Focal Adhesion maturation**

Integrins and associated proteins can be considered as mechanical sensors, as they integrate information about the mechanical properties from sources like: the ECM, adjacent cells or direct physical stimuli. Accordingly, the cells can respond by adapting their intracellular organization, shape or stiffness. Furthermore, cells can also influence the mechanical properties of their environment by changing the composition, stiffness or topography of the ECM. These cellular functions are particularly important in the field of **mechanobiology**, a multidisciplinary field where cellular biology, biophysics, engineering as well as computational and structural biology converge to understand how cells sense, integrate and respond to extracellular and intracellular mechanical signals and translate that information into biological responses (Jansen et al. 2015; Gefen 2010). How integrin-mediated adhesions translate those mechanical signals into biochemical signals is known as **mechanosignaling (Figure 8)**. The coupling of both mechanosensing and mechanosignaling is defined as **mechanotransduction** (Stutchbury et al. 2017). Integrin-mediated mechanotransduction plays a key role in cell adhesion, by permitting the maturation of nascent adhesions into focal adhesions (FAs).

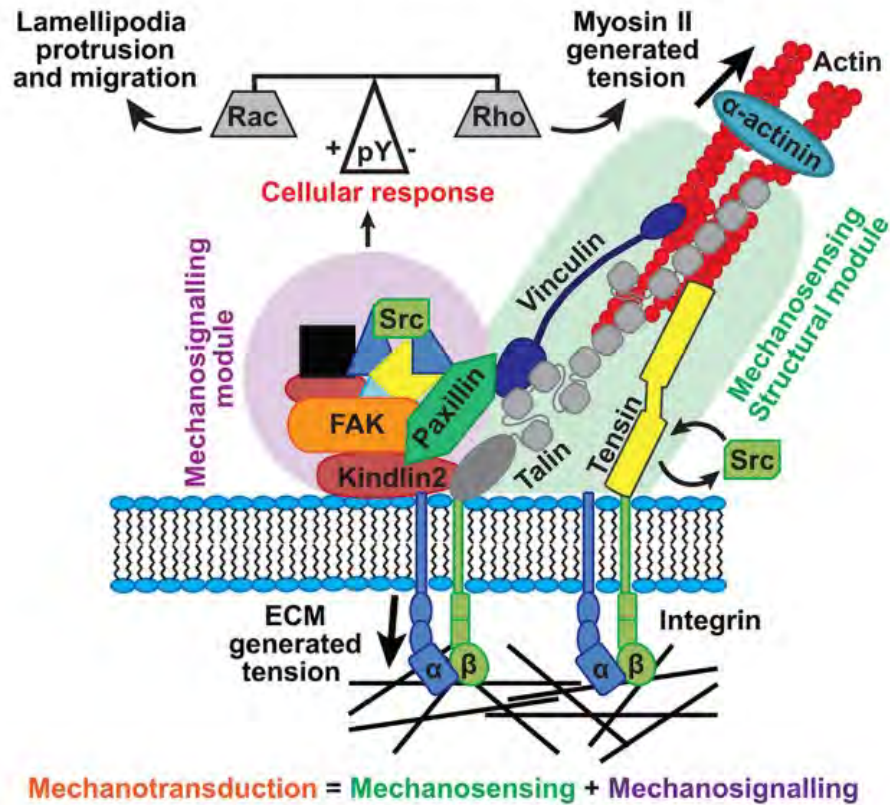


Figure 8. Components associated with the cell to extracellular matrix adhesion structures. The process of mechanotransduction involves the participation of cellular modules or molecular assemblies, organized in order to perceive the mechanical properties of their extracellular environment (mechanosensing module). This information is further translated into biochemical signals that the cell can integrate according to the intracellular signaling networks in order to respond accordingly to the environment stimuli (mechanosignalling module). The process of coordinating the information between the extracellular to intracellular (or *vice versa*) mechanical forces is known as mechanotransduction (Stutchbury et al. 2017).

The adhesion maturation process involves an increase in size and composition, but also impacts on the lifetime for these structures, as the smaller they are, the more labile too. Cells can form nascent adhesions at the leading edges of migration at lamellipodia. These structures are $< 0.25\mu\text{m}^2$ and their formation and mechanical formation and stability mostly depends on the F-actin polymerization, rather than the actomyosin II pulling forces (Choi et al. 2008; Gardel et al. 2010; **Figure 9**). Nascent adhesions can further grow and mature into Focal complexes (FC) at the rear part of the lamellipodia and this maturation is correlated with the presence of alpha-actinin. alpha-actinin acts as

a short-term template bundling actin filaments and recruiting other adaptor and signaling proteins like the Focal Adhesion Kinase (Choi et al. 2008; Gardel et al. 2010; **Figure 9**). Focal complexes then mature into Focal Adhesions through a process involving the stretching of talin under actomyosin contraction (Gardel et al. 2010). We will develop this process further with more structural details in the section devoted to talin and mechanotransduction,

More recent findings also give new light on the maturation process, as the periphery of FAs can interact indirectly with the microtubules. This interaction is mediated by KANK1, a protein able to interact with talin molecules surrounding the FAs forming a cortical microtubule stabilization complex (CMSC) that, as its name suggests, helps to further stabilize these adhesion structures (Bouchet et al. 2016). The microtubule recruitment at zones located behind the leading edge or retracting cell zones, is important, because this is associated to FA disassembly by different mechanisms (Broussard, Webb, and Kaverina 2008).

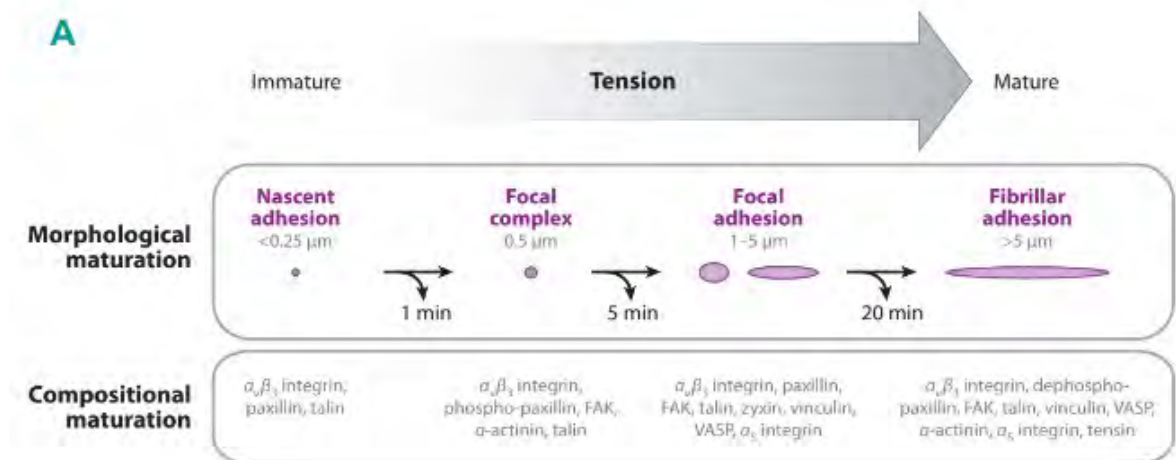


Figure 9. Maturation of integrin-mediated adhesion structures. IDACS are represented in purple. The large arrow on top represents tension exerted by the actin polymerization or actomyosin contraction during mechanotransduction. The curved black arrow indicate possible adhesion turnover and timescale (from Gardel et al. 2010).

Talin structure and mechanotransduction

Talin is a 270 kDa with two main isoforms in vertebrates, talin1 and talin2 sharing 76% sequence similarity. Talin1 is the main isoform found in cell to ECM adhesion structures. At the structural level, talin has 18 domains: an N-term globular head domain or FERM domain (50 kDa) that can stably bind to integrin's cytoplasmic domains and an elongated rod domain formed by 13 helical bundles or rod domains (R1-R13) comprised of 62 α -helices. Talin can bind to actin fibers via three actin binding sites and contains a dimerization domain at its C-terminus there (**Figure 10**). The active or "open" form of talin1 is best characterized. In the "closed" or inactive state, talin cannot bind to integrins and the vinculin binding sites are not available. A structural model for talin's activation priming suggests that the interaction of the subdomain F2 of the FERM domain with PIP₂ is occluded by its interaction with R12 in the inactive form (Dedden et al. 2019).

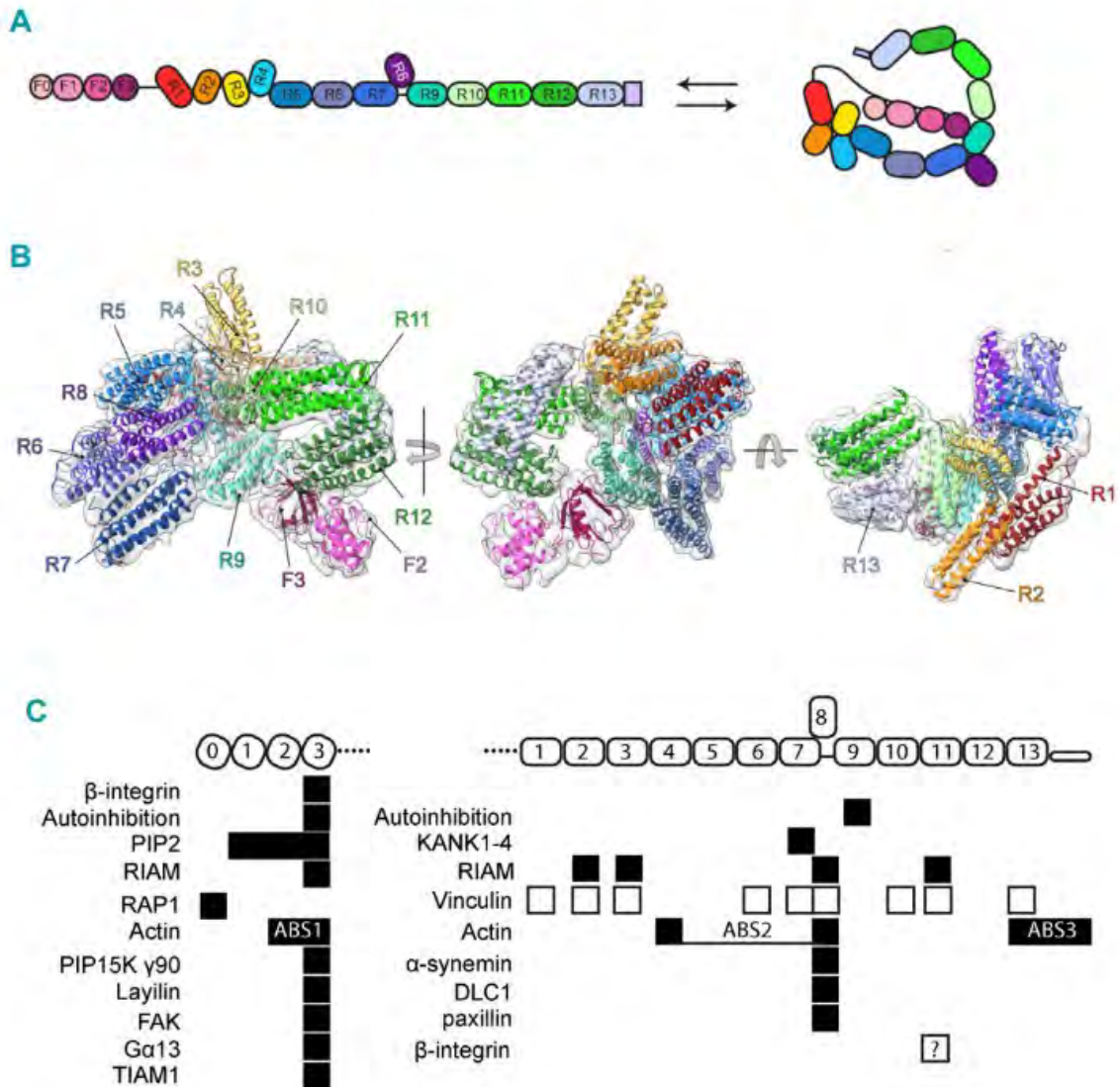


Figure 10. Talin structural organization and binding partners. (A) Schematics for the organization of the 18 domains of talin and (B) three views for the structural fitting into a Cryo-EM density map. (C) As talin is considered as a signaling hub from integrin dependent adhesions to the ECM, several talin partners are listed. (Dedden et al. 2019 & Goult, Yan, and Schwartz 2018).

Talin is a key component of the force transduction layer in FAs, acting as a mechanosensor that couples the force between the ECM and the intracellular environment (Goult, Yan, and Schwartz 2018; Han and de Rooij 2016). When cells adhere to a soft substrate, the talin molecule does not stretch sufficiently to unveil VBSs that remained buried into helix bundles, failing to recruit vinculin and reinforce

cytoskeletal anchorage before integrins detach from the ECM (**Figure 11**). In contrast, during mechanotransduction, when the substrate is sufficiently stiff, the actomyosin contraction-dependent stretching of talin leads the unfolding of talin helix bundles, unveiling of the VBSs, vinculin recruitment and activation and reinforced cytoskeletal tethering via Vt binding to F-actin (**Figure 11**). Elegant studies using magnetic tweezers have established a hierarchy in the pulling forces required to unfold the various talin helix bundles, suggesting a gradual response in vinculin recruitment at focal adhesions during mechanotransduction (Yao et al. 2016; Dedden et al. 2019). Consistently, in studies combining the tracking of focal adhesions during their maturation and quantitative fluorescent microscopy analysis, it was found that talin and vinculin formed pre-complexes in nascent adhesions, and that vinculin recruitment occurred at a high rate when these nascent adhesions undergo maturation into mature focal adhesions (Han et al. 2021). Whether in cells, the recruitment of vinculin and its activation solely depends on the exposure of talin VBSs, required a combinatorial stimulation is a matter of debate.

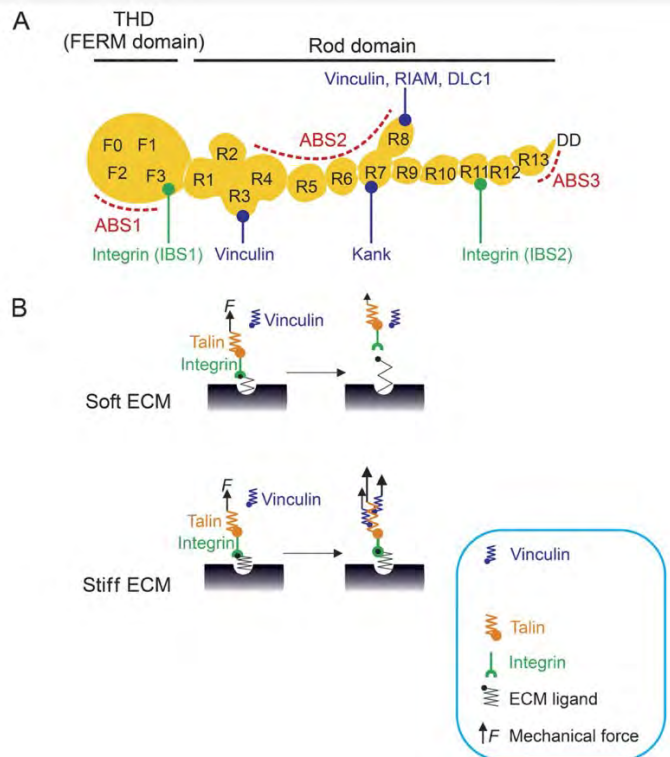


Figure 11. Conformational changes associated with the mechanical unfolding of talin. The helix bundles from the talin rod domain can unveil vinculin binding sites in response to the mechanical stretching of the molecule by actomyosin contraction (Sun et al., 2016).

4. Vinculin

- **Structure and evolutionary aspects**

The vinculin-homology family comprises evolutionary related proteins composed of four to five interconnected helical bundles. In vertebrates, the vinculin family includes, α -catenin and α -catulin. Strikingly, vinculin family members can be traced back to the Opisthokonta clade comprising Fungi, Metazoa and unicellular related groups. A maximum-likelihood phylogeny for the vinculin family was proposed by Miller *et al.* by comparing the relatedness of 96 VIN protein sequences, indicating its presence at the emergence of multicellularity among different groups (**Figure 12**) (Miller et al. 2013; Gielata et al. 2022).

More recently, a structural and functional analysis of a vinculin family member present in the sponge *Oscarella pearsei* (*Op*) compared both the sequence and domain architecture with the vinculin and α -catenin present in vertebrates (*G. gallus* and *M. musculus* respectively), indicating the existence of a conserved architectural pattern. The *Op* ortholog was detected by fluorescence microscopy in both cell-cell and cell-matrix adhesion connecting them to the actin cytoskeleton, suggesting a functional contribution in those structures. Notably, the presence of a D2 helical bundle, a domain involved in the head domain stability and autoinhibition of F-actin binding, is a particular feature present among vinculin homologues, but not in α -catenin, α -catulin or the *Op* VIN ortholog (Miller et al. 2018; Gielata et al. 2022).

Vinculin was originally described as a protein mediating the attachment of actin stress fibers to cell adhesion sites and in association with α -actinin (Geiger 1979). The name “vinculin” derives from the latin word “*vinculum*” which means to bond, union and/or unity (Peng et al. 2011). Vinculin’s structural, biochemical and cellular related properties concerning this study will be developed further in the following sections.

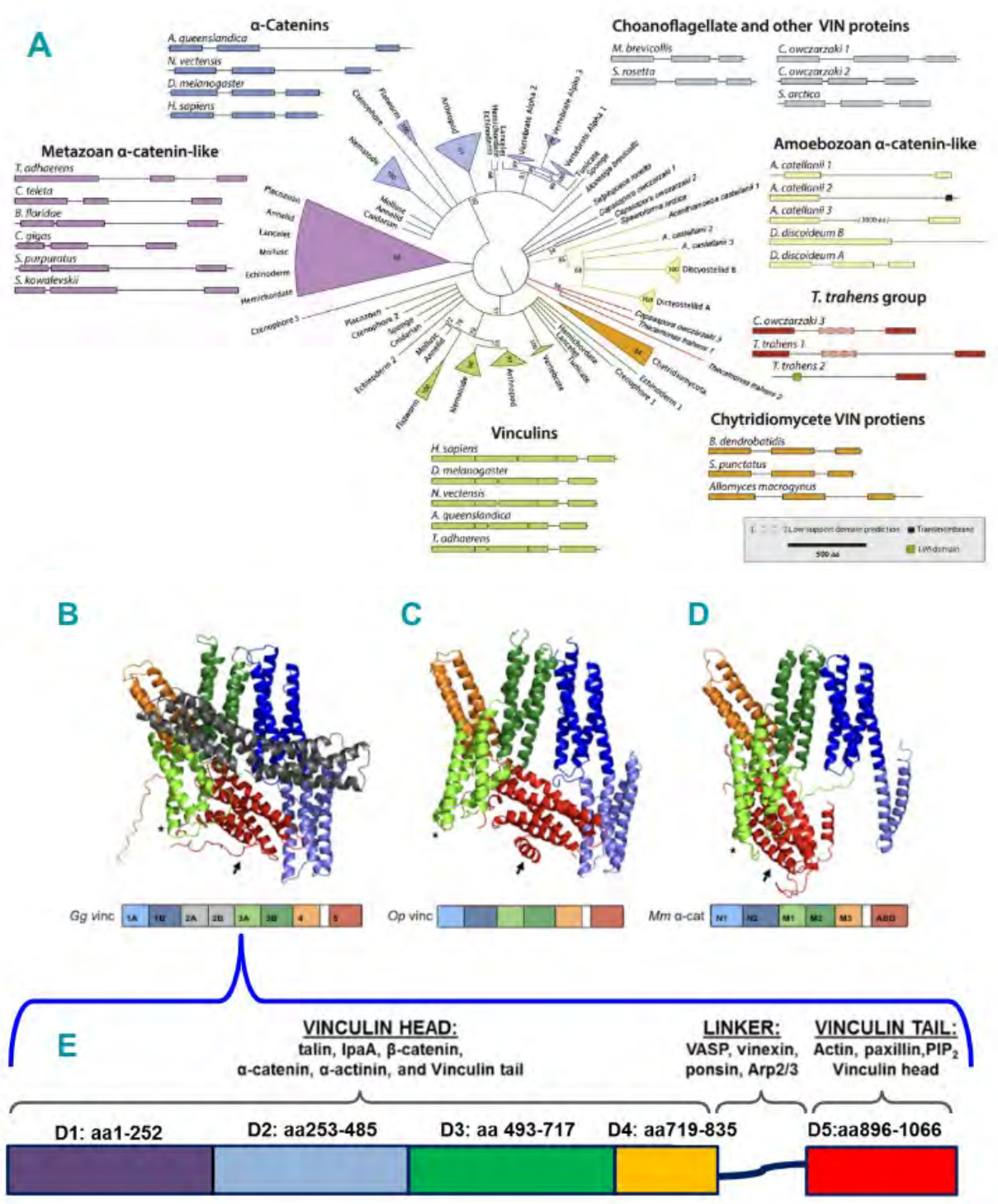


Figure 12. Vinculin family members among metazoans/non-metazoans and

comparison of domain architecture. (A) A maximum likelihood phylogeny for 96 proteins belonging to the VIN family. Different domain architectures corresponds to the number of the VIN domains found in the sequences analyzed the and color codes represent the different clades included in this phylogeny (B-D) Comparison of domain architectures among members from the VIN family vinculin and α -catenin present in vertebrates (B and D) with the vinculin orthologue found in the sponge Op. Their corresponding domain schematics is depicted below. The architectural organization of the VIN family member α -catulin, highly resembles the one from α -catenin (D). (E) Binding partners identified with vinculin's head, linker and tail domains including: vinculin activators (VBSs), kinases, phosphatases, adaptor proteins, actin regulators, lipids and actinn (adapted from Miller et al., 2013, Miller et al., 2018 and Bays and DeMali, 2017).

Vinculin comprises three main regions: a N-term globular head and a C-term tail domain composed of α -helix bundles, and a less organized proline-rich linker region (PRR) connecting them (Ziegler, Liddington, and Critchley 2006). The crystal structures corresponding to chicken and human vinculin revealed the presence of conserved subdomains composed by antiparallel α -helix bundles denoted as D1 to D5, with D5 corresponding to the F-actin binding tail domain or Vt. D1–D3 are composed of two four-helix bundles connected by a common long α -helix (Figure 13; Borgon et al. 2004; Bakolitsa et al. 2004). D4 and D5 (Vt) only contain one helix-bundle. At the basal state, vinculin is maintained folded through intramolecular interactions between Vh and mainly D1, with the D1-D2-D3 subdomains organizing as a pincer holding Vt (Figure 13; Borgon et al. 2004; Bakolitsa et al. 2004).

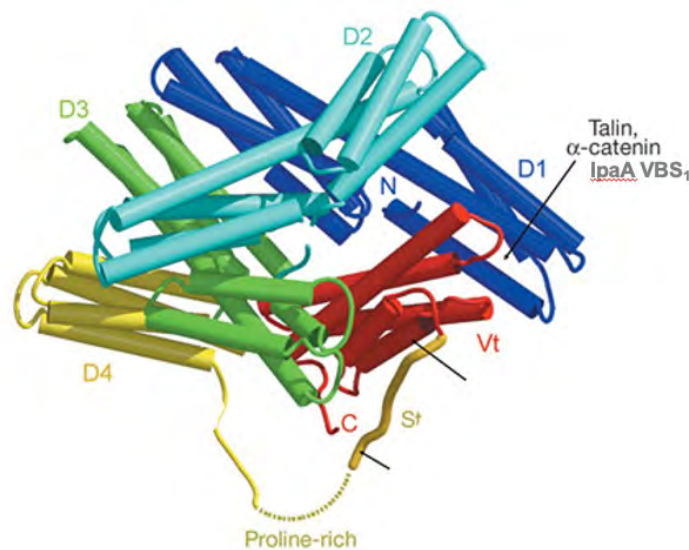


Figure 13. Crystal structure of human vinculin. The vinculin head is composed of the conserved D1-D4 subdomains. Intramolecular interactions between Vt and D1 maintain vinculin in its folded conformation (from Bakolitsa et al. 2004).

- ***Vinculin functions***

Vinculin is a component of focal adhesions and of cadherin-based intercellular junctions. Its decreased expression is often observed in cancer cells and has been associated with increased cell tumorigenesis. Vinculin deficiency leads to cell adhesion defects explaining its importance in embryonic development and in cardiomyopathies. Vinculin is an integral component of focal complexes also called nascent adhesions, along with other proteins such as paxillin and p125 FAK and is required for the enlargement of these into large focal adhesions. While in cultured cells, vinculin is not essential for the formation of adhesion structures, it is required to strengthen the link between integrin and cadherin receptors with the actin cytoskeleton and plays a key role in mechanotransduction. As a result, vinculin-deficient cells form cell protrusions called lamellipodia or filopodia that are unstable and are more motile (Varnum-Finneey et al. 1994). However, increased motility in vinculin-deficient cells is associated with defects in directed migration, consistent with the role of vinculin in stabilizing adhesions (Coll et al. 1995). Recently, vinculin was shown to form so called “catch bonds” with actin filaments, which as opposed to “slip bonds”, correspond to bonds that are revealed when actin filaments are subjected to pulling forces (Huang et al. 2017). Interestingly, these catch bonds are significantly more stable when the force is applied towards the pointed end of actin filaments relative to the barbed ends, consistent with the polarity of actin filaments subjected to the actomyosin contraction during the maturation of focal adhesions in cells (Huang et al. 2017). The property of vinculin to form catch-bonds with actin filaments, that are stabilized by force and with an asymmetric directionality may account for a role of vinculin in organizing the polarity of the actin cytoskeleton at cell-cell and cell-matrix adhesion structures. As illustrated in these studies, in the past two decades, our understanding of how vinculin strengthens cytoskeletal anchorage has largely benefited from structural studies and biophysical approaches, elucidating how binding of vinculin to F-actin is regulated in a force-dependent manner. These aspects linked to mechanotransduction will be developed in subsequent sections.

In addition to reinforcing cytoskeletal anchorage, vinculin was shown to regulate the dynamics of actin polymerization / depolymerization. When stimulated with *Shigella* IpaA, vinculin promotes the partial capping of actin filaments' barbed end (Ramarao et al., FEBS 2007). Also, Vt by itself shows full capping activity towards the barbed ends of actin filaments (Leclainche et al. 2010). The capping activity of vinculin observed in vitro may account for its stabilizing role at focal adhesions by preventing actin polymerization and protrusion formation.

Finally, vinculin can bundle actin filaments, either through its oligomerization via Vt, as will be developed further, or by forming scaffolds with talin (Thompson et al., 2013). Boujemaa-Paterski et al recently showed that through its interaction with talin, vinculin induces the formation of actin bundles with mixed polarity that affect the organization and dynamics of actin network dependent of the Arp2/3 complex nucleator (Boujemaa-Paterski et al. 2020). How these diverse vinculin functions are regulated remains unclear.

- ***Vinculin Binding Sites and vinculin activation***

Vinculin interacts with partners containing a vinculin binding site (VBS), which refers to an amphipathic α -helix of a typical size of around 20 residues. VBSs can be found in proteins such as talin, α -actinin or α -catenin involved in mechanosensing. In these proteins, the VBSs remain hidden into helical bundles and can be gradually exposed through a force-dependent unfolding of the helix bundle (Kluger et al. 2020).

In addition to VBS-containing cellular proteins, different intracellular pathogens such as *Shigella spp.* or *Chlamydia spp.* Express bacterial effector proteins with VBSs exposed independent of mechanotransduction. These bacterial VBS-containing proteins are required during host cell invasion by these pathogens events (Park et al. 2011; Kluger et al. 2020). Overall, structural, biochemical and bioinformatic characterization of both endogenous and exogenous VBSs have led to define a consensus optimal VBS sequence as: *LXXAAXXVAXXVXXLIXXA*, with the hydrophobic residues facing the same side in

the α -helix (**Table 1**) (Gingras et al. 2005; Kluger et al. 2020)

Talin-1	
VBS 4/VBS1	L L Q A A K G L A G A V S E L L R S A
VBS 6	L M Q L A A K A V A T S A A A E L V L K A
VBS 9	V G A A A T A V T Q A A L N E L L Q H V
VBS 11	M V R Q A R I L A Q A T S D L V N A I
VBS 12/VBS2	L L S A A K I L A D A T A K M V E A A
VBS 27	L L A A A A R A V T D S I N Q L I T M C
VBS 33	F V Q S A K E V A N S T A N L V K T I
VBS 36	L A G H S R T V S D S I K K L I T S M
VBS 46/VBS3	L I E C A R R V S E K V S H V L A A L
VBS 50	L I N A V K D V A K A L G D L I S A T
VBS 58	I L E A A K S I A A A T S A L V K A A
IpaA	
VBS IpaA1	I Y K A A K D V T T S L S K V L K N I
VBS IpaA2	I Y E K A K E V S S A L S K V L S K I
VBS IpaA3	I F E A S K K V T N S L S N L I
Alpha-Actinin Isoforms (reverse)	
VBS alpha 1/4	I Q N E V E N I T R A I T T L L Q E W
VBS alpha 2	I Q T E V E N I T R A I T T L L L E W
VBS alpha 3	V Q N E V E N I T R A I S T L L Q E W
Other VBS	
α -Catenin VBS	I V A E C N A V R Q A L Q D L L S E Y
RIAM-VBS	I D Q M F S T L L G E M D L L T Q S L
Sca4 VBS C	I Y N K A R E V I N A V N P V I E A L
Sca4 VBS N	L L N A A T A L S G S M Q Y L L N Y V
TarP-VBS1 (GPIC)	L L E A A R N T T T M L S K T
Vinexin (predicted)	L L E R E L A K L S A E D K D L R A I
Metavinculin (predicted in the linker region)	I N Q P M M M A A R Q L H D E A R K W

Table 1. Reported VBSs and sequence similarities. The color code indicates the biochemical properties of aminoacid residues with single letter code as follows: A: small hydrophobic; V, P: medium hydrophobic; I, L, F, M, Y, W: large hydrophobic; S, C: small hydrophilic; T, N: medium hydrophilic; Q, H: large hydrophilic; K, R: large basic; D: medium acidic; E: large acidic (Modified from Kluger et al. 2020).

Vinculin activation is triggered by an interaction with a VBS that can alter the stability between the head-tail domains in the closed conformation (i.e D1-Vt or D4-Vt). All activating VBSs reported to date interact with the first helix-bundle of D1. The canonical view on the vinculin activation mostly derived from structural analysis by studying the D1 domain bound to a talin's VBS, where it was showed that the vinculin D1 domain transits a conformational change after the insertion of the amphipathic α -helix by converting its four-helix bundle into a heterodimeric five-helix bundle by a mechanism named helical bundle conversion. This mechanism was theorized to be sufficient to disrupt the stability of the acidic pocket formed between residues at the interphase between D1 and Vt domain (Izard et al. 2004). These findings were important as vinculin activation was revealed as a result from conformational changes in D1 head subdomain.

A complementary model of vinculin activation includes the participation of molecules such as phosphatidylinositol-4,5-bisphosphate (PIP₂) besides the D1-VBS interaction.

PIP₂ binding to vinculin has also been proposed to promote its opening, but it is not clear to what extent it interferes with F-actin binding (H. Chen, Choudhury, and Craig 2006; Carisey and Ballestrem 2011). As discussed further, PIP₂ was also shown to promote vinculin oligomerization via Vt. Later studies also highlighted a complementary role of the F-actin binding to the Vt in order to maintain vinculin in a fully activated conformation (H. Chen, Choudhury, and Craig 2006; Carisey and Ballestrem 2011). This model is referred to as the combinatorial activation model, as it considers necessary the presence of secondary activators to overcome the tight intermolecular interaction between the vinculin D1-Vt and other head domains with the Vt domain (**Figure 14**; H. Chen, Choudhury, and Craig 2006; Carisey and Ballestrem 2011).

Finally, endogenous post-translational modifications such as serine or threonine residues phosphorylation, have also emerged as mechanisms regulating vinculin's activity, recruitment or lifetime into different adhesomes (Bays and DeMali 2017). Vinculin derived Foerster Resonance Energy Transfer (**FRET**) probes have been used to characterize the localization of active-inactive states of vinculin in living cells. These studies showed that vinculin remains mostly in an inactive/closed state at the cytoplasm, however, the active/open state was associated with its recruitment to cell adhesion sites presumably after the unveiling of talin's VBSs on those adhesion sites (H. Chen et al. 2005).

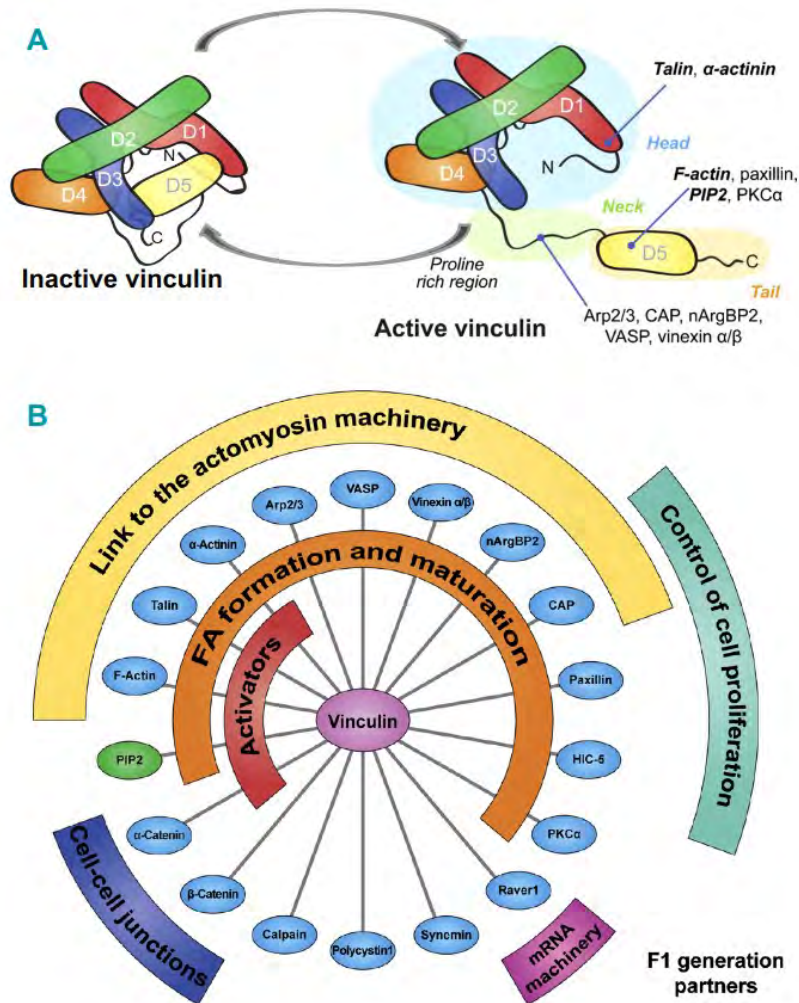


Figure 14. Schematics of vinculin activation and binding partners. A) General representation of the different vinculin domains in the open and closed conformation. After vinculin activation by binding a VBS the tail domain D5 is released and binding sites to other protein partners are unveiled as indicated by the blue lines. B) Direct binding patterns reported to vinculin (circles) and the diverse cellular processes or functions they're associated with (adapted from Carisey and Ballestrem, 2011).

- **Vinculin allosteric changes: the input of structural modeling.**

The intrinsic complexity of protein's structure-function relationship has made it a problem attractive to handle with methods of computational modeling. Specifically, Molecular Dynamic (MD) modeling is a method aimed to collectively trace the movement of atoms in a protein during the transition between at least two given conformational

states. As such, after the MD simulation provides the measurements for covariance of coordinates among the atoms in a molecule, the principal values for direction (Eigenvectors) and the magnitude of their displacement (Eigenvalues) can be obtained. Those models normally can include data about the formation and disruption of contact residues (Berendsen and Hayward 2000; Yiwen Chen and Dokholyan 2006).

Furthermore, in terms of biological functions, it has been proposed that the structural rearrangements that a protein presents after binding to its partner in a protein-ligand or protein-protein interaction are already predisposed in the structural vicinity of the native state. In other words, the most probable conformational (thermodynamic) pathways that a protein is likely to transit between two different states (i.e inactive/active or unbound/bound states) can be recapitulated by analyzing their intrinsic conformational predisposition(s) in its apo/native form (Berendsen and Hayward 2000). Experimental data have showed agreement with this proposal and some researchers have even proposed that this structure-encoded properties imply that: **i)** a protein possesses a fingerprint or unique landscape of dynamic fluctuations (at equilibrium conditions) that depends in its 3D structure; and **ii)** those fluctuations or predispositions might be functionally or even evolutionary constrained (Tobi and Bahar 2005).

Different teams have studied vinculin through different structure-based modeling (**SBM**) approaches in order to understand the transition between the inactive to active states normally including: **1)** the helical bundling conversion after VBS insertion in the D1 domain; **2)** the relationship (contacts) among subdomains in the apo/native state and during the activation process and; **3)** the inclusion of pulling forces as expected after Vt-F-actin interaction in a different direction (or even opposite) from the one acting on the D1-VBS complex.

A pioneering study from Chen and Dokholyan used an MD approach to analyze the structural changes from vinculin full length in its (near) native conformation and after binding to talin VBS1 (Yiwen Chen and Dokholyan 2006). Near its native conformation, the dominant conformational motions found for vinculin in this study

were the following:

- The “expansion-retraction” cycles between the PRR and the D5(Vt) domains. The twisting motion at the region connecting the two helix bundles from the D2 domain.
- An intrinsic flexibility of the head domain, specifically holding and releasing of Vt by the pincer-like organization D1-D2-D3 as described previously by its crystal structure (Borgon et al. 2004; Bakolitsa et al. 2004).
- A shift to a near parallel reorganization of the major axis of the D1, D2 and Vt subdomains.

Importantly, the D1-Vt contact interphase was maintained stable through those conformational fluctuations in the near native conformation. Additionally, by comparing the apo form before and after increasing the temperature of the system, the authors calculated the level of inter-domain association-dissociation and found that the D1-Vt and D1-D2 were more resilient compared with the other inter-domain interactions. Interestingly, the D1-Vt and D1-D2 interdomains were also resilient to the inclusion of talin VBS1 in D1, suggesting the importance of additional signals during vinculin activation (Yiwen Chen and Dokholyan 2006).

Multiple studies have revisited the modeling of vinculin’s structural behavior during its activation by considering different assumptions on the model to identify the pathways that might be taking place during mechanotransduction. For instance, Sun et al. used SBM to predict the possible conformational transitions that vinculin might follow during its activation process (L. Sun et al. 2017). They compared simulations of talin VBS3-dependent helical bundle conversion on vinculin D1 under the absence or presence of opposing pulling forces between the D1-VBS3 complex and Vt, to mimic F-actin pulling. The bi-molecular simulations predicted different free energy barriers separating four different states: **N** → **I** → **C** → **D** (*Native* → *Inactive-intermediate VBS binding* → *Helical bundle converted* → *Intramolecular Dissociation or Active*).

Interestingly, when the simulations included moderate to high opposing pulling forces (>40 pN), two conformational pathways were distinguished during vinculin activation; the first one from **I** → **C** → **D** states, the second one appeared to proceed directly from

I → D (Figure 15). These findings suggest an activation shortcut, depending on the applied force and involving the disruption of the D4-Vt binding interphase even before the helical bundle conversion takes place.

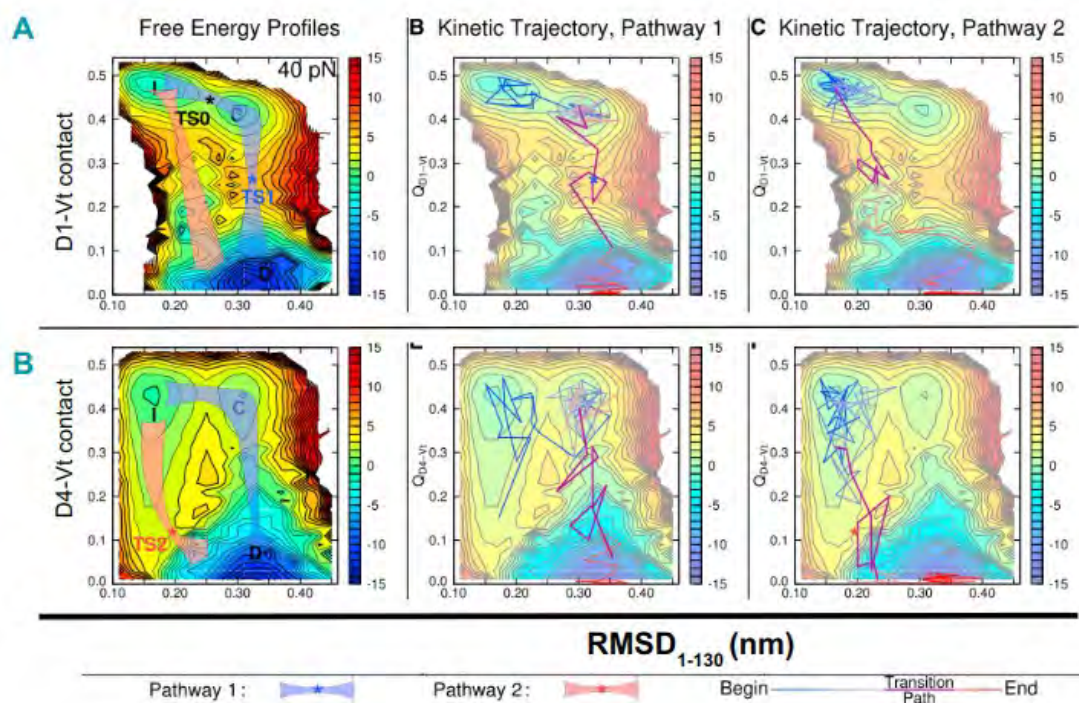


Figure 15. Vinculin can change its conformation on the D1-D4 domains in a two-step process as analyzed *in silico* and *in vitro*. **A)** This structural based modeling approach proposed the ability of the vinculin head domain to use two alternative routes driving the conformational changes related to vinculin activation, one transiting from the inactive, non-bound form to an intermediate one where the VBS is bound to the D1 domain, the second route was only apparent when modeling the behavior of the head domain under the presence of pulling forces as expected during its activation *in vivo*. In order to release its tail domain from the rest of the protein. **B)** Experimental detection of a transitory state on full length vinculin proteins subject to the passage through a gasified ion-trap in order to detect the probable conformational changes associated with the gas collision area to energy necessary to transit intermediate conformational changes on vinculin and derivatives (from Sun et al. 2017).

Together, these modeling studies suggest that VBS binding to D1 may not be enough to disrupt the vinculin head interaction with the tail domain. However, pulling forces applied to the head domain predicted an alternative pathway independent of helical-bundle conversion promoted by the insertion of the activating VBS in D1.

The role of pulling forces during vinculin activation has also been emphasized through single-molecule studies measuring the mechanical stability of D1 bound to a talin or α -catenin VBS (Le, Yu, and Yan 2019). These studies showed that complexes can remain stable until a 20-30 pN force range before dissociating (Le, Yu, and Yan 2019). In contrast, Klugger *et al.* found that D1 in complex with different VBSs derived from talin, α -actinin, and *Shigella's* IpaA can stand loading forces up to 45-60 pN and that the preferred or more stable orientation of the complexes were by pulling the VBS in a shear-like manner, with the VBS properly docked to D1 and independent of the N-terminal or C-terminal D1 orientation (Klugger et al. 2020). Differences between these two studies might be due to the experimental design used to measure the single molecule binding forces, since Le et al. used magnetic tweezers as opposed to AFM (Atomic Force Microscopy) for Klugger et al. Nonetheless, both studies confirmed that D1-VBS complexes can remain stably associated, even under force range where the D1 second helix bundle unfolds (Le, Yu, and Yan 2019; Klugger et al. 2020).

The study from Klugger et al. also included an MD approach further supporting unfolding of the D1 second helix-bundle before dissociation of VBS from the D first helix-bundle. Additionally, the authors studied the effects of shear-like (tangential) pulling and the zipper-like (perpendicular) pulling on full length vinculin tethered at its C-terminus with talin VBS11 bound to D1. Major conformational rearrangements were predicted in those simulations involving the reorientation of the D1, D2 and D3 interphases without unfolding events (Klugger et al. 2020).

Structural analysis combined with biochemical data and cell transfection experiments data has further provided evidence for non-binary open \rightarrow close transitions of the head domain conformational changes during vinculin's activation (Chorev et al. 2018). Chorev et al. compared WT vinculin and two vinculin mutant constructs bearing T12 and T12-A974K that destabilize the contacts between Vh-Vt. Comparison of their conformational plasticity through ion-mobility mass spectrometry indicated that the different vinculin T12 and T12-A974K variants showed a pronounced presence of an

intermediate population of conformers defined as “semi-open” (Chorev et al. 2018). This comparison showed three favored states that the authors classified as [closed → semi-open → open], that the T12 vinculin was more susceptible to adopt the semi-open conformer and that T12-A974K proceeded directly to the open state (Chorev et al. 2018). These results are consistent with an intermediate “semi-open” conformation during vinculin activation (L. Sun et al. 2017). At the cellular levels, transfection of the T12 and T12-A974K vinculin variants in vinculin null cells led to an increase in the cell size, length, and number of adhesions per cell when compared to wild-type vinculin, in accordance to facilitated transition from the semi-open to open states.

A recent study has proposed an alternative model for vinculin activation that also includes major rearrangements of the vinculin head subdomains, but without the need to dissociate or extend the D5 (Vt) as suggested in the classical activation model. Stec and Stec applied an **TLSDM** (translation / liberation / screw molecular dynamics) modeling approach to refined vinculin crystal structures (Stec and Stec 2022). This method grossly considers the crystal structure of a protein as a snapshot of the dynamic properties of large groups of atoms in motion and the way they might behave dynamically. The TLSDM algorithm is aimed to find an optimal number of non-overlapping, contiguous segments in a protein even if a group is apparently separated by a hinge region or flexible loop (Painter and Merritt 2006). The TLSDM analysis identified units **I**, **II** and **III** corresponding to D1, D2 and D3 respectively, and predicted a module **IV** including D4 and D5 even if not connected by a shared helix as in the other units (Stec and Stec 2022). This is contrasting to the canonical view of the linker region as being unstable and primed to separate D5 from the rest of the protein. A complementary folding analysis detected the stability and instability hotspots in the protein sequence (**Figure 16**). Specifically, instability regions were found around vinculin residue 50 corresponding to the binding site for activating VBS and the proline rich region (Stec and Stec 2022).

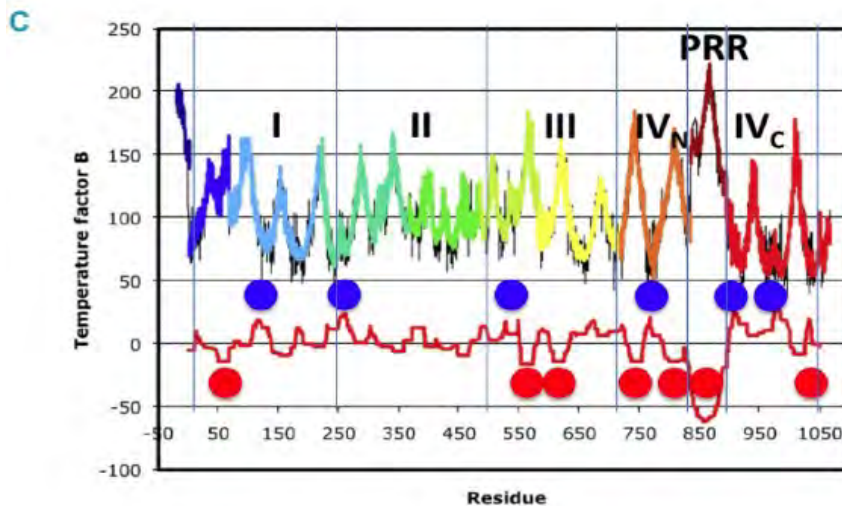
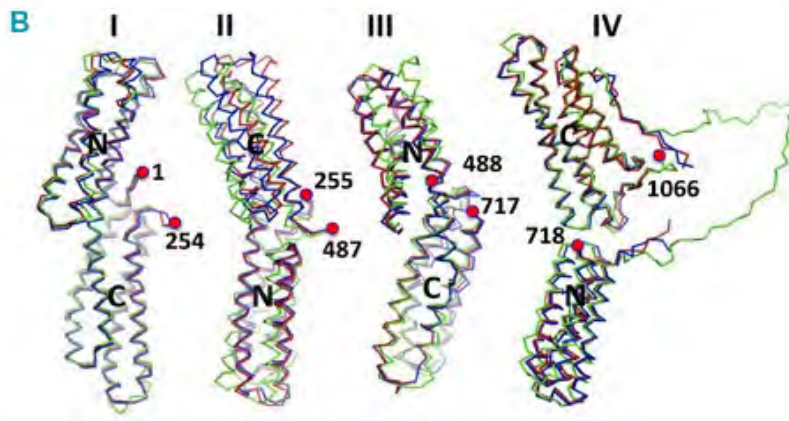
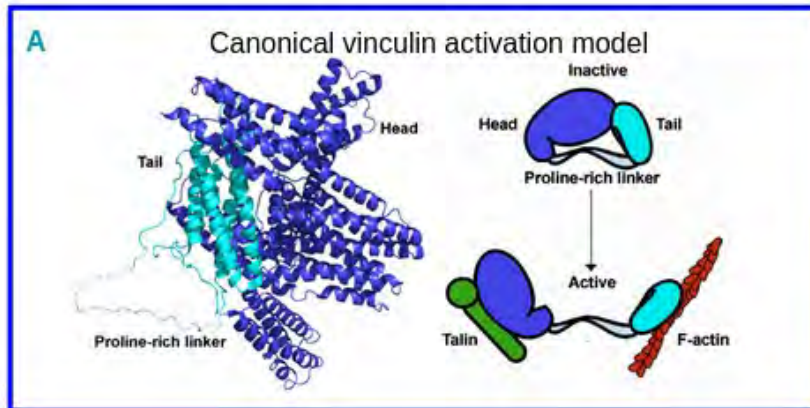


Figure 16. Canonical vinculin activation model and model of mechanical unfolding without Vt separation. (A) Derived from early EM observations of vinculin and extended in after the obtention of the full-length vinculin crystal structure, the standard model of vinculin activation involves the convergence of signals including the VBS binding to the first helical bundle of the D1 domain and the interaction with F-actin in order to release the pincer-like holding of the tail domain, efficiently couple the mechanical tension between the adhesion

molecules and the actin cytoskeleton. **(B)** The model proposed by Stec and Stec involves major rearrangements of the four pairs of helical bundles contained in vinculin but the model proposed doesn't involve the separation of the tail domain D5 from the rest of the protein. Instead, proposes a novel model where the D4 and D5 form a stable interacting interphase that allows the domains to remain bound even after major conformational reorganizations under mechanical tension. **(C)** Shows the predicted sites of stability (blue dots) and instability (red dots), and its position along the protein sequence. A notable recurrence of stability hotspots is predicted to keep the stable interaction between D4 and D5 (Thompson, Tolbert, and Campbell 2013; Stec and Stec 2022).

As a summary, in this study, Stec and Stec proposes an alternative to the standard model of vinculin activation involving:

- the opening of vinculin while preserving folding integrity of units and mechanical stability. Examples of this mechanical stability have been identified in spring-like ankyrin domains (G. Lee et al. 2006) and as it has been suggested by biochemical data and MD predictions (Le, Yu, and Yan 2019; Chorev et al. 2018; Kluger et al. 2020).
- D4-D5 as a single unit stabilized by non-covalent bonds.
- a new model of activation with a reorientation of all the four pairs of helical bundles (super-bundle) of vinculin, and D5 (Vt) not separating from the other domains.
- protein “instability” sites able to bind activating or auxiliary proteins (i.e. VBS binding sites in D1 or PRR binding proteins Arp2/3, VASP).

This study also highlights the importance of the linker-PRR domain as a stabilizer between D4 and D5, and acting as a multiple adaptor for molecules related to vinculin activation as well as actin-regulators (PIP₂, VASP or Arp2/3).

- ***Vinculin oligomerization***

Early studies aimed to characterize the structural features of purified vinculin proteins by means of electron microscopy ((**EM**) methods such as negative staining and rotary shadowing. In those studies, were identified not only a globular head and their corresponding smaller tail domains of individual vinculin molecules, but also the formation of higher-order structures formed by association of both head-head and tail-tail interactions under high salt or low ionic buffer conditions (**Figure 17**). Such structures resembled more a parachute or a bouquet of balloons, being the tail-tail

interaction the more recurrent one (Molony and Burridge 1985; Milam 1985).

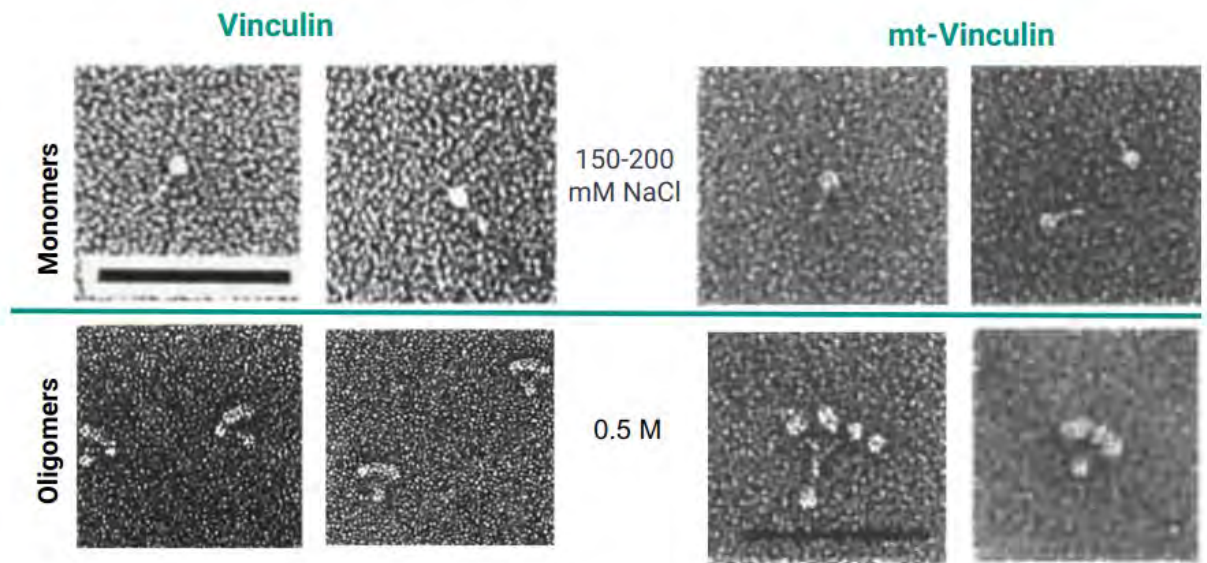


Figure 17. Electron microscopy images for monomeric and oligomeric forms of vinculin and metavinculin. (A) Vinculin and metavinculin head and tail domains can be discerned in its monomeric form as globular structures. (B) After increasing the salt concentration or a mild ionic strength buffer, both vinculin and metavinculin adopt an oligomeric form consisting of head-head or tail-tail interactions that resemble parachutes or bouquets of balloons.

There is evidence that the Vt by itself can oligomerize at higher concentration, a scenario that looks certainly not feasible in vivo conditions as it requires $>300 \mu\text{M}$ concentrations to form homodimers (Shen et al. 2011). On the other hand, there is evidence about the formation of Vt oligomers when in the presence of PIP_2 or F-actin. All subsequent studies focused on oligomerization mediated by Vt, providing with convincing in vitro evidence of vinculin dimerization or trimerization (Chinthalapudi et al. 2014, 2015).

Vt binding to F-actin and actin bundling

The structure of the vinculin tail Vt is detailed in **Figure 18**. Vt in the context of full-length vinculin or as an isolated domain corresponds to a five-helix bundle connected to unstructured N-terminal and C-terminal arms. The N-terminal arm or strap, interacts with H1 and H2 of the helix bundle, as well as with the C-terminal arm. The loop between H1 and H2 interacts with both N-terminal strap and the C-terminal arm, creating

a hairpin structure. This C-terminal hairpin is important to maintain the Vt structure and may insert into the plasma membrane to regulate the mechanical properties of vinculin (Diez et al. 2009).

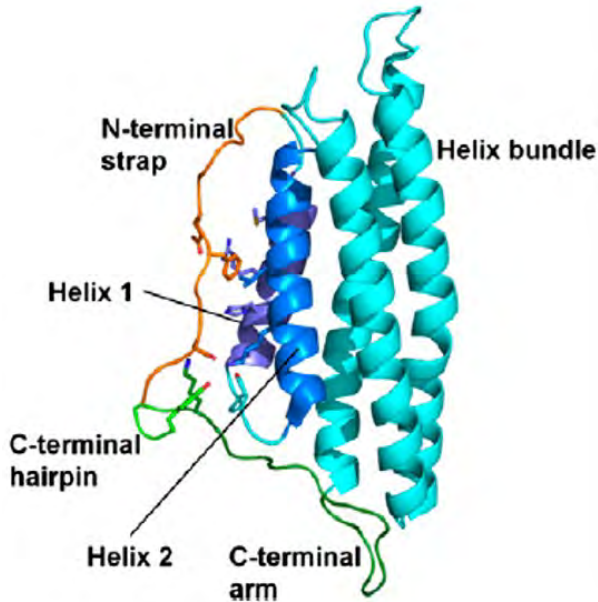


Figure 18. Crystal structure of Vt. The C-terminal hairpin connects the N-terminal strap to the C-terminal arm and is important to maintain the Vt structure (from Diez et al. 2009).

The precise interface implicating Vt binding to F-actin is still unclear. While structural models are available, mutagenesis studies aiming at conforming these models were performed on Vt constructs with deletions in the N-terminal strap, C-terminal arm or helices that affect the stability of the helix bundle, and therefore must be considered with caution. One study by Janssen et al, based on rigid docking on low resolution negative stain EM suggests that Vt interact with two surfaces on adjacent actin protomers (Janssen et al. 2006). In this model, the upper actin protomer corresponding to the pointed end of the actin filament interact with H2 and H3 of Vt, while the lower actin protomer corresponding to the barbed end interacts with H3, H4 and the C-terminal arm (Janssen et al. 2006; **Figure 19A**).

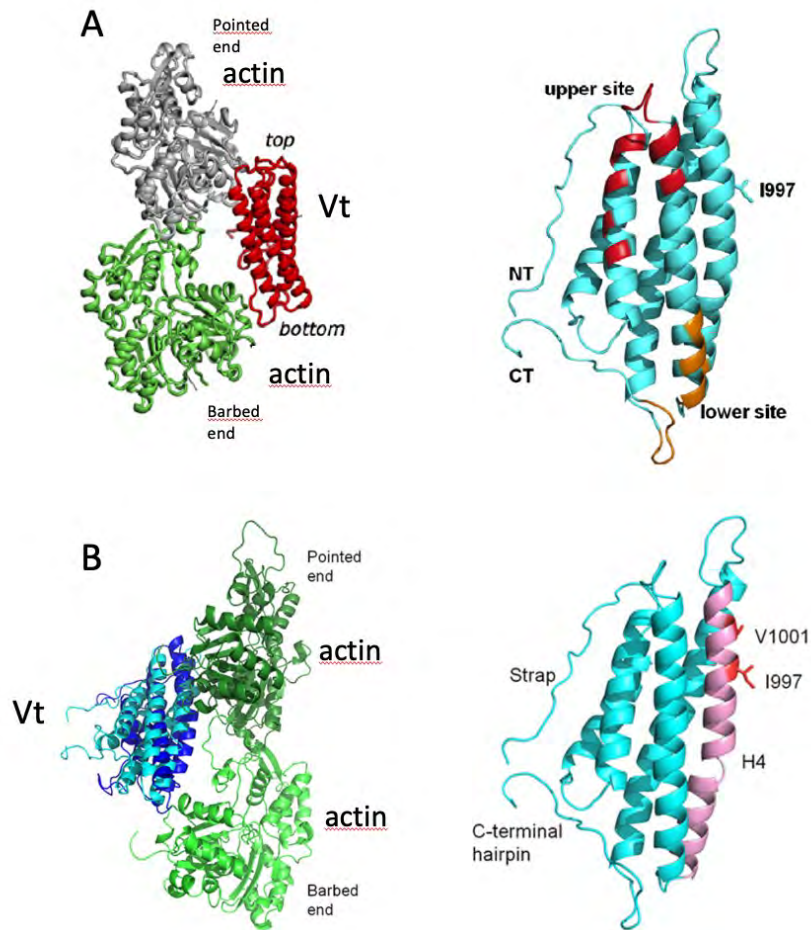


Figure 19. Vt interaction with F-actin. Two contrasting models of Vt interaction with F-actin based on docking of crystal structures in EM envelopes. A) Janssen et al. 2006. B, Thompson et al. 2014.

This study, however, is challenged by the structural heterogeneity proposed for actin filaments, that may present diverse structural modes (Galkin et al. 2010), as well as by the low resolution of the EM analysis. A higher resolution (ca 20 Å) study by Thompson et al. also based on the docking of the Vt crystal structure on reconstruction of negative stain EM data of Vt bound to actin filaments, suggest that Vt interact with one actin protomer with a single interface involving H4 and H5 (**Figure 18B**). This latter study is in phase with the effects of single mutations that interfere with Vt binding to F-actin (Thompson et al. 2014).

Further studies indicate that Vt undergoes significant conformational changes upon binding to F-actin (Kim et al. 2016). Notably, during binding of Vt to F-actin, the H1

helix was observed to dissociate from the Vt helix bundle to promote dimerization (Kim et al. 2016; **Figure 20**). The direct implication of H1 in actin bundling was demonstrated by mutagenizing residues buried in the apo Vt, but exposed in the Vt F-actin bound state. It was found that the single mutation M898A did not affect vinculin binding to F-actin but virtually abrogated actin bundling (Kim et al. 2016). The geometry of vinculin at focal adhesion predicts that actin bundling activity is favored during mechanotransduction, since tensile forces oriented towards the pointed end of actin filaments would prevent the refolding of H1 in the Vt helix bundle (**Figure 20**).

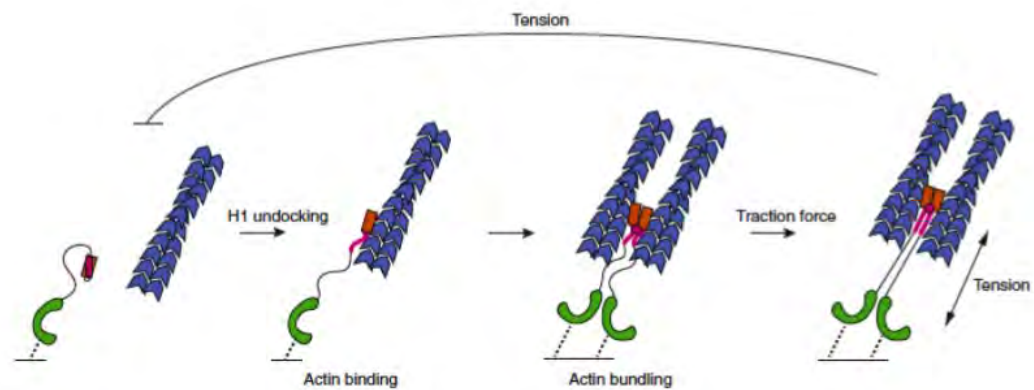


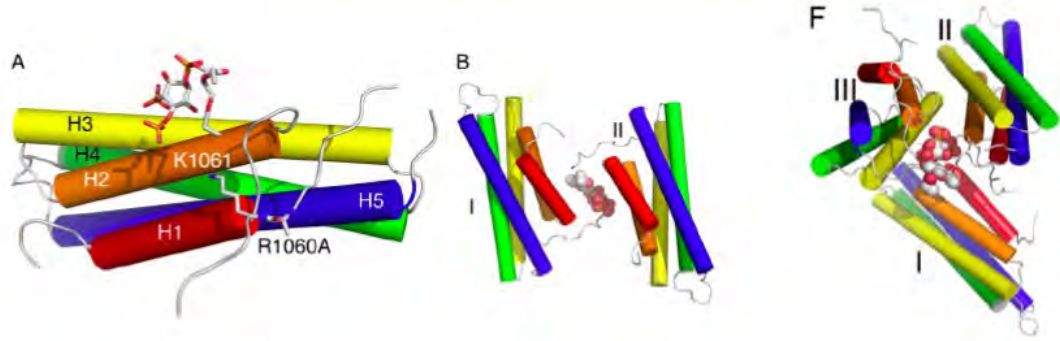
Figure 20. Model for Vt-mediated actin bundling from Thompson et al. 2016. Binding of Vt to F-actin induces dissociation from the Vt bundle of the H1 helix that triggers dimerization.

PIP₂ mediated Vt dimerization and trimerization

PIP₂ binding has been implicated in many functions of vinculin, including its association with the plasma membranes, regulating the interaction with other ligands such as VASP and F-actin, or the life-time of vinculin at focal adhesions (Chinthalapudi et al. 2014). In vitro, PIP₂ was shown the oligomerization of vinculin via Vt to induce the formation of dimers and trimers (Chinthalapudi et al. 2014).

While there is convincing in vitro evidence concerning PIP₂-mediated oligomerization of vinculin by Vt, the role of oligomerization in actin bundling is still unclear during the formation of integrin dependent adhesions. As for F-actin binding, the interpretation of

mutational analysis of Vt to identify the functional effects of PIP₂ binding to Vt in cell adhesion is difficult, since in many studies, this was performed using constructs deleted for the C-terminal hairpin to prevent membrane association or containing multiple mutations that could potentially affect the structure of Vt (Chandrasekar et al. 2005). However, a more recent comprehensive study showing the 3.2 Å resolution crystal structure of PIP₂ bound-vinculin oligomers provided with a basis for the role of PIP₂ binding to vinculin in cell adhesion (Chinthalapudi et al. 2014). This structure shows that PIP₂ binding to vinculin does not implicate the canonical positively charged lysine-rich sequence found in Pleckstrin-Homology (PH) domain of other PIP₂ binding proteins. PIP₂ binds to the N-terminal strap of Vt, promotes its unfurling (Chinthalapudi et al. 2014) and induces Vt dimerization by “sandwiching” the loops between H1 and H2 of two Vt protomers (**Figure 21**). Trimerization occurs when a third Vt molecule interact via its H3 helix with PIP₂ sandwiched between a Vt dimer. Here, single point mutations such as K1061Q, that does not interfere with the Vh-Vt interaction or binding to F-actin, prevent binding to PIP₂ containing vesicles. Introduction of these lipid-binding deficiency mutations in full-length vinculin affects the organization of the actin cytoskeleton and impaired cell migration in cell wound-closure assays (Chinthalapudi et al. 2014). These phenotypes could be attributed to different dynamics of the the PIP₂-binding deficient vinculin variant at focal adhesions measured in Fluorescence After Photobleaching (FRAP) experiments. These experiments showed that a large pool of the PIP₂-binding deficient vinculin variant was immobile, while the remaining pool showed significantly shorter life-time at focal adhesions than parental vinculin. These findings provide with convincing evidence that PIP₂ binding to vinculin regulates its mode of recruitment as well as its stability at focal adhesions. However, how the findings connect with the role of PIP₂ in Vt oligomerization remains unclear.



(Chinthalapudi et al., 2014)

Figure 21. PIP₂-induced dimerization and trimerization of Vt. PIP₂ binds to the N-terminal strap and induces Vt dimerization and trimerization by “sandwiching” the loops between H1 and H2 of two Vt protomers.

6. Interaction of IpaA VBSs with vinculin and talin

During the initial stages of interaction with epithelial cells, *Shigella* is captured by thin cellular extensions termed filopodia (Mattila and Lappalainen, 2008). Key to their probing function, filopodia act as "sticky fingers" that can express active integrins and exert pulling forces through filopodial actin filaments connected to the retrograde flow (Mattila and Lappalainen, 2008). Filopodial adhesions may break or stabilize depending on the interaction established and the counterforce exerted by the substrate, a property used by *Shigella* to invade cells without constitutively adhering to host cell surfaces (Romero et al. 2011). While there may show differences in terms of their composition and sensing ability in different cell types, filopodia share common features, forming three types of adhesion structures: 1) basal adhesions have an extended lifetime and are required for elongation and retraction of filopodia; 2) shaft adhesions are more transient and control the advance of the plasma membrane leaflet (veil) between two filopodia; 3) tip adhesions can trigger signals leading to the disassembly of shaft adhesions (Gomez et al. 2001; Hu et al. 2014). How these filopodial adhesions are differentially regulated is unclear. Interestingly, along with integrins, talin, vinculin, as well as markers of mature focal adhesions have been described in filopodial shaft adhesions indicating that these may be subjected to high tensile forces (Hu et al. 2014). During *Shigella* invasion, the large majority of events involve filopodial capture [4]. While the majority of

filopodial capture occurs at the filopodial tip (ca 75%), a significant fraction of bacteria (25%) interacts with the shaft of filopodia adhering to the substrate and subsequently "surf" on the filopodial surface to reach the cell cortex as described for some invading viruses (Romero et al. 2011; Chang et al. 2016). In this latter case, filopodia remain extended and bound to the substrate, in contrast to adhesion at the tip of swirling filopodia that leads to its retraction (Romero et al. 2011; Bornschlogl et al. 2013). This peculiar mode of bacterial invasion exclusively relies on a limited number of T3SS complexes estimated in the order of 50-100 on the bacterial surface, with only those being active (< 5) located at one bacterial pole (Jaumouille et al. 2008; Collet et al. 2018). That such limited number of T3SS complexes promotes bacterial adhesion during filopodial retraction suggests unusually high adhesion strength for each contact. This issue is of importance since no specific cell receptor has been identified for *Shigella* or other bacterial T3SS tip complex components. Intriguingly, while there is no known *Shigella* adhesin promoting constitutive cell adhesion, the IcsA surface autotransporter involved in intra-cellular actin-based motility was shown to act as a transient adhesin during *Shigella* invasion, with the concerted action of a still uncharacterized *Shigella* T3SS effector (Brockte et al., 2014).

Our laboratory previously showed that the T3SS effector IpaA induced bacterial anchoring by binding to vinculin. IpaA contains three exposed VBSs located within its 145 carboxyterminal residues (IpaA VBS1-3). Structure-function studies of individual IpaA VBSs have provided valuable clues on their function as a super mimic of endogenous vinculin VBSs (Valencia-Gallardo et al. 2015). Accordingly, IpaA VBS1 acts as a high affinity activating VBS interacting with the first helix bundle of D1 (**Figure 22**; Izard et al. 2006). As opposed to activating VBSs, IpaA VBS2 interacts with the second helical bundle of D1 in an additional manner that does not induce major conformational changes but that confers an unmatched high affinity IpaA-vinculin interaction (**Figure 22**; Tran Van Nhieu and Izard 2007).

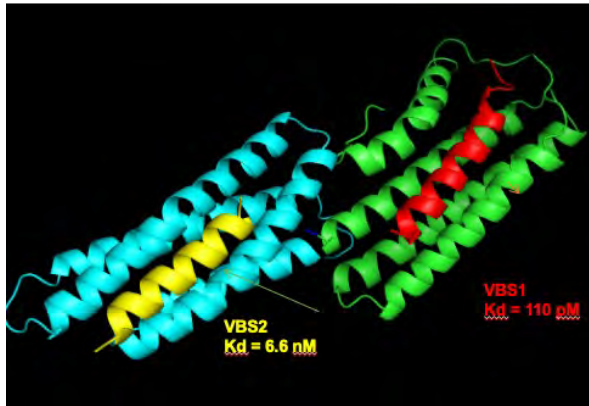


Figure 22. Structure of IpaA VBS1-2 bound to D1. The structure is reconstructed from the crystal structures of IpaA VBS1 bound to D1 (Bois et al. 2006) and IpaA VBS2 bound to D1 (Tran Van Nhieu et al. 2007). Green: D1 first helix bundle. Cyan: D1 second helix bundle. Red: IpaA VBS1. Yellow: IpaA VBS2. The respective K_d for IpaA VBS interaction with D2 is indicated.

In recent studies, our laboratory found that IpaA VBS3 acts as a site that binds to vinculin as well as talin (Valencia-Gallardo et al. 2019). IpaA VBS3 represents the first single helix described with such dual property. The unique property of IpaA VBS3 to also bind talin is linked to the presence of a 2 positively charged residues (IpaA R489 and K498) that orientates the VBS3 helix in the groove of the talin H1-H4 bundle (**Figure 23A**). Interestingly, among the 11 talin VBSs, only talin helix 46 shows similar features (**Figure 23A**). As for vinculin binding to talin, IpaA VBS3 binding to the talin R1 bundle requires the removal of the talin H5 inhibitory helix, but not the unfurling of the talin H1-H4 bundle observed for vinculin binding (**Figure 23B**). The team's results suggest that IpaA VBS3 targets and stabilizes a semi-stretched talin conformer controlling filopodial dynamics and favoring bacterial capture during the early stages of invasion (**Figure 23C**; Valencia-Gallardo et al. 2019).

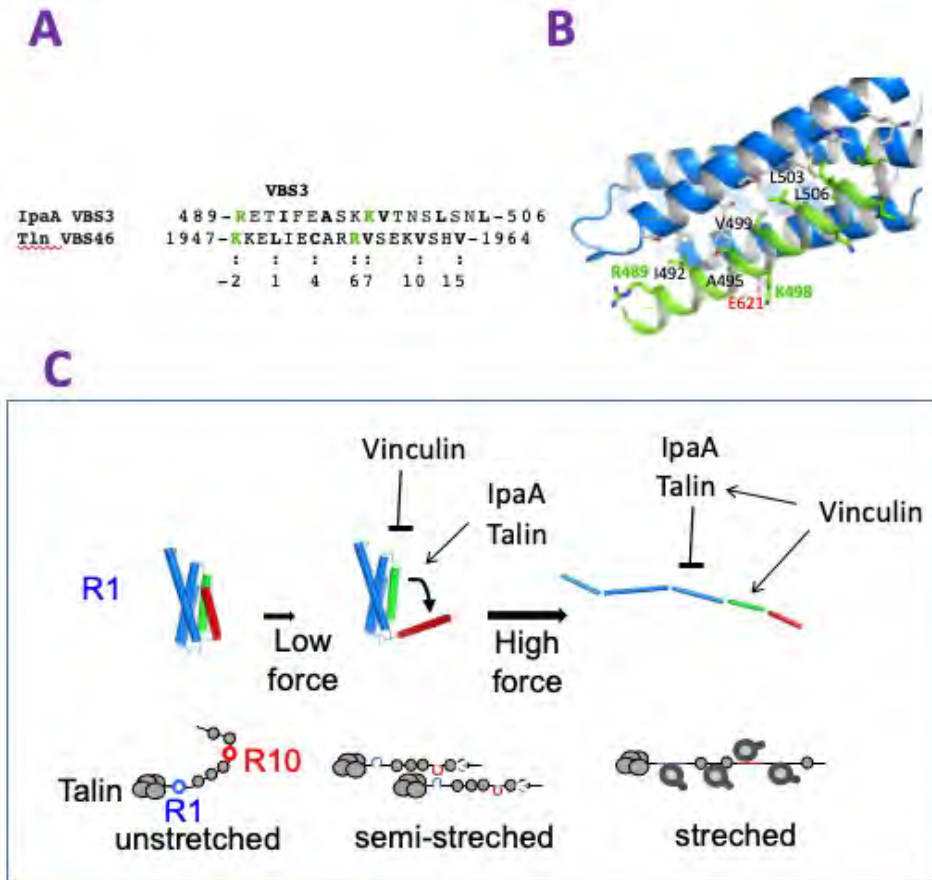


Figure 23. IpaA VBS3 binding to talin stabilizes a semi-folded talin conformer favoring bacterial capture by filopodia. **A**, sequence alignment of IpaA VBS3 and talin VBS46. Green: positively charged residues. Bold: hydrophobic residues. **B**, crystal structure of IpaA VBS3 (green) bound to talin H1-H4 (blue). The IpaA residues contacting talin H1-H4 are indicated in green and black. Red: talin E621 interacting with IpaA K498. **C**, model for stabilization of a semi-stretched talin conformer by IpaA VBS3. At low forces such as those exerted by filopodia, unfolding of talin H1 permits IpaA VBS3 binding to H1-H4. At higher forces, unfolding of H1-H4 leads to IpaA VBS3 dissociation and binding of vinculin. The talin VBS46 in the R10 bundle may play a similar stabilizing role for semi-stretched talin.

THESIS RATIONALE

In addition, another set of the team's findings indicates that when targeting vinculin in concert with IpaA VBS1-2, IpaA VBS3 reveals a novel mode of vinculin activation, that we term "supra-activation", because it involves the unfolding of the vinculin head

and unveiling of binding sites that were not reported before [article 1]. As opposed to endogenous vinculin ligands, the VBSs in IpaA are not buried in helical bundle and are fully exposed. This property likely enables IpaA to act in an opportunistic manner, targeting talin at the tip of filopodia through its unique VBS3, or promoting vinculin supra-activation through the combination of its three VBSs. Remarkably, the evidence suggests that through the unveiling of these sites on the vinculin head domain, IpaA VBS1-3 lead to the formation of vinculin trimers (ref). When expressed in cells IpaA VBS1-3 lead to the formation of large focal adhesions that form independent of mechanotransduction [article 1].

These findings presented in the article 1 of the “Results” section and set the basis for my PhD project, aiming at further characterizing the implications of vinculin supra-activation. To this aim, based on structural models obtained from the mass spectrometry analysis of IpaA-vinculin complexes, I undertook to design mutations in vinculin predicted to interfere with IpaA VBS3 binding to D1D2 and characterize their effects on D1D2 trimerization and focal adhesions’ formation.

II. RESULTS

ARTICLE 1

SUMMARY

The *Shigella* effector IpaA co-opts the focal adhesion protein vinculin to promote bacterial invasion. Here, we show that IpaA triggers an unreported mode of vinculin activation through the cooperative binding of its three vinculin-binding sites (VBSs) leading to vinculin oligomerization via its D1 and D2 head subdomains and highly stable adhesions resisting actin relaxing drugs. Using cross-linking mass spectrometry, we found that while IpaA VBSs1-2 bound to D1, IpaA VBS3 interacted with D2, a subdomain masked to other known VBSs. Structural modeling indicated that as opposed to canonical activation linked to interaction with D1, these combined VBSs interactions triggered major allosteric changes leading to D1D2 oligomerization. A cysteine-clamp preventing these changes and D1D2 oligomerization impaired growth of vinculin microclusters and cell adhesion. We propose that D1D2-mediated vinculin oligomerization occurs during the maturation of adhesion structures to enable the scaffolding of high-order vinculin complexes, and is triggered by *Shigella* IpaA to promote bacterial invasion in the absence of mechanotransduction. Thus, IpaA-VBSs trigger the formation of stable cell adhesions independent of mechanotransduction, in contrast to regular adhesions formed in cells.

My contribution to this work consisted in performing the analysis of time-lapse experiments showing how before and after the presence of actomyosin contraction molecules (the Rho-kinase inhibitor Y27632), cells co-transfected full length Vinculin-mCherry and with GFP-VBS-123 (A483), but not with Vinculin-mCherry and GFP-VBS-12 (A524) (Figure 5.b), or Vinculin-mCherry alone (Figure 5.a), showed an important resistance to adhesion disassembly mediated by (Y27632) and even an increase in vinculin positive adhesions after the treatment (Figures 5.c and Figure 5.d). This resistance to cell adhesion disassembly molecules was corroborated by analyzing the late cell adhesion marker VASP in time-lapse imaging experiments were cells cotransfected with mCherry-VASP and GFP-VBS-123 also remained stable for longer periods of time as compared to controls (Figures 5.e, 5.f, and 5.g).

ARTICLE 1

***Shigella ipaA* mediates actin bundling through diffusible vinculin oligomers with activation imprint**

Running title: IpaA induces vinculin oligomerization

Cesar Valencia-Gallardo^{1-3*}, Daniel-Isui Aguilar-Salvador^{1-3*}, Hamed Khakzad^{1-3§}, Benjamin Cocom-Chan¹⁻³, Charles Bou-Nader^{4,5§}, Christophe Velours⁶, Yosra Zarrouk¹⁻³, Christophe Le Clainche⁷, Christian Malosse⁸, Diogo Borges Lima⁸, Nicole Quenech'Du⁹⁻¹⁰, Bilal Mazhar⁹⁻¹⁰, Sami Essid¹⁻³, Marc Fontecave^{4,5}, Atef Asnacios¹¹, Julia Chamot-Rooke⁸, Lars Malmström¹², Guy Tran Van Nhieu^{1-3¶*}

¹Team “Ca²⁺ signaling and Microbial Infections”, I2BC, 91190 Gif-sur-Yvette, France.

²Institut National de la Santé et de la Recherche Médicale U1282, 91190 Gif-sur-Yvette, France.

³Centre National de la Recherche Scientifique UMR9198, 91190 Gif-sur-Yvette, France.

⁴Laboratoire de Chimie des Processus Biologiques, Collège De France, 75005 Paris, France.

⁵Centre National de la Recherche Scientifique UMR8229, 75005 Paris, France

⁶Fundamental Microbiology and Pathogenicity Laboratory, UMR 5234 CNRS-University of Bordeaux, SFR TransBioMed, 33076 Bordeaux, France

⁷Université Paris-Saclay, CEA, CNRS, Institute for Integrative Biology of the Cell (I2BC), 91198, Gif-sur-Yvette, France

⁸Mass Spectrometry for Biology Utechs, Institut Pasteur, USR 2000, CNRS, 75015 Paris, France

⁹CIRB, Collège de France, 75005 Paris, France.

¹⁰Institut National de la Santé et de la Recherche Médicale U1050, Paris, France

¹¹Laboratoire Matière et Systèmes Complexes, UMR 7057 CNRS & Université Paris Diderot, Sorbonne Paris Cité, Paris, France

¹²Division of Infection Medicine, Department of Clinical Sciences, Lund University, Lund, Sweden.

*. §equal contribution

¶For correspondence: E-mail: guy.tran_van_nhieu@ens-paris-saclay.fr. Present address: I2BC. Inserm U1282. CNRS UMR9198. Gif-sur-Yvette.

Running title: IpaA promotes vinculin oligomerization

Keywords: *Shigella*; *invasion*; *vinculin*; *adhesion*; *actin*; *bundling*

Abstract

Upon activation, vinculin reinforces cytoskeletal anchorage during cell adhesion. Activating ligands classically disrupt intramolecular interactions between the vinculin head and tail domain that binds to actin filaments. Here, we show that *Shigella* IpaA triggers major allosteric changes in the head domain leading to vinculin homo-oligomerization. Through the cooperative binding of its three vinculin-binding sites (VBSs), IpaA induces a striking re-orientation of the D1 and D2 head subdomains associated with vinculin oligomerization. IpaA thus acts as a catalyst producing vinculin clusters that bundle actin at a distance from the activation site and trigger the formation of highly stable adhesions resisting the action of actin relaxing drugs. Unlike canonical activation, vinculin homo-oligomers induced by IpaA appear to keep a persistent imprint of the activated state in addition to their bundling activity, accounting for stable cell adhesion independent of force transduction and relevant to bacterial invasion.

Introduction

Shigella, the causative agent of bacillary dysentery, invades epithelial cells by injecting type III effectors that locally reorganize the actin cytoskeleton (Ogawa, Handa et al. 2008, Valencia-Gallardo, Carayol et al. 2015, Mattock and Blocker 2017). Shigella invasion involves limited contacts with host cells and critically depends on the type III effector IpaA that promotes cytoskeletal anchorage by targeting the (FA) adhesion proteins talin, and vinculin (Romero, Grompone et al. 2011, Valencia-Gallardo, Carayol et al. 2015, Valencia-Gallardo, Bou-Nader et al. 2019). During integrin-mediated cell adhesion, talin acts as a mechanosensor by exposing its vinculin binding sites (VBSs) that recruit and activate vinculin, reinforcing anchorage to the actin cytoskeleton in response to mechanical load (Humphries, Wang et al. 2007, Parsons, Horwitz et al. 2010, Lavelin, Wolfenson et al. 2013, Ciobanasu, Faivre and Le Clainche 2014, Atherton, Stutchbury et al. 2015). Shigella cannot generate the type of mechanical load required for strong cytoskeletal anchorage, therefore, scaffolding of talin, and vinculin at bacterial invasion sites exclusively relies on IpaA. IpaA contains three vinculin binding sites (VBSs) in its carboxyterminal moiety, with diverse functions inferred from the crystal structures of complexes containing the VBS peptide (Izard, Tran Van Nhieu et al. 2006, Tran Van Nhieu and Izard 2007). Vinculin is classically described as a head domain (Vh) connected to a tail domain (Vt) by a flexible linker (Bakolitsa, Cohen et al. 2004). Vh contains three repetitions (D1-D3) of a conserved domain consisting of two antiparallel α -helix-bundles and a fourth α -helix bundle D4 (Bakolitsa, Cohen et al. 2004). A proline-rich unstructured linker bridges D4 and a

five-helix bundle Vt containing the carboxyterminal F-actin binding domain (Bakolitsa, Cohen et al. 2004). Under its inactive folded form, intramolecular interactions between Vh and Vt prevent ligand binding. IpaA VBS1, as for all VBSs described to activate vinculin, interacts with the first helical bundle of the D1 domain, promoting major conformational changes that disrupt the Vh-Vt intramolecular interactions and free the vinculin F-actin binding region (Izard, Evans et al. 2004). IpaA VBS2, in contrast, interacts with the second helical bundle of D1 (Tran Van Nhieu and Izard 2007), hence, its association with IpaA VBS1 results in a very high affinity and stable IpaA VBS1-2:D1 complex, with an estimated KD in the femtoM range (Tran Van Nhieu and Izard 2007). Functional evidence indicates that IpaA VBS3 cooperates with IpaA VBS1-2 to stimulate bacterial invasion (Park, Valencia-Gallardo et al. 2011, Valencia-Gallardo, Bou-Nader et al. 2019). IpaA VBS3, as an isolated peptide, acts as IpaA VBS1 by interacting with the vinculin D1 first helical bundle and promotes vinculin activation (Park, Valencia-Gallardo et al. 2011). IpaA VBS3, however, can also interact with talin to stimulate bacterial capture by filopodia during the early *Shigella* invasion phase of host cells (Valencia-Gallardo, Bou-Nader et al. 2019). The structural data indicate that IpaA VBS3 stabilizes the H1-H4 helix bundle expected to form in a partially stretched talin conformer at the low force range exerted by filopodia (Valencia-Gallardo, Bou-Nader et al. 2019). Intriguingly, IpaA VBS3 shares with talin VBS10 (H46) the ability to bind to vinculin and talin H1H4, suggesting a complex interplay between talin and vinculin during mechanotransduction (Valencia-Gallardo, Bou-Nader et al. 2019). Unlike talin

VBSs, IpaA VBSs are not buried into helix bundles, presumably enabling targeting of vinculin and talin in a serendipitous manner.

In addition to strengthening cytoskeletal anchorage, vinculin has also been implicated in the bundling of actin filaments through dimerization via its tail domain (Vt), triggered by F-actin or phosphatidylinositol(4, 5) bisphosphate (PIP₂) binding (Johnson and Craig 2000, Janssen, Kim et al. 2006, Chinthalapudi, Rangarajan et al. 2014). Consistent with a key role in Vt-mediated actin bundling, mutations in Vt that prevent PIP₂-binding lead to defects in FA dynamics and formation (Chinthalapudi, Rangarajan et al. 2014). Also, mutations that prevent Vt dimerization or alter C-terminal hairpin involved in actin bundling lead to defects in FA formation and cell spreading, although the correlation between F-actin bundling activity and the amplitude of adhesion defects is unclear (Shen, Tolbert et al. 2011). The role of Vt-induced dimerization in scaffolding, however, remains unclear since it cannot simply explain the formation of high-order complexes. The formation of these high-order vinculin complexes could implicate the recruitment of other vinculin-binding partners or vinculin oligomerization mechanisms other than through Vt, possibly through Vh-Vh interactions observed in the so-called “parachute” structures (Molony and Burridge 1985). Of interest, upon activation, vinculin is known to promote the scaffolding of adhesion components during FA growth and maturation, a process that may also implicate its oligomerization (Thompson, Tolbert et al. 2013). More recently, through its interaction with branched actin networks and the bundling activity of talin-vinculin scaffolds, vinculin was also proposed to regulate the dynamics of actin polymerization at

adhesion structures (Boujemaa-Paterski R, Martins B et al. 2020). These studies also pointed to the observation that vinculin-mediated actin bundling occurred at the site of vinculin activation (Boujemaa-Paterski R, Martins B et al. 2020), thereby imposing a frame spatially limiting the actin bundling activity of vinculin during adhesion maturation.

Here, we investigated the role of vinculin at the cell cortical sites of *Shigella* invasion, where all three IpaA VBSs are expected to bind target vinculin (Valencia-Gallardo, Bou-Nader et al. 2019). We show that the combined action of IpaA VBSs, induce major conformational changes in the vinculin head domain, a process that we coined “supra-activation”. These changes lead to the formation of vinculin homo-oligomers promoting the bundling of actin filaments at a distance from the activation site. Our results suggest that vinculin “supra-activation” also occurs during mechanotransduction and is required for maturation of cell adhesions.

Results

IpaA VBS1-3 are required for full recruitment of vinculin at *Shigella* contact sites

IpaA VBS3 targets a partially unfolded talin conformer, during early bacterial capture by filopodia, but is not expected to bind to fully activated talin (HYPERLINK "" \l "_heading=h.3fwokq0"Valencia-Gallardo, Bou-Nader et al. 2019). Instead, at higher force ranges associated with FA maturation at the cell cortex, IpaA VBS3 is expected to target vinculin in combination with IpaA VBS1, 2. To test this, we analyzed adhesion structures induced by *Shigella* during bacterial invasion.

As shown in Fig. 1a and as previously reported (Tran Van Nhieu and Izard 2007), *Shigella* triggers the IpaA-dependent recruitment of vinculin at phagocytic cups (Fig. 1a, arrows, and 1b, WT). Vinculin recruitment was strongly reduced at bacterial contact sites induced by *ipaA/VBS3* expressing only IpaA VBS3 (Figs.1a, b, VBS3 and S1, Park, Valencia-Gallardo et al. 2011). *ipaA/VBS3* triggered the recruitment of small vinculin patches but large phagocytic cups as observed for the wild-type strain were not detected (Figs. 1a, arrows and 1b). We previously identified mutations A495K and K498E in IpaA VBS3 affecting talin- but not vinculin-binding (Valencia-Gallardo, Bou-Nader et al. 2019). We found that these mutations did not affect the recruitment of vinculin small patches triggered by IpaA VBS3, consistent with a direct role of IpaA VBS3 in vinculin binding at bacterial contact sites (Figs. 1a, b, A495K and K498E; Fig. S1). Consistent with previous talin staining results, IpaA also induced the formation of vinculin-containing FAs

distal to bacterial invasion sites (Fig. 1a, arrowheads; Valencia-Gallardo, Bou-Nader et al. 2019). In contrast to bacterial contact sites, these distal FAs formed at similar extents for WT *Shigella* and *ipaA*/VBS3 but were affected in talin-binding deficient VBS3 derivatives (Figs. 1a, arrowheads, 1c and S1), suggesting that vinculin recruitment at distal FAs occurred indirectly through talin.

These results indicate that IpaA VBS3 binding to vinculin is required for the full recruitment of this cytoskeletal linker at phagocytic cups during *Shigella* invasion. In contrast, IpaA VBS3 appears to play a distinct role in bacterial-induced distal FAs, for which its talin-binding property is critical while vinculin binding is dispensable. These findings point at different functions of IpaA VBS3, contrasting with a mere role in vinculin scaffolding during *Shigella* invasion.

IpaA induces vinculin higher order oligomerization

Previous analytical size exclusion chromatography (SEC) studies suggested that IpaA can bind to multiple vinculin molecules through its three VBSs (Park, Valencia-Gallardo et al. 2011). In the proposed model and akin to the model proposed for talin VBSs during mechanotransduction, each IpaA VBS binds to one vinculin molecule through interaction via the first bundle of the vinculin D1 subdomain, leading to its activation (Fig. 2a) (Park, Valencia-Gallardo et al. 2011). This view supports a redundant role for IpaA VBSs inconsistent with a differential role of IpaA VBS3 suggested in the previous set of experiments.

To further characterize the role of IpaA VBS3 on vinculin binding, we studied the effects of the IpaA derivatives containing VBS1-2 (AVBS1-2) or VBS1-3 (AVBS1-3) on binding to derivatives containing different subdomains of

the vinculin head (D1-D4) using SEC-MALS (Size Exclusion Chromatography-Multi-Angle Light Scattering) (Fig. 2b). When analyzing binding of AVBS1-3 to the D1 first subdomain of vinculin corresponding residues 1 -257 and consistent with previous SEC results (Park, Valencia-Gallardo et al. 2011), AVBS1-3:D1 complexes with a molar ration of 1:1, 2:1 and 3:1 were observed likely corresponding to the scaffolding of D1 molecules on the 3 IpaA VBSs based on the predicted molecular mass of the complexes (Fig. 2c). We then analyzed complexes formed upon incubation of AVBS1-3 with a construct containing vinculin residues 1-834 (D1D4), corresponding to full-length human vinculin (HV) devoid of the carboxyterminal F-actin binding domain (Fig. 2b). As shown in Fig. 2d, we found 1:1 D1D4:AVBS1-3 but unexpectedly, complexes containing 2 and 3 D1D4 molecules were also observed (Fig. 2d). Similar complexes containing 2 and 3 molecules of a derivative containing only the vinculin residues 1-484 (Fig. 2f, D1D2) upon incubation with AVBS1-3, indicating that vinculin oligomerization only required the vinculin D1 and D2 sub-domains. By contrast, when AVBS1-2 was incubated with D1D2, 1:1 and 2:0 - 2:1 D1D2:AVBS1-2 complexes were detected, but no D1D2 trimers (Fig. 2e). Because of the small size of AVBS1-2 and AVBS1-3 and the low extinction coefficient difference between complex partners, the detection limits of the SEC-MALS equipment did not allow to unambiguously distinguish between 2:0 and 2:1 D1D2: AVBS1-2 or 3:0 and 3:1 D1D2:AVBS1-3 complexes. However, the discrepancy between the determined and expected molecular masses of the complexes, as well as the slopes observed for the molecular mass argued that the peak corresponded to 2:0 and 2:1, or 3:0 and 3:1

complexes in equilibrium (Figs. 2 d-f). In line with this, quantitative SDS-PAGE analysis of the peak fractions indicated a molar ratio comprised between 2:0-2:1 and 3:0-3:1 for D1D2:AVBS1-2 and D1D2:AVBS1-3, respectively, consistent with a mixture of inter-exchanging complexes present in the corresponding peaks (Fig. S2).

These results suggest that binding of IpaA VBS1-3 to vinculin triggers conformational changes leading to the formation of vinculin trimers.

IpaA promotes major conformational changes in the vinculin D1 D2 domains

To further investigate mechanism responsible for vinculin oligomerization, we performed binding assays with vinculin derivatives immobilized onto a solid phase to restrict conformational changes. By constraining conformation of vinculin derivatives, we expected to prevent the formation of higher order oligomers observed in solution, while enabling binding of IpaA VBSs to initial sites on the vinculin derivative conformers. These assays indicated that AVBS1-3 and AVBS1-2 bound to vinculin with a similar affinity as estimated in Fig. S3a by their EC50 (95% confidence interval) of 6.1 (4.2-9.0) and 3.7 (1.7-8.1) nM, respectively. Strikingly, a large difference was observed in the binding plateau, indicating that vinculin presented more binding sites for AVBS1-3 than for AVBS1-2 (Fig. S3a). D1D2 presented more binding sites than the D1 domain only, suggesting the presence of additional sites on the D2 domain (Fig. S3b). Consistently, BN-PAGE showed the formation of 1:1, as well as a 1:2 D1D2:AVBS1-3 complexes, observed

with increasing AVBS1-3 molar ratio (Fig. S3c). In contrast, single 1:1 complexes were observed for D1:AVBS1-3, D1:AVBS1-2 or D1D2-AVBS1-2 (Figs. S3c-h), indicating that IpaA VBS3 was required to reveal additional sites on the D2 domain. These results suggested that as for immobilization on solid phase, the presence of Coomassie brilliant blue in BN-PAGE interfered with higher order vinculin oligomerization while enabling binding to the vinculin derivative monomer. Together, these results suggested that the formation of vinculin oligomers triggered by AVBS1-3 required the IpaA VBS3 dependent exposure of binding sites on D2. These findings were unexpected, since vinculin activating ligands have been described to bind to a single site on the D1 domain of vinculin.

To map interactions between AVBS1-2 and AVBS1-3 with D1D2, complexes were cross-linked, subjected to proteolysis and analyzed using Liquid Chromatography coupled to Mass Spectrometry (LC-MS) (Star Methods). Intermolecular links were identified from the characterization of cross-linked peptides, and along with identified intramolecular links, used to produce structural models (Suppl. Tables 1-3 and Figs. S4a, b; Star Methods). The D1:AVBS1-2 complex showed links consistent with a "canonical" conformer expected from established structures (Izard, Tran Van Nhieu et al. 2006, Tran Van Nhieu and Izard 2007) (Fig. S4c). Similar links were identified for the D1D2:AVBS1-2 complex, with a majority of links observed with the D1 domain (Fig. S4d). For both complexes, the structure shows interactions between IpaA VBS1 and VBS2 with the D1 first and second bundles, respectively, leading to helical bundle reorganization of D1 associated with vinculin activation (Izard, Evans et al. 2004;

Figs. S4c, d). For the D1D2:AVBS1-3 complex, MS-based structural modeling reveals two major conformers accounting for the majority of links. In a first "closed" conformer, IpaA VBS1 and VBS2 interact with the D1 bundles in a similar manner as for AVBS1-2, where the relative positioning of D1 and D2 is globally conserved compared to apo D1D2 or the D1D2:AVBS1-2 complex (Fig. 3a and Figs. S4d, e). In this "closed" conformer, IpaA VBS3 interacts with an interface formed by the H5 (residues 128-149) and H8 (residues 222-250) helices in the second bundle of D1, and the H13 (residues 373-397) helix in the second bundle of D2 (Figs. 3a, b). The second "open" conformer, however, shows a major re-orientation of D1 and D2 subdomains with their major axis forming an angle value of ca 82° compared to the 25° observed in the native vinculin structure or the first conformer, with IpaA VBS3 docking sidewise through extensive interaction with the H5 (residues 128-149) and H8 (residues 222-250) helices of D1 (Figs. 3c, d, light blue helices). Since this latter conformer was observed for AVBS1-3 but not for AVBS1-2, we posited that it was involved in the formation of higher order D1D2 complexes and homotrimer. To test this, we engineered mutations substituting residue Q68 in the first D1 bundle and A396 in the second D2 bundle for cysteine residues, expected to prevent the formation of the open conformer upon disulfide bridge formation (Fig. 3e) by preventing major conformational shifts of the D1 and D2 domains. In control experiments, disulfide bridge formation was detected in D1D2 and full-length HV containing the Q68C and A396C mutations, expected to act as a clamp preventing the major conformational changes induced by AVBS1-3 (Figs. S5a-c).

As shown in Fig. 3f, two and three upper-shifted D1D2 bands were visualized by clear native PAGE upon incubation with AVBS1-2 and AVBS1-3, respectively. Quantitative 2nd dimension SDS-PAGE analysis of the upper-shifted bands 2 and 3 upon incubation with AVBS1-3 indicated a D1D2:AVBS1-3 molar ratio superior to 3, suggesting these likely corresponded to the 2:0-2:1 and 3:0-3:1 higher order D1D2 complexes observed in the SEC-MALS analysis (Figs. 2, S2 and S5e), although with a different representativity perhaps linked to electrophoretic conditions. The cysteine clamp Q68C A396C (CC) in D1D2 did not prevent the exposure of additional sites on D2 or 1:1 complex formation induced by AVBS1-2 or AVBS1-3. However, CC prevented the formation of higher order complexes for D1D2 as well as for full-length vinculin (Figs. 3f, and S5f, HV-CC). We coined "supra-activation" the mode of vinculin activation induced by AVBS1-3 involving major conformational changes in the vinculin head to distinguish it from the canonical activation associated with the dissociation of vinculin head-tail domains.

IpaA mediates actin bundling and vinculin-talin co-clusters at a distance from activation site

To further characterize the role of vinculin "supra-activation", we performed actin co-sedimentation assays. As expected, the cysteine-clamp had little effects on vinculin canonical activation, since the majority of cysteine-clamped full-length vinculin (HV-CC) associated with actin filaments upon incubation with AVBS1-2 or AVBS1-3 (Figs. S6a, b). We then tested the ability of vinculin oligomers to promote actin bundling by performing low-speed sedimentation assays (Star

Methods). As shown in Fig. 4, vinculin alone did not promote actin bundling (Figs. 4a, b, HV). Upon incubation with AVBS1-3, up to 30% of the total actin pool sedimented, consistent with AVBS1-3-mediated vinculin actin bundling. This actin bundling activity was associated with the low-speed co-sedimentation of vinculin with actin (Fig. 4a). In contrast, no such actin bundling activity was observed for HV-CC even upon incubation with AVBS1-3 (Figs. 4a, b). Together, these results suggest that vinculin oligomers triggered by IpaA-mediated vinculin supra-activation bundle actin filaments.

Next, we asked how vinculin oligomers promoted actin bundling relative to the site of AVBS1-3-mediated supra-activation. Indeed, vinculin homo-oligomers are not expected to remain bound to AVBS1-3 but to diffuse away from activation sites. To test this, we designed a solid-phase assay where GST-AVBS1-3 was coated on 1 μ M-diameter fluorescent beads (Star Methods). Control experiments indicated that GST-AVBS1-3 showed little desorption from beads up to 2 hours following coating (Figs. S6c, d). HV was fluorescently labeled and incubated with GST-AVBS1-3-coated beads in actin polymerization assays (Star Methods). As shown in Fig. 4c, vinculin clusters were clearly detected in association with actin bundles, away from AVBS1-3-coated beads. As expected, such vinculin clusters were observed to a much lesser extent with beads coated AVBS1-2, control GST, and the HV-CC cysteine clamp construct (Figs. 4c, d). Also, consistent with low-speed actin sedimentation results, actin bundling was prominent upon incubation with AVBS1-3-coated beads, relative to AVBS1-2- and GST-coated beads and was not observed for HV-CC (Figs. 4c, d). These results are consistent with the

formation of vinculin homo-oligomers induced by AVBS1-3-mediated supra-activation, bundling actin filaments away from the activation sites.

Talin VBSs promote higher order clustering of IpaA-induced vinculin oligomers

During canonical activation, vinculin simultaneously binds to talin and actin filaments through its N-terminal and C-terminal domain. We then used fluorescent vinculin clustering assays to ask whether in addition to actin bundling, AVBS1-3-mediated vinculin oligomers could interact with talin. In the design of these experiments, we aimed to mimic the multiplicity of VBSs present per talin molecule expected to play an additional scaffolding role in vinculin cluster formation at FAs. For this purpose, we coated 100 nm-beads with the vinculin binding H1-H4 helices from the R1 talin bundle at a calculated density of one H1H4 molecule / 86 nm^2 and co-incubated these beads along with AVBS1-3- beads and vinculin in actin polymerization assays. As shown in Fig. 5a, Tln-beads co-localized with vinculin clusters induced by AVBS1-3-coated beads consistent with binding of vinculin oligomers to talin. As expected, very few clusters were observed for AVBS1-2-coated beads (Fig. 5a). In addition, the integrated density of vinculin clusters showed striking difference between AVBS1-2 and AVBS1-3, with AVBS1-3-induced clusters being on average 9-times brighter than AVBS1-2-induced clusters (Figs. 5a, left panels and 5b). These marked differences suggested additional clustering levels mediated by multivalent talin beads. To confirm this, we quantified the density of Tln-beads per vinculin clusters based on their integrated fluorescence intensity. As shown in Fig. 5c, talin beads showed a

recruitment that was 2.3-fold higher at vinculin clusters induced by AVBS1-3 relative to AVBS1-2, suggestive of higher order clustering.

Together, the results indicate that as opposed to canonical activation, vinculin supra-activation leads to the formation of homo-oligomers mediating actin bundling and binding to talin, a property promoting another levels of clustering by multivalent VBSs. Following diffusion, vinculin oligomers show persistent F-actin binding and bundling activity at a distance from the activation site.

Vinculin supra-activation promotes actin bundling and adhesion expansion

We next tested the effects of vinculin supra-activation on FA formation by introducing the cysteine clamp in full length vinculin fused to mCherry (CC-HV) and analyzed its effects following transfection in MEF vinculin-null cells. As shown in Fig. 6a, vinculin led to the formation of larger and more numerous talin-containing FAs than mock-transfected vinculin null cells, consistent with residual vinculin activation (Figs. 6a, b). In contrast, CC-HV-expressing cells formed significantly fewer and smaller FAs than cells transfected with vinculin (Figs. 6a-e). A more detailed analysis indicated that the average width of adhesions formed by CC-HV was remarkably conserved with an average of 0.96 ± 0.27 (SD) μm (Figs. 6f, h, i). This was in sharp contrast with FAs formed by wild-type vinculin showing a larger dispersion in average width (1.31 ± 0.57 (SD) μm) and reaching up to several microns (Figs. 6g-i). In addition, stress fibers and thick actin bundles connecting FAs were observed for HV, but not CC-HV expressing cells (Figs. 6a,

f, g). These results suggest that vinculin supra-activation impaired in CC-HV, is involved in the growth of adhesion structures and actin bundling during FA maturation.

To clarify the role of IpaA-mediated vinculin supra-activation in FA dynamics, we analyzed the effects of AVBS1-2 and AVBS1-3 expression in C2.7 cells, a vinculin-expressing myoblastic cell line, which form prominent FAs well suited for dynamic TIRF (total internal reflection fluorescence) microscopy analysis. As shown in Figs. 6j-l and S6a, b, cells transfected with GFP-AVBS1-2 formed more numerous and larger peripheral FAs as well as actin-rich ruffles compared to control cells. GFP-AVBS1-3 transfected cells formed even larger and more numerous FAs, but with significantly less actin ruffles than GFP-AVBS1-2 transfected cells (Figs. 6j-l and S7a, b). Strikingly, GFP-AVBS1-3-induced FAs were extremely stable, with a median duration of at least 84 min, while GFP-AVBS1-2-transfected and control cells showed FAs with a comparable median duration of less than 25 min (Figs. S7c, d; Suppl. movie 1). This increased FA stability in GFP-AVBS1-3 transfectants was predominantly due to decreased rates of FA disassembly with a 2-fold decrease in median instant rates relative to control cells (Figs. S7e, f; Suppl. movie 1). These results indicate that AVBS1-3-induced vinculin supra-activation promotes the expansion and increased stability of FAs.

IpaA-induced focal adhesions form independent of mechanotransduction

The stability of IpaA-induced FAs suggests that their formation may be less dependent on mechanotransduction. To test this, we analyzed the effects of the acto-myosin relaxing Rho-kinase inhibitor Y27632. Strikingly, vinculin-labeled

FAs induced by GFP-AVBS1-3 resisted the action of Y27632, with a five- and four-times slower median rate of FA disassembly relative to control cells and GFP-AVBS1-2 transfectants, respectively (Figs. 7a-c Suppl. movie 2). Large FAs were even observed to form in GFP-AVBS1-3 transfectants following addition of the inhibitor (Figs. 7a-c), a process that was not observed for other samples, including cells transfected with GFP fused to the vinculin D1 domain (vD1) reported to delay talin refolding following stretching (del Rio, Perez-Jimenez et al. 2009, Margadant, Chew et al. 2011, Carisey, Tsang et al. 2013) (Figs. 7a-c; Suppl. movie 2). GFP-AVBS1-3 also delayed the Y27632-induced removal of the late adhesion marker VASP (Fig. S8; Suppl. movie 3).

These findings are consistent with our in vitro results showing the catalysis by IpaA of vinculin oligomers with persistent activity. The resistance of VASP to the action of Y27632 in IpaA-induced FAs suggests that vinculin oligomers contribute to the scaffolding of this late FA marker.

Discussion

Shigella invades host cells through a triggering mode implicating discrete number of contacts between the T3SS and host cells (Valencia-Gallardo, Carayol et al. 2015). How IpaA promotes bacterial attachment to the cell surface by reinforcing cytoskeletal tethering to limited bacterial contact sites has been an open question. Here, we show that IpaA induces the supra-activation of vinculin associated with unveiling of binding sites on the D2 subdomain and major conformational changes of the vinculin head. Vinculin supra-activation leads to the formation of vinculin homo-oligomers that bundle actin filaments and bind to talin. Strikingly, IpaA-

induced vinculin oligomers diffuse away from activation sites, a property associated with the expansion of adhesion structures at bacterial contact sites during *Shigella* invasion. Our studies also suggest that vinculin supra-activation is also involved in the maturation of cell adhesions, independent of bacterial invasion: i) a cysteine-clamp inhibiting vinculin supra-activation, but not canonical activation prevents the formation of mature adhesions; ii) IpaA VBS1-3 that mediates vinculin supra-activation accelerates the speed of cell adhesion but at a steady state, the strength of cell adhesion does not differ from that of control cells. These results suggest that IpaA VBS1-3 mediates vinculin supra-activation through the unique organization and joint action of its three VBSs, but that canonical activation also leads to supra-activation when combined with mechanotransduction. Consistent with this, we also found that during *Shigella* invasion, vinculin supra-activation triggered by IpaA VBS1-3 is required for full adhesion formation at bacterial contact sites, canonical activation mediated by a single IpaA VBS is sufficient for FA formation at basal membranes distal from bacteria.

Interestingly, molecular dynamics simulations suggest that stretching of the vinculin during mechanotransduction also results in the exposure of the vinculin head D2 subdomain (Kluger, Braun et al. 2020). It is therefore tempting to speculate that mechanotransduction also leads to vinculin homo-oligomerization that we observed for IpaA through intermolecular interactions between the D1-D2 domains. Whether vinculin stretching alone, or an additional interaction between a VBS and D2 in a manner similar to IpaA VBS3 is required during mechanotransduction is not known. Of interest, IpaA VBS3 shares homology with

the talin VBS corresponding to helix 46 (Valencia-Gallardo, Bou-Nader et al. 2019). This suggests that talin H46 helix could play such a role during vinculin supra-activation.

There are important differences, however, that one can expect from vinculin supra-activation depending on IpaA or mechanotransduction. These differences could account for the extreme stability of FAs in IpaA VBS1-3- compared to IpaA VBS1-2-transfectants during cell treatment with actin relaxing drugs. Indeed, IpaA acts as a catalyst leading to the persistent production of vinculin oligomers independent of the stretching of vinculin by cytoskeletal forces. During vinculin canonical activation, however, oligomers will form as a function of the stretching force and disassemble when the force is released.

Vinculin oligomers are sufficiently biochemically stable to be observed in our SEC-MALS, native gel or fluorescence microscopy analysis, suggesting the stabilization of conformers via inter-protomer interactions. Because of this property, vinculin supra-activation may correspond to a switch defining a threshold during the formation of adhesion structures. Indeed, because of their relative stability, their ability to simultaneously bundle actin filaments, bind to talin and to diffuse away from activation sites, vinculin oligomers following supra-activation are expected to promote the expansion and strengthening of adhesion structures through diffusion and capture by talin VBSs. Consistently, our studies show that supra-activation-deficient cysteine clamped vinculin only support the formation of small adhesion structures ($< 1 \mu\text{m}$ width) with limited actin bundling, while supra-activation proficient vinculin promotes the formation of large FAs and actin

bundles. Our talin-bead scaffolding assays indicate that vinculin cluster formation is further driven by the multiplicity of talin VBSs (Fig. S7, grey arrows). Because of the multiplicity of VBSs on talin molecules, co-clustering between vinculin oligomers and talin is likely to play a role in adhesion expansion (Fig. S7). Vinculin- has been shown to immobilize and bundle actin filaments from Arp2/3 branched networks (Boujemaa-Paterski, Martins et al. 2020). In this case, however, bundling was shown to occur at activation sites and proposed to occur through talin-vinculin scaffolds (Boujemaa-Paterski, Martins et al. 2020). This activity is in contrast with diffusible bundling activity associated with vinculin oligomers that we describe here, which may promote clustering at a distance from activation sites. Clustering of adhesions at different scales is believed to play a major role in adhesive processes through the regulation of functional units (Mege and Ishiyama 2017). At the molecular levels, integrin clustering in adhesions is not fully understood; it may be induced by ligand-binding and integrin homo-oligomerization via integrin trans-membrane domains (Karimi, O'Connor et al. 2018). Nanoclusters consisting of hundreds of integrin molecules were proposed to correspond to elementary units that merge to form nascent adhesions (Changede and Sheetz 2017). Vinculin oligomers following supra-activation could provide an additional basis for the expansion of adhesions through the bundling of actin filaments and scaffolding of cytoskeletal linkers in response to increasing actomyosin pulling force (Fig. S9). As opposed to physiological substrates, single bacteria cannot sustain the range of counterforces associated with the strengthening of adhesion structures during mechanotransduction and integrin-mediated adhesion

to the substrate. Actin bundling and scaffolding triggered by IpaA-induced vinculin oligomers may *Shigella* with means to strengthen its adhesion during bacterial invasion independent of mechanotransduction (Fig. S9a). Importantly, the view of IpaA catalyzing the formation of vinculin activated vinculin oligomers may explain its potency and how a limited number of this injected type III effector can have major impact on the global cell adhesion properties, distal from bacterial invasion sites (Fig. S9b). Understanding how vinculin supra-activation and oligomer formation regulate the composition and properties of adhesions at *Shigella* invasion sites will likely have important implications for cell adhesion and will be the focus of future investigation.

Limitations of the study

We describe a novel mode of vinculin supra-activation induced by the *Shigella* type III effector IpaA. Whether vinculin supra-activation also occurs during cell adhesion during the maturation of adhesion structures will required further investigation.

ACKNOWLEDGEMENTS

The authors thank Gauthier Mercante for technical help, Philippe Maily for help with image analysis and René-Marc Mège for insightful discussions and reading of the manuscript. This work was supported by grants from Inserm, CNRS and Collège de France to the CIRB, as well as grant from the PSL Idex project “Shigaforce”. DIAS and BCC are recipients of a PhD fellowship from a CONACYT scholarship. CV-G and DIAS also received support from the Memolife Labex. HK and LM were supported by Swiss National Science Foundation (grant

no. SNF P2ZHP3_191289) and the Knut and Alice Wallenberg Foundation (grant no. KAW 2016.0023), respectively. This work has also benefited from the facilities and expertise of the Macromolecular Interaction Platforms of I2BC.

AUTHOR CONTRIBUTIONS

CV-G and DIAS conceived and performed most of the experimental works, data analysis and wrote the manuscript. BCC, SE and BM analyzed TIRF experiments. CV and CB-N performed the SEC-MALS analysis. BCC and YZ performed native gel analysis of vinculin complexes. CM and JCR designed and performed the LC-MS analysis. DBL analyzed the cross-linked mass spectrometry data. HK and LM generated structural models. CL provided help for the actin co-sedimentation assays. GTVN designed the project and wrote the manuscript.

FIGURES AND LEGENDS

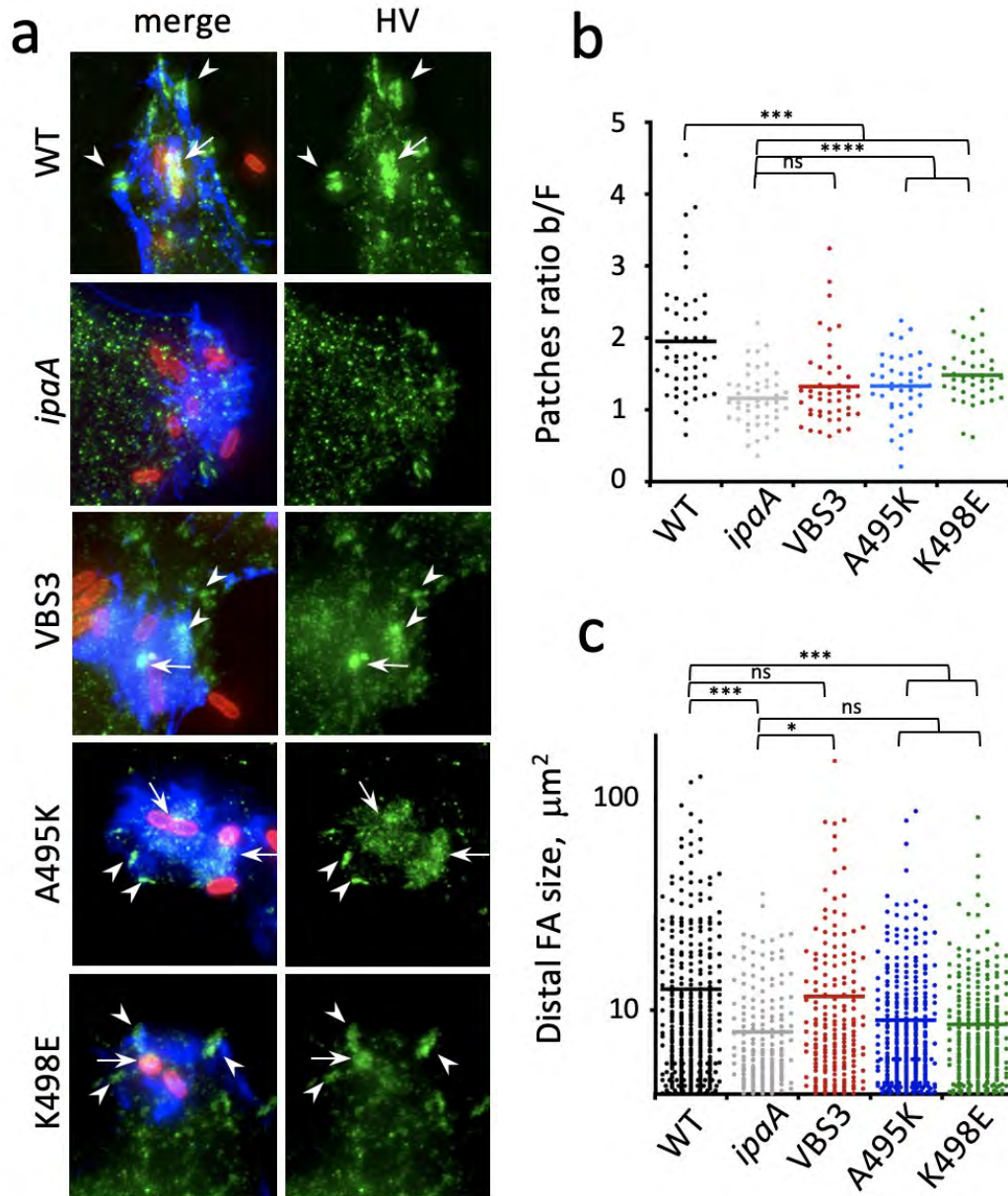


Figure 1. Vinculin recruitment at *Shigella* contact sites and distal adhesion structures during bacterial invasion.

HeLa cells were challenged with bacteria for 30 min at 37°C, fixed and processed for immunofluorescence staining. *ipaA* mutant complemented with: full-length IpaA

(WT); control vector (*ipaA*); IpaA Δ VBS1-2 (VBS3); IpaA Δ VBS1-2 A495K (A495K); IpaA Δ VBS1-2 K498E (K498E). **a**, representative micrographs. Merge: maximum projection of deconvolved confocal planes. vinculin: confocal plane corresponding to the cell basal surface. Red: bacteria; green: vinculin. Blue: F-actin. Vinculin recruitment at bacterial contact sites (arrows) and distal adhesion structures (arrowheads). Scale bar = 5 μ m. **b**, vinculin recruitment at bacterial contact sites was quantified as the ratio of average fluorescence intensity of vinculin labeling associated with the bacterial body over that of actin foci (Star Methods, Fig. S1). The average ratio \pm SEM is indicated. WT: 1.94 ± 0.11 (48 foci, N = 2); *ipaA*: 1.15 ± 0.05 (46 foci, N = 2); VBS3: 1.32 ± 0.08 (45 foci, N = 2); A495K: 1.33 ± 0.07 (42 foci, N = 2); K498E: 1.48 ± 0.06 (38 foci, N = 2). **c**, large vinculin adhesion structures were scored as detailed in the Star Methods section. Average FA size \pm SEM μ m²: WT: 12.54 ± 0.76 (393 FAs, N = 2); *ipaA*: 8.48 ± 0.49 (201 FAs, N = 2); VBS3: 11.59 ± 1.08 (207 FAs, N = 2); A495K: 8.96 ± 0.45 (376 FAs, N = 2); K498E: 8.56 ± 0.44 (291 FAs, N = 2). Mann and Whitney test: *: $p < 0.05$; ***: $p < 0.005$; ****: $p < 0.001$.

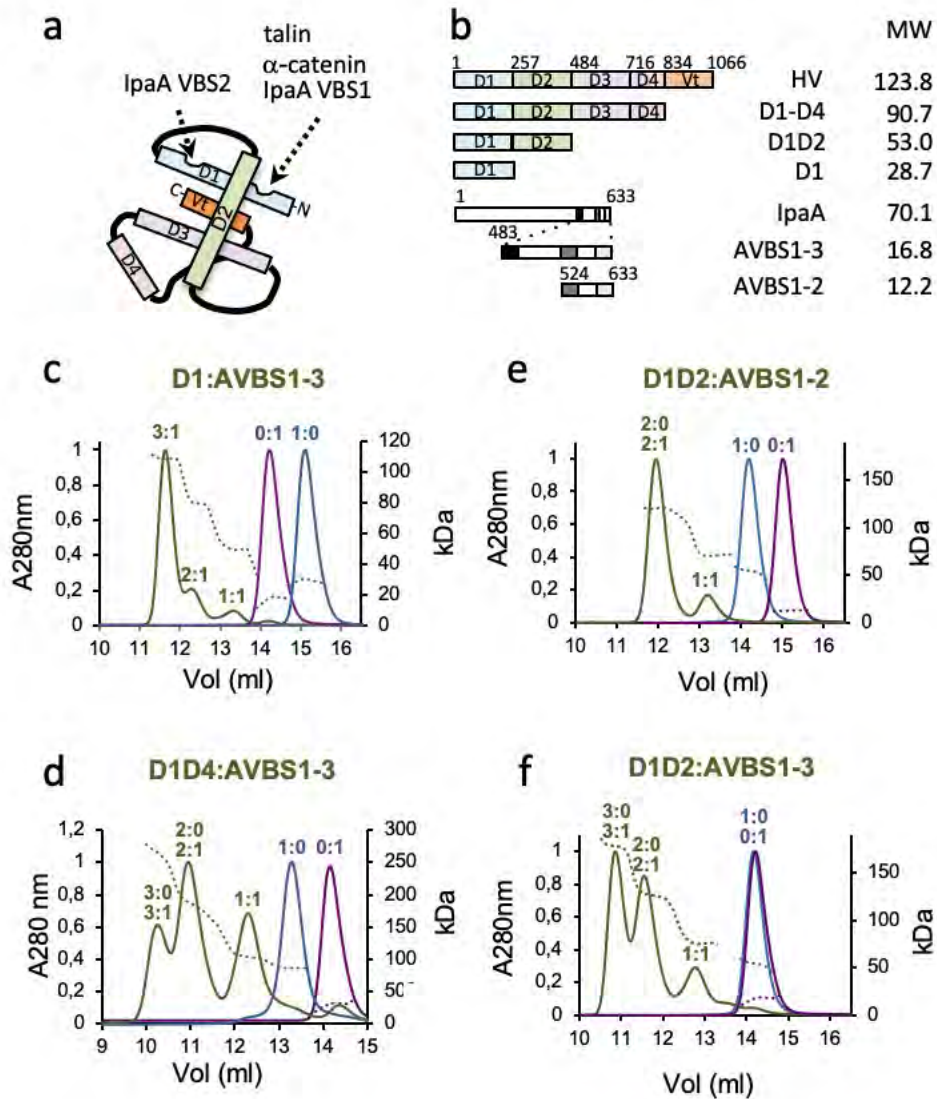


Figure 2. IpaA promotes vinculin homo-oligomerization

a, Scheme of folded vinculin (HV). The binding sites and corresponding ligands are indicated. **b**, Scheme of vinculin and IpaA constructs. vinculin domains and IpaA VBSs are depicted as boxes. The numbers indicate the start residue of each domain. MW: molecular weight in kDa. **c-f**, green: SEC elution profiles of complexes formed between AVBS1-3 (**c**, **d**, **f**) or AVBS1-2 (**e**) and the indicated vinculin derivatives; blue: the indicated vinculin derivative alone; purple: AVBS1-2 (**e**) or AVBS1-3

alone (c, d, f). The indicated complex stoichiometry was inferred from the molecular weight estimated by MALS. Dotted line: molecular weight.

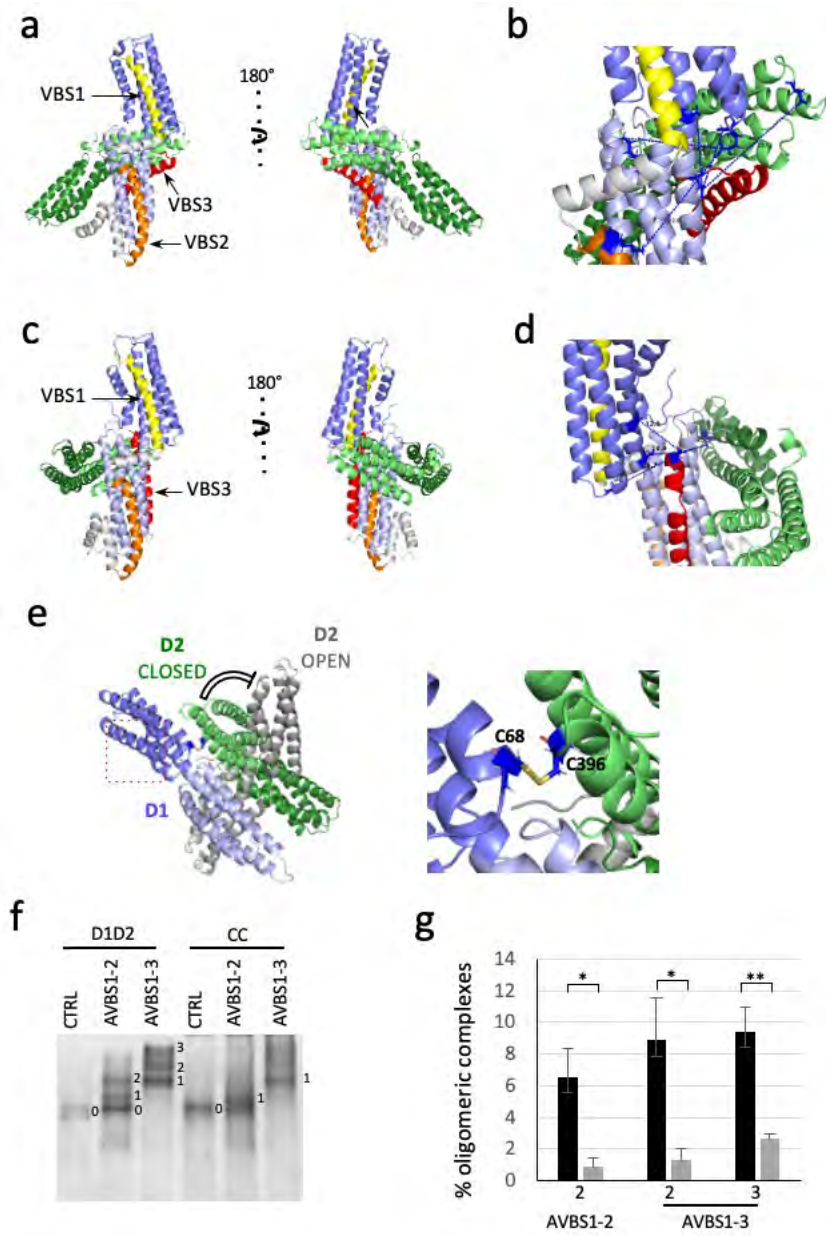


Figure 3. IpaA promotes major conformational changes in the vinculin D1 D2 domains

a-e) Structural models of D1D2-IpaA VBS1-3. Pale blue: D1 first bundle. Dark blue: D1 second bundle. Pale green: D2 first bundle. Dark green: D2 second bundle.

Yellow: IpaA VBS1. Orange: IpaA VBS2. Red: IpaA VBS3. **a, b**, “closed” conformer; **c, d**, “open” conformer. **h, j**, higher magnification of the IpaA VBS3-D1D2 interaction in (**b**) and (**d**) showing the identified cross-linked distance between residues in Å. IpaA VBS1-3 were docked on the surface of Vinculin D1D2 and verified using MS cross-link constraints. TX-MS protocol (Hauri, Khakzad et al. 2019) in combination with MS constraints was used to unify and adjust the final model, which justifies over 100 cross-links. **e**, Structural model of cysteine-clamped vinculin. Green: D2 in the closed conformer. Grey: D2 domain in the open conformer. Black: C68-C396 cysteine clamp preventing the switch from closed to open conformers. Right panel: enlarged view of the cystein clamp shown in the inset in the left panel. **f**, native gel analysis of vinculin D1D2 and IpaA derivatives. D1D2 or the double cysteine mutant D1D2 (CC) were incubated with the indicated IpaA derivatives and analyzed by native PAGE followed by Coomassie staining. The numbers next to the band indicate upper-shifted bands of D1D2:AVBS1-2 or D1D2:AVBS1-3 complexes. Note the absence of higher order complexes for the CC mutant. **g**, the band integrated intensity corresponding to the indicated shifted bands were quantified using ImageJ. Values are expressed as the percent of total protein amounts in the corresponding sample. Solid bars: D1D2. Grey bars: CC.

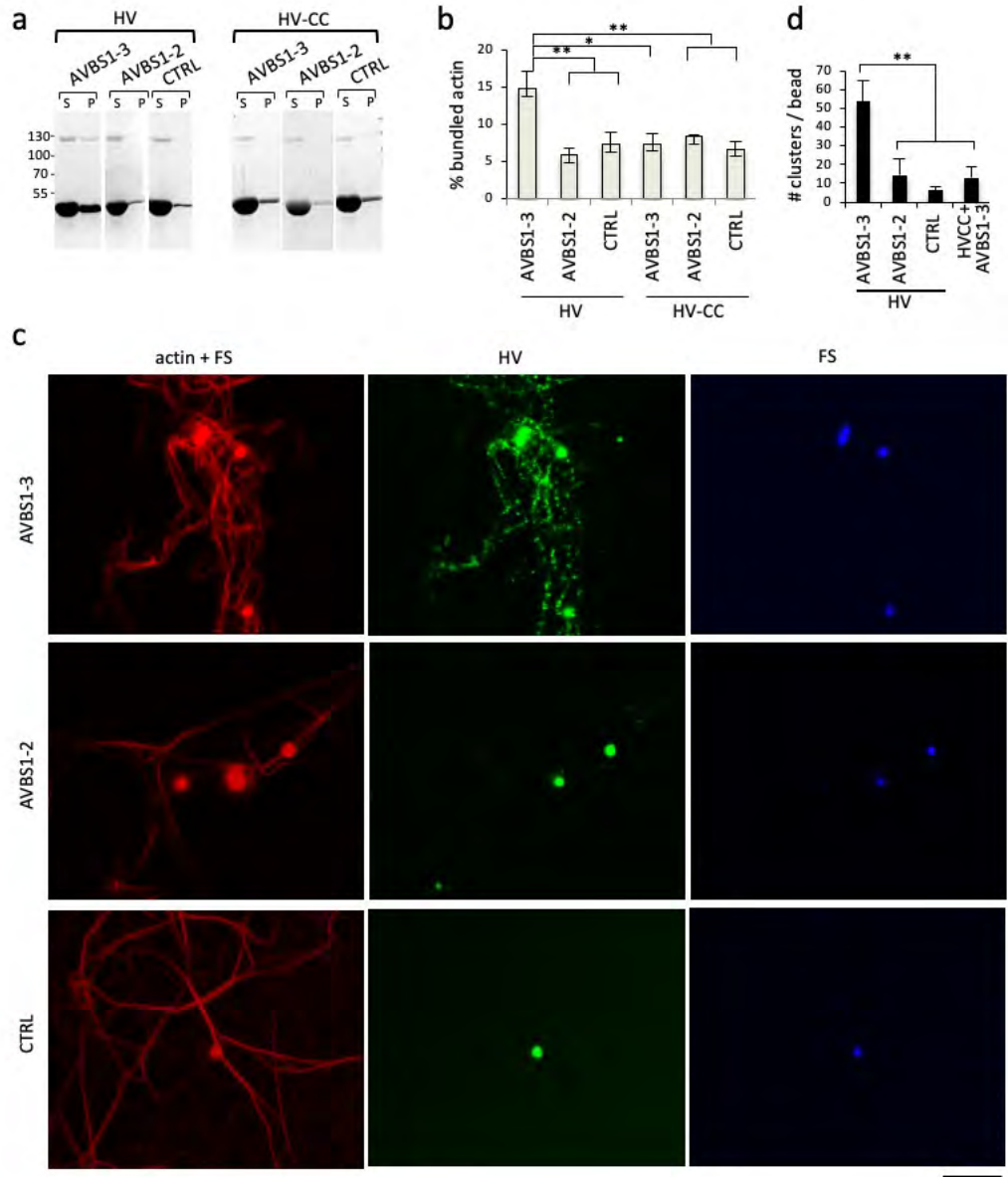


Figure 4. IpaA-induced vinculin oligomers promote actin bundling at a distance from activation sites.

a, b, actin sedimentation assays. HV: full-length human vinculin; HV-CC: cysteine-clamp derivative. Actin was allowed to polymerize at a final concentration of 20-30 μ M in the presence of the indicated proteins. Samples were centrifuged at 14,000 g for 10 min to pellet actin bundles, respectively. **a**, representative SDS-PAGE analysis using a 10% polyacrylamide gel followed by Coomassie staining. S:

supernatant; P: pellet. **b**, the band integrated intensity corresponding to actin was quantified using ImageJ. Values are expressed as the percent of actin in the pellet fraction relative to the total actin amounts in the supernatant and pellet fractions normalized to control. **b**, percent of bundled actin; HV (n = 9, N = 4); HV-CC (n = 6, N = 3). **c**, Representative micrographs of fluorescently labeled actin polymerized in the presence of Bodipy-vinculin and coated beads. Beads were coated with AVBS1-3, AVBS1-2 or GST (CTRL). red: actin; green: Bodipy-vinculin; blue: beads. Numerous vinculin clusters are observed at a distance from AVBS1-3 coated-beads. **d**, the numbers of vinculin clusters per bead \pm SEM are shown for the indicated samples (N= 3, HV+AVBS1-3: 1292; N= 2, HV+AVBS1-2: 120; N=2, HV+GST (CTRL): 56; N=2, HVCC+AVBS1-3: 80). Scale bar = 5 μ m. Mann and Whitney. *: p < 0.05; **: p < 0.01.

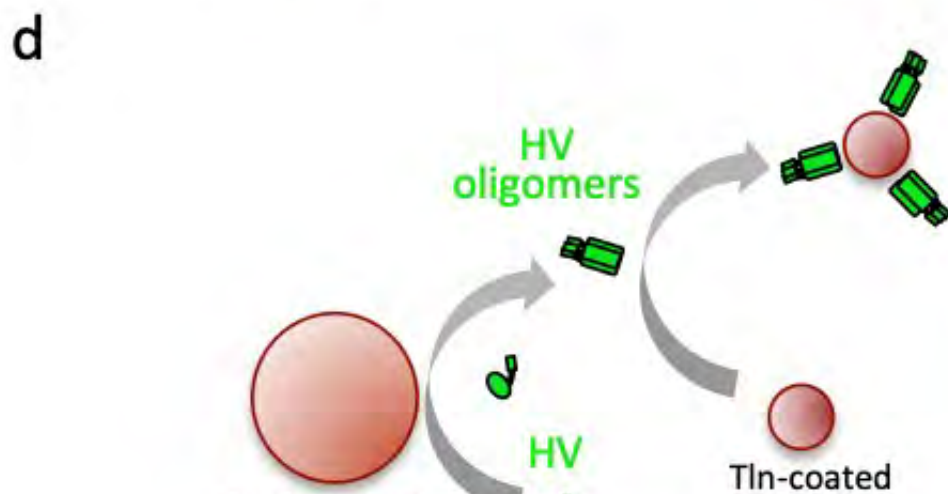
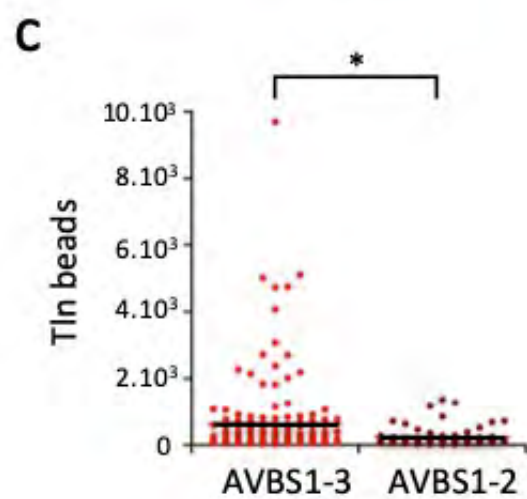
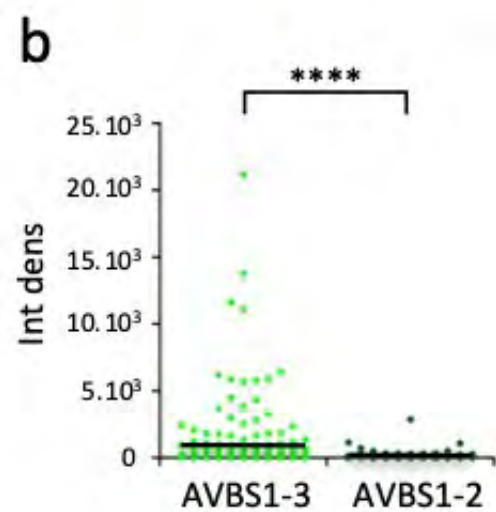
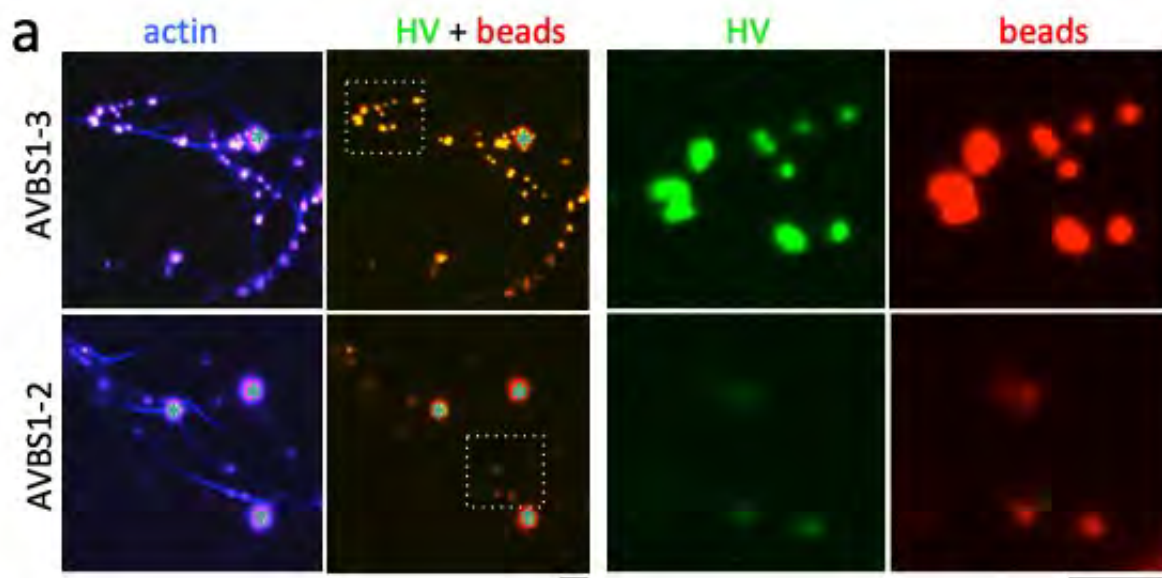


Figure 5. Vinculin oligomers are clustered by talin VBSs.

Fluorescent actin was allowed to polymerize in the presence of vinculin, 1 μm -diameter red fluorescent beads coated with the indicated sample and 100 nm-diameter red fluorescent beads coated with talin H1-H4. **a**, representative micrographs. Blue: actin. Green: vinculin; red: 1 μm - and 100 nm-red fluorescent coated beads. The cyan stars indicate GST-AVBS1-2 / GST-AVBS1-3 –coated 1 μm beads. Right panels are higher magnification of the insets shown in the left panels. Scale bar = 1 μm . **b**, normalized integrated density of vinculin clusters. HV+AVBS1-3: 204 clusters, N =2; HV+AVBS1-2: 142 clusters, N =2. **c**, normalized integrated density talin H1-H4 beads. HV+AVBS1-3, 148 clusters, N =2; HV+AVBS1-2: 64 clusters, N =2. Mann and Whitney. *: p = 0.023; ****. p = 0.00018. **d**, model for vinculin oligomers clustering by talin VBSs. Bead-immobilized AVBS1-3 catalyzes the formation of vinculin oligomers, that diffuse away from activation site. Vinculin oligomers binding to Tln-coated beads results in higher order cluster formation.

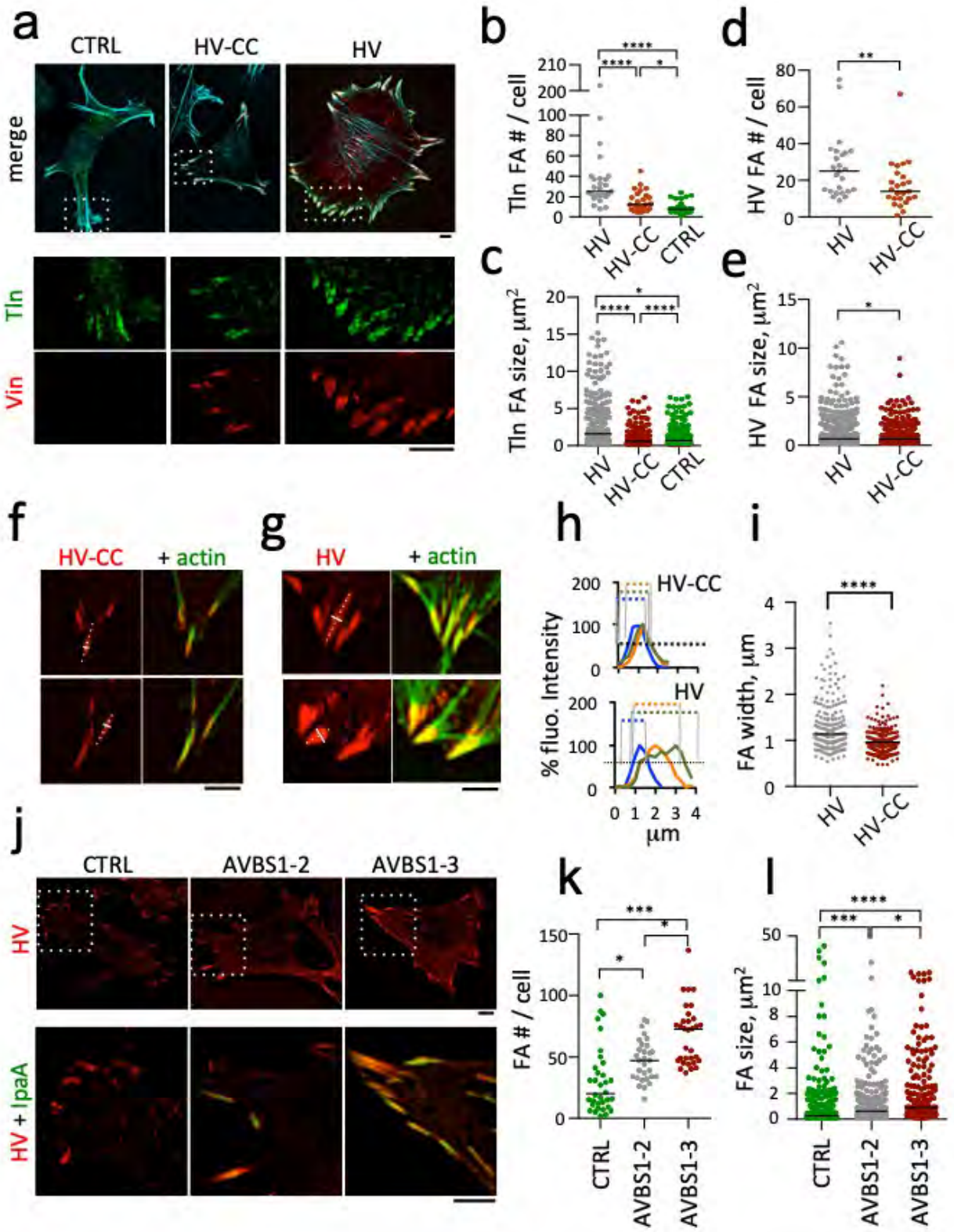


Figure 6 – vinculin supra-activation promotes the merging of adhesions clusters.

Cells were transfected, fixed and processed for fluorescence microscopy analysis of FAs. **a, f, g, j**, representative fluorescence micrographs; red: Vinculin-mCherry; green: GFP-talin (**a**) or F-actin (**f, g**); cyan: F-actin (**a**). Scale bar = 5 μm . **a-i**, MEF vinculin null cells; transfection with GFP-talin (CTRL); talin co-transfection with full-length HV-mCherry (HV) or HV Q68C A396C-mCherry (CC-HV). **j-l**, C2.7 cells; transfection with vinculin (CTRL); vinculin co-transfection with GFP-AVBS1-2 or GFP-AVBS1-3. **b-e, k, l**: the FA number per cell and size were determined using a semi-automatic detection program (Star Methods). Bar: median size. FAs analyzed for: **b, c**, GFP-talin; **d, e, h, i, k, l**, HV or CC-HV. **b-e**, CTRL: n=28, N=3; HV: n = 25, N = 3; CC-HV: n = 25, N = 3. **h**, representative plot profiles from linescans (solid white lines) orthogonal to the main FA axis (dashed white lines) in (**f**) and (**g**). **i**, FA width determined as the full width half-maximum by linear interpolation from plot profiles in (**h**); HV: 181 FAs, 6 cells, N = 2. CC-HV: 101 FAs, 14 cells, N = 3. Mann-Whitney test with Bonferroni multiple comparison correction. *: $p < 0.05$; **: $p < 0.01$; ***: $p < 0.005$; ****: $p < 0.001$. **j-l**, n > 30 cells, N = 3. Dunn's multiple comparisons test. *: $p < 0.05$; ***: $p < 0.005$.

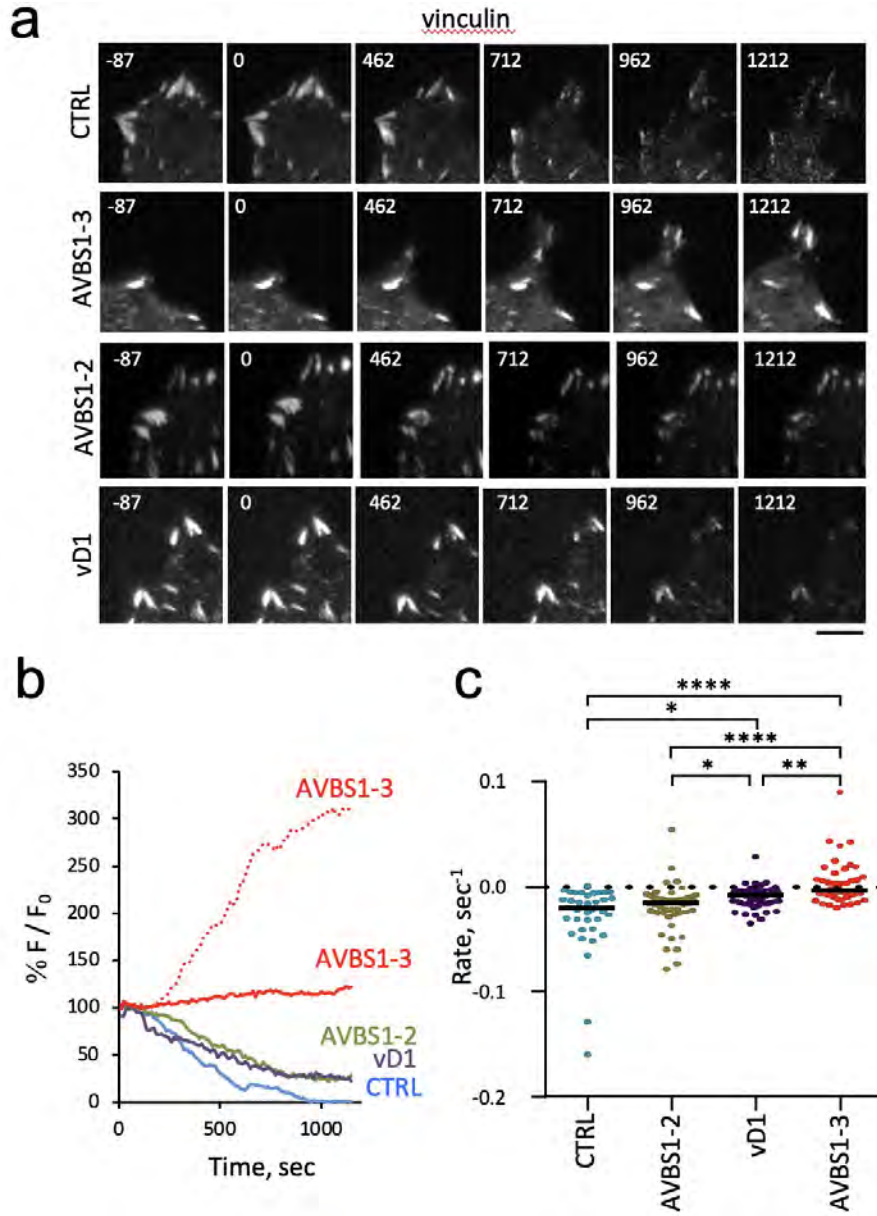
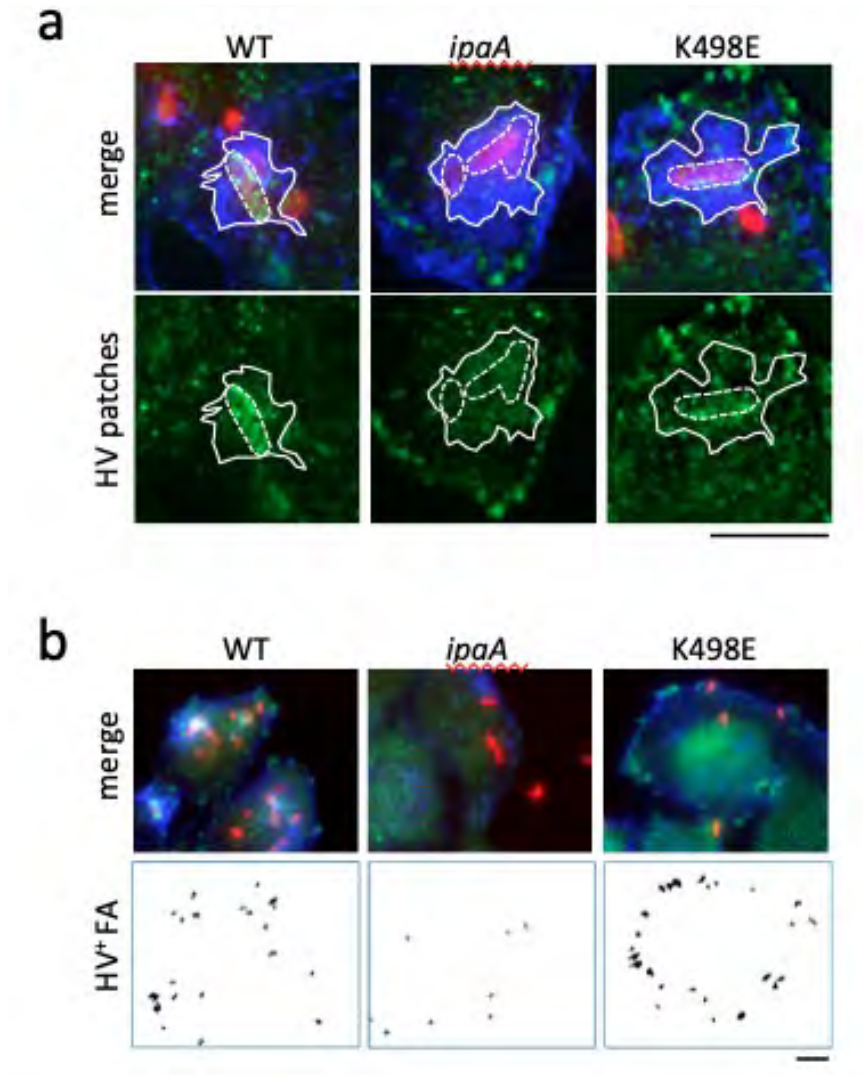


Figure 7. IpaA-mediated vinculin supra-activation stimulates cell adhesion independent of mechanotransduction. TIRF microscopy of C2.7 cells transfected with mCherry-vinculin alone (CTRL) or co-transfected with GFP-AVBS1-2 (AVBS1-2), GFP-vD1 (vD1), or GFP-AVBS1-3 (AVBS1-3). Adhesion kinetic parameters were determined from time-lapse acquisitions following cell treatment with 100 μ M Y-

27632. **a**, representative time series acquisitions. Numbers indicated the elapsed time in seconds, with the inhibitor added at $t = 0$. Scale bar = 5 μm . **b**, % F/F_0 : average fluorescence intensity of adhesions expressed as a percent of initial fluorescence. Solid lines: representative traces corresponding to single adhesions for the indicated samples in the corresponding color. The dashed redline illustrates FA assembly in GFP-AVBS1-3 transfected cell, seldom observed with the other samples. **c**, initial rates of adhesion assembly / disassembly inferred from linear fits. Number of adhesions analyzed: **c**, $N = 5$. CTRL: 84; vD1: 75; AVBS1-2: 140; AVBS1-3: 97. Dunn's multiple comparisons test. *: $p < 0.05$; ****: $p < 0.001$.

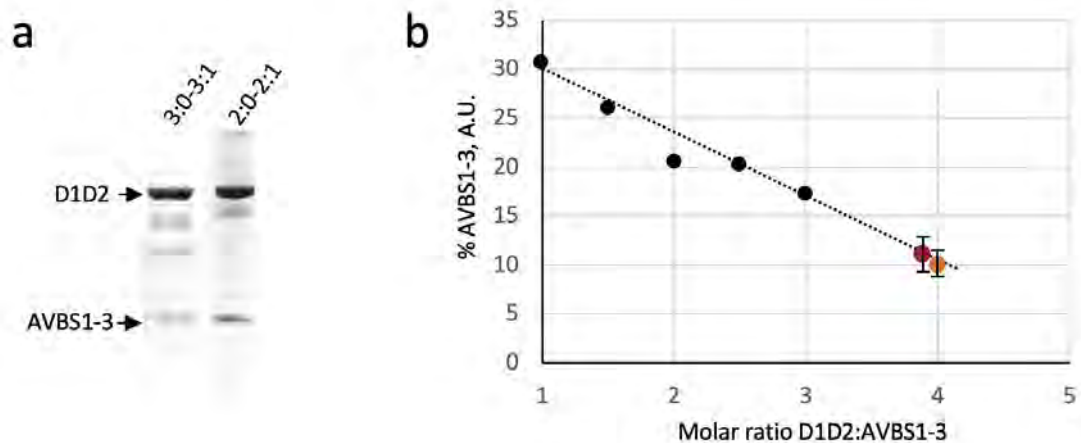
SUPPLEMENTARY INFORMATION



Supplementary Fig. 1. Quantification of IpaA-dependent vinculin recruitment during *Shigella* invasion.

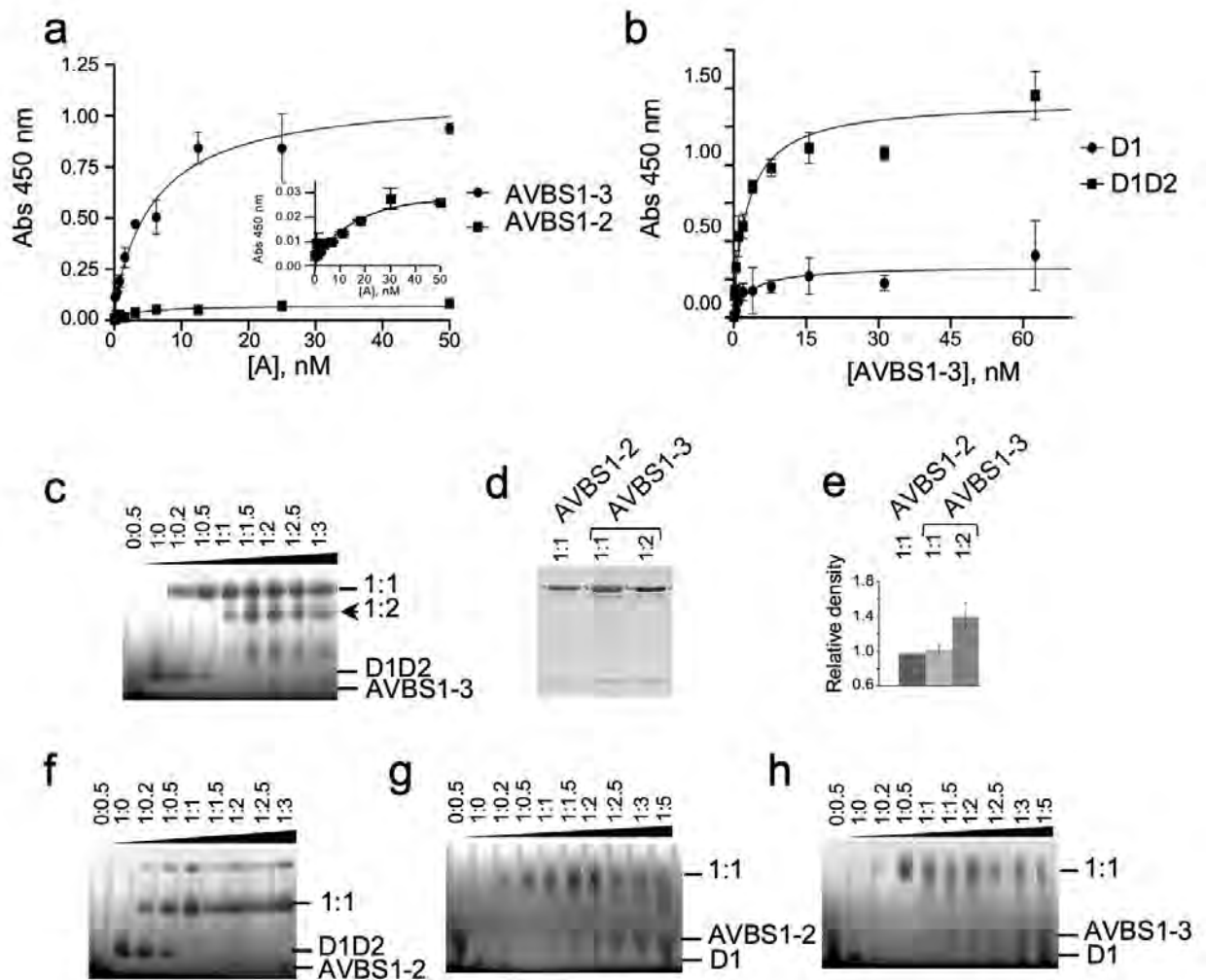
HeLa cells were challenged with bacteria for 30 min at 37°C, fixed and processed for immunofluorescence staining. Merge: maximal projections of confocal planes. Red, bacterial LPS; green, vinculin; blue, F-actin. vinculin: vinculin labeling. **a, b,**

representative micrographs. *ipaA* mutant complemented with: full-length IpaA (WT); control vector (*ipaA*); IpaA Δ VBS1-2 K498E (K498E). Scale bar = 5 μ m. **a**, ROI delineated by: solid lines, actin foci (F); dotted lines, bacterial bodies (b). Vinculin recruitment at the bacterial body was quantified as the ratio of the average fluorescence intensity of vinculin labeling of (b) over that of (F). **b**, HV+ FA: large vinculin adhesions were quantified from images corresponding to the confocal plane of the cell basal surface as described in the Star Methods section.



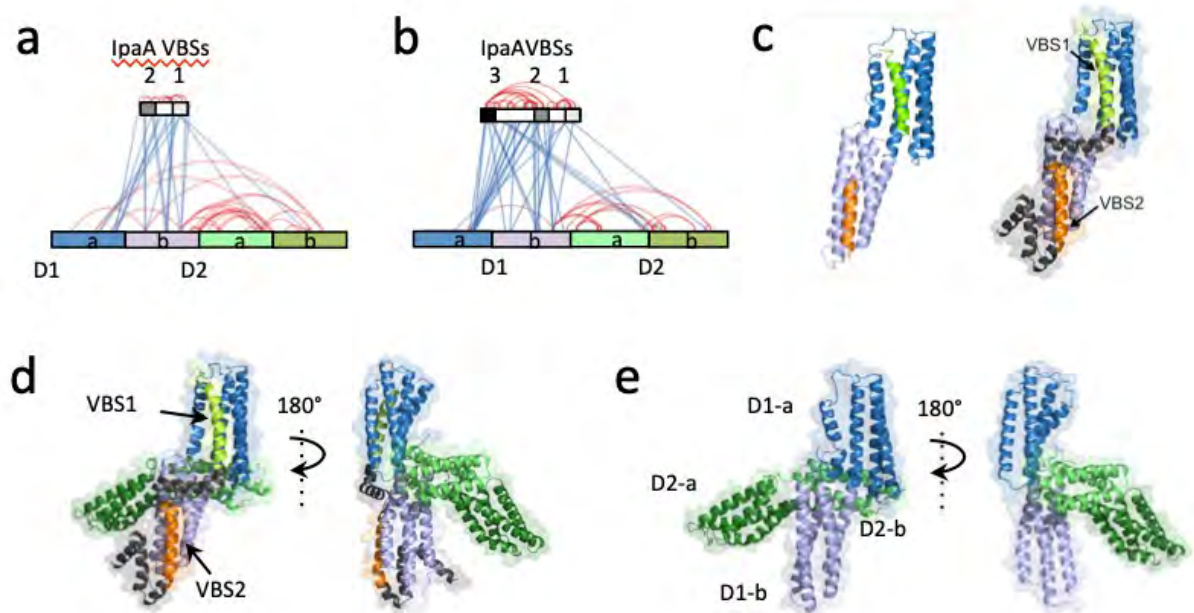
Supplementary Fig. 2. Determination of the D1D2:AVBS1-3 molar ratio in peaks obtained in SEC-MALS analysis. **a**, Representative SDS-PAGE analysis using a 10% polyacrylamide gel followed by Coomassie blue staining of the fractions corresponding to the 3:0-3:1 and 2:0-2:1 peaks shown in the SEC-MALS in Fig. 2f. The arrows point at D1D2 and AVBS1-3. **b**, the band integrated intensities were quantified using ImageJ. The values obtained for AVBS1-3 were multiplied by a factor of 3.15 to account for the difference in mass relative to D1D2. The percent of AVBS1-3 relative to the D1D2 and AVBS1-3 total amounts (% AVBS1-3) was

plotted as a function of the D1D2:AVBS1-3 molar ratio. The values correspond to the average determination \pm SEM (N = 3). Black circles: reference samples using defined D1D2:AVBS1-3 molar ratio. Red circles: molar ratio determined for the indicated peak fraction. Red: 3:0-3:1 peak. Orange: 2:0-2:1 peak. The determined D1D2:AVBS1-3 molar ratio of 3.8 and 3.9 for the 3:0-3:1 and 2:0-2:1 peaks, respectively, are consistent with a mixture of hetero- and homo-oligomers (2:0-2:1 and 3:0-3:1) in each peak.



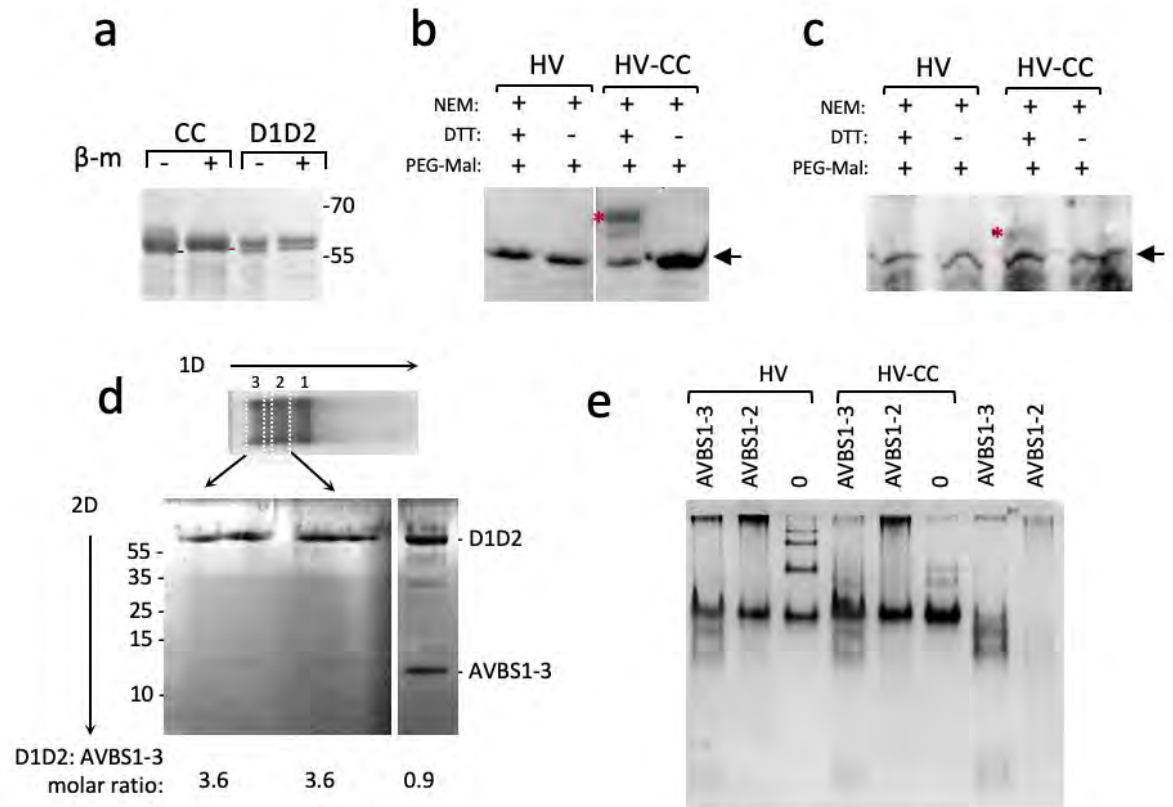
Supplementary Fig. 3. IpaA VBS3 reveals multiple binding sites on vinculin.

a, b, Solid phase binding assays. **a**, coating: vinculin; ligands: AVBS1-3 (solid circles); AVBS1-2 (solid squares). The inset shows binding of AVBS1-2 with an extended Y-axis. **b**, coating: D1 (solid circles) or vinculin D1D2 (solid squares); ligand: AVBS1-3. **c, f-h**, BN-PAGE in 6-18% polyacrylamide gradient gels and Coomassie staining analysis of D1D2:AVBS1-3 (**c**), D1D2:AVBS1-2 (**f**), D1:AVBS1-2 (**g**) or D1:AVBS1-3 (**h**) complexes. The molar ratio is indicated above each lane. Arrowheads indicate protein alone, or complex migration at the indicated molar ratio. **d**, bands were recovered from BN-PAGE and analyzed in a second dimension SDS-PAGE in a 15% poly-acrylamide gel and Coomassie staining. Bands were analyzed by densitometry. **e**, ratio of density values for the D1D2:AVBS1-2 complex (empty bar) and D1D2:AVBS1-3 complexes corresponding to the upper (light grey bar) or lower (dark grey bar) shifts.



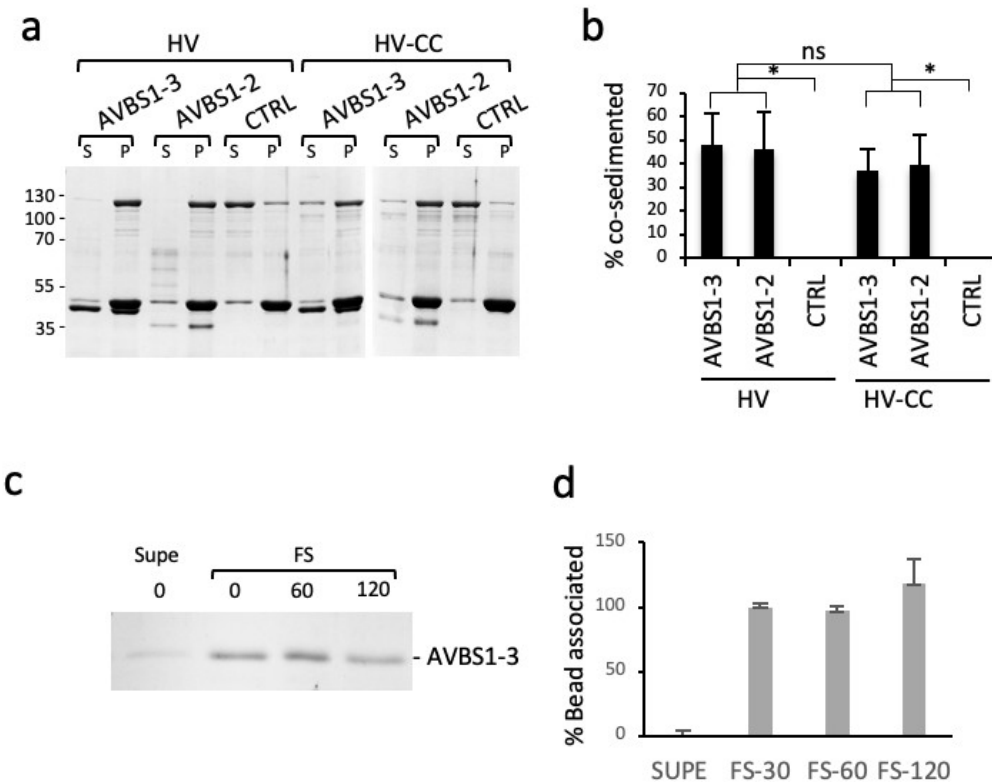
Supplementary Figure 4. Structural models of vD1:AVBS1-2.

a, b, EDC cross-link map from mass spectrometry analysis (LC-MS/MS) of vinculin D1D2-IpaA VBS1-2 (**a**) and D1D2-IpaA VBS1-3 (**b**) following extraction of 1:1 complexes from BN-PAGE. Blue lines: inter-molecular links. Red lines: intra-molecular links. Note the links between IpaA VBS3 and the D2 second bundle. Cross-linked residues are detailed in Suppl. Table 1. **c**, left, structure predicted from the resolved vD1: IpaA VBS1: and vD1:IpaA VBS2 crystal structures (Izard, Tran Van Nhieu et al. 2006, Tran Van Nhieu and Izard 2007); right, structural model of vD1:IpaA VBS1-2. The model was established using RosettaCM protocol and accounts for 19 inter and intra-molecular cross-links out of 24 identified (Suppl. Table 1). Structural models of: **d**, D1D2:AVBS1-2. **e**, D1D2. AVBS1-2 were docked on the surface of Vinculin D1D2 using MS cross-link constraints. TX-MS protocol in combination with MS constraints was used to unify and adjust the final model, which justifies over 100 cross-links.



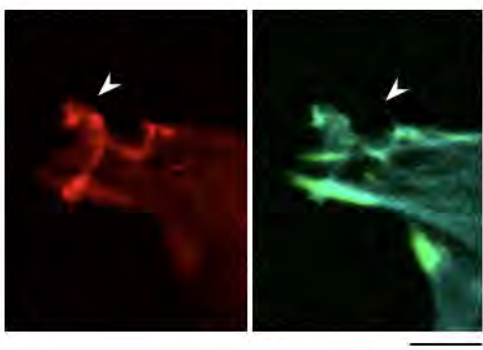
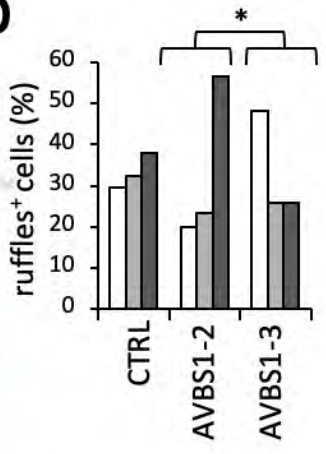
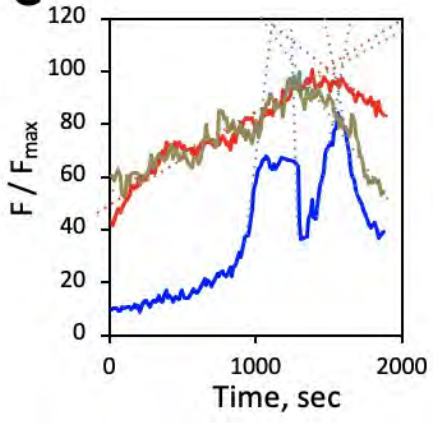
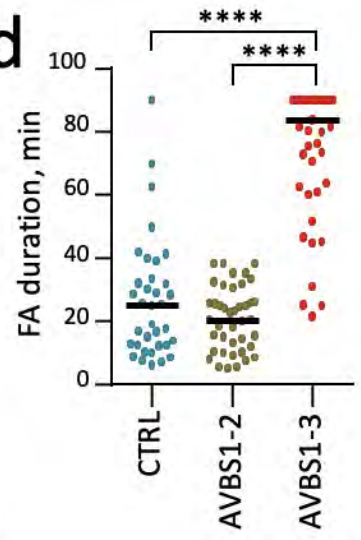
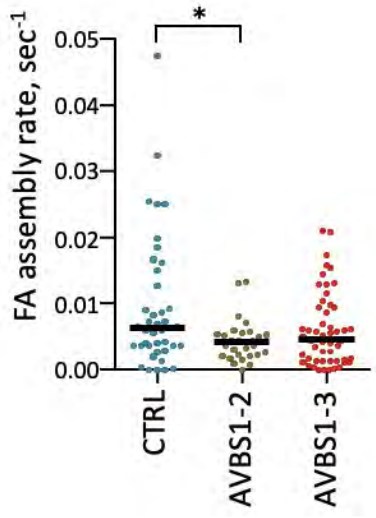
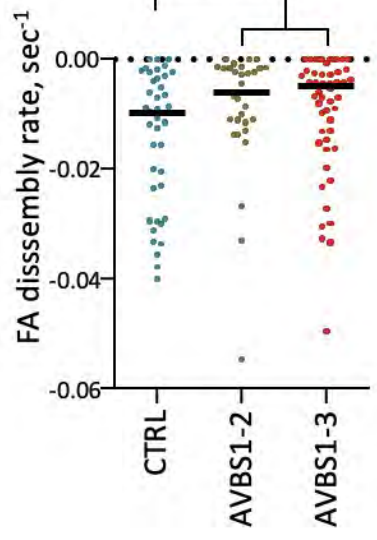
Supplementary Figure 5. The Q68C A396C D1D2 mutant does not form high order complexes. Representative gels revealed by Coomassie blue staining. **a**, Disulfide bridge formation in D1D2. D1D2: wild-type sequence. CC: D1D2 Q68C A396C. SDS-PAGE analysis using a 10 % polyacrylamide gel. + β -metOH: samples were boiled in Laemmli sample loading buffer containing 5 mM beta-mercaptoethanol prior to SDS-PAGE. The molecular weight markers in kDa are indicated. The black and red bars point to the respective migration of unreduced and reduced D1D2 Q68C A396C, respectively. **b**, **c**, Disulfide bridge formation in HV-CC. HV: full-length vinculin. HV-CC: HV Q68C A396C. Purified proteins (**b**) or samples pulled-down from lysates of HeLa cells transfected with pC1-HV8His or PC1-HVCC8His (Suppl. Star Methods) were treated with NEM, prior to reduction or not with DTT and

treatment with PEG-Mal as indicated (Suppl. Star Methods). The red star points at the shifted band associated with the PEGylation of reduced disulfide bridge in HV-CC. **d**, bands corresponding to the shifts 2 and 3 observed upon incubation of D1D2 with AVBS1-3 (Fig. 3f) were dissected from native gels (1D). 2D: second dimension SDS-PAGE analysis using a 10 % polyacrylamide gel. Right strip: analysis of the reaction sample at a D1D2:AVBS1-3 molar ratio = 1. The numbers below the samples correspond to the D1D2:AVBS1-3 molar ratio determined by scanning densitometry. **e**, Clear Native-PAGE analysis in a 6-18% polyacrylamide gradient gel of HV and HV-CC complexes in the presence of AVBS1-3, AVBS1-2 at a molar ration of 1: 2 or buffer alone (0) as indicated.

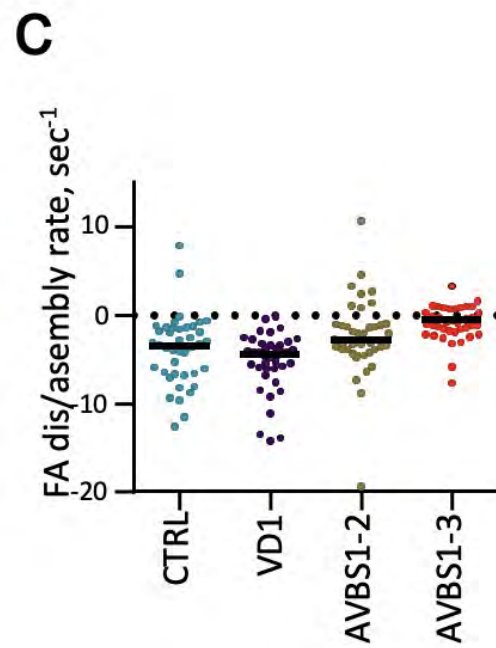
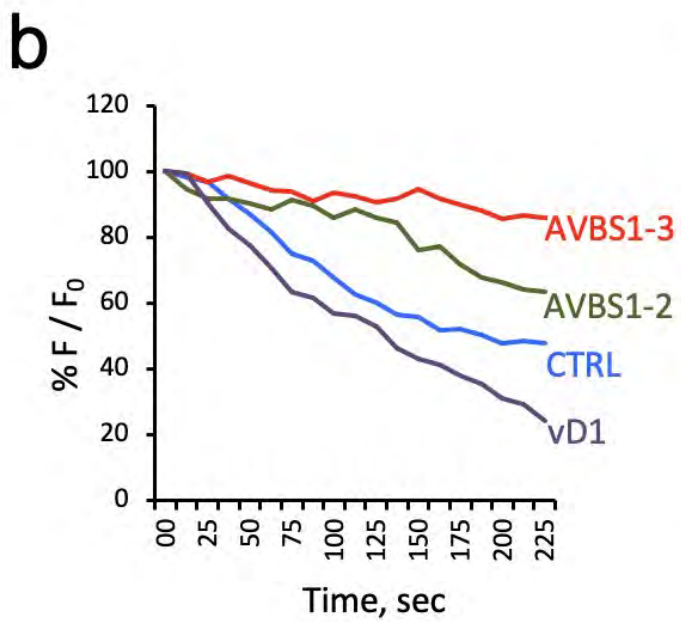
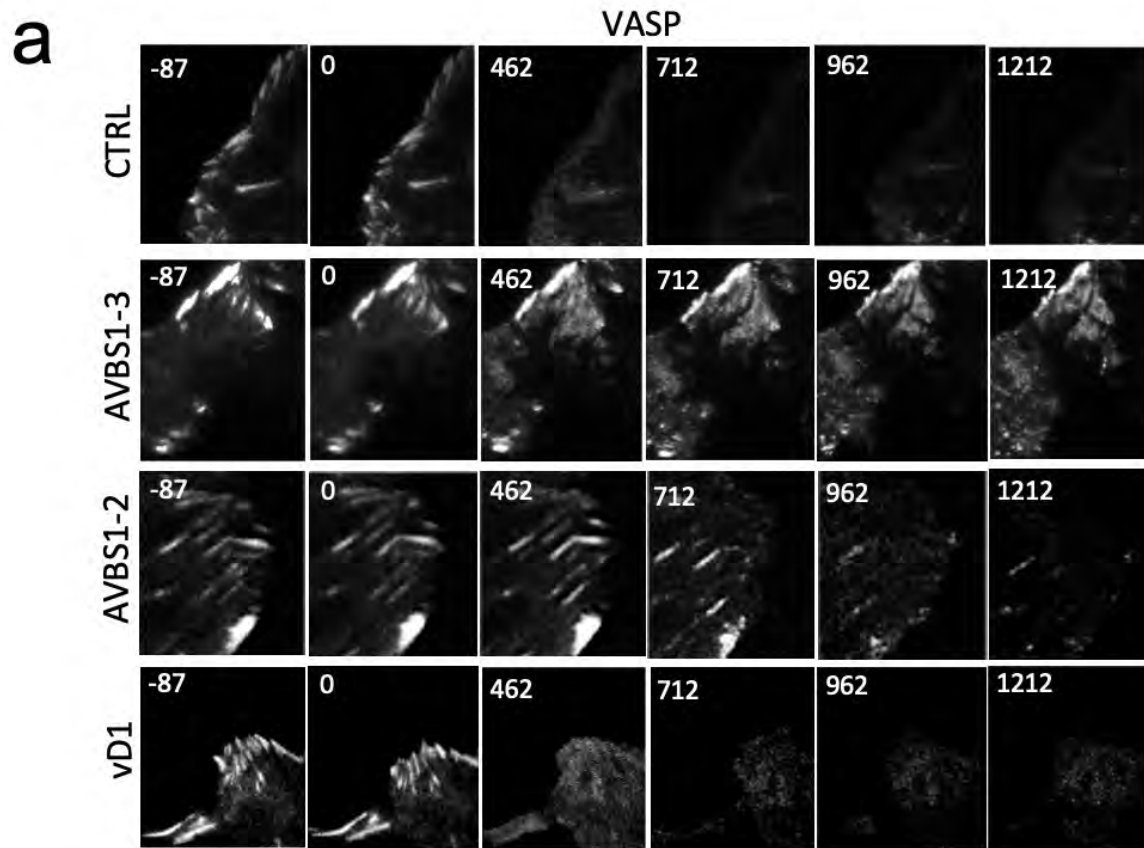


Supplementary Figure 6. IpaA-induced vinculin oligomers mediate actin bundling at a distance from activation sites.

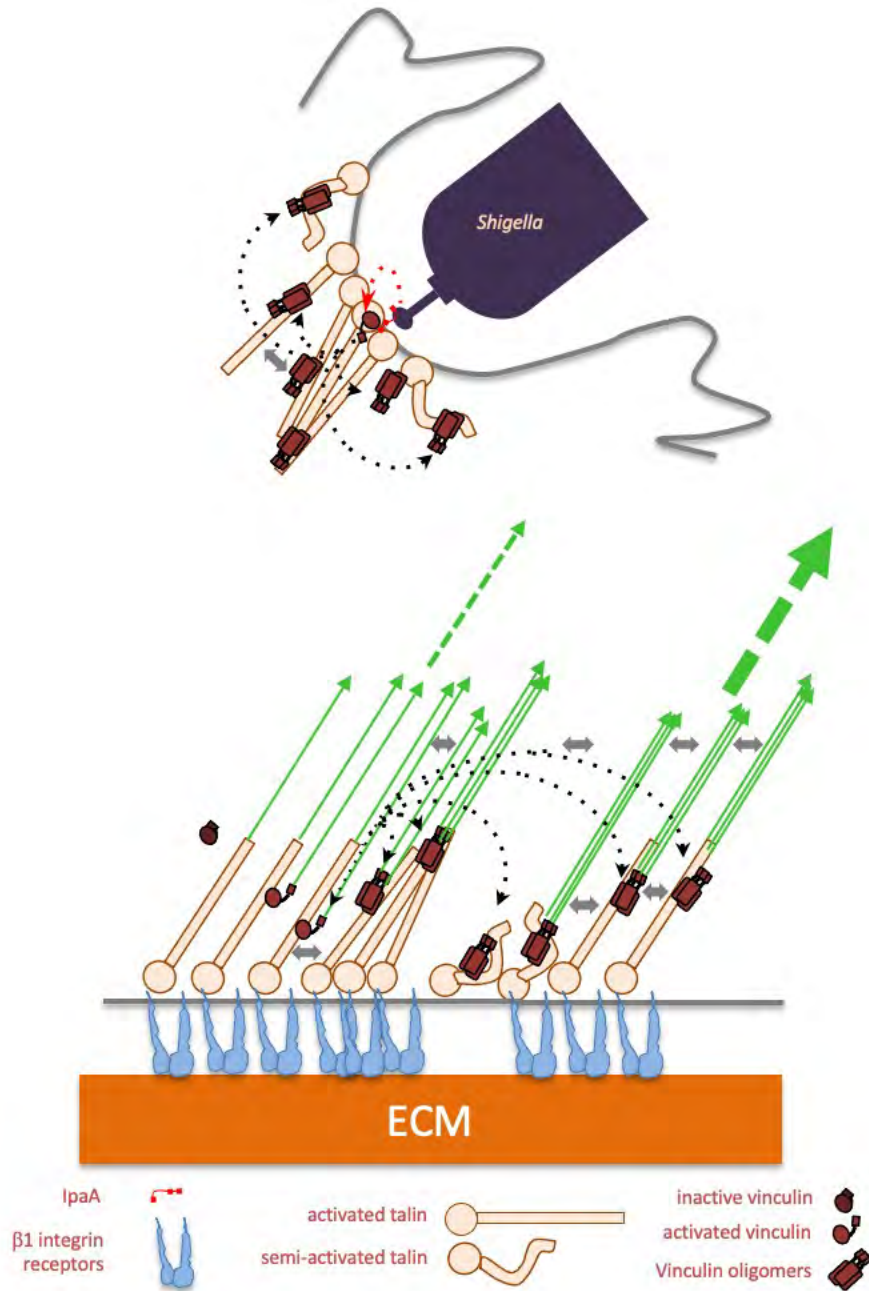
a, b, actin sedimentation assays. HV: full-length human vinculin; HV-CC: cysteine-clamp derivative. Actin was allowed to polymerize at a final concentration of 10 μ M in the presence of the indicated proteins. Samples were centrifuged at 110,000 g for 30 min to pellet actin filaments. S: supernatant; P: pellet. **a, c**, representative SDS-PAGE analysis using a 10% polyacrylamide gel and Coomassie staining. **b, d**, the band integrated intensity corresponding to HV or HV-CC (**b**) or GST-AVBS1-3 (**d**) were quantified using ImageJ. Values are expressed as the percent of protein amounts in the pellet fraction relative to the total protein amounts in the supernatant and pellet fractions. **b**, percent of co-sedimented vinculin (n = 3, N = 3) or HV-CC (n = 3, N = 3). **c**, analysis of fluorosphere coating with GST-AVBS1-3. Fluorospheres were coated with GST-AVBS1-3 at a final concentration of 2 μ M in PBS, washed three times by centrifugation and resuspension in PBS, and incubated in F-actin buffer. At the time points indicated in min, samples were centrifuged for 2 min. Beads were resuspended in Laemmli loading sample buffer, incubated for 10 min at 95C and bead-associated protein were analyzed by SDS-PAGE using a 10% polyacrylamide gel. The supernatant was subjected to trichloroacetic acid precipitation at a final concentration of 5%, prior to acetone wash and SDS-PAGE analysis. Supe: supernatant. FS: beads-associated samples. **d**, average percent of the initial bead-associated amounts of GST-AVBS1-3. N= 3.

a**b****c****d****e****f**

Supplementary Figure 7. Actin ruffles and TIRF analysis of FA dynamics in AVBS1-2 and AVBS1-3 transfectants. a b, CTRL: C2.7 cells. IpaA VBS1-2: GFP-IpaA VBS1-2 transfectants. IpaA VBS1-3: GFP-IpaA VBS1-3 transfectants. **a**, representative fluorescence micrographs. Arrows: adhesions; arrowheads: ruffles. Green: GFP; red: vinculin; cyan: actin. **b**, percent of cells with ruffles \pm SEM. Cells with: no ruffles (empty bars); small ruffles (light grey bars); large ruffles (dark grey bars). *: Pearson's Chi-squared test (N=3, n > 30, p = 0.036). **c-f**, C2.7 cells were transfected with vinculin-mCherry (HV), vinculin-mCherry and GFP-IpaA VBS1-2 (AVBS1-2) or vinculin and GFP-IpaA VBS1-3 (AVBS1-3). The dynamics of vinculin-mCherry-labeled FAs were analyzed by TIRF microscopy. **c**, traces correspond to the variations of average fluorescence intensity of a representative single FA (F) normalized to its maximal average fluorescence intensity over the analyzed period in seconds (F_{max}). Blue: vinculin; green: vinculin + AVBS1-2; red: vinculin + AVBS1-3. **d**, FA duration. **e, f**, instant assembly (**b**) or disassembly (**c**) rates were inferred from the slopes of linear fits as depicted in **a**), with a Pearson correlation value > 0.85. HV: n = 41, N = 3; HV + AVBS1-2: n = 31, N = 2; HV + AVBS1-3: n = 55, N = 3. Mann-Whitney U test. *: p < 0.05.



Supplementary Figure 8. IpaA-mediated vinculin supra-activation stimulates cell adhesion independent of mechanotransduction. TIRF microscopy of C2.7 cells transfected with mCherry-VASP alone (CTRL) or co-transfected with GFP-AVBS1-2 (AVBS1-2), GFP-vD1 (vD1), or GFP-AVBS1-3 (AVBS1-3). Adhesion kinetic parameters were determined from time-lapse acquisitions following cell treatment with 100 μ M Y-27632. **a**, representative time series acquisitions. Numbers indicated the elapsed time in seconds, with the inhibitor added at $t = 0$. Scale bar = 5 μ m. **b**, % F/F_0 : average fluorescence intensity of adhesions expressed as a percent of initial fluorescence. Solid lines: representative traces corresponding to single adhesions for the indicated samples in the corresponding color. The dashed redline illustrates FA assembly in AVBS1-3 transfected cell, seldom observed with the other samples. **c**, initial rates of adhesion assembly / disassembly inferred from linear fits. Number of adhesions analyzed: **c**, N = 4. CTRL: 42; IpaA VBS1-3: 43; IpaA VBS1-2: 40; vD1: 40. Dunn's multiple comparisons test. *: $p < 0.05$; ****: $p < 0.001$.



Supplementary Figure 9. Scheme of IpaA-mediated vinculin supra-activation and oligomerization during *Shigella* invasion and FA maturation. Top, IpaA induces vinculin supra-activation through the concerted action of the three IpaA VBS1-3 (red dotted arrow) at bacterial contact sites during *Shigella* invasion, leading to vinculin

homo-oligomers diffusing away from activation sites (black dotted arrows). These vinculin oligomers are further clustered by talin, resulting in expansion of the bacterial adhesion structures. Bottom, vinculin canonical activation by talin VBSs combined with acto-myosin pulling force during mechanotransduction leads to supra-activation and oligomer formation. These oligomers diffuse from activation sites (black dotted arrows) and are captured by talin VBSs and actin fibers (green), leading to actin bundling and focal adhesion expansion associated with increased pulling force (dotted green arrows).

SUPPLEMENTARY TABLES

#	Exp. MH ⁺	Primary Score	Peptide Sequence	IpaA VBS1-2	Hv D1
32670	4457.1	3.28	IDDTSAELLTDDISDLKNNNDITAENN NIYK - MA K MIDER	D604	K173
32798	1924.16	2.61	INN K LK - ELLPVLISAMK	K540	E200
33042	4613.23	3.70	IDDTSAELLT D DISDLKNNNDITAENN NIYK - NLGPGMT K MAK	D594	K170
33042	4613.23	3.70	IDDTSAELLT D DISDLKNNNDITAENN NIYK - NLGPGMT K MAK	D595	K170
33042	4613.23	4.11	IDDTSAELLTDDISDLKNNNDITAENN NIYK - NLGPGMT K MAK	D604	K170
33322	5310.64	4.48	IDDTSAELLTDDISDLKNNNDITAENN NIYK - VGKETVQTTE D QILKR	K600	D67
33334	2347.28	2.51	DVTTSLS K VLK - MSA E INEIIR	K625	E240
33432	2138.26	2.88	VL K NINKD - ELLPVLISAMK	K628	E200
33496	2315.32	3.09	AA K DVTTSLSK - ELLPVLISAMK	K617	E200
34822	2642.55	2.68	AKEVSSALS K VLSK - ELLPVLISAMK	K579	E200

38218	3685.86	3.87	NINKD - TIESILEPVAQQISHLVIMHEEGEVDG K	K632	E31
38218	3685.86	3.66	NINKD - TIESILEPVAQQISHLVIMHEEGEVDG K	K632	E28
#	Exp. MH⁺	Primar y Score	Peptide Sequence	Hv D1	
34075	2342.29	3	ELLPVLISAMK - NLGPGMTKMAK	E200	K170
36135	3088.67	2.62	NFTVEKMSAEINEIR - ELLPVLISAMK	K236	E200
#	Exp. MH⁺	Primar y Score	Peptide Sequence	IpaA VBS1-2	
14281	3051.56	3.52	NYVTETNADTIDKNHAIYEK - INNKLK	E554	K540
15477	3342.67	2.74	NYVTETNADTIDKNHAIYEK - AKEVSSALSK	E554	K571
17603	3141.54	2.71	NYVTETNADTIDKNHAIYEK -	K562	K572

			EVSSALSK		
31359	4483.2	2.64	IDDTSAELLTDDISDLKNNNDITAENN NIYK - A K EVSSALSK	E590	K571
31996	2965.5	2.94	IDDTSAELLTDDISDLK - AA K DVTTSLSK	D598	K617
31996	2965.5	2.51	IDDTSAELLT D DISDLK - AA K DVTTSLSK	D594	K617
32705	4586.24	4.1	IDDTSAELLTDDISDLKNNNDITAENN NIYK - AA K DVTTSLSK	E608	K617
33253	3291.74	3.81	IDDTSAELLT D DISDLK - A K EVSSAL S K V LSK	D595	K579
33997	5328.54	4.76	IDDTSAELLTDDISDLKNNNDITAENN NIYK - ID D TSAELLTDDISDLK	K600	D586
34007	4655.33	4.78	IDDTSAELLT D DISDLKNNNDITAENN NIYK - DVTTSL S K V LK	D594	K625

Suppl. Table 1. Cross-linked residues characterized in the D1:IpaA VBS1-2 complex (XL-amino acids of each protein are bolded in the sequences).

#	Exp. MH ⁺	Primary Score	Peptide Sequence	IpaA VBS1-2	Hv D1D2
20480	3470.68	3.86	NYVTETNADTIDKNHAIYEK - NLGPGMT K MAK	E554	K170
23021	3883.92	3.71	NYVTETNADTID K NHAIYEK - ETVQTTEDQILKR	K562	E60
24707	3117.73	5.00	AKEVSSALSKVLSK - VGKETVQTTEDQILK	K579	E66
36724	4612.22	4.82	IDDTSAELLTDDISDLKNNNDITAENN NIYK - NLGPGMT K MAK	D604	K170
39712	5255.49	3.79	IDDTSAELLTDDISDLKNNNDITAENN NIYK - NLGPGMT K MA K MIDER	D598	K173
39893	5162.6	4.51	IDDTSAELLTDDISDLKNNNDITAENN NIYK - ALA K QVATALQNLQTK	E590	K464
40011	2641.56	4.45	AKEVSSALSKVLSK - ELLPVLISAMK	K579	E200
41002	3047.64	3.99	L K VTDANIR - GILSGTSDLLLTFDEAEVR	K542	E128
41440	3944.01	3.86	IDDTSAELLTDDISDLK -	D598	K366

			AQQVSQGLDVLTA K VENAAR		
42699	3685.87	4.03	NINKD - TIESILEPVAQQISHLVIMHEEGEVDG K	K632	E31
#	Exp. MH ⁺	Primary Score	Peptide Sequence	Hv D1D2	
25162	3323.71	4.54	LNQA K GWLRDPSASPGDAGEQAIR - ALASIDSK	K281	D274
30025	3169.64	4.03	GQGSSPVAMQKAQQVSQGLDVLTA K - VENAAR	K352	E368
30045	3278.66	3.69	VLQLTSWDE D AWASK - K LEAMTNSKQSIK	D275	K381
30201	3695.87	3.82	LNQA K GWLRDPSASPGDAGEQAIR - MSA E INEIIR	K281	E240
31264	3251.77	5.03	ALAK Q VATALQNLQTKTNR - RQGK G DSPEAR	K464	E458
31264	3251.77	4.50	ALAK Q VATALQNLQTKTNR - RQGK G DSPEAR	K464	D455
31620	2516.36	3.44	ALASIDSKLNQA K - MSA E INEIIR	K295	E240

35256	3787.88	4.12	GILSGTSDLLLTDFDEAEVR - GSSHHHHHHSSGLVPR	E128	G12
38115	3310.75	4.29	GILSGTSDLLLTDFDEAEVR - AVANSRPAKAAVH	E147	K507
39508	3685.90	3.56	GQGSSPVAMQKAQQVSQGLDVLTA K - MSAEINEIR	K352	E240
40134	3129.61	2.19	NQGIEEALKNRNFTVEKMSAEINEIR	E224	K236
40285	3184.71	4.81	AQQVSQGLDVLTAKVENAAR - SLGEISALTSK	K366	E437
40296	2280.32	3.69	ELLPVLISAMK - LNQA K GWLR	E200	K281
40351	3255.72	4.00	AQQVSQGLDVLTAKVENAAR - MSAEINEIR	K366	E240
40571	4536.51	4.44	GDSPEARALAKQVATALQNLQTK - SLGEISALTSKLADLRRQ GK	D455	K444
40881	3704.92	4.32	KIDAAQNWLADPNGGPEGEEQIR - ELLPVLISAMK	K387	E200
40923	3100.63	3.94	AQQVSQGLDVLTAKVENAAR - KLEAMTNSK	E368	K373

41473	3723.01	4.34	GQGSSPVAMQKAQQVSQGLDVLTA K - ELLPVLISAMK	K352	E200
41482	4633.41	3.54	TIESILEPVAQQISHLVIMHEEGEVDG K - KLEAMTNSKQSIK	E28	K381
42201	3294.83	3.66	AQQVSQGLDVLTA K VENAAR - ELLPVLISAMK	K366	E200
#	Exp. MH⁺	Primar y Score	Peptide Sequence	IpaA VBS1-2	
15424	3050.56	3.57	NYVTETNADTIDKNHAIYEK - INN KLK	E554	K540
16531	3340.67	3.55	NYVTETNADTIDKNHAIYEK - A KEVSSALS K	E558	K571
16865	3341.67	4.11	NYVTETNADTIDKNHAIYEK - A KEVSSALS K	E554	K571
34602	4584.25	4.05	IDDTSA ELL TDDISDLKNNNDITAENN NIYK - A AKDVT TSLSK	E590	K617
35202	4586.25	5.2	IDDTSA ELL TDDISDLKNNNDITAENN NIYK - A AKDVT TSLSK	D594	K617
35824	4583.26	3.43	IDDTSA ELL TDDISDLKNNNDITAENN	E608	K617

			NIYK - AAK D VTTSLSK		
39340	4911.48	4.37	IDDTSAELLT D DISDLKNNNDITAENN NIYK - AKEVSSALS K VLSK	D595	K579
39340	4911.48	4.06	IDDTSAELLT D DISDLKNNNDITAENN NIYK - AKEVSSALS K VLSK	D598	K579
39340	4911.48	3.83	IDDTSAELLT D DISDLKNNNDITAENN NIYK - AKEVSSALS K VLSK	E590	K579
39730	3291.74	3.64	IDDTSAELLT D DISDLK - A K EVSSALS K VLSK	D595	K571
40244	4655.32	4.35	IDDTSAELLT D DISDLKNNNDITAENN NIYK - DVT T SL S K V L K	D594	K625
40244	4655.32	4.35	IDDTSAELLT D DISDLKNNNDITAENN NIYK - DVT T SL S K V L K	D595	K625

Suppl. Table 2. Cross-linked residues characterized in the D1D2:IpaA VBS1-2 complex (XL-amino acids of each protein are bolded in the sequences).

#	Exp. MH ⁺	Primary Score	Peptide Sequence	IpaA VBS1-3	Hv D1D2
1323 7	3014.59	3.29	DITKSTTEHR - VGKETVQTTEDQILKR	K530	E66
1467 1	2518.38	2.49	SKDITK - VGKETVQTTEDQILKR	K526	E66
1479 1	2556.44	2.35	INNKLK - VGKETVQTTEDQILKR	K540	E66
1780 6	2621.29	3.10	GSPGIPGDTYLTR - QQELTHQEHR	G517	E181
2003 9	2571.40	3.08	LKVTDANIR - ETVQTTEDQILKR	K542	E66
2052 6	3651.79	3.37	NYVTETNADTIDKNHAIYEK - NSKNQGIEEALK	E554	K219
2098 5	3469.67	3.01	NYVTETNADTIDKNHAIYEK - NLGPGMTKMAK	D558	K170
2293 6	3468.66	2.62	NYVTETNADTIDKNHAIYEK - NLGPGMTKMAK	E554	K170

2313 7	4011	3.29	NYVTETNADTID K NHAIYEK - VG K ETVQTTEDQILK	D561	K59
2541 8	3725.82	3.27	NYVTETNADTID K NHAIYEK - ETVQTTEDQILK	K562	E66
2541 8	3725.82	3.72	NYVTETNADTID K NHAIYEK - E TVQTTEDQILK	K562	E60
2761 8	3161.66	3.21	G SPGIPGDTYLTR - VG K ETVQTTEDQILKR	G517	E60
2761 8	3161.66	3.61	G SPGIPGDTYLTR - VG K ETVQTTEDQILKR	G517	D67
2836 6	2918.61	3.18	EVSSALS K VLSK - VG K ETVQTTEDQILK -	K579	E66
2999 6	1977.96	3.06	G SPGIPGDTYLTR - MIDER	G517	D176
3649 7	2772.45	3.78	G SPGIPGDTYLTR - AQQVSQGL D VLTAK	G517	D361
3661 5	4613.23	3.68	IDDTSAELLT D DISDLKNNNDITAENN NIYK - NLGPGMT K MAK	D594	K170

3663 2	2214.27	3.22	AKEVSSALSK - ELLPVLISAMK -	K571	E200
3753 6	3824.86	2.64	GSPGIPGDTYLTR - KIDAAQNWLADPNGGPEGEEQIR	G517	D389
4026 3	3413.78	3.79	GSPGIPGDTYLTR - AQQVSQGLDVLTA K VENAAR	D484	K366
4043 2	5992.94	5.1	IDDTSA E LLTDDISDLKNNNDITAENN NIYK - GQGSSPVAMQKAQQVSQGLDVLTA K	E590	K362
4067 9	2708.42	3.25	SKDITK - GILSGTSDLL L TFDE A AEVR	K526	E128
4099 4	3074.69	3.12	KVTNSLSNLISLIGTK - ETVQTT E DQILK	K498	E66
4118 7	4612.22	2.86	IDDTSA E LLTDDISDLKNNNDITAENN NIYK - NLGPGMT K MAK	E590	K170
4181 6	2387.41	3.65	DVTTSLSK V LK - ELLPVLISAMK	K625	E200
4332 6	3137.65	3.41	AAKDVTT S L S K - GILSGTSDLL L TFDE A AEVR	K625	E128
4353	3542.88	3.63	IDDTSA E LLTDDISDLK -	D594	K464

7			ALAKQVATALQNLQTK		
4361 2	3604.91	3.34	VTNSLSNLISLIGTKSGTQER - ETVQTTEDQILK	K513	E66
4508 1	3350.71	3.48	GSPGIPGDTYLTR - GILSGTSDLLTFDEAEVR	G517	D121
5347 4	5745.03	4.09	NINKD - TIESILEPVAQQISHLVIMHEEGEVDG KAIPDLTAPVAAVQAAVSNLVR	K632	E31
#	Exp. MH⁺	Primary Score	Peptide Sequence	Hv D1D2	
1758 2	1670.89	3.51	VGKETVQTTEDQILK	K59	E66
1758 2	1670.89	3.38	VGKETVQTTEDQILK	K59	D67
2600 0	3322.71	4.03	LNQAKGWLDRDPSASPGDAGEQAIR - ALASIDSK	K281	D374
3090 1	3169.64	3.79	GQGSSPVAMQKAQQVSQGLDVLTA K - VENAAR	K352	E368
3103	3695.87	3.81	LNQAKGWLDRDPSASPGDAGEQAIR -	K281	E240

1			MSAEINEIR		
3582 7	3665.8	3.75	KIDAAQNWLADPNGGPEGEEQIR - MSAEINEIR	K387	E240
3821 5	3040.71	3.43	VGKETVQTTEDQILKR - ELLPVLISAMK	K59	K200
3973 4	3614.9	4.15	GQGSSPVAMQKAQQVSQGLDVLTA - SLGEISALTSK	K352	E437
4021 8	3580.72	3.88	VLQLTSWDEDAWASKDTEAMK - MSAEINEIR	K261	E240
4041 8	2881.63	3.77	QVATALQNLQTKTNR - ELLPVLISAMK	K476	E200
4055 9	3184.71	4.71	AQQVSQGLDVLTAKVENAAR - SLGEISALTSK	K366	E437
4056 0	2280.32	3.35	ELLPVLISAMK - LNQAKGWLR	E200	K281
4060 4	2553.46	3.78	ALASIDSKLNQAK - ELLPVLISAMK	K276	E200
4114 0	2892.69	3.97	ALAKQVATALQNLQTK - ELLPVLISAMK	K464	E200
4159	4173.16	5.49	GQGSSPVAMQKAQQVSQGLDVLTA	K366	E375

8			VENAAR - KLEAMTNSK		
4159	4173.16	5.8	GQGSSPVAMQKAQQVSQGLDVLTA K	E368	K373
8			VENAAR - K LEAMTNSK		
4159	4173.16	4.98	GQGSSPVAMQKAQQVSQGLDVLTA K	D361	K373
8			- VENAAR K LEAMTNSK		
4168	3726.02	3.87	GQGSSPVAMQKAQQVSQGLDVLTA K	K352	E200
2			- ELLPVLISAM K		
4238	3293.83	4.63	AQQVSQGLDVLTA K VENAAR -	K366	E200
7			ELLPVLISAM K		
4238	3293.83	3.3	AQQVSQGLDVLTA K VENAARK -	E368	K281
7			LNQA K GWLR		
#	Exp. MH⁺	Primar y Score	Peptide Sequence	IpaA VBS1-3	
1739	3339.66	3.31	NYVTETNADTIDKNHAIYEK -	D561	K571
8			A K EVSSALSK		
1763	3341.68	3.44	NYVTETNADTIDKNHAIYEK -	D558	K571
0			A K EVSSALSK		

1763 0	3341.68	4.19	NYVTETNADTIDKNHAIYEK - AKEVSSALSK	E554	K571
2007 1	3141.53	3.53	NYVTETNADTIDKNHAIYEK - AKEVSSALSK	K562	E572
2015 0	3349.69	4.44	NYVTETNADTIDKNHAIYEK - LKVTDANIR	D558	K542
2015 0	3349.69	4.03	NYVTETNADTIDKNHAIYEK - LKVTDANIR	D561	K542
3516 3	4584.24	3.59	IDDTSAELLTDDISDLKNNNDITAENN NIYK - AAKDVTTSLSK	D594	K617
3516 3	4584.24	3.49	IDDTSAELLTDDISDLKNNNDITAENN NIYK - AAKDVTTSLSK	D595	K617
3538 2	4586.24	3.35	IDDTSAELLTDDISDLKNNNDITAENN NIYK - AAKDVTTSLSK	E590	K617
3596 7	4584.24	4.42	IDDTSAELLTDDISDLKNNNDITAENN NIYK - AAKDVTTSLSK	D598	K617
3596 7	4584.24	4.95	IDDTSAELLTDDISDLKNNNDITAENN NIYK - AAKDVTTSLSK	E608	K617

3596 7	4584.24	4.52	IDDTSAELLTDDISDL K NNNDITAENN NIYK - AAKD V TTSLSK	K600	D618
3596 7	4584.24	4.22	IDDTSAELLTDDISDL K NNNDITAENN NIY K - AAKD V TTSLSK	K614	D618
3596 7	4584.24	4.94	IDDTSAELLTDDISDL K NNNDITAENN NIYK - AAKD V TTSLSK	D604	K617
3988 1	2845.52	4.73	VTNSLSNLISLIGT K SGTQER - ELQEK	K513	E520
3988 1	2845.52	4.62	VTNSLSNLISLIGT K SGTQER - ELQEK	K513	E523
4004 4	4655.33	5.07	IDDTSAELLT D DISDL K NNNDITAENN NIYK - D V TTSLSK V L K	D594	K625
4004 4	4655.33	4.86	IDDTSAELLT D DISDL K NNNDITAENN NIYK - D V TTSLSK V L K	D595	K625
4004 4	4655.33	4.45	IDDTSAELLTDDISDL K NNNDITAENN NIYK - D V TTSLSK V L K	D598	K625
4004 4	4655.33	4.44	IDDTSAELLTDDISDL K NNNDITAENN NIYK - D V TTSLSK V L K	E590	K625

4006 5	3092.6	3.51	IDDTSAELLT DD ISDLK - EVSSALSKVLSK	D594	K579
4006 5	3092.6	3.38	IDDTSAELLT DD ISDLK - EVSSALSKVLSK	D594	K579
4006 9	3093.61	3.36	IDDTSAELLT DD ISDLK - EVSSALSKVLSK	D598	K579
4009 5	2988.61	4.48	VTNSLSNLISLIGTKSGTQER - VTDANIR	K513	D545
4044 8	3252.74	3.81	VTNSLSNLISLIGTKSGTQER - ETIFEASKK	K513	E494
4060 3	5153.62	4.36	IDDTSAELLT DD ISDLKNNNDITAENN NIYK - K VTNSLSNLISLIGTK	D594	K498
4060 3	5153.62	4.46	IDDTSAELLT DD ISDLKNNNDITAENN NIYK - K VTNSLSNLISLIGTK	D595	K498
4060 3	5153.62	4.56	IDDTSAELLT DD ISDLKNNNDITAENN NIYK - K VTNSLSNLISLIGTK	D598	K498
4060 3	5153.62	3.99	IDDTSAELLT DD ISDLKNNNDITAENN NIYK - K VTNSLSNLISLIGTK	D604	K498

4060 6	5153.62	3.53	IDDTSA E LLTDDISDLKNNNDITAENN NIYK - K VTNSLSNLISLIGTK	E590	K498
4111 6	2593.44	3.85	K VTNSLSNLISLIGTK - E TIFEASK	K498	E490
4114 2	3909.09	4	E TIFEASK K VTNSLSNLISLIGTK - G SPGIPGDTYLTR	E490	G477

Suppl. Table 3. Cross-linked residues characterized in the D1D2 -IpaA VBS1-3 1:1 complex (XL-amino acids of each protein are bolded in the sequences)

STAR METHODS

RESOURCE AVAILABILITY

Lead contact

Further information and requests for resources and reagents should be directed to and will be fulfilled by the lead contact, Guy Tran Van Nhieu (guy.tranvannhieu@i2bc.paris-saclay.fr).

Materials availability

Availability of plasmids, resources and reagents generated in this study may be subjected to restriction due to patent application N°PVT/ EP2016/073287.

Data and code availability

Any additional information required to reanalyze the data reported in this paper is available from the lead contact upon request.

Data

All data reported in this paper not related to the patent application N°PVT/ EP2016/073287 will be shared by the lead contact upon request.

Code

This paper does not report original code.

METHODS DETAILS

Plasmids and constructs

Human vinculin constructs were generated by polymerase chain reaction using the forward primer 5' GCGCATATGCCAGTGTTTCATACG-3' and reverse primers 5'-CGTCGACTCACCAGGCATCTTCATCGGC-3' for D1 (residues 1-258) or 5'-CGTCGACTCAGTGTACAGCTGCTTTG-3' for D2 (residues 1-492) using a plasmid containing full-length octahistidine-tagged human vinculin (pET3a-vinculin 8His, residues 1–1,066), as template (Bakolitsa, Cohen et al. 2004), and cloned into the NdeI-Sall sites of pet15b (Novagen) to obtain pET15b-D1 and pET15b-D1D2, respectively. The Q68C and A396C cysteine substitution for the cysteine clamp were introduced into pet15b-D1D2 by site-directed mutagenesis using the 5'-GAGACTGTTCAAACCACTGAGGATTGCATTTTGAAG-3' and 5'-ATCGATGCTGCTCAGAACTGGCTTTGCGATCCAAAT-3' primers, respectively. The pGFP-vD1 plasmid was generated by polymerase chain reaction using the forward primer 5'-ACCCGGGATCCCGCC-3' and reverse primer 5'-ACCCGGGACCAGGCA-3', and cloned into pEGFP. The pmCherry-human vinculin (HV) and pmCherry-VASP plasmids were from Addgene. Stealth siRNA anti-human vinculin was from Invitrogen (reference number 1299001). The cysteine clamp was introduced in pmCherry N1-vinculin by exchanging the NheI-PspXI fragment with the corresponding XbaI-PspXI fragment of pET15b-D1D2 -Q68C A396C. Introduction of the cysteine clamp in full length vinculin was performed by swapping the *SexAI-BsrgI* fragment from pET15b-D1D2-Q68C-A396C and pET3a-vinculin 8His.

The IpaA constructs GFP-AVBS1-2 and GFP-AVBS1-3 were generated by polymerase chain reaction (PCR) and cloning into pcDNA3.1 NT-GFP Topo TA (Invitrogen) using the 5'-TCAAAGGACATTACAAAATCC-3' and 5'-

GCGATATCATGGCCAGCAAAGG-3' forward primers, respectively, and the 5'-GCGCGGCCGCTTAATCCTTATTGATATTC-3' reverse primer. The GST-AVBS1-3 construct was generated by PCR using 5'-GGCGAATTCCCGGAGACACATATTTAACACG-3' forward and 5'-GCCGTCGACTTAATCCTTATTGATATTCT-3' reverse primers and cloning into the *EcoRI-Sall* of pGEX-4T-2 (GE Lifesciences). pGST-AVBS1-2 was previously described (Ramarao, Le Clainche et al. 2007). The pGFP-vD1 plasmid was generated by polymerase chain reaction using the forward primer 5'-ACCCGGGATCCCGCC-3' and reverse primer 5'-ACCCGGGACCAGGCA-3', and cloned into pEGFP. The pmCherry-human vinculin (HV) and pmCherry-VASP plasmids were from Addgene. Stealth siRNA anti-human vinculin was from Invitrogen (reference number 1299001). All constructs were verified by DNA sequencing. Plasmids pC1-HV8His and pC1HV-CC8His were generated by replacing the 1.1 Kb *EcoRV-NotI* fragment of pmCherryN1-HV and pmCherryN1-HV-CC, respectively, by the 764 bp *EcoRV-NotI* fragment from pET3a-vinculin 8His.

Cell lines and bacterial strains

HeLa cells (ATCC CCL-2) were incubated in RPMI (Roswell Park Memorial Institute) medium containing 5% FCS (fetal calf serum, Gibco®) in an incubator with 5% CO₂. C2.7 myoblasts (Mitrossilis, Fouchard et al. 2009), MEF and MEF vinculin null cells (Humphries, Wang et al. 2007) were routinely grown in DMEM 1 g / L glucose containing 10 % FCS in a 37°C incubator containing 10 % CO₂. For transfection experiments, cells were seeded at 2.5 x 10⁴ cells in 25 mm-diameter coverslips. Cells were transfected with 3 µg of pGFP-AVBS1-2 or pGFP-AVBS1-3

plasmids with 6 μ l JetPEI transfection reagent (Polyplus) for 16 hours following the manufacturer's recommendations. C2.7 mice myoblasts cells were fixed in PBS containing 3.7% paraformaldehyde for 20 min at 21°C and permeabilized with 0.1% Triton X-100 for 4 min at 21°C.

The wild type *Shigella flexneri*, isogenic mutants, and complemented *ipaA* mutant strains, as well as wild type *Shigella* expressing the AfaE adhesin were previously described (Izard, Tran Van Nhieu et al. 2006). Bacterial strains were cultured in trypticase soy broth (TCS) medium at 37°C. When specified, antibiotics were added at the following concentrations: carbenicillin 100 μ g/ml, kanamycin 20 μ g/ml.

Cell challenge with *Shigella* strains

HeLa cells seeded at 4×10^5 cells in coverslip-containing 34 mm-diameter wells the day before the experiment. After 16 hours, cells were challenged with *Shigella* strains coated with poly-L-lysine, as follows. Bacteria grown to an OD_{600 nm} of 0.6 - 0.8 were washed three-times by successive centrifugation at 13 Kg for 30 sec and resuspension in EM buffer (120 mM NaCl, 7 mM KCl, 1.8 mM CaCl₂, 0.8 mM MgCl₂, 5 mM glucose, and 25 mM HEPES, pH = 7.3). Samples were resuspended in EM buffer containing 50 μ g/ml poly-L-lysine and incubated for 15 min at 21°C, washed three times in EM buffer and resuspended in the same buffer at a final OD of OD_{600 nm} = 0.2. Cell samples were washed three times in EM buffer and challenged with 1 ml of the bacterial suspension and incubated at 37°C. Samples were fixed

with PBS containing 3.7% PFA after 30 min incubation. Samples were processed for immunofluorescence microscopy.

Immunofluorescence staining

Cells were processed for immunofluorescence staining using the Vin11.5 anti-vinculin monoclonal antibody (ref. V4505, Sigma-Aldrich) and anti-mouse IgG antibody coupled to Alexa 546 (Jackson Research) and Phalloidin-Alexa 633 (Invitrogen), as described previously (Tran Van Nhieu and Izard 2007). Bacteria were labeled using anti-LPS rabbit polyclonal antibody followed by anti-rabbit IgG antibody coupled to Alexa 525 as described (Izard, Tran Van Nhieu et al. 2006). Samples were analyzed using an Eclipse Ti inverted microscope (Nikon) equipped with a 60 x objective, a CSU-X1 spinning disk confocal head (Yokogawa), and a Coolsnap HQ2 camera (Roper Scientific Instruments), controlled by the Metamorph 7.7 software. Analysis of fluorescent actin filaments was performed using a Leica confocal SP8 using a 63 x objective.

Protein purification

BL21 (DE3) chemically competent *E. coli* (Life Technologies) was transformed with the expression constructs. D1 and D1D2 were purified essentially as described (Papagrigoriou, Gingras et al. 2004, Park, Valencia-Gallardo et al. 2011). For the IpaA derivatives, bacteria grown until $OD_{600nm} = 1.0$ were induced with 0.5 mM IPTG and incubated for another 3 hrs. Bacteria were pelleted and washed in binding buffer 25 mM Tris PH 7.4, 100 mM NaCl and 1 mM beta-mercaptoethanol, containing Complete™ protease inhibitor. Bacterial pellets were resuspended in 1/50th of the original culture volume and lyzed using a cell disruptor (One shot model, Constant

System Inc.). Proteins were purified by affinity chromatography using a GSTrap HP affinity column (GE Healthcare) and size exclusion chromatography (HiLoad S200, GE Healthcare). Samples were stored aliquoted at -80°C at concentrations ranging from 1 to 10 mg/ml.

Protein complex formation analysis

Proteins were incubated at a concentration of 30 µM in binding buffer for 60 min at 4°C. Samples were analyzed by SEC-MALS using an HPLC (Shimadzu), a 24 ml Superdex 200 Increase 10/300 GL filtration column (GE Healthcare) and a MiniDAWN TREOS equipped with a refractometer Optilab T-rEX (Wyatt Technology) connected in series, to separate constructs according to their Stokes radius and determine the molar mass of macromolecules in solution. Data were analyzed using the ASTRA 6.1.7.17 software (Wyatt Technology Europe). Protein complex formation was visualized by PAGE under non-denaturing conditions using a 7.5% polyacrylamide gel, followed by Coomassie blue staining.

Solid-phase binding assay

96-well Maxisorp (Nunc) ELISA plates were coated with 30 nM of full-length vinculin, vinculin constructs or IpaA proteins at the indicated concentrations in binding buffer (25 mM Tris PH 7.4, 100 mM NaCl and 1 mM β-mercaptoethanol). Samples were blocked with PBS-BSA 2%, washed and incubated with IpaA or vinculin proteins in binding buffer containing 0.2% BSA at room temperature for one hour. After incubation, the plates were washed and incubated with an anti-IpaA (dilution 1/2000^e) polyclonal primary antibody³ or anti-vinculin (dilution 1/2000^e)

Vin11.5 monoclonal antibody (Sigma-Aldrich) in binding buffer containing 0.2% BSA for one hour at room temperature. Plates were washed and incubated with an HRP-coupled secondary anti-rabbit or anti-mouse IgG antibody (1/32000°) (Jackson ImmunoResearch) for one hour. The reaction was revealed by adding 100 μ l of tetramethylbenzidine (Sigma-Aldrich) for 15 min, stopped by adding 50 μ l of 0.66N H₂SO₄ and the absorbance was read at 450 nm (Dynatech MR400).

BN-PAGE (Blue Native – Polyacrylamide Gel Electrophoresis) protein native gel analysis and complex cross-linking

25 μ M of vinculin constructs were incubated with different molar ratios of IpaA proteins in a 1X BN-PAGE buffer (250 mM ϵ -aminocaproic acid and 25 mM Bis-Tris PH 7,0) at 4°C for one hour. The protein mixtures were separated in a one-dimension native BN-PAGE electrophoresis as described (Eubel and Millar 2009). For vinculin-IpaA protein ratio assay, vinculin-IpaA bands containing the complexes separated by BN-PAGE were cut, sliced and boiled in 2 x Laemmli SDS buffer followed by SDS-PAGE. The second dimension SDS-PAGE gels were stained (colloidal Coomassie staining) and the density of the bands was determined using Image J. The normalized vinculin:IpaA ratio of the complexes was compared using a non-parametric Kruskal-Wallis rank sum test (R statistical software).

For crosslinking vinculin-IpaA complex, bands containing the complexes were cut, sliced and electroeluted in native conditions (15 mM Bis-Tris pH 7.0 and 50 mM Tricine) inside a closed dialysis membrane (SpectraPor). The soluble complexes were

recovered and their buffer exchanged twice into an amine-free cross-link buffer in 25 mM HEPES pH 7.0 containing 100 mM NaCl using 10MWCO ZEBA desalting columns (Thermo Scientific). The fractions containing the complexes were incubated for 1 hr at 4°C with 10 mM N-hydroxysulfosuccinimide and 5 mM EDC (Sigma-Aldrich) following the manufacturer's recommendations. The cross-linking reaction was stopped by adding 50 mM Tris pH 7.4 and incubating for 20 minutes. Samples were denatured in 2x SDS Laemmli buffer for 5 min at 95°C and complexes were eluted from gel slices following SDS-PAGE.

Liquid Chromatography Mass spectrometry (LC-MS)

Complexes obtained after the cross-linking step were loaded onto a 4-20% polyacrylamide gradient gels and Coomassie stained. The bands containing the complexes were cut and submitted to tryptic digestion (Shevchenko, Tomas et al. 2006). The experiments were performed in duplicates for the 3 complexes D1:AVBS1-2, D1D2: AVBS1-2 and D1D2:AVBS1-3. Peptides obtained after tryptic digestion were analyzed on a Q Exactive Plus instrument (Thermo Fisher Scientific, Bremen) coupled with an EASY nLC 1 000 chromatography system (Thermo Fisher Scientific, Bremen). Sample was loaded on an in-house packed 50 cm nano-HPLC column (75 µm inner diameter) with C18 resin (1.9 µm particles, 100 Å pore size, Reprosil-Pur Basic C18-HD resin, Dr. Maisch GmbH, Ammerbuch-Entringen, Germany) and equilibrated in 98 % solvent A (H₂O, 0.1 % FA) and 2 % solvent B (ACN, 0.1 % FA). A 120 minute-gradient of solvent B at 250 nL.min⁻¹ flow rate was applied to separate peptides. The instrument method for the Q Exactive Plus was set up in DDA mode (Data Dependent Acquisition). After a survey scan in the Orbitrap

(resolution 70 000), the 10 most intense precursor ions were selected for HCD fragmentation with a normalized collision energy set up to 28. Charge state screening was enabled, and precursors with unknown charge state or a charge state of 1 and >7 were excluded. Dynamic exclusion was enabled for 35 or 45 seconds respectively.

Analysis of disulfide bridge by PEG-Maleimide modification

The determination of disulfide bridge formation in HV-CC was performed as previously described with minor modifications (Braakman, Lamriben et al. 2017; Pant, Oh, and Mysore 2021). Briefly, for in vitro determination, 2 µg of purified HV or HV-CC were first incubated with 50 mM NEM PEG-Mal, NEM (N-ethylmaleimide), prior to reduction by incubation in 50 mM DTT (dithiothreitol). Alternatively, control samples were first reduced by incubation in 50 mM DTT, prior to NEM treatment. All samples were then incubated in 8 mM PEG-Mal (Sigma Aldrich, 63187). All incubation steps were carried out for 40 min at 21°C in 150 mM Tris pH 6.8, 0, 1%SDS (incubation buffer). Samples were precipitated and washed twice with acetone prior to resuspension between incubation steps. For determination of disulfide bridge formation in cells, HeLa cells were transfected with plasmids pC1-HV8His or pC1HV-CC8His the day preceding the experiment. Cells were scraped in 200 µls of ice-cold incubation buffer containing 1 mM AEBSF (4-(2-aminoethyl)benzenesulfonyl fluoride). Cell lysates were transferred to Eppendorf tubes on ice, 1800 µls of 150 mM Tris pH 6.8 containing 1 mM DTT (wash buffer) were added, and samples were clarified by centrifugation for 10 min at 13,000 g at 4°C. Clarified lysates were transferred to a fresh Eppendorf tube and subjected to pull-down by incubation with 40 µls of Ni Sepharose 6 Fast flow resin (Sigma Aldrich Pharmaceuticals) for 40 min at

4°C using an end-over-end roller. Samples were washed three times with 500 µls wash buffer. Samples were then subjected to NEM and DTT treatment prior to PEG-Mal modification as described above for purified proteins. Samples were resuspended in Laemmli loading sample buffer and SDS-PAGE analysis using a 7.5% polyacrylamide gel. For purified proteins, gels were analyzed by Coomassie blue staining. For proteins pulled-down from cell lysates, samples were analyzed by anti-vinculin Western blot analysis using the Vin11.5 mouse monoclonal antibody (Sigma Aldrich Pharmaceuticals) at a 1:5000 dilution.

Actin sedimentation assays

Actin was purified from rabbit muscle as described previously (Ciobanasu, Faivre et al. 2015). For actin co-sedimentation assays 5 µM actin was incubated in F-actin buffer (2 mM Tris pH7.5, 0.2 mM CaCl₂, 0.5 mM beta-mercaptoethanol, 0.2 mM ATP, 100 mM KCl, 2 mM MgCl₂) for 60 min at 21°C. When indicated, HV, HV-CC, AVBS1-3 and AVBS1-2 were added at a 2 µM final concentration. Samples were centrifuged at 110,000 g for 30 min at 4°C. For actin bundling assays, actin was allowed to polymerize at the indicated concentration and samples were centrifuged at 14,000 g for 10 min at 31°C. Proteins in pellets and supernatants were analyzed by SDS-PAGE on a 10% polyacrylamide gel followed by Coomassie blue staining. For quantification, protein band integrated densities were determined using ImageJ. The percentage of pelleted protein is calculated relative to the total amounts of the corresponding protein in the supernatant and pellet.

Fluorescent microscopy analysis of actin bundling by vinculin oligomers.

HV and HV-CC were labeled using BodipyTM FL NHS Ester (Succinimidyl Ester) (ThermoFisher, D2184) following the manufacturer's instruction. Actin was fluorescently labeled with AlexaFluor 594 Succinimidyl Ester as previously described (Ciobanasu, Faivre et al. 2015). To immobilize protein on beads, 30 μ ls of 1 μ m-diameter red Fluorospheres (Molecular Probes, F8887) were incubated with 2 μ M GST-AVBS1-3, GST-AVBS1-2 or GST as a control in 200 μ l PBS for 120 min with end-over-end rolling at 4°C. Beads were washed three-times by successive centrifugation for 2 min at 14,000 g and resuspension in 200 μ l PBS. 100 nm-diameter red Fluorospheres were coated with 2 μ M of talin H1-H4 (Papagrigoriou, Gingras et al. 2004) using a similar procedure. For each sample, 30 μ l of the coated-bead suspension were centrifuged 2 min at 14,000 g, the supernatant was discarded and pelleted beads were resuspended in F-actin buffer containing 3.5 μ M actin, 1.5 μ M AlexaFluor 594 -labeled actin, and HV or HV-CC at 1 μ M final concentration in a total volume of 10 μ l. Samples were incubated for 15 min at 21°C, Phalloidin AlexaFluor 594 (Thermofisher, A12831) was added at a final concentration of 100 nM and incubation was allowed to proceed for another 45 min. Samples were mixed with

DAKO mounting medium (DAKO, S3023), placed on a slide and covered by a 22 x 22 mm coverslip. Samples were analyzed using a Leica SP8 confocal microscope using a 63 x oil immersion objective, at an image resolution of 2048 x 2048, zoom 4.

Data analysis

The identification of cross-linked peptides from LC-MS data was performed using SIM-XL v. 1.3 (Lima, de Lima et al. 2015), with the following search parameters: EDC as cross-linker, a tolerance of 20 ppm for precursor and fragment ions, trypsin fully specific digestion with up to three missed cleavages. Carbamidomethylation of cysteines was considered as a fixed modification. All initial identification of cross-linked peptides required a primary score of SIM-XL greater than 2.5 for inter-links and 2.0 for intra-links or loop-links. As single incorrect cross-link identification might lead to a different model, a manual post-validation of the search engine results at the MS2 level was thus performed. A 2D-map showing the protein-protein interaction was generated as an output (Figs. 2a,b). Only peptides present in the 2 replicates are gathered in Supplementary Tables 1-3 and were used for the modeling.

Modeling

We used the distance constraints obtained from cross-linking MS data (Suppl. Tables 1-3) to guide the protein structure modeling using the TX-MS protocol as described by Hauri, Khakzad et al. (Hauri, Khakzad et al. 2019). In short, TX-MS uses the Rosetta comparative modeling protocol (RosettaCM) (Song, DiMaio et al. 2013), and the flexible backbone docking protocol (RosettaDock) (Gray 2006) to generate models and evaluate how well each model explains the MS constraints using a novel scoring function. Here, a total of 100,000 models was generated, of which the highest-scoring

model is displayed in (Fig. 3c), supported by a total of 100 inter and intra-molecular cross-links.

TIRF (Total Internal Reflection Microscopy) analysis

C2.7 cells were transfected with pmCherry-vinculin or pmCherry-VASP and the indicated plasmids as described above. Samples were mounted onto a TIRF microscopy chamber on a stage of an Eclipse Ti inverted microscope (Nikon) equipped with an Apo TIRF 100 x N.A. 1.49 oil objective heated at 37°C. TIRF analysis was performed using the Roper ILAS module and an Evolve EM-CCD camera (Roper Scientific Instruments). When mentioned, Y-27632 was used at 100 μ M. Image acquisition was performed every 12.5 seconds for 30 to 90 minutes.

Invasion assays

Tissue culture Transwell inserts (8 μ m pore size; Falcon, Franklin Lakes, NJ) were coated for 3 hours with 10 μ g of Matrigel following the manufacturer's instructions (Biocoat, BD Biosciences, San Jose, CA). Inserts were placed into 24-well dishes containing 500 μ l of RPMI medium supplemented with 1% fetal calf serum. 5×10^4 melanoma cells were added to the upper chamber in 250 μ l of serum-free RPMI medium. After 24 hours, transmigrated cells were scored by bright field microscopy. Experiments were performed at least three times, each with duplicate samples.

QUANTIFICATION AND STATISTICAL ANALYSIS

Vinculin clusters induced by AVBS1-2- and AVBS1-3-coated beads were analyzed using the ImageJ 2.1.0/1.53c software. Briefly, for each set of experiments, sum projection images of confocal planes were thresholded using identical parameters between samples. Clusters were detected using the “Analyze particle” plug-in, setting

a minimal size of 570 nm². The vinculin cluster integrated fluorescence density was arbitrarily expressed as the percent of the mean integrated fluorescence density determined for vinculin clusters induced by GST-coated beads (Fig. 2) or AVBS1-2-coated beads (Fig.3).

Quantification of vinculin recruitment at the close vicinity of invading bacteria was performed on the sum projection of confocal planes corresponding to *Shigella*-induced actin foci. ROIs were drawn to delineate the actin foci (F) and the bacterial body (b) from the corresponding wavelength channel as shown in Fig. S1. The vinculin recruitment index was calculated as the ratio of the average fluorescence intensity corresponding to vinculin labeling associated with (b) corrected to background over that of (F). For the quantification of the number and size of large adhesion structures induced by *Shigella* invasion in HeLa cells, the confocal fluorescent microscopy plane corresponding to the vinculin-labeled cell basal plane was processed using the imageJ FFT / Bandpass followed by particle analysis plugins with a low size threshold set at 3.54 μm². A semi-automated protocol using Icy software was developed for the quantification of adhesion structures in C2.7 cells (de Chaumont, Dallongeville et al. 2012). Confocal fluorescent microscopy planes were used to detect vinculin structures using HK means thresholding and overlaid binary masks obtained from the threshold projections of F-actin labeled images (Max-entropy method). FAs were detected as spots positive for both vinculin mCherry and actin structures using Wavelet Spot Detector. The number of adhesions was analyzed using Dunn's multiple comparisons test. The statistical analysis of cell motility was

performed in the R software. Medians were compared using a Wilcoxon rank sum test and dispersion by Median absolute dispersion (MAD) parameter.

KEY RESOURCES TABLE

REAGENT or RESOURCE	SOURCE	IDENTIFIER
Antibodies		
Vin11.5	Sigma-Aldrich	ref. V4505
Polyclonal anti- <i>Shigella</i> serotype V lipopolysaccharide	Valencia-Gallardo et al., 2019	
Bacterial and virus strains		
<i>Shigella flexneri</i> serotype V	Valencia-Gallardo et al., 2019	M90T
<i>Shigella flexneri</i> serotype V <i>ipaA</i> mutant	Valencia-Gallardo et al., 2019	M90T <i>ipaA</i>
Biological samples		
Non applicable		
Chemicals, peptides, and recombinant proteins		
N-hydroxysulfosuccinimide	MERCK	106627-54-7
1-ethyl-3-carbodiimide hydrochloride	Sigma-Aldrich	25952-53-8
N-ethylmaleimide	Sigma-Aldrich	128-53-0
dithiothreitol	Sigma-Aldrich	16096-97-2
PEG-Mal	Sigma-Aldrich	63187
Bodipy TM FL NHS Ester	ThermoFisher	D2184
Y-27632	Sigma-Aldrich	129830-38-2
Critical commercial assays		
Non applicable		
Deposited data		
Non applicable		
Experimental models: Cell lines		
HeLa cells	ATCC	ATCC CCL-2
C2.7 cells	Mitrossilis et al., 2009	
MEF vinculin null cells	Humphries, Wang et al. 2007	
Experimental models: Organisms/strains		
Non applicable		
Oligonucleotides		
5' GCGCATATGCCAGTGTTCATACG-3'	This study	vD1 For
5'-CGTCGACTCACCAGGCATCTTCATCGGC-3'	This study	vD1 Rev
5'-CGTCGACTCAGTGTACAGCTGCTTTG-3'	This study	vD2 Rev
5'-GAGACTGTTCAAACCACTGAGGATTGCATTTTGAAG-3'	This study	HV-Q68C mut

5'- ATCGATGCTGCTCAGAACTGGCTTTGCGAT CCAAAT-3'	This study	HV-A396C mut
5'-ACCCGGGATCCCGCC-3'	This study	GFP-vD1 For
5'-ACCCGGGACCAGGCA-3'	This study	GFP-vD1 Rev
5'-TCAAAGGACATTACAAAATCC-3'	This study	GFP-AVBS1-2 For
5'-GCGATATCATGGCCAGCAAAGG-3'	This study	GFP-AVBS1-3 For
5'- GCGCGGCCGCTTAATCCTTATTGATATTC- 3'	This study	GFP-AVBS Rev
5'- GGCGAATCCCGGAGACACATATTTAACA CG-3'	This study	GST-AVBS1-3 For
5'- GCCGTCGACTTAATCCTTATTGATATTCT- 3'	This study	GST-AVBS1-3 Rev
5'-ACCCGGGATCCCGCC-3'	This study	GFP-vD1 For
5'-ACCCGGGACCAGGCA-3'	This study	GFP-vD1 Rev
Recombinant DNA		
pET15b-D1	This study	
pET15b-D1D2	This study	
pET15b-D1D2-CC	This study	
pGFP-vD1	This study	
pmCherry N1-HV-CC	This study	
pGFP-AVBS1-2	This study	
pGFP-AVBS1-3	This study	
pGST-AVBS1-2	Ramaro et al., 2007	
pGST-AVBS1-3	This study	
pC1-HV8His	This study	
pC1HV-CC8His	This study	
pmCherry-human vinculin	Addgene	
pmCherry-VASP	Addgene	
Software and algorithms		
Icy	De Chaumont et al., 2012	
Rosetta modeling	Song et al., 2013	
RosettaDock	Gray, 2006	
ASTRA 6.1.7.17	Wyatt Technology Europe	
Other		
Non applicable		

Suppl. movie 1. TIRF analysis of vinculin-mCherry expressing C2.7 cells co-transfected with a GFP fusion to the indicated construct. The time is indicated in seconds.

Suppl. movie 2. TIRF analysis of vinculin-mCherry expressing C2.7 cells co-transfected with a GFP fusion to the indicated construct. The time is indicated in seconds. At time "0", addition of the Rho kinase inhibitor Y-27632 was added at 100 μM final concentration.

Suppl. movie3. TIRF analysis of VASP-mCherry expressing C2.7 cells co-transfected with a GFP fusion to the indicated construct. The time is indicated in seconds. At time "0", addition of the Rho kinase inhibitor Y-27632 was added at 100 μM final concentration.

Suppl. Movie 4. 1205Lu melanoma cells 1205Lu melanoma cells were transfected with the indicated constructs. Cells were perfused in a microfluidic chamber and allowed to adhere for 20 min prior to application of shear stress reaching 22.2 dynes.cm⁻². The elapsed time is indicated in seconds.

REFERENCES

- Atherton, P., B. Stutchbury, D.Y. Wang, D. Jethwa, R. Tsang, E. Meiler-Rodriguez, P. Wang, N. Bate, R. Zent, I.L. Barsukov, B.T. Goult, D.R. Critchley and C. Ballestrem (2015). "Vinculin controls talin engagement with the actomyosin machinery". *Nat. Commun.* **4**;6:10038. doi: 10.1038/ncomms10038.
- Bakolitsa, C., D. M. Cohen, L. A. Bankston, A. A. Bobkov, G. W. Cadwell, L. Jennings, D. R. Critchley, S. W. Craig and R. C. Liddington (2004). "Structural basis for vinculin activation at sites of cell adhesion." *Nature* **430**(6999): 583-586.
- Boujemaa-Paterski, R., B. Martins, M. Eibauer, C. Beales, B. Geiger and O. Medalia (2020). "Talin-activated vinculin interacts with branched actin networks to initiate bundles." *eLife* **9**: e53990.
- Braakman, I., Lamriben, L., van Zadelhoff, G., & Hebert, D. N. (2017). Analysis of disulfide bond formation. *Current Protocols in Protein Science*, 90, 14.1.1–14.1.22. doi: 10.1002/cpps.43.
- Carisey, A., R. Tsang, A. M. Greiner, N. Nijenhuis, N. Heath, A. Nazgiewicz, R. Kemkemer, B. Derby, J. Spatz and C. Ballestrem (2013). "Vinculin regulates the recruitment and release of core focal adhesion proteins in a force-dependent manner." *Curr Biol* **23**(4): 271-281.
- Changede, R. and M. Sheetz (2017). "Integrin and cadherin clusters: A robust way to organize adhesions for cell mechanics." *Bioessays* **39**(1): 1-12.
- Chinthalapudi, K., E. S. Rangarajan, D. N. Patil, E. M. George, D. T. Brown and T. Izard (2014). "Lipid binding promotes oligomerization and focal adhesion activity of vinculin." *J Cell Biol* **207**(5): 643-656.
- Ciobanasu, C., B. Faivre and C. Le Clainche (2014). « Actomyosin-dependent formation of the mechanosensitive talin-vinculin complex reinforces actin anchoring ». *Nat. Commun.* **5**: 3095. doi: 10.1038/ncomms4095.
- Ciobanasu, C., B. Faivre and C. Le Clainche (2015). "Reconstituting actomyosin-dependent mechanosensitive protein complexes in vitro." *Nat. Protoc.* **10**: 75-89.
- de Chaumont, F., S. Dallongeville, N. Chenouard, N. Herve, S. Pop, T. Provoost, V. Meas-Yedid, P. Pankajakshan, T. Lecomte, Y. Le Montagner, T. Lagache, A. Dufour and J. C. Olivo-Marin (2012). "Icy: an open bioimage informatics platform for extended reproducible research." *Nat Methods* **9**(7): 690-696.
- del Rio, A., R. Perez-Jimenez, R. Liu, P. Roca-Cusachs, J. M. Fernandez and M. P. Sheetz (2009). "Stretching single talin rod molecules activates vinculin binding." *Science* **323**(5914): 638-641.

- Eubel, H. and A. H. Millar (2009). "Systematic monitoring of protein complex composition and abundance by blue-native PAGE." Cold Spring Harb Protoc **2009**(5): pdb prot5221.
- Gray, J. J. (2006). "High-resolution protein-protein docking." Curr Opin Struct Biol **16**(2): 183-193.
- Gutierrez, E., B. G. Petrich, S. J. Shattil, M. H. Ginsberg, A. Groisman and A. Kasirer-Friede (2008). "Microfluidic devices for studies of shear-dependent platelet adhesion." Lab Chip **8**(9): 1486-1495.
- Hauri, S., H. Khakzad, L. Happonen, J. Teleman, J. Malmstrom and L. Malmstrom (2019). "Rapid determination of quaternary protein structures in complex biological samples." Nat Commun **10**(1): 192.
- Humphries, J. D., P. Wang, C. Streuli, B. Geiger, M. J. Humphries and C. Ballestrem (2007). "Vinculin controls focal adhesion formation by direct interactions with talin and actin." J Cell Biol **179**(5): 1043-1057.
- Izard, T., G. Evans, R. A. Borgon, C. L. Rush, G. Bricogne and P. R. Bois (2004). "Vinculin activation by talin through helical bundle conversion." Nature **427**(6970): 171-175.
- Izard, T., G. Tran Van Nhieu and P. R. Bois (2006). "*Shigella* applies molecular mimicry to subvert vinculin and invade host cells." J Cell Biol **175**(3): 465-475.
- Janssen, M. E., E. Kim, H. Liu, L. M. Fujimoto, A. Bobkov, N. Volkmann and D. Hanein (2006). "Three-dimensional structure of vinculin bound to actin filaments." Mol Cell **21**(2): 271-281.
- Johnson, R. P. and S. W. Craig (2000). "Actin activates a cryptic dimerization potential of the vinculin tail domain." J Biol Chem **275**(1): 95-105.
- Karimi, F., A. J. O'Connor, G. G. Qiao and D. E. Heath (2018). "Integrin Clustering Matters: A Review of Biomaterials Functionalized with Multivalent Integrin-Binding Ligands to Improve Cell Adhesion, Migration, Differentiation, Angiogenesis, and Biomedical Device Integration." Adv Healthc Mater **7**(12): e1701324.
- Kluger, C., L. Braun, S. M. Sedlak, D. A. Pippig, M. S. Bauer, K. Miller, L. F. Milles, H. E. Gaub and V. Vogel (2020). "Different Vinculin Binding Sites Use the Same Mechanism to Regulate Directional Force Transduction." Biophys J **118**(6): 1344-1356.
- Lavelin, I., H. Wolfenson, I. Patla, Y. I. Henis, O. Medalia, T. Volberg, A. Livne, Z. Kam and B. Geiger (2013). "Differential effect of actomyosin relaxation on the dynamic properties of focal adhesion proteins." PLoS One **8**(9): e73549.
- Lima, D. B., T. B. de Lima, T. S. Balbuena, A. G. C. Neves-Ferreira, V. C. Barbosa, F. C. Gozzo and P. C. Carvalho (2015). "SIM-XL: A powerful and user-friendly tool for peptide cross-linking analysis." J Proteomics **129**: 51-55.

- Margadant, F., L. L. Chew, X. Hu, H. Yu, N. Bate, X. Zhang and M. Sheetz (2011). "Mechanotransduction in vivo by repeated talin stretch-relaxation events depends upon vinculin." PLoS Biol **9**(12): e1001223.
- Mattock, E. and A. J. Blocker (2017). "How Do the Virulence Factors of *Shigella* Work Together to Cause Disease?" Front Cell Infect Microbiol **7**: 64.
- Mege, R. M. and N. Ishiyama (2017). "Integration of Cadherin Adhesion and Cytoskeleton at Adherens Junctions." Cold Spring Harb Perspect Biol **9**(5).
- Mitrossilis, D., J. Fouchard, A. Guiroy, N. Desprat, N. Rodriguez, B. Fabry and A. Asnacios (2009). "Single-cell response to stiffness exhibits muscle-like behavior." Proc Natl Acad Sci U S A **106**(43): 18243-18248.
- Molony, L. and K. Burridge (1985). "Molecular shape and self-association of vinculin and metavinculin." J Cell Biochem **29**(1): 31-36.
- Ogawa, M., Y. Handa, H. Ashida, M. Suzuki and C. Sasakawa (2008). "The versatility of *Shigella* effectors." Nat Rev Microbiol **6**(1): 11-16.
- Pant, K. D., Oh, S., & Mysore, K.S. (2021). Protocol for determining protein cysteine thiol redox status using western blot analysis. STAR Protocols, Volume 2, Issue 2, 100566, ISSN 2666-1667.
- Papagrigoriou, E., A. R. Gingras, I. L. Barsukov, N. Bate, I. J. Fillingham, B. Patel, R. Frank, W. H. Ziegler, G. C. Roberts, D. R. Critchley and J. Emsley (2004). "Activation of a vinculin-binding site in the talin rod involves rearrangement of a five-helix bundle." EMBO J **23**(15): 2942-2951.
- Park, H., C. Valencia-Gallardo, A. Sharff, G. Tran Van Nhieu and T. Izard (2011). "Novel vinculin binding site of the IpaA invasin of *Shigella*." J Biol Chem **286**(26): 23214-23221.
- Parsons, J. T., A. R. Horwitz and M. A. Schwartz (2010). "Cell adhesion: integrating cytoskeletal dynamics and cellular tension." Nat Rev Mol Cell Biol **11**(9): 633-643.
- Ramarao, N., C. Le Clainche, T. Izard, R. Bourdet-Sicard, E. Ageron, P. J. Sansonetti, M. F. Carlier and G. Tran Van Nhieu (2007). "Capping of actin filaments by vinculin activated by the *Shigella* IpaA carboxyl-terminal domain." FEBS Lett **581**(5): 853-857.
- Romero, S., G. Grompone, N. Carayol, J. Mounier, S. Guadagnini, M. C. Prevost, P. J. Sansonetti and G. T. Van Nhieu (2011). "ATP-mediated Erk1/2 activation stimulates bacterial capture by filopodia, which precedes *Shigella* invasion of epithelial cells." Cell Host Microbe **9**(6): 508-519.
- Shen, K., C. E. Tolbert, C. Guilluy, V. S. Swaminathan, M. E. Berginski, K. Burridge, R. Superfine and S. L. Campbell (2011). "The vinculin C-terminal hairpin mediates F-actin bundle formation, focal adhesion, and cell mechanical properties." J Biol Chem **286**(52): 45103-45115.

Shevchenko, A., H. Tomas, J. Havlis, J. V. Olsen and M. Mann (2006). "In-gel digestion for mass spectrometric characterization of proteins and proteomes." Nat Protoc **1**(6): 2856-2860.

Smalley, K. S., M. Lioni, M. Dalla Palma, M. Xiao, B. Desai, S. Egyhazi, J. Hansson, H. Wu, A. J. King, P. Van Belle, D. E. Elder, K. T. Flaherty, M. Herlyn and K. L. Nathanson (2008). "Increased cyclin D1 expression can mediate BRAF inhibitor resistance in BRAF V600E-mutated melanomas." Mol Cancer Ther **7**(9): 2876-2883.

Song, Y., F. DiMaio, R. Y. Wang, D. Kim, C. Miles, T. Brunette, J. Thompson and D. Baker (2013). "High-resolution comparative modeling with RosettaCM." Structure **21**(10): 1735-1742.

Thompson, P. M., C. E. Tolbert and S. L. Campbell (2013). "Vinculin and metavinculin: oligomerization and interactions with F-actin." FEBS Lett **587**(8): 1220-1229.

Tran Van Nhieu, G. and T. Izard (2007). "Vinculin binding in its closed conformation by a helix addition mechanism." EMBO J **26**(21): 4588-4596.

Valencia-Gallardo, C., C. Bou-Nader, D. I. Aguilar-Salvador, N. Carayol, N. Quenech'Du, L. Pecqueur, H. Park, M. Fontecave, T. Izard and G. Tran Van Nhieu (2019). "*Shigella* IpaA Binding to Talin Stimulates Filopodial Capture and Cell Adhesion." Cell Rep **26**(4): 921-932 e926.

Valencia-Gallardo, C. M., N. Carayol and G. Tran Van Nhieu (2015). "Cytoskeletal mechanics during *Shigella* invasion and dissemination in epithelial cells." Cell Microbiol **17**(2): 174-182.

ARTICLE 2

Polar interactions determine head domain-mediated vinculin oligomerization induced by *Shigella* IpaA

SUMMARY:

Vinculin is a protein associated to reinforce integrin adhesion structures. The protein's D1 and D5 subdomains have been extensively studied for its binding capacity to VBSs and F-actin, respectively, where two pulling forces act on vinculin at the same time (force-dependent activation) and can induce specific conformational changes on vinculin. However, *Shigella's* IpaA effector protein could mimic those changes and this way of vinculin activation is designated as the force-independent activation model. Previous findings of the effects of *Shigella's* IpaA-VBSs interacting with vinculin's D1D2 subunits, showed the induction of conformational changes in solution on the D1D2 subunits (as observed in structural modeling from those proteins forming complexes), and cells transfected with the IpaA-VBSs formed stable adhesions resistant to acto-myosin relaxation treatment. In this work, we found that single residue substitution at the surface on D1 and D2 altered the capacity of the protein to form oligomeric complexes with IpaA-VBSs as shown by biochemical assays. This suggests that D1D2 contact regions participate in maintaining the structural integrity and interdomain interactions during force dependent conformational changes. As suggested by the altered size and shape of Focal Adhesions on cells transfected with non-canonical D1 or D2 full length vinculin variants suggests. Then, the vinculin "head" domain might be involved in a mechanosensitive activation of the protein instead of involving an active-inactive state, as previously reported in studies targeting the D1-D5 interaction

ARTICLE 2

Polar interactions determine head domain-mediated vinculin oligomerization induced by *Shigella* IpaA

Benjamin COCOM-CHAN¹⁻³, Hamed KHAKZAD¹⁻³, Cesar VALENCIA-GALLARDO¹⁻³, Yosra ZARROUK¹⁻³, Guy TRAN VAN NHIEU^{1-3*}

¹Team “Ca²⁺ signaling and Microbial Infections”, I2BC, 91190 Gif-sur-Yvette, France.

²Institut National de la Santé et de la Recherche Médicale U1282, 91190 Gif-sur-Yvette, France.

³Centre National de la Recherche Scientifique UMR9198, 91190 Gif-sur-Yvette, France.

* correspondance : guy.tranvannhieu@i2bc.paris-saclay.fr

Running title: IpaA-induced head domain-vinculin oligomerization

Keywords: *vinculin; head domain; oligomerization; cell adhesion*

Abstract

Vinculin is a component of focal adhesions strengthening integrin receptors association to the actin cytoskeleton during mechanotransduction. While vinculin activation leading to its association with actin filaments has been particularly studied, the role and mechanism of vinculin oligomerization remain unclear. The *Shigella* IpaA effector binds to vinculin to promote efficient bacterial invasion of host cells. Unlike canonical activating ligand, IpaA interacts with the vinculin subdomains D1 and D2 via its three Vinculin Binding Sites (VBSs), promoting major allosteric changes leading to D1D2 domain-mediated trimerization. Here, we built on structural models of allosteric conformers of D1D2:IpaA complexes to design mutations and analyzed their effects on IpaA-induced trimer formation using native gel shift assays. We show that charge inversions or affecting polar interactions at residues in D1D2 interfacing IpaA VBS3, or targeting a distal putative coiled-coil motif in D2 reduced the rates of D1D2 trimer formation. Introduction of these mutations in full length vinculin led to a decrease in the number and size of focal adhesions, with distinct elongated focal adhesions associated with the coiled-coil mutation. These findings suggest that IpaA hijacks a cell endogenous head-domain mediated vinculin oligomerization process involved in the maturation of focal adhesion.

I performed the experiments and generated all the data related to this work, with the exception of the SEC analysis in Figure 1A.

Introduction

Vinculin is a cytoskeletal linker of integrin-mediated matrix adhesions as well as cadherin-based cell-cell junctions (Goldman, 2016; Bays and De Mali, 2017). It plays an important role in cell adhesion processes, motility and development and its functional deficiency is associated with major diseases including cancer and cardiomyopathies (Peng et al., 2011). Vinculin associates with a number of ligands, including focal adhesion and intercellular junction components, lipids, signaling proteins as well as proteins regulating the organization and dynamics of the actin cytoskeleton (Goldman, 2016; Bays and De Mali, 2017). The role of vinculin in integrin-mediated adhesion has been particularly studied (Atherton et al., 2016; Parsons et al., 2010). Vinculin is recruited at focal adhesions and reinforces the link between integrins and the actin cytoskeleton. The extent of vinculin recruitment determines the growth and maturation of focal adhesions, associated with the scaffolding of adhesion components and mechanotransduction linked to the actomyosin contraction (Atherton et al., 2016; Parsons et al., 2010). While the precise mechanisms leading to vinculin activation potentially involving combinatorial stimulation and recruitment at focal adhesions inside cells are not fully understood, *in vitro* biomimetic mechanical and structure-function studies have enlightened major aspects of the role of vinculin in cell adhesion (Yan et al., 2015).

Vinculin is classically described as a three-domain protein containing an aminoterminal globular head domain (Vh), a flexible linker domain, and a F-actin -binding tail domain (Vt). Vh contains three subdomains D1-D3 and a half-subdomain D4. Each subdomain corresponds to conserved repeats and consists of two four/five helix bundles connected by a long alpha-helix (Goldman, 2016). At the inactive state, vinculin is maintained folded by intramolecular interactions between Vh and Vt. All ligands activating vinculin contain a vinculin binding site (VBS), corresponding to 20-25 residues structured into an amphipathic α -helix that interacts with the first helix-bundle of D1 (Gingras et al., 2005). Insertion of the activating VBS in the D1 first helix bundle leads to the reorganization of the bundle and destabilizes the interaction between D1 and Vt (Izard et al., 2004). More than 70 VBSs or predicted VBSs have been identified in the various

vinculin ligands, often containing multiple VBSs (Kluger et al., 2020). These VBSs, however, are often buried into helix bundles and their exposure regulates vinculin activation (Kluger et al., 2020). Force-induced stretching of a vinculin ligand such as talin, acting as mechanosensor, provides with a means to expose the VBSs during integrin-mediated adhesion (Sun et al., 2016; Goult et al., 2021). Talin binds to F-actin via at least two sites in its rod domain and to integrin cytoplasmic domains via its amino-terminal FERM domain. During mechanotransduction, talin stretching by the actomyosin contraction exposes vinculin binding sites (VBSs) that are buried in helix bundles of the rod domain in the native state (Yan et al., 2015). Exposed talin VBSs in turn bind to vinculin and relieve the intramolecular interactions between the vinculin head (Vh) and tail (Vt) domains, unveiling the F-actin-binding site in Vt (Goult et al., 2021). Since talin contains 11 VBSs in helix bundles unfolding at different force amplitudes, the stretching force-dependent interaction between talin and vinculin serves as a mechanism to strengthen actin cytoskeletal anchorage as a function of substrate stiffness (Yan et al., 2015; Yao et al., 2016). While in vitro, vinculin interaction with a VBS is sufficient to promote its opening and interaction with F-actin, vinculin activation in cells may result from a combinatorial stimulus including interaction with phosphatidylinositol (4,5)-biphosphate (PIP₂) or phosphorylation (Izard and Brown, 2016; Aurnheimer et al., 2015).

Intracellular bacterial pathogens such as *Chlamydia*, *Rickettsia*, and *Shigella* express ligands diverting vinculin functions to promote virulence (Thwaites et al., 2015; Park et al., 2011; Valencia-Gallardo, 2015). Among these, the *Shigella* type III effector IpaA was shown to target vinculin via three VBSs present at its carboxyterminal domain (Valencia-Gallardo, 2015). Unlike other host cell endogenous VBSs, IpaA VBSs are not buried into helix bundles and therefore likely act in concert to promote bacterial invasion. IpaA VBS1 and VBS2 bind to the first and second bundles of D1, respectively, conferring binding to vinculin with a very high affinity and the IpaA property to act a “super-mimic” of endogenous activating VBSs (Izard et al., 2006; Tran Van Nhieu and Izard, 2007). The role of IpaA VBS3 appears more complex and likely underline the role of IpaA in different processes during bacterial invasion. In addition to

vinculin, IpaA VBS3 also binds to talin and may stabilize a partially stretched talin conformer present in filopodial adhesions, thereby favoring bacterial capture by filopodia at initial stages of the bacterial invasion process (Park et al., 2011; Valencia-Gallardo et al., 2019). IpaA VBS3 was also shown to bind to the vinculin D2 subdomain, when IpaA VBSs 1-2 are bound to D1 (Valencia-Gallardo et al., 2022). Binding of IpaA VBS1-3 to D1D2 trigger major conformational changes, coined “supra-activation”, leading to D1D2 homo-oligomerization via the D1D2 head subdomains and the formation of D1D2 trimers (Valencia-Gallardo et al., 2022). IpaA-induced vinculin “supra-activation” enables invasive *Shigella* to promote strong adhesion in the absence of mechanotransduction (Valencia-Gallardo et al., 2022). However, analysis of defects a vinculin cysteine-clamp variant, deficient for vinculin supra-activation while still proficient for canonical activation, suggests that vinculin head domain oligomerization also occurs during mechanotransduction and is required for vinculin-dependent actin bundling and the maturation of focal adhesions into large adhesion structures (Valencia-Gallardo et al., 2022).

While seminal studies based on rotary shadow electron microscopy analysis reported the formation of vinculin mediated by Vh-Vh as well as Vt-Vt interactions in vitro, studies on vinculin oligomerization have essentially focused on Vt-Vt interactions (Molony and Burridge, 1985). Phosphatidylinositol (4, 5) bisphosphate (PIP₂) binding to vinculin was shown to promote vinculin oligomerization and PIP₂-binding deficient vinculin showed defects in the organization of the actin cytoskeleton, as well as increased turn-over of focal adhesions (Bakolitsa et al., 1999; Chinthalapudi et al., 2014). Binding of F-actin was also reported to induced the formation of vinculin tail dimers, likely different than those induced by PIP₂, and mutants in the Vt C-terminal hairpin responsible for F-actin-induced dimerization showed defects in actin bundling associated with a decrease in size and number of focal adhesions (Johnson and Craig, 2000; Bakolitsa et al., 1999). Vinculin establishes catch bond with a significantly increased lifetime when the force was applied towards the pointed end of actin filaments, consistent with the polarity of actomyosin contraction (Huang et al., 2017). However, while mechanotransduction triggers vinculin recruitment associated with the

maturation, enlarging of focal adhesions and actin bundling, how Vt-mediated vinculin oligomerization may be regulated by to actomyosin contraction remains unclear (Thompson et al., 2013). Vinculin head-domain (Vh) mediated oligomerization could provide with a force-dependent mechanism, since vinculin was reported to acts as a mechanosensor, with its head domain undergoing conformational changes under applied force, showing increased binding to ligand such as MAPK1 (Garakni et al., 2017). Here, we report the effects of mutation in vinculin D1D2 altering the formation of trimers induced by IpaA. We identified D1D2 polar residues predicted to contact IpaA VBS3 and showed their involvement in IpaA-induced trimerization. We show that these mutations affect the formation of focal adhesions supporting the notion that Vh-Vh mediated vinculin oligomerization akin to that induced by *Shigella* IpaA also occurs during the maturation of cell adhesion structures.

Results

Design of mutations in D1D2 affecting IpaA-induced trimer formation

The modeled structures indicated that the IpaA VBS3 interacted with D2 and triggers a reorganization of the D1 and D2, where the major axis of these subdomains undergoes a 30 % angle displacement relative to the apo D1D2 or D1D2 in complex with IpaAVBS1-2 only (Fig. 1B, Valencia-Gallardo et al., 2022). This “open” D1D2 conformer is associated with D1D2-mediated trimerization of vinculin (ref), since IpaA VBS1-2 was found to form D1D2:IpaA 1:1 and 2:0-2:1 complexes, while IpaA VBS1-3 also triggered the formation of 3:0-3:1 complexes (Valencia-Gallardo et al., 2022). We hypothesized that IpaA VBS3 induced allosteric changes led to the exposition of a domain in D1D2 responsible for trimerization* and that mutations in D2 at residues interfacing IpaA VBS3 should affect trimer formation. To test this, we scrutinized interfacing residues between IpaA VBS3 and D1D2 in the D1D2:IpaA VBS1-3 conformers.



As shown in Fig. 1B, in the close D1D2:IpaA conformer, the IpaA VBS3 helix mostly interacts with the H10 long helix of D2. We could identify a set of putative polar

interactions and salt bridges, with IpaA residues T492, E495, K499 and S503 interacting with vinculin residues N393, K139, D389 and K386, respectively (Fig. 1C). In the open conformer, the IpaA VBS3 helix mainly interacts with the H4 long helix of D1, with IpaA residue K499 interacting with vinculin E243. Of note, in this open conformer, an electrostatic clash between vinculin K139 and IpaA K499 may contribute to the dynamics of the IpaA VBS3 during its interaction with different allosteric conformers leading to D1D2 oligomerization (Fig. 1D). All identified vinculin residues were substituted for a charged residue to introduce a charge inversion or disrupt polar interactions using site directed mutagenesis (Materials and Methods, Table 1). We also introduced a mutation at vinculin residue N379 in H10 of D2 that is not expected to establish contact with IpaA VBS3 in the close or open conformer. In this rationale, mutations affecting IpaA VBS3's interface with the close D1D2 conformer are expected to alter its initial docking of IpaA VBS3 on D1D2, whereas the E143K charge inversion would destabilize the open conformer and alter subsequent allosteric changes leading to trimer formation.

Independent of the IpaA VBS3-D1D2 interface, the hidden Markov model-based algorithm MARCOIL predicts the presence of a coiled-coil domain in the same H10 D2 helix between vinculin residues 348 to 393, buried into the D2 helix bundles and adjacent to the IpaA VBS3 interaction sites in the close D1D2 conformer (Fig. S1). This putative coiled-coil domain contains the classical a-g heptad sequence at residues 367-373, with the V367 and A373 corresponding to the “a” and “d” hydrophobic residues, respectively, presumed to intersperse their non-polar side chains at the α -helices interfaces during oligomerization. In our working model, interaction between IpaA VBS3 with D1D2 reveals an oligomerization domain present in D1D2 responsible for trimerization (Valencia-Gallardo et al., 2022), which could involve this putative coiled-coil domain. To test the role of this domain in D1D2 trimerization, we introduced the V367D substitution predicted to disrupt supercoiled helix packing (Fig. S1).

Quantitative analysis of D1D2 trimer formation using CN-PAGE

In previous works, we showed that IpaA induced the formation of D1D2:IpaA 1:1, as well as dimeric complexes and trimeric D1D2 complexes rapidly associating and dissociating an IpaA molecule in SEC-MALS experiments (Valencia-Gallardo et al., 2022). Here, we studied the effects of increasing IpaA molar ratio using SEC and CN-PAGE. As shown in Fig. 2, at a D1D2:IpaA 1:1 molar ratio, the major peaks with similar amplitude corresponded to the 1:0 and likely the D1D2 trimeric complexes (Fig. 2A, peaks A and C). At a D1D2:IpaA 1:1.5 molar ratio, the D1D2 trimeric complexes represented the major peak (Fig. 2A, peak A). Upon increasing of IpaA molar ratio, a major shifted band (Fig. 2B, A') could also be observed in CN-PAGE followed by Coomassie blue staining, with apo D1D2 rapidly disappearing (Fig. 2B, C') and the formation of intermediate shifted bands (Fig. 2B). The similarity between the distribution of the bands with increasing molar ratio of IpaA in CN-PAGE and the SEC peaks suggested that the A and A' peaks corresponded to trimeric D1D2 complexes. To confirm this, we dissected the A' band from CN-PAGE and analyzed it in a second dimension using regular SDS-PAGE (Materials and Methods) and compared the amounts of D1D2 and IpaA relative to those present in fractions from the SEC peak A. As shown in Fig. 2C, the relative amounts of D1D2 and IpaA were similar for both A and A' samples, with an estimated molar ratio of 3.8 and 3.2, respectively, both values being consistent with a mixture of D1D2:IpaA 3:0 and 3:1 complexes inferred from the SEC-MALS analysis (Valencia-Gallardo et al., 2022).

We used scanning densitometry, to determine the rates of D1D2 trimer formation and D1D2 monomer disappearance normalized to the initial amounts of D1D2 (Materials and Methods). As shown in Fig. 2D, the appearance of D1D2 trimers and disappearance of apo D1D2 as a function of increasing IpaA molar ratio could be nicely adjusted to linear fits with a Pearson coefficient $R^2 > 0.95$. The CN-PAGE assay was used to determine a rate of D1D2 trimer appearance of 1.51 AU^{-1}  **xx** (SEM), and D1D2 monomer disappearance of -1.06 AU^{-1}  **xx** (SEM).

Characterization of D1D2 mutations affecting trimer formation

We estimated that the CN-PAGE assay was sufficiently robust and reproducible to determine potential differences in rates of trimer formation in the various D1D2 variants. All mutations were introduced in D1D2 and the corresponding variants were purified to homogeneity (Fig. S2). Samples were incubated with increasing molar ratio of the IpaA vinculin-binding domain (aVBD) and analyzed by CN-PAGE followed by Coomassie staining (Materials and Methods). As shown in Figs. 3 and S3, the majority of mutants showed decrease rates of trimer formation (Figs. 3, S3 and Table 2). The rates of D1D2 trimer formation and monomer disappearance were then inferred from linear fits, following quantification by scanning densitometry.

As shown on Table 2, mutations could be distinguished in three types based on to their effects on the rates of D1D2 trimer formation and monomer disappearance. Mutations D389R, E143K and V367D showed delayed rates of D1D2 trimer formation, but no difference in D1D2 monomer disappearance. Mutations K386D, K386G and K139E showed delayed rates of D1D2 trimer formation, as well as increased rates in D1D2 monomer disappearance. The last type of mutations corresponding to N379E and N393D showed no significant effects on trimer formation, but increased rates in monomer disappearance. These results suggest a key role for a knot of polar and charge interactions associated with the D389, K386, and K139 vinculin residues adjacent to IpaA K499 in D1D2 trimerization. Vinculin residue E143 that affects D1D2 trimerization also potentially interacts with IpaA K499 in the open D1D2 conformer. The D389R and E143K charge inversions did not affect monomer disappearance, whereas other polar mutations with the exception of vinculin V367D targeting the coiled-coil domain led to increase rates of monomer disappearance. While difficult to explain, these results suggest a succession of allosteric interaction between IpaA VBS3 and D1D2 where salt bridges and polar interactions play distinct roles.

Of interest, the mutations in these vinculin residues D389R, E143K, K386D, K386G and K139E appear to also show a delay in the decrease of monomer disappearance for aVBD molar ratio inferior to 0.15 relative to that induced in wild-type D1D2 (Figs. 3 and S3), suggesting impairment of initial interaction steps between IpaA and D1D2. The

delayed rates of trimer formation associated with V367D also suggest a role for the potential coiled-coil domain. The absence of effects on the rates of D1D2 monomer disappearance for the D389R, E143K and V367D mutations is consistent with the impairment of steps subsequent to the D1D2 1:1 complex formation, involved in D1D2 dimerization or trimerization.

Effects of mutations impairing D1D2 trimerization on focal adhesions

Vinculin oligomerization has been mainly studied *in vitro* and reported to occur through the Vt-tail domain upon PIP₂ stimulation (Thomson et al., 2013). In cells, however, the role of vinculin oligomerization in cell adhesion structures remain unclear. Our studies using a cysteine clamp variant of vinculin deficient for head-domain mediated oligomerization suggest that this property is required for the maturation into large focal adhesions independent of *Shigella* IpaA (Valencia-Gallardo et al., 2022).

To further investigate the role of head domain-mediated vinculin oligomerization in cell adhesions, we transferred mutations altering D1D2 trimerization into full length vinculin fused to mCherry and studied the ability of the vinculin variants to form focal adhesions following transfection in MEF vinculin null cells (Materials and Methods). We studied mutations targeting the knot of polar interactions at the C-terminal extremity of the H10 helix in D2, involved in interaction with IpaA VBS3.

As shown in Fig. 4, cells expressing the D389R, E143 and V367D variants showed a strong spreading defect relative to cells expressing parental mCherry-vinculin, while no significant difference was observed for the K386D variant (Figs. 4A and 4B). These results correlated with a strong reduction of focal adhesions in the D389R, E143 and V367D variants with median numbers of FAs \pm SD / cell ranging from 45 \pm 5 to 64 \pm 8, compared to 110 \pm 11 for cells expressing parental vinculin (Figs. 4A and 4C). A reduction of the mean number of FAs per cell was also observed for the K386D variant, albeit of lesser amplitude (Figs. 4A and 4C). The decrease in FAs number per cell was also associated with a decrease in their average size in the D389R and E143K variants (Figs. 4A and 4D). We observed no significant decrease in the average FA size for the

K386D, consistent with a defect in cell adhesion of lesser amplitude for this latter variant relative to the D389R and E143K variants (Figs. 4A and 4D). Interestingly, the V367D variant also did not show a significant difference in the average FA size compared to control cells expressing parental mCherry-vinculin (Fig. 4D), despite a significant reduction in the number of FAs per cell. The FAs in the V367D variant, although similar in size, looked different than those in control cells, being mostly at the cell periphery and particularly elongated (Fig. 4A). This qualitative difference was confirmed by quantification of the AR index, showing a pronounced difference for the V367D variant compared to the other samples (Fig. 4E).

Discussion

In this work, we identified polar residues located at the C-terminal extremity of the H10 helix in vinculin D2 involved in D1D2 trimerization induced by *Shigella* IpaA. Among mutations reducing IpaA-induced D1D2 trimer formation, we identified the charge inversions at vinculin D389R and E143K that do not affect the rates of monomer disappearance, while the K386D/G polar mutations also led to increased rates of monomer disappearance. IpaA vinculin interaction is mediated by 3 VBSs, IpaA VBS1 and VBS2 interacting with the first and second bundle of D1, respectively. The high affinity of IpaA VBS1-2 to D1 is likely to drive the initial steps leading to the formation of a D1D2: IpaA 1:1 complex, independent of IpaA VBS3. From our modeled structures of the D1D2:IpaA 1:1 complexes, the vinculin D389R and E143K mutations are expected to disfavor IpaA VBS3 binding to the close and open D1D2 conformer, respectively. Hence, the effects of these mutations are in line with specific effects on IpaA VBS3 allosteric changes leading to D1D2 oligomerization without affecting formation of IpaA VBS1, 2-dependent 1:1 D1D2:IpaA complex.

The effects of the K386D/G mutations inversely affecting the rates of D1D2 trimer formation and monomer disappearance are more difficult to explain. There are two possible explanations to explain the increase rates of D1D2 monomer disappearance: i, these polar mutations may increase the rates of IpaA binding to D1D2. This possibility is unlikely because of the predominant role of IpaA VBS1-2 in driving the formation of

a D1D2:IpaA 1:1 complex and because these mutations were precisely designed to interfere with IpaA VBS3 interaction with D1D2; ii, they may stabilize an allosteric D1D2 conformer subsequent to the formation of the D1D2:IpaA 1:1 complex, thereby favoring the formation of this latter complex and accelerating monomer disappearance. This possibility is counter-intuitive because it implies that these polar mutations have opposite effects on favoring the formation of an D1D2:IpaA intermediate complex while disfavoring the formation of the trimer. However, it needs to be envisioned since the IpaA VBS3 helix is unlikely to function in the same iterative manner during D1D2 dimerization and resolution into a D1D2 homotrimer, and rather interacts with different subset of residues during these processes. The effects of the K139E mutation also impairing D1D2 trimer formation and accelerating monomer disappearance may be explained in a related yet different manner. Indeed, in apoD1D2, K139 establish a salt bridge with D389 that likely stabilize the D1D2 in the close conformation. The vinculin K139E charge inversion may therefore destabilize D1D2 to favor the formation of intermediate D1D2:IpaA complexes.

We found that the V367D predicted to disrupt the putative CC in D2 H10 affected trimer formation, suggesting a role for this motif in IpaA-induced D1D2 oligomerization. In the structures of apo D1D2 of full-length vinculin, this motif is located at a region of the D2 subdomain exposed on the surface of the vinculin head, but situated at the interface between the D1 and D2 bundle with insufficient space between the subdomains to accommodate another D2 helix bundle for oligomerization. Because the coiled-coil heptad motif is located adjacent to the IpaA VBS3 interaction site with the C-terminal extremity of the H10 helix, one could speculate that IpaA VBS3 binding induces the conformational changes associated with the exposition of this heptad motif. However, this motif remains at the interface of the D1 and D2 subdomains in the open conformer, suggesting that if it plays a role in D1D2 oligomerization, this coiled-coil motif should be exposed in another subsequent intermediate D1D2 conformer.

Our findings based on a clamped-mutant of vinculin proficient for canonical activation but deficient for supra-activation suggest that the head-domain mediated

oligomerization of vinculin akin to that induced by IpaA is required for the maturation of adhesions into large focal adhesions (Valencia-Gallardo et al., 2022). The observed effects of the D1D2 mutations support this hypothesis, since the D389R and E143K mutations introduced into full-length vinculin severely affected the number and size of on focal adhesions. While showing reduced and smaller focal adhesions, the amplitude of these defects was less in the K389D vinculin variant. These findings may be related to the different effects of this mutation observed in vitro relative to the D389R and E143K mutations, and to the accumulation of intermediate vinculin oligomeric complexes. Indeed, we previously found that in replating experiments, IpaA favored the rapid adhesion of cell to the substrate, but that similar levels of adhesion were detected over prolonged incubation upon canonical activation including that induced by an IpaA variant deleted for VBS3 (Valencia-Gallardo et al., 2022). The findings suggested that IpaA could promote the supra-activation of vinculin in the absence of mechanotransduction, but that canonical activation associated with mechanotransduction could also induce supra-activation. It is possible that the accumulation of oligomeric complexes linked to the K386D mutation compensate the defect of IpaA-induced trimers, during mechanotransduction.

The size reduction of focal adhesions in D1D2 mutants was more specifically observed at the levels of peripheral adhesions, while little difference was observed for ventral adhesions relative to parental vinculin. These ventral adhesions appeared thin and elongated, consistent with fibrillar adhesions known to remain stable independent of force (Sun et al., 2016). These observations are consistent with head domain-mediated vinculin oligomerization occurring at high force regime. As opposed to other mutations, the V367D mutation led to a drastic reduction of the number of focal adhesions but did not affect their average size. Instead, the V367D variant mostly formed elongated adhesions at the cell periphery. While the role of the putative coiled-coil domain targeted by the V367D mutation deserves clarification, the effects on the focal adhesion morphology associated with this particular mutation is consistent with the impairment in a process during vinculin oligomerization and focal adhesion formation that is different than the other mutations.

Materials and Methods

Bacterial strains, cells and plasmids

The bacterial strain used for the purification of D1D2 construct is *E. coli* BL21 (DE3) from Invitrogen. *E. coli* DH5- α F⁻ *endA1 glnV44 thi-1 recA1 relA1 gyrA96 deoR nupG purB20 ϕ 80dlacZ Δ M15 Δ (lacZYA-argF) U169, hsdR17(rK-mK+), λ - was used for the purification of aVBD. MEF and MEF vinculin null cells (Humphries, Wang et al. 2007) were grown in DMEM 1 g / L glucose containing 10 % FCS in a 37°C incubator containing 10 % CO₂.*

The pGEX4T2-AVBS1-3 encoding aVBD and the pET15b-D1D2 plasmids were described previously. The mutations in D1D2 were introduced by site-directed mutagenesis using pET15b-D1D2 as a matrix and the primer pairs indicated in Table 1. The pmCherry-human vinculin (HV) and was from Addgene. Mutations in D1D2 were transferred in mCherry-HV by exchanging the NheI-PspXI fragment with the corresponding XbaI-PspXI fragment of pET15b-D1D2.

Protein purification

BL21 (DE3) competent *E. coli* was transformed with the pET15b-D1D2 variant constructs. D1D2 were purified as described (Park, Valencia-Gallardo et al. 2011). For the IpaA derivatives, DH5-a competent *E. coli* was transformed with pGEX-4T2-AVBS1-3. Bacteria were grown at 37°C with shaking until OD_{600nm} = 1.0 were induced with 1 mM IPTG and incubated for another 2 hrs. Bacteria were pelleted and washed in ice-cold lysis buffer containing 25 mM Tris PH 7.4, 100 mM NaCl and 1 mM beta-mercaptoethanol, containing Complete™ protease inhibitor. All subsequent steps were performed at 4°C. Bacterial pellets were resuspended in 1/20th of the original culture volume and lyzed using a microfluidizer (LM20, Microfluidics). Cell debris were pelleted by centrifugation at 8000 xg for 20 min. Clarified lysates were subjected to affinity chromatography using a GStrap HP affinity column (GE Healthcare). Briefly, following incubation with the clarified lysates, the column was washed with five column volumes prior to incubation in PBS containing 100 μ g / ml Thrombin (Cytiva,

ref 27084601) for 16 hours at 21°C. aVBD was then eluted in PBS and further subjected to purification using size exclusion chromatography using a Superdex 200 10/300 GL (Ge Healthcare). Samples were stored aliquoted at -80°C at concentrations ranging from 1 to 10 mg/ml.

SEC analysis

D1D2 and aVBD were at the indicated molar ratio, with D1D2 at a final concentration of 20 µM, for 60 minutes at 21°C. 200µl of the protein mixtures were analyzed by size-exclusion chromatography (SEC) on a Superdex 200 10/300 GL (GE Healthcare) using a GE ÄKTA FPLC™ (Fast Protein Liquid Chromatograph, GMI) and a collection volume of 200 µl per fraction and 20ml of total collected volume. The SEC buffer was 25 mM Tris-HCl pH 7.2, 100 mM NaCl.

CN-PAGE

The D1D2 variants and aVBD were at the indicated molar ratio, with D1D2 at a final concentration of 20 µM, for 60 minutes at 21°C. Protein complex formation was visualized by PAGE under non-denaturing conditions using a 7.5% polyacrylamide gel, followed by Coomassie blue staining, as described previously (ref).

Cell transfection

For transfection experiments, cells were seeded at 1×10^4 cells on 25 mm-diameter coverslips coated with fibronectin at a concentration of 20 µg / ml. Cells were transfected with 1 µg of the pGEX-4T2-D1D2 construct and 4 µls JetPEI transfection reagent (Polyplus) for 16 hours following the manufacturer's recommendations.

Fluorescence confocal microscopy analysis

Samples were fixed in PBS containing 3.7 % paraformaldehyde for 60 min at 21°C, prior to processing for fluorescence staining of F-actin using Phalloidin-Alexa 488 as previously described (Valencia-Gallardo et al., 2022). Samples were analyzed using an Eclipse Ti inverted microscope (Nikon) equipped with a 60 x objective APO TIRF oil

immersion (NA: 1.49), a CSU-X1 spinning disk confocal head (Yokogawa), and a Prime 95B sCMOS camera (Photometrics) controlled by the Metamorph 7.7 software.

Image analysis

Focal adhesions were analyzed using the ImageJ 2.1.0/1.53c software. For each set of experiments, the confocal plane corresponding to the basal plane was subjected to thresholding using strictly identical parameters between samples. Adhesion clusters were detected using the “Analyze particle” plug-in, setting a minimal size of 3.5 μm^2 .

Statistical analysis

The number of adhesions was analyzed using Dunn's multiple comparisons test. The median area was compared using Mann-Whitney test. Differences in the rates of D1D2 trimer formation and monomer disappearance based were analyzed using an ANCOVA test.

Acknowledgements

The research was supported by fundings from the Inserm and CNRS. GTVN is a recipient of the grant ANR-21-CE35-0007-03 CALPLYCX. DA and BCC received funding from the CONACYT. HK received a grant from the Swiss National Science Foundation (grant no. SNF P2ZHP3_191289).

References

1. Bays JL, DeMali KA. Vinculin in cell-cell and cell-matrix adhesions. *Cell Mol Life Sci.* 2017 Aug;74(16):2999-3009. doi: 10.1007/s00018-017-2511-3. Epub 2017 Apr 11. PMID: 28401269; PMCID: PMC5501900.
2. Goldmann WH. Role of vinculin in cellular mechanotransduction. *Cell Biol Int.* 2016 Mar;40(3):241-56.
3. Peng X, Nelson ES, Maiers JL, DeMali KA. New insights into vinculin function and regulation. *Int Rev Cell Mol Biol.* 2011;287:191-231.
4. Atherton P, Stutchbury B, Jethwa D, Ballestrem C. Mechanosensitive components of integrin adhesions: Role of vinculin. *Exp Cell Res.* 2016 Apr 10;343(1):21-27.
5. Parsons JT, Horwitz AR, Schwartz MA. Cell adhesion: integrating cytoskeletal dynamics and cellular tension. *Nat Rev Mol Cell Biol.* 2010 Sep;11(9):633-43.
6. Yan J, Yao M, Goult BT, Sheetz MP. Talin Dependent Mechanosensitivity of Cell Focal Adhesions. *Cell Mol Bioeng.* 2015;8(1):151-159.

7. Kluger C, Braun L, Sedlak SM, Pippig DA, Bauer MS, Miller K, Milles LF, Gaub HE, Vogel V. Different Vinculin Binding Sites Use the Same Mechanism to Regulate Directional Force Transduction. *Biophys J*. 2020 Mar 24;118(6):1344-1356.
8. Gingras AR, Ziegler WH, Frank R, Barsukov IL, Roberts GC, Critchley DR, Emsley J. Mapping and consensus sequence identification for multiple vinculin binding sites within the talin rod. *J Biol Chem*. 2005 Nov 4;280(44):37217-24.
9. Izard T, Evans G, Borgon RA, Rush CL, Bricogne G, Bois PR. Vinculin activation by talin through helical bundle conversion. *Nature*. 2004 Jan 8;427(6970):171-5.
10. Sun Z, Guo SS, Fässler R. Integrin-mediated mechanotransduction. *J Cell Biol*. 2016 Nov 21;215(4):445-456.
11. Goult BT, Brown NH, Schwartz MA. Talin in mechanotransduction and mechanomemory at a glance. *J Cell Sci*. 2021 Oct 15;134(20):jcs258749.
12. Yao M, Goult BT, Klapholz B, Hu X, Toseland CP, Guo Y, Cong P, Sheetz MP, Yan J. The mechanical response of talin. *Nat Commun*. 2016 Jul 7;7:11966. doi: 10.1038/ncomms11966.
13. Izard T, Brown DT. Mechanisms and Functions of Vinculin Interactions with Phospholipids at Cell Adhesion Sites. *J Biol Chem*. 2016 Feb 5;291(6):2548-55.
14. Auernheimer V, Lautscham LA, Leidenberger M, Friedrich O, Kappes B, Fabry B, Goldmann WH. Vinculin phosphorylation at residues Y100 and Y1065 is required for cellular force transmission. *J Cell Sci*. 2015 Sep 15;128(18):3435-43.
15. Thwaites TR, Pedrosa AT, Peacock TP, Carabeo RA. Vinculin Interacts with the Chlamydia Effector TarP Via a Tripartite Vinculin Binding Domain to Mediate Actin Recruitment and Assembly at the Plasma Membrane. *Front Cell Infect Microbiol*. 2015 Nov 30;5:88.
16. Park H, Lee JH, Gouin E, Cossart P, Izard T. The rickettsia surface cell antigen 4 applies mimicry to bind to and activate vinculin. *J Biol Chem*. 2011 Oct 7;286(40):35096-103.
17. Valencia-Gallardo CM, Carayol N, Tran Van Nhieu G. Cytoskeletal mechanics during *Shigella* invasion and dissemination in epithelial cells. *Cell Microbiol*. 2015 Feb;17(2):174-82.
18. Izard T, Tran Van Nhieu G, Bois PR. *Shigella* applies molecular mimicry to subvert vinculin and invade host cells. *J Cell Biol*. 2006 Nov 6;175(3):465-75.
19. Tran Van Nhieu G, Izard T. Vinculin binding in its closed conformation by a helix addition mechanism. *EMBO J*. 2007 Oct 31;26(21):4588-96. doi: 10.1038/sj.emboj.7601863. Epub 2007 Oct 11. Erratum in: *EMBO J*. 2008 Mar 19;27(6):922.
20. Park H, Valencia-Gallardo C, Sharff A, Tran Van Nhieu G, Izard T. Novel vinculin binding site of the IpaA invasin of *Shigella*. *J Biol Chem*. 2011 Jul 1;286(26):23214-21.
21. Valencia-Gallardo C, Bou-Nader C, Aguilar-Salvador DI, Carayol N, Quenech'Du N, Pecqueur L, Park H, Fontecave M, Izard T, Tran Van Nhieu G. *Shigella* IpaA Binding to Talin Stimulates Filopodial Capture and Cell Adhesion. *Cell Rep*. 2019 Jan 22;26(4):921-932.

22. Valencia-Gallardo C, Aguilar-Salvador D, Khakzad H, Cocom-Chan B, Bou-Nader C, Velours C, Zarrouk Y, Le Clainche C, Malosse C, Borges Lima D, Quenech'Du N, Mazhar B, Essid S, Fontecave M, Asnacios A, Chamot-Rooke J, Malmström L, Tran Van Nhieu G. BioRxive. doi: <http://doi.org/10.1101/2022.11.07.515412>.
23. Molony L, Burridge K. Molecular shape and self-association of vinculin and metavinculin. *J Cell Biochem.* 1985;29(1):31-6.
24. Bakolitsa C, de Pereda JM, Bagshaw CR, Critchley DR, Liddington RC. Crystal structure of the vinculin tail suggests a pathway for activation. *Cell.* 1999 Dec 10;99(6):603-13. doi: 10.1016/s0092-8674(00)81549-4. PMID: 10612396.
25. Chinthalapudi K, Rangarajan ES, Patil DN, George EM, Brown DT, Izzard T. Lipid binding promotes oligomerization and focal adhesion activity of vinculin. *J Cell Biol.* 2014 Dec 8;207(5):643-56.
26. Johnson RP, Craig SW. Actin activates a cryptic dimerization potential of the vinculin tail domain. *J Biol Chem.* 2000 Jan 7;275(1):95-105.
27. Huang DL, Bax NA, Buckley CD, Weis WI, Dunn AR. Vinculin forms a directionally asymmetric catch bond with F-actin. *Science.* 2017 Aug 18;357(6352):703-706.
28. Thompson PM, Tolbert CE, Campbell SL. Vinculin and metavinculin: oligomerization and interactions with F-actin. *FEBS Lett.* 2013 Apr 17;587(8):1220-9.
29. Garakani K, Shams H, Mofrad MRK. Mechanosensitive Conformation of Vinculin Regulates Its Binding to MAPK1. *Biophys J.* 2017 May 9;112(9):1885-1893.

Figure and legends

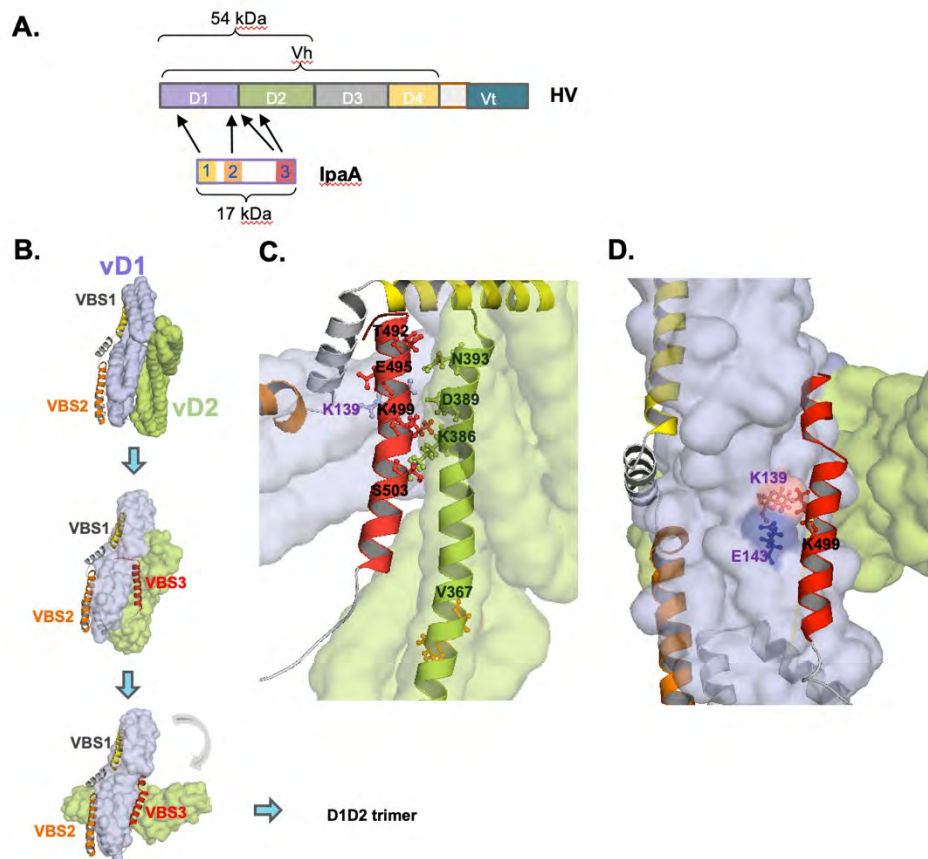


Fig. 1 Design of D1D2 mutations targeting IpaA VBS3 contact sites

A, Schematic organization of vinculin subdomains and IpaA vinculin-binding domain. The molecular weight of the vinculin D1D2 and IpaA vinculin-binding domains is indicated. The arrows point at binding of: IpaA VBS1 to the D1 first bundle, IpaA VBS2 to the second D1 bundle, IpaA VBS3 binding to the D1D2 interface and D2 second bundle. **B-D,** TX-MS based models of D1D2: aVBD. The vinculin D1 and D2 are shown as grey and green surface structures, respectively. IpaA VBSs are shown as ribbon structures. **B,** Top: IpaA VBS1-2 binds to a D1D2 that adopts a conformation similar to that of apoD1D2 (close conformer). Concomitant binding of IpaA VBS3 to the D2 first bundle leads to a similar D1D2 conformation (Middle, while binding of IpaA

VBS3 to the D1D2 interface induces a major conformational change (open conformer) with a 30° tilt in the relative orientation of the D1 and D2 major axis. **C**, **D**, higher magnifications showing the IpaA VBS3(red) interface with D1 D2 in the close (**C**) and open (**D**) conformer. The residues potentially involved in polar interactions via their side chains are indicated. In the open conformer, IpaA K499 may interact with E143 or clash with K139 on vinculin D1.

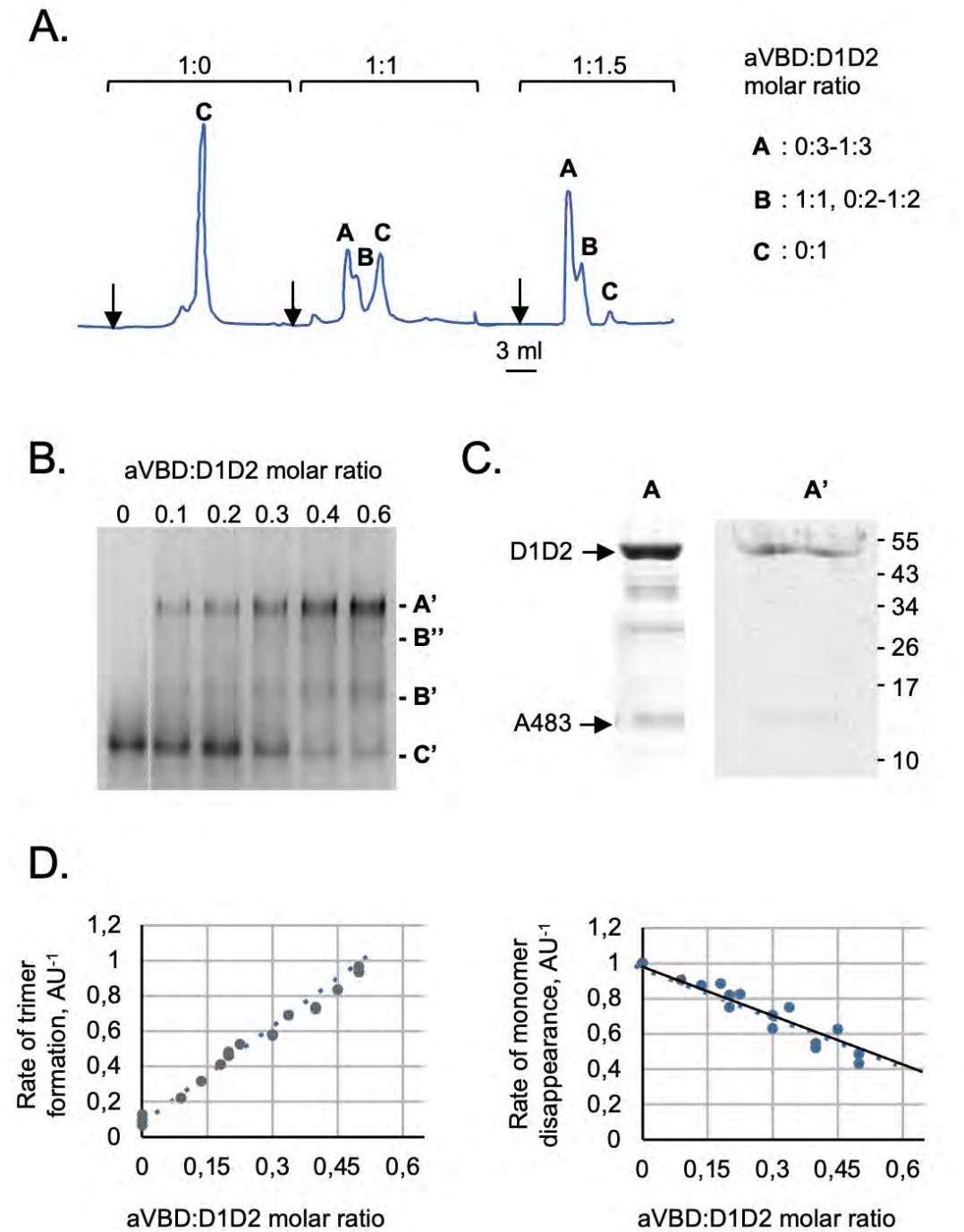


Fig. 2. A CN-PAGE assay to study IpaA-induced D1D2 trimer formation

A, B. aVBD and D1D2 were mixed at the indicated molar ratio, with D1D2 at a final concentration of 20 μ M, and incubated for 60 min at 21°C prior to analysis. **A**, SEC analysis using an Increase Superdex 200 (Materials and Methods). The indicated stoichiometry is inferred from previous SEC-MALS analysis (ref) molecular and the mass of complexes in peaks A, B and C estimated from molecular weight standards as a function of the respective elution volume. **B**, CN-PAGE using a 10 % polyacrylamide native gel followed by Coomassie blue staining. C': monomeric D1D2, B' and B'': aVBD:D1D2 complexes. **C**, SDS-PAGE followed by Coomassie blue staining of samples corresponding to peak A in SEC fractionation as shown in panel A (A) and eluted following dissection of band A' as shown in Panel D (A'). Densitometry analysis of the bands indicated a D1D2:aVBD ratio of 3.8 and 3.2 for sample A and A', respectively, consistent with 3:0-3:1 aVBD complexes. **D**, the integrated intensity of bands corresponding to trimeric (A') or monomeric D1D2 (C) were scanned by densitometry, and normalized to that of monomeric D1D2 in the absence of aVBD. The graphs are representative of at least three independent experiments.

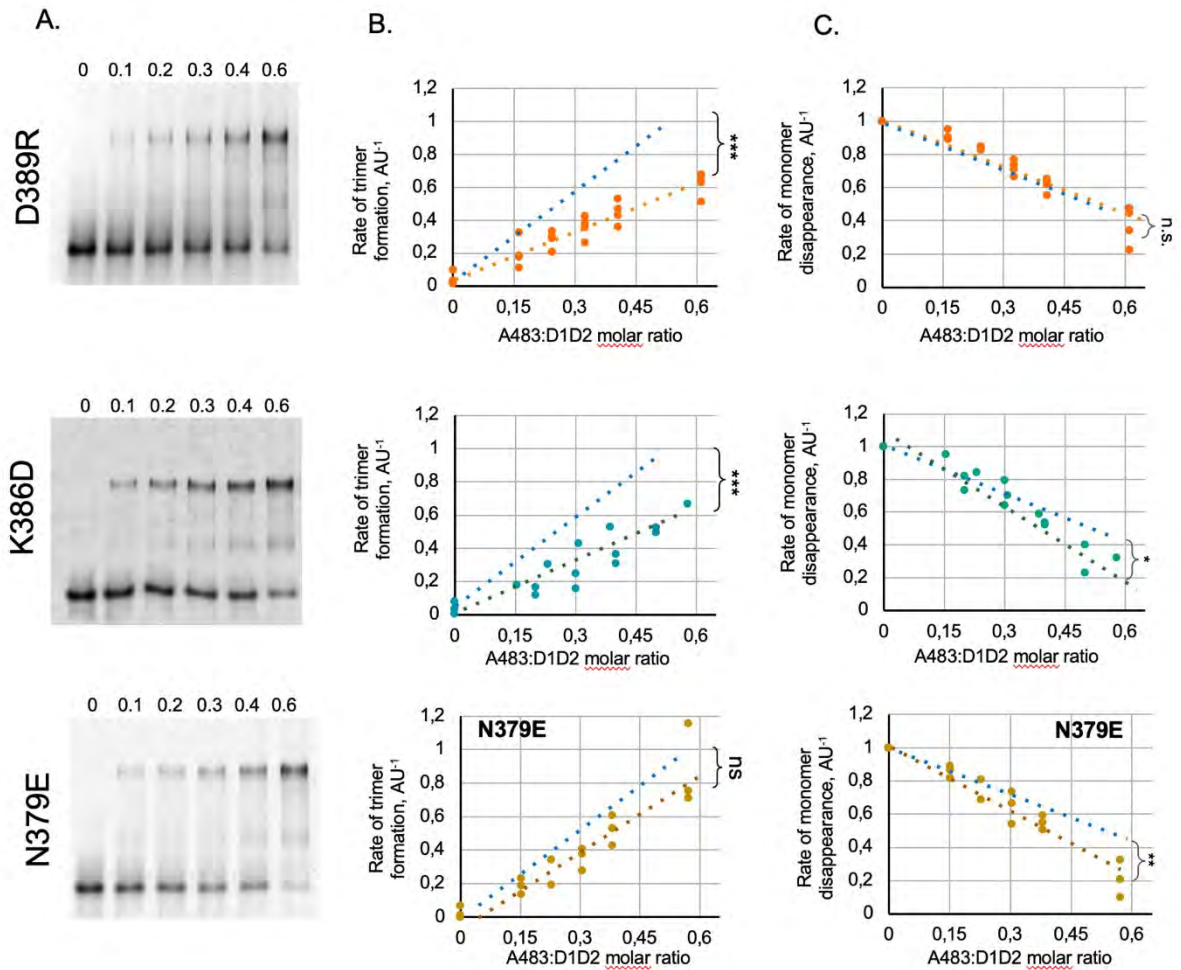


Fig. 3. Effects of mutations on D1D2 trimer formation and monomer disappearance.

A, CN-PAGE using a 10 % polyacrylamide native gel followed by Coomassie blue staining of aVBD-induced complex formation with the indicated D1D2 variant. The aVBD:D1D2 molar ratio is indicated above each lane. **B**, **C**, the integrated intensity of bands corresponding to trimeric (**B**) or monomeric D1D2 (**C**) were scanned by densitometry, and normalized to that of monomeric D1D2 in the absence of aVBD. The graphs are representative of at least three independent experiments. The blue dashed lines correspond to linear fits obtained for parental D1D2. ANCOVA test: *: $p < 0.05$; **: $p < 0.01$; ***: $p < 0.005$. ns: not significant.

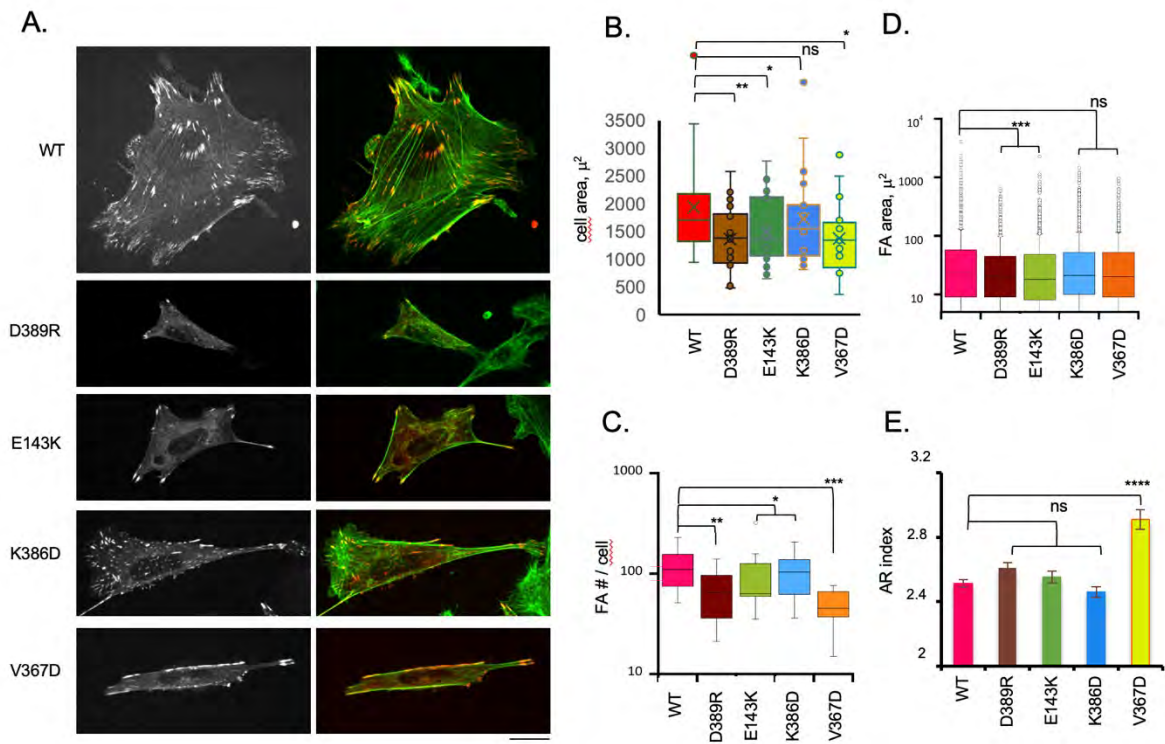


Fig. 4. Effects of D1D2 mutations affecting D1D2 trimer formation on focal adhesions. MEF vinculin $-/-$ cells were transfected with HV-mCherry variants bearing the indicated mutation. Samples were fixed and processed for fluorescence staining of F-actin. **A**, Left panels: HV mCherry. Right panels: green: F-actin; red:HV mCherry. **B**, cell spreading area. **C**, average number of FAs per cell ($n > 20$, $N = 2$); **D**, average FA size; **E**: AR index corresponding to the major over minor axis of FA. **C-E**, ($n > 2500$, $N = 2$). Mann-Whitney: *: $p < 0.05$; **: $p < 0.01$; ***: $p < 0.005$. ns: not significant.

D1D2 mutation	primers
D389R	5'-CATTGCAAAGAAGATCCGTGCTGCTCAGAACTGGC-3' 5'-GCCAGTTCTGAGCAGCACGGATCTTCTTTGCAATG-3'
E143K	5'-AGGAATTTTGaaaTATCTTACAGTG-3' 5'-CACTGTAAGATAtttCAAATTCCT-3'
K386D	5'-GAGCATTGCagacAAGATCGATGC-3' 5'-GCATCGATCTTgtcTGCAATGCTC-3'
K386G	5'-CAAAGCAGAGCATTGCAGGCAAGATCGATGCTGCTC-3' 5'-GAGCAGCATCGATCTTGCCTGCAATGCTCTGCTTTG-3'
K139E	5'-TAGAGTTTGCgaaGGAATTTTGG-3' 5'-CCAAAATTCCttcGCAAACCTCTA-3'
V367D	5'-CTCACAGCAAAAAGTGGAAAATGCAGCTCGC-3' 5'-GCGAGCTGCATTTTCCACTTTTGCTGTGAG-3'
N393D	5'-GATCGATGCTGCTCAGGACTGGCTTGCAGATCCAAATG-3' 5'-CATTTGGATCTGCAAGCCAGTCCTGAGCAGCATCGATC-3'
N379E	5'-GCTGGAAGCCATGACCGAATCAAAGCAGAGCATTGC-3' 5'-GCAATGCTCTGCTTTGATTCGGTCATGGCTTCCAGC-3'

Table 1. Primers used in this study.

D1D2 construct	Rate of trimer formation AU ⁻¹	Rate of Monomer Disappearance AU ⁻¹
WT	1.51	-1.06
D389R	0.95 ***	-1.06 ^{n.s.}
E143K	1.10 ***	-0.88 ^{n.s.}
V367D	1.19 ***	-0.88 ^{n.s.}
K386D	0.99 ***	-1.29
K386G	1.12 **	-1.39 *
K139E	1.04 ***	-1.42 *
N393D	1.30 ^{n.s.}	-1.32 *
N379E	1.48 ^{n.s.}	-1.38 **

Table 2. Rates of D1D2 trimer formation and monomer disappearance.

The rates of trimer formation and monomer disappearance for the indicated D1D2 variants were inferred from linear fits (Materials and Methods). ANCOVA test: *: $p < 0.05$; **: $p < 0.01$; ***: $p < 0.005$. ns: not significant.

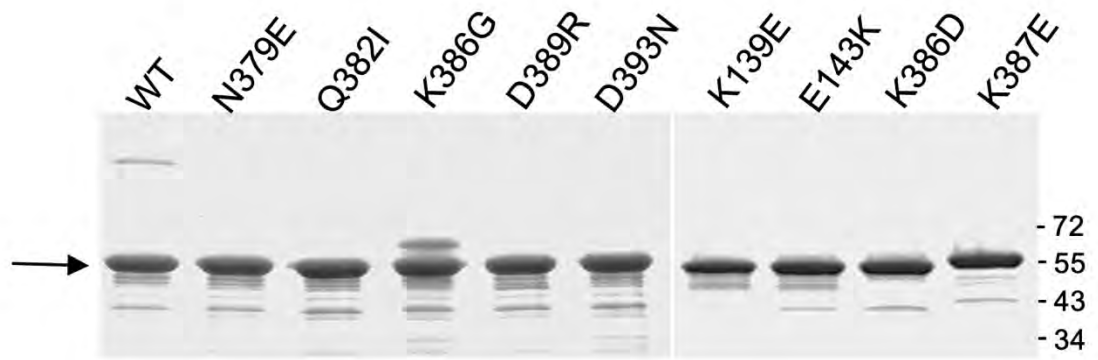


Fig. S2. SDS-PAGE purified D1D2 variants

D1D2 variants expressed in *E. coli* BL21 (DE3) and purified by affinity chromatography (Materials and Methods) were analyzed by SDS-PAGE using a 10 % polyacrylamide gel followed by Coomassie staining. The size of the molecular weight markers is indicated in kDa. The arrow points at D1D2 constructs.

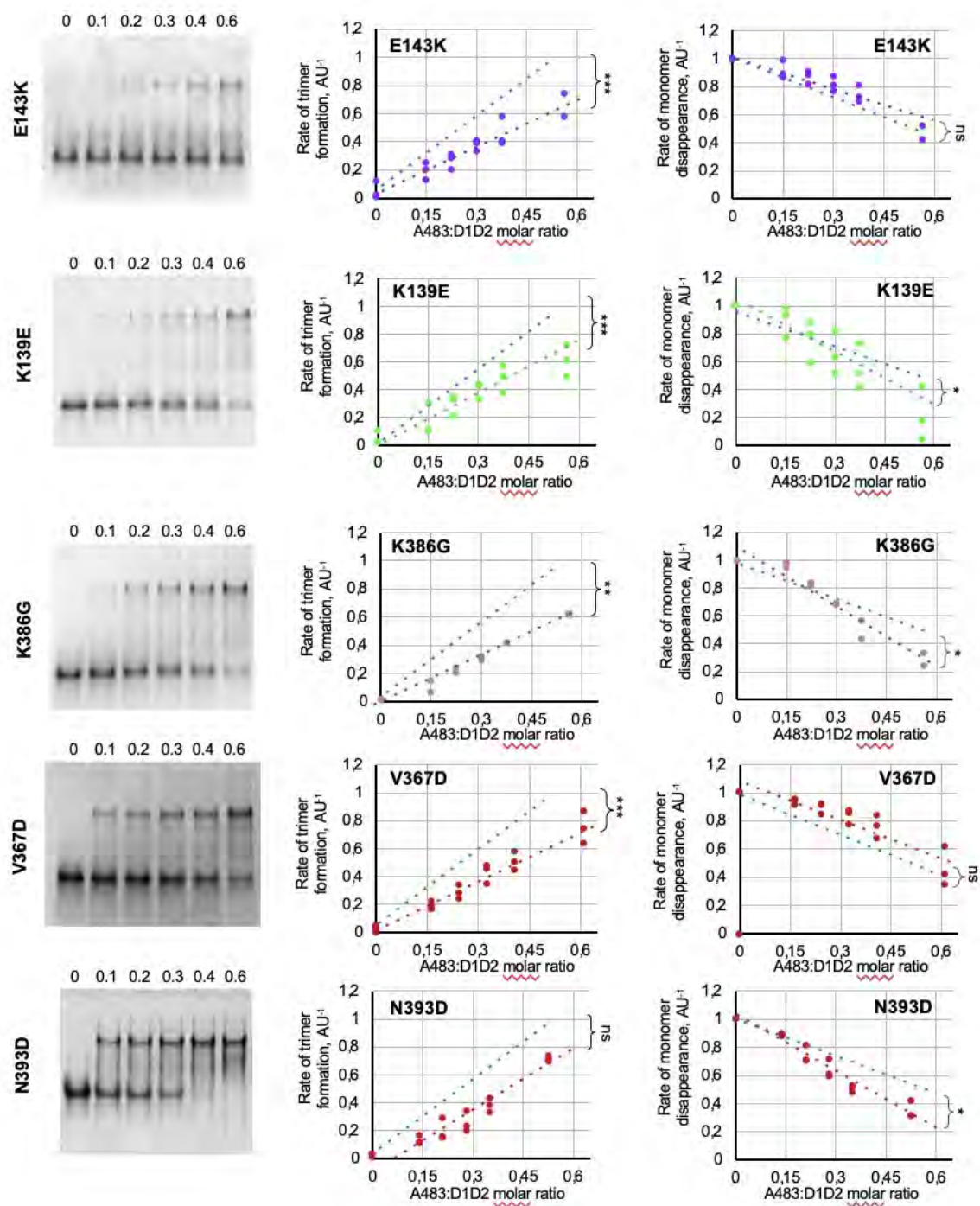


Fig. S3. Effects of D1D2 mutations on IpaA-induced trimer formation and monomer disappearance.

Left panels, CN-PAGE using a 10 % polyacrylamide native gel followed by Coomassie blue staining of aVBD-induced complex formation with the indicated D1D2 variant. The aVBD:D1D2 molar ratio is indicated above each lane. **Center and right panels,**

The aVBD:D1D2 molar ratio is indicated above each lane. **Center and right panels,**

the integrated intensity of bands corresponding to trimeric (**center**) or monomeric D1D2 (**right**) were scanned by densitometry, and normalized to that of monomeric D1D2 in the absence of aVBD. The graphs are representative of at least three independent experiments. The blue dashed lines correspond to linear fits obtained for parental D1D2. ANCOVA test: *: $p < 0.05$; **: $p < 0.01$; ***: $p < 0.005$. ns: not significant.

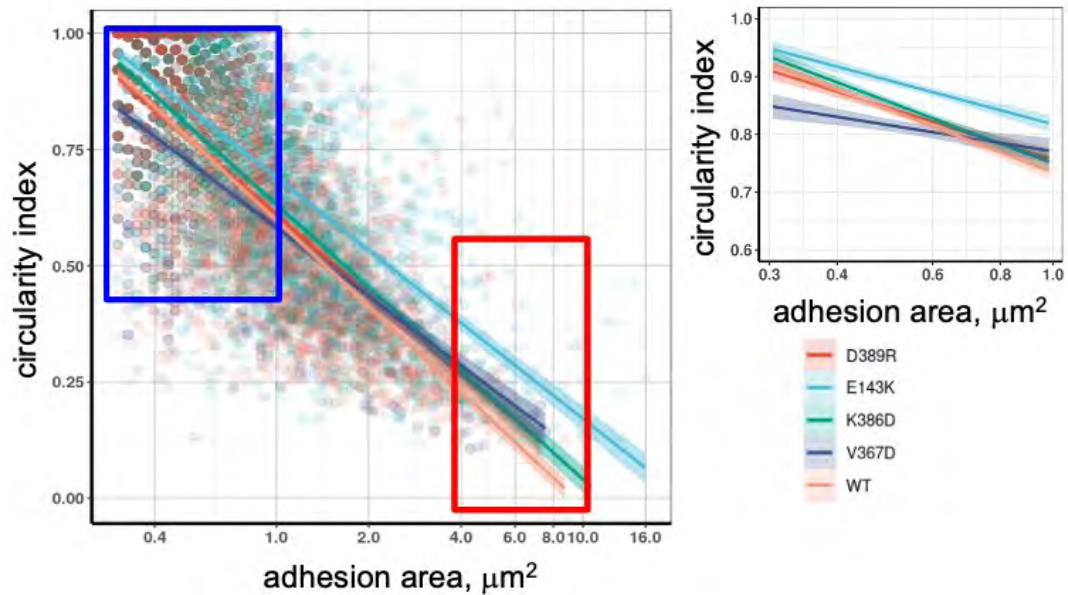


Figure S4. Focal adhesion size plotted as a function of their circularity index. Left: each dot corresponds to an adhesion structure labeled with the vinculin variant indicated by the color code. The linear fit for each variant is shown. Right: linear fits for small adhesion structures (area $< 1 \mu\text{m}^2$). Note the more elongated adhesions for the V367D variant.

SUPPLEMENTARY RESULTS #1

IpaA VBS1-3 transfection increases the kinetics and strength of cell adhesion

Authors : Daniel Isui Aguilar¹, Benjamin Cocom-Chan¹, Cesar Valencia-Gallardo¹, Delphine Javelaud², Alain Mauviel², Jacques Fattacioli³, Guy Tran Van Nhieu¹

¹ Equipe Signalisation Calcique et Infections Microbiennes, CIRB, Collège de France, 75005 Paris, France. From November 2021 : I2BC - Inserm U1280-CNRS UMR9198 Gif-sur-Yvette.

² Institut Curie, PSL Research University, INSERM U1021, CNRS UMR3347, Team “TGF- β and Oncogenesis“, Equipe Labellisée LIGUE 2016, F-91400, Orsay, France. Université Paris-Sud, F-91400, Orsay, France.

³ PASTEUR, Département de Chimie, École Normale Supérieure, PSL University, Sorbonne Université, CNRS, 75005 Paris, France. Institut Pierre-Gilles de Gennes pour la Microfluidique, 75005 Paris, France

Goal :

In these experiments, we tested the effects of IpaA VBS1-3 (A483) on the kinetics of cell adhesion using a microfluidic chamber.

Materials and Methods

Cell lines, plasmids and transfection

The IpaA constructs GFP-A524 and GFP-A483 were generated by polymerase chain reaction (PCR) and cloning into pcDNA3.1 NT-GFP Topo TA (Invitrogen) using the 5'-TCAAAGGACATTACAAAATCC-3' and 5'-GCGATATCATGGCCAGCAAAGG-3' forward primers, respectively, and the 5'-GCGCGGCCGCTTAATCCTTATTGATATTC-3' reverse primer. 1205Lu melanoma cells (Smalley, Lioni et al. 2008) were grown in RPMI + Glutamax medium

(RPMI1640) supplemented with 10 % fetal calf serum (FCS) and non-essential aminoacids in a 37°C incubator with 5 % CO₂. For transfection experiments, cells were seeded at 2.5 x 10⁴ cells in 25 mm-diameter coverslips. Cells were transfected with 3 µg of pGFP-A524 or pGFP-A483 plasmids with 6 µls JetPEI transfection reagent (Polyplus) for 16 hours following the manufacturer's recommendations. C2.7 mice myoblasts cells were fixed in PBS containing 3.7% paraformaldehyde for 20 min at 21°C and permeabilized with 0.1% Triton X-100 for 4 min at 21°C. 1205Lu melanoma cells were processed for adhesion under shear stress experiments in microfluidic chambers.

Microfluidics cell adhesion assay

Analysis of cell detachment under shear stress was based on previous works (Gutierrez, Petrich et al. 2008). 1205Lu melanocytes were transfected with the indicated constructs, then labeled with 2 µM calcein-AM (Life Technologies) in serum-free DMEM for 20 minutes. Cells were detached by incubation with 2 µM Cytochalasin D (Sigma-Aldrich) for 40 minutes to disassemble FAs, followed by incubation in PBS containing 10 mM EDTA for 20 minutes. Cells were washed in EM buffer (120 mM NaCl, 7 mM KCl, 1.8 mM CaCl₂, 0.8 mM MgCl₂, 5 mM glucose and 25 mM HEPES at pH 7.3) by centrifugation and resuspended in the same buffer at a density of 1.5 x 10⁶ cells/ml. Calcein-labeled transfected cells and control unlabeled cells were mixed at a 1:1 ratio and perfused onto a 25 mm-diameter glass coverslips (Marienfeld) previously coated with 20 µg/ml fibronectin and blocked with PBS containing 2% BSA (Sigma-Aldrich) in a microfluidic chamber on a microscope stage at 37°C. We used a commercial microfluidic setup (Flow chamber system 1C,

Provitro) and a Miniplus3 peristaltic pump (Gilson) to adjust the flow rate in the chamber. Microscopy analysis was performed using a LEICA DMRIBe inverted microscope equipped with a Cascade 512B camera and LED source lights (Roper Instruments), driven by the Metamorph 7.7 software (Universal imaging). Cells were allowed to settle for the indicated time prior to application of a 4 ml/min, flow corresponding to a wall shear stress of 22.2 dyn/cm² (2.22 Pa). Acquisition was performed using a 20 X objective using phase contrast and fluorescence illumination (excitation 480 ± 20 nm, emission 527 ± 30 nm). Fluorescent images were acquired before and after flushing to differentiate between target and control cells. Phase contrast images were acquired every 200 ms. Fold enrichment was defined as the ratio between of attached labeled and unlabeled cells.

Results

GFP-A483 induced higher yields of adherent cells when replating was performed with short kinetics, with a 5-fold increase over control cells and GFP-A524 transfectants, respectively, for 10 min replating (Fig. 1a). By contrast, little difference in adhesion yield was detected between samples at 15 min suggesting that IpaA predominantly affected the early dynamics of cell adhesion (Fig. 1a). To extend these findings, we measured cell adhesion strength using controlled shear stress in a microfluidic chamber and 1025 Lu melanoma cells (Smalley, Lioni et al. 2008). We first controlled the efficacy of anti-vinculin siRNA treatment in these cells (Figs. 1b, c). Consistent with replating experiments, when cells were allowed to adhere to fibronectin-coated surfaces for more than 25 min, little difference in resistance to shear stress could be detected between GFP-A483 and GFP transfected cells samples (Figs. 1d, e). In contrast, similar

to cells depleted for by siRNA treatment, cells transfected with the clamped vinculin version showed a decreased ability to adhere in comparison to wild-type vinculin-transfected cells (Fig. 1e).

However, when shear stress was applied after less than 20 min following cell incubation, GFP-A483-transfected cells showed significantly higher resistance to shear stress up to 22.2 dynes.cm⁻² than GFP-A524- or GFP-transfected cells, with 1.7 ± 0.2 - and 0.9 ± 0.14-fold enrichment ± SD of adherent cells for GFP-A483 and GFP-A524-transfected cells versus control GFP-transfected cells, respectively (Fig. 1f).

These results are in full agreement with effects observed for A483 on adhesion structures and suggest that A483-mediated vinculin supra-activation accelerates endogenous processes occurring during mechanotransduction to promote strong adhesion.

REFERENCES

- Mitrossilis, D., et al., *Single-cell response to stiffness exhibits muscle-like behavior*. Proc Natl Acad Sci U S A, 2009. **106**(43): p. 18243-8.
- Gutierrez, E., et al., *Microfluidic devices for studies of shear-dependent platelet adhesion*. Lab Chip, 2008. **8**(9): p. 1486-95.
- Smalley, K.S., et al., *Increased cyclin D1 expression can mediate BRAF inhibitor resistance in BRAF V600E-mutated melanomas*. Mol Cancer Ther, 2008. **7**(9): p. 2876-83.

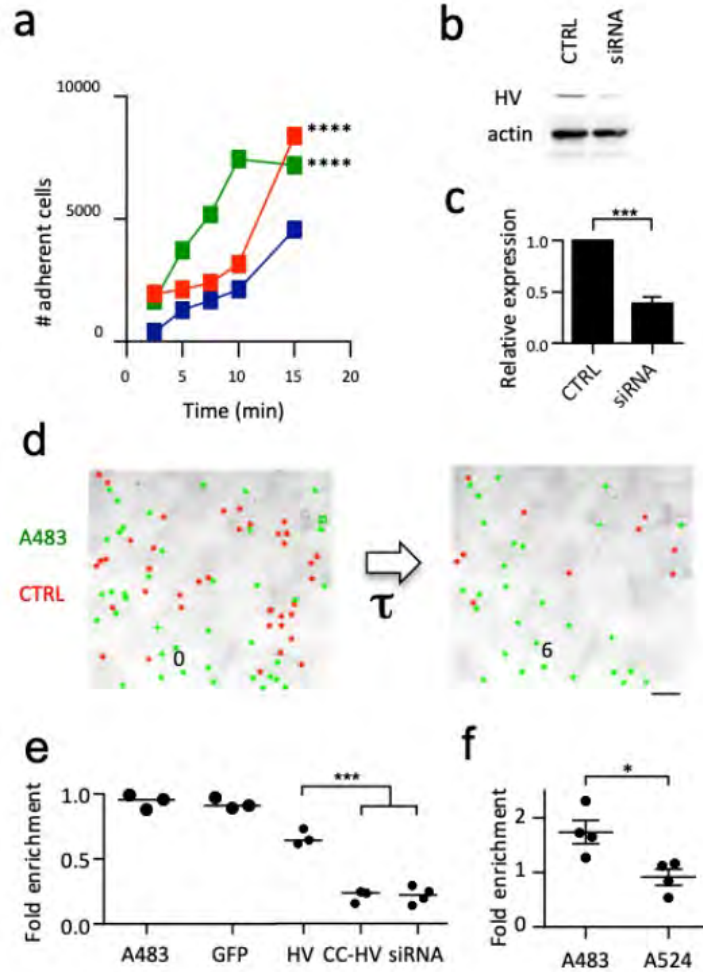


Figure 1. IpaA VBS 1-3 increases the kinetics and strength of cell adhesion

a, 1205Lu melanoma cells were transfected with GFP alone (blue), GFP-IpaA VBS1-2 (A524, red) or GFP-IpaA VBS1-3 (A483, green), lifted up by trypsinization and plated for the indicated time on Fn N-coated coverslips. Samples were washed, fixed and adherent cells were scored microscopically. The total number of adherent cells scored is indicated. GFP: 3223 cells, N = 4; A524: n=7418, N = 4; A4 483: n =5668, N = 4. Chi square corrected with Bonferroni multiple comparison correction. ****: $p < 0.0001$. **b, c**, 1205Lu melanoma cells were mock-transfected (CTRL) or treated with anti-vinculin siRNA (siRNA, Materials and Methods). **b**, anti-vinculin Western blot analysis. **c**, average HV band intensity normalized to that of control cells. Unpaired t test. ****: $p = 0.005$. **d-f**, transfected cells were with calcein (Materials and Methods) and mixed with the same ratio of control cells. Cells were perfused in a microfluidic chamber and allowed to adhere prior to shear stress application for: **d, e**, 30-60 min; **f**, 20 min. **d**, representative fields. The number indicates the elapsed time (seconds) after shear stress application. **e, f**, scatter plot of the ratio of adherent cells with respect to non-transfected cells, **e**, A483 (N = 3, n = 557); GFP (N = 3, n = 490); HV: vinculin mCherry (N = 3, n = 481); CC-HV: vinculin Q68C A396C-mCherry (N = 3, n = 259); siRNA: cells treated with anti-vinculin siRNA (N = 3, n = 395). **f**, A483 (N = 4, n = 610) or A524 (N = 4, n = 433) transfected cells vs control cells (1594 cells, N = 4). Unpaired t test. *: $p = 0.0229$.

SUPPLEMENTARY INFORMATION #2

A role for IpaA K499 in vinculin supra-activation

Authors : Benjamin Cocom-Chan¹Guy Tran Van Nhieu¹

¹ Equipe Signalisation Calcique et Infections Microbiennes. I2BC - Inserm U1280-
CNRS UMR9198 Gif-sur-Yvette.

Goal:

We tested the effects of the IpaA K499E charge inversion predicted to affect the interaction with vinculin D389 and E143 in the close or open D1D2 conformers, respectively, on D1D2 trimerization.

Materials and Methods

Plasmids

The IpaA mutation was introduced in plasmid pGEX-4T2-IpaA VBS1-3 by site directed mutagenesis using the following primers 5'-TAGAGTTTGCGAAGGAATTTTGG-3' and 5'- CCAAAATTCCttcGCAA ACTCTA-3'. Protein purification and CN-PAGE were performed as described in article 2.

CN-PAGE

Aliquots of 10/40 µl were loaded into 7.5% polyacrylamide mini-gels (1mm width) by using standard gel recipes but substituting SDS for water. Runnings were performed during 150-180 min at 25mA per gel were used in order to observe the bands corresponding to the monomers and the higher order oligomers 3:1 or oligomer (cold conditions were preferred during the runnings). D1D2-E143K was the only one requiring 180 min in order to observe higher bands. Molar ratios of D1D2:IpaA-

VBS123 were between 1:0→1:1. The gels were stained using colloidal Coomassie R-250 blue.

Band intensities corresponding to the monomer, higher order oligomer or intermediate species were measured using ImageJ with a fixed rectangular area (adjusted with the max width for the monomer and max high order oligomer for the height). A reference area outside the lanes used for the running reactions was included to subtract the background. Values were plotted and then normalized in order to compare the in vitro phenotypes between D1D2 wt and the variant.

Results

Figure 1 shows that the IpaA VBS1-3 K499E variant induces less D1D2 trimerization (yellow trace) compared to the WT IpaA VBS 1-3. A slight increase in intermediate complexes (red trace), suggesting that IpaA stabilizes hetero-complexes.

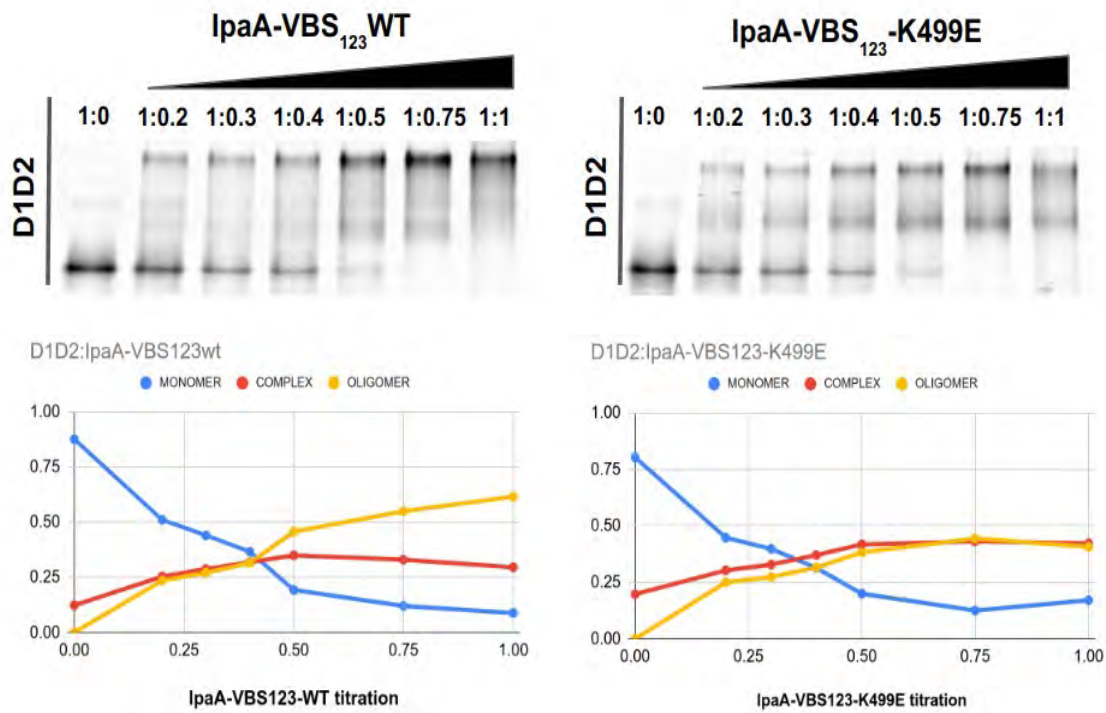


Fig. 1. Effects of IpaA VBS1-3 K499E on D1D2 trimer formation and monomer disappearance. Top, CN-PAGE using a 10 % polyacrylamide native gel followed by Coomassie blue staining of IpaAVBS1-3 or incubated with vinculin D1D2. The IpaA VBS1-3:D1D2 molar ratio is indicated above each lane. Bottom, the integrated intensity of bands corresponding to trimeric (yellow), intermediate complex (red) or monomeric (blue) D1D2

were scanned by densitometry, and normalized to that of monomeric D1D2 in the absence of IpaA VBS1-3. The graphs are representative of at 2 independent experiments.

III. DISCUSSION

The ability of IpaA to induce vinculin activation in the absence of mechanotransduction suggests that IpaA-VBSs uses an alternative mechanism to the one occurring in cells during force transmission events, as cells when cells are adhering to a stiff substrate. Our assays using purified protein versions of IpaA-VBSs or IpaA-VBSs variant interacting with vinculin D1D2, showed that this interaction is mostly dependent on the D1a:VBS interaction as is the case for endogenous vinculin partners talin, alpha-actinin or alpha-catenin. However, whereas the VBS exposure is driven in a sequential manner by mechanical signals for endogenous vinculin partners, IpaA does not require a mechanical input to unveil their VBSs, as they're already exposed. Thus, this might facilitate the successive states necessary for the vinculin activation process.

Evidence for the possible roles of D1D2 and full length vinculin oligomeric forms in cells is needed. Nonetheless, as we observed, the D1D2:IpaA-VBSs hetero-complex is stable even under the native gel running conditions, this might have implications yet to be fully elucidated. One possibility is to act as an actin bundling protein at distance, probably as a short term molecular memory for the pulling direction being exerted from the acto-myosin cytoskeleton associated to the cell adhesion sites, a role that in cells occurs for example during mechanical-pulling dependent calpain cleavage of the talin rod domain, a function that has important implications during the cell adhesion growth, turnover and cellular survival (Saxena et al. 2017).

Another possibility is that *Shigella*'s IpaA-VBSs act as adhesion enhancer, as they don't possess cleavage sites. This could allow the bacteria to proliferate, as in the case of *Chlamydia* spp. infected cells lining the mucosas, where TarP, a T3SS effector protein harboring two or three VBSs at its C-term domain (Whitewood et al. 2018). Similarly to IpaA, *Chlamydia*'s TarP enhances the cell adhesion number formation and those adhesions are resistant to the effect of blebbistatin, an inhibitor of myosin II, as cells remain attached to the intestinal epithelium this could favor to the bacteria to spread the infection process to other neighboring cells (Pedrosa et al. 2020).

Regarding the molecular level mechanisms, the alternative pathway that IpaA might exploit to activate vinculin during *Shigella spp.* infection could depend on the cooperative action of VBS1 and VBS2 allowing VBS3 to interact with the interphase between D1 and D2 and induce a conformational change that might drive the rotation of D2 respecting D1 in a counterclockwise manner (C. Valencia-Gallardo et al. 2022). However, the rotation it suffers under mechanical tension, according to SMD simulations from Kluger et al. indicates that D2 rotates respect to D1 in a clockwise direction (Kluger et al. 2020). Nonetheless, mechanisms could lead to similar results as they involve a major conformational change in the vinculin head domain in order to induce the release of the D5 (tail) domain to couple the mechanical tension after associating with F-actin. The conformational steps following this interaction remain to be further described.

Substitution of residues located at the interphase of D1-D3 contact regions might also lead to reinforce the idea that the vinculin head domain is playing an important role in terms of acting as a regulator during mechanically-dependent vinculin conformational changes. Additionally, the D2-D3 interphase might play a similar role in regulating the amount or degree of conformational plasticity during mechanically dependent or independent changes in conformation. Consequently, the binding of F-actin to vinculin D5, might depend on the collective behavior of the protein, as the interdomain region shows a strong stability (Stec and Stec 2022) and their binding interactions might be coevolving in order to permit the protein to maintain its proper function.

In reference to the predicted association between the vinculin H1 helix located at the D5 or vinculin tail, this should be addressed in the future, as this predicted interaction and specific conformational state should take place under specific conditions to be determined experimentally. Nonetheless, it is reasonable to speculate that, if this endogenous VBS from vinculin can interact with the D1 first helix bundle, this interaction might take place under a non-characterized conformational state as those vinculin states remain less characterized.

A possible explanation for this observation might be related to the PIP₂ binding capacity mediated by basic residues located in the H1 and H2 from D5, and this interaction mediates the turnover of vinculin on those adhesions as their amino acid substitution not only extends the lifetime of vinculin FA and promotes its upwards shift relocalization in the z-axis, but affects the turnover of the same (Thompson et al. 2017). In our structural prediction the endo-VBS helix is spanning both H1 and H2 residues, and particularly, the R910 and K911 residues are located at similar sites as the K498 and K499 in the IpaA's VBS3 to D1 structures. Those positively charged residues are also facing the outer side when in complex with D1, therefore both PIP₂ binding and the endo-VBS to D1 binding are not necessarily mutually exclusive between them and this might be involved in the regulation of vinculin when recruited to the FA sites. Targeting both R910 and K911 on full length vinculin transfection experiments could help to discard this hypothesis and shed some light on the vinculin regulation by PIP₂ at the integrin signaling layer in FAs.

In relation to our cell transfection experiments, our results suggest that single residue substitution could have an important impact on the phenotype at the level of cell adhesion morphology and proper cell spreading. For instance, the FA phenotype corresponding to the mutation at the residue E143K located in D1, but facing near a contact region to D2, showed more rounded adhesions than the WT along different adhesion's sizes. However, cells transfected with this variant formed less adhesions and spread less. This might indicate that E143K substitution in full length vinculin reduces the capacity of the protein to respond to the mechanical pulling from the actin stress fibers, either by a reduced binding capacity to F-actin at the D5 domain, or a resistance to experience conformational changes derived from mechanical signals. In both cases, the biochemical analysis of purified protein variants should be addressed in further details.

In comparison to the observations on residue substitutions located at the surface of the D1 and D2 domains, the V367D residue substitution is located inside the D2 helical

bundle. Interestingly, when trying to identify if the IpaA-VBSs can form complexes with purified vinculin D2 proteins in native-PAGE conditions no bands or complexes were visible (Valencia-Gallardo et al., unpublished), this suggests that the folded form of the D2 domain is stabilized by interacting with the other vinculin domains and there is no in vitro evidence for the IpaA-VBSs binding to D2 alone, even under protein-protein docking simulation conditions (data not shown).

This is an scenario important to consider as the prediction of the coiled-coil motif with their particular combination of hydrophobic and charged residues is located exactly in the middle of the alpha-helix and connecting the two bundles of D2 (Delorenzi and Speed 2002). This indicates the importance of keeping its structure in the folded architecture in order to resist unfolding under mechanical stress (see Kluger et al. 2020). And as other molecular dynamics predictions based on the vinculin suggests, D2 is more likely to experience major conformational as its orientation axis respecting the pulling force angle from the VBS bound to D1 and the actin cytoskeleton is almost perpendicular (Yiwen Chen and Dokholyan 2006). This is important to consider vinculin as a non-linear mechanosensor (compared to talin) and not only as a scaffolding or adaptor in cell adhesion structures.

Accordingly, cells expressing the full-length vinculin V367D variant presented adhesions structures already elongated at the initial steps of formation according to its size (Article 2, **Figure S4**), might suggest that the protein is more sensitive to suffer conformational changes even at low levels of pulling forces from the actin cytoskeleton and probably before the tension from myosin pulling is exerted and the adhesions can increase in size.

Altogether, the substitution of single residues altering either the proper interactions at the surface of interdomain interactions or avoiding the proper folding of the domains itself, can have larger range effects at the level of altering the size and anisotropy of focal adhesions at different stages of maturation, as inferred from the adhesion area to circularity relationship (Article 2, **Figure S4**). As the cell adapts their intracellular

environment through the alignment of the actin stress fibers to the ECM patterning and stiffness properties initially imposed by their environment, they also change in shape their cell adhesions accordingly (Tamiello et al. 2016). This suggests that the inter-domain contact regions, as well as the integrity of domains itself are key to modulate the coupling of mechanical inputs imposed to vinculin D1 by VBS binding and D5 (F-actin pulling) domains. Which suggests by the cell adhesion shape measurements that vinculin can act as a mechanosensitive component.

Additional cell transfection experiments with the FLVmCherry variants will be necessary to understand the observations described in this work, as the extent of cell migration capacity by time lapse imaging studies, the recruitment of adhesion maturation markers such as VASP or alpha-actinin or tensin; as well as their ability to resist the relaxation exerted from the acto-myosin pulling forces from actin stress fibers (i.e. Y-27632).

Also, in order to clarify the molecular mechanisms underlying the FA phenotypes observed in cell transfection experiments, purifying full length vinculin proteins and evaluating their *in vitro* ability of F-actin bundling or co-sedimentation assays might be necessary. Regarding the conformational states associated with the vinculin head domain variants, the response to mechanical pulling forces analyzed by AFM microscopy analysis or SMD simulations should be considered.

In terms of the “clutch model hypothesis” we should not forget that this the observed phenotypes associated to cells transfected with the vinculin variants analyzed so far, do not take into account the implications for the proper functioning of other subcomponents from the “molecular clutch” such as talin or alpha-actinin, that is also involved in the maximum force transmission between the integrin layer and the actin regulatory layer, as the protein is involved, not only because can work as a traction force generation, but also work as an actin bundling protein. These roles do not overlapped with talin or vinculin functions in the force transmission layer (Case and Waterman 2015). Additionally, we should consider that the efficiency of the force

transmission also depends on the actomyosin pulling forces, the ECM rigidity and the binding unbinding rates between those components, as there exists different optimal forces for the different components (Elosegui-Artola, Trepap, and Roca-Cusachs 2018). Therefore, the picture depicted by the “molecular clutch hypothesis” might still be reductionist compared to the mechanisms involved in living systems, as even the ECM does exert biological functions beyond acting as a passive substrate.

Compared to the VBS-D1 binding and to the binding of D5 to F-actin from vinculin, we found that D1 and D2 residues located at sites different from those interactions can have an important impact on vinculin’s activity. As our *in vitro* assays showed, the vinculin:IpaA-VBSs protein complexes and oligomer formation can be diminished independently of their D1:VBS binding capacity, and this might be due to an alternative conformation imposed by the residue substitutions into their D1D2 apo-protein form. Also, in our cell transfection experiments we observed that when transferring those substitutions into full length protein variants, a reduced cell spreading and altered FA morphology was observed in cells. That might be explained by an underestimated role for the vinculin domain organization regulating the response of the protein to mechanical pulling tension, independently of their VBS or actin binding activities, which supports the idea of vinculin acting as a mechanosensitive component in cellular adhesion structures.

GENERAL CONCLUSION

Vinculin has been mostly considered as a scaffolding protein in cell adhesion structures. However, vinculin can bind to different regulatory molecules in cell adhesions like kinases, phosphatases, adaptor proteins, actin regulators or lipids (Bays and DeMali 2017). In order to do so, vinculin should change its conformation into an “active” form with an elusive structural conformation when present in cell adhesions. As these structures to function traits are evolutionary conserved, different intracellular pathogens have coevolved molecular mechanisms to bypass those mechanical-dependent structural

changes by targeting vinculin binding and activation through proteins harboring VBS motifs (Murphy and Brinkworth 2021), in order to “hijack” the cells to form adhesion-like structures in the absence of mechanical traction.

Shigella's IpaA it has an exceptional capacity to activate vinculin without the need for additional signals and induce mechanical-independent conformational changes, as compared to the activation involving not only the binding of other proteins and the presence of actin pulling forces on the protein. In this study, we found that single amino acid substitutions located at the D1 or D2 domains, but not at sites involved in the VBS or F-actin binding. We observed an altered ability of the protein to be recruited at sites under mechanical stress, as observed in our *in vitro* experiments using IpaA exposed VBSs; as well as the ability of the protein to properly respond to the pulling forces acting in the intracellular environment in cells transfected with full length vinculin variants (specially the E143K and the V367D variants). Thus, reducing the cell spreading capacity and FA morphology. Altogether, the aminoacid residue substitution in the vinculin D1 and D2 domains revealed that the integrity in the “head” domain of the protein is as important as VBS or F-actin binding interaction to regulate the activity of vinculin during the mechanical-dependent activation process, what provides more evidence to consider the protein as a mechanosensor and not only a protein adaptor or scaffold.

PERSPECTIVES

Two observations can be further explored derived from this work, the first corresponds to corroborate the presence of an endogenous-VBS motif predicted to be located at the H1 helix from the vinculin D5 domain, and the possible implications for vinculin functions in cell, probably by targeting residue substitutions. The second corresponds to the characterization of the molecular mechanisms underlying the observed phenotypes observed after altering vinculin “head” domain, specifically the vinculin variants E143K and the V367D. Both variant associated FA phenotypes suggested that the former is unable to properly connect the FAs with the actin stress

fibers, and the later seems to be more sensitive to the actin pulling forces, as it was observed that D2 C-C variant present elongated adhesions since the early stages of adhesion formation.

IV. BIBLIOGRAPHY

- Akeda Y, Galán JE. Chaperone release and unfolding of substrates in type III secretion. *Nature*. 2005 Oct 6;437(7060):911-5.
- Bakolitsa, Constantina, Daniel M. Cohen, Laurie A. Bankston, Andrey A. Bobkov, Gregory W. Cadwell, Lisa Jennings, David R. Critchley, Susan W. Craig, and Robert C. Liddington. 2004. "Structural Basis for Vinculin Activation at Sites of Cell Adhesion." *Nature* 430 (6999): 583–86.
- Barczyk, Malgorzata, Sergio Carracedo, and Donal Gullberg. 2010. "Integrins." *Cell and Tissue Research* 339 (1): 269–80.
- Bays, Jennifer L., and Kris A. DeMali. 2017. "Vinculin in Cell-Cell and Cell-Matrix Adhesions." *Cellular and Molecular Life Sciences: CMLS* 74 (16): 2999–3009.
- Berendsen, H. J., and S. Hayward. 2000. "Collective Protein Dynamics in Relation to Function." *Current Opinion in Structural Biology* 10 (2): 165–69.
- Bonnans, Caroline, Jonathan Chou, and Zena Werb. 2014. "Remodelling the Extracellular Matrix in Development and Disease." *Nature Reviews. Molecular Cell Biology* 15 (12): 786–801.
- Borgon, Robert A., Clemens Vornrhein, Gerard Bricogne, Philippe R. J. Bois, and Tina Izard. 2004. "Crystal Structure of Human Vinculin." *Structure* 12 (7): 1189–97.
- Bornschlogl, T., et al., Filopodial retraction force is generated by cortical actin dynamics and controlled by reversible tethering at the tip. *Proc Natl Acad Sci U S A*, 2013. 110(47): p. 18928-33.
- Bouchet, Benjamin P., Rosemarie E. Gough, York-Christoph Ammon, Dieudonné van de Willige, Harm Post, Guillaume Jacquemet, Af Maarten Altelaar, Albert Heck Jr, Benjamin T. Goult, and Anna Akhmanova. 2016. "Talin-KANK1 Interaction Controls the Recruitment of Cortical Microtubule Stabilizing Complexes to Focal Adhesions." *eLife* 5 (July). <https://doi.org/10.7554/eLife.18124>.
- Boujemaa-Paterski R, Martins B, Eibauer M, Beales CT, Geiger B, Medalia O. Talin-activated vinculin interacts with branched actin networks to initiate bundles. *Elife*. 2020 Nov 13;9:e53990.
- Broussard, Joshua A., Donna J. Webb, and Irina Kaverina. 2008. "Asymmetric Focal Adhesion Disassembly in Motile Cells." *Current Opinion in Cell Biology* 20 (1): 85–90.
- Brotcke Zumsteg, A., et al., IcsA is a *Shigella flexneri* adhesin regulated by the type III secretion system and required for pathogenesis. *Cell Host Microbe*, 2014. 15(4): p. 435-45.
- Campbell, Iain D., and Martin J. Humphries. 2011. "Integrin Structure, Activation, and Interactions." *Cold Spring Harbor Perspectives in Biology* 3 (3). <https://doi.org/10.1101/cshperspect.a004994>.
- Carisey, Alex, and Christoph Ballestrem. 2011. "Vinculin, an Adapter Protein in Control of Cell Adhesion Signalling." *European Journal of Cell Biology* 90 (2-3): 157–63.
- Case, Lindsay B., and Clare M. Waterman. 2015. "Integration of Actin Dynamics and Cell Adhesion by a Three-Dimensional, Mechanosensitive Molecular Clutch." *Nature Cell Biology* 17 (8): 955–63.

- Chang, K., et al., Filopodia and Viruses: An Analysis of Membrane Processes in Entry Mechanisms. *Front Microbiol*, 2016. 7: p. 300
- Chandrasekar, I., Stradal, T.E., Holt, M.R., Entschladen, F., Jockusch, B.M. and Ziegler, W.H. (2005) Vinculin acts as a sensor in lipid regulation of adhesionsite turnover. *J. Cell Sci.* 118, 1461–1472,
- Changede, Rishita, Haogang Cai, Shalom J. Wind, and Michael P. Sheetz. 2019. “Integrin Nanoclusters Can Bridge Thin Matrix Fibres to Form Cell-Matrix Adhesions.” *Nature Materials* 18 (12): 1366–75.
- Changede, Rishita, and Michael Sheetz. 2017. “Integrin and Cadherin Clusters: A Robust Way to Organize Adhesions for Cell Mechanics.” *BioEssays: News and Reviews in Molecular, Cellular and Developmental Biology* 39 (1): 1–12.
- Changede, Rishita, Xiaochun Xu, Felix Margadant, and Michael P. Sheetz. 2015. “Nascent Integrin Adhesions Form on All Matrix Rigidities after Integrin Activation.” *Developmental Cell* 35 (5): 614–21.
- Chen, Hui, Dilshad M. Choudhury, and Susan W. Craig. 2006. “Coincidence of Actin Filaments and Talin Is Required to Activate Vinculin.” *The Journal of Biological Chemistry* 281 (52): 40389–98.
- Chen, Hui, Daniel M. Cohen, Dilshad M. Choudhury, Noriyuki Kioka, and Susan W. Craig. 2005. “Spatial Distribution and Functional Significance of Activated Vinculin in Living Cells.” *The Journal of Cell Biology* 169 (3): 459–70.
- Chen, Yiwen, and Nikolay V. Dokholyan. 2006. “Insights into Allosteric Control of Vinculin Function from Its Large Scale Conformational Dynamics.” *The Journal of Biological Chemistry* 281 (39): 29148–54.
- Chen, Yunfeng, Hyunjung Lee, Haibin Tong, Martin Schwartz, and Cheng Zhu. 2017. “Force Regulated Conformational Change of Integrin $\alpha\beta$.” *Matrix Biology: Journal of the International Society for Matrix Biology* 60-61 (July): 70–85.
- Chinthalapudi, Krishna, Dipak N. Patil, Erumbi S. Rangarajan, Christoph Rader, and Tina Izard. 2015. “Lipid-Directed Vinculin Dimerization.” *Biochemistry* 54 (17): 2758–68.
- Chinthalapudi, Krishna, Erumbi S. Rangarajan, Dipak N. Patil, Eric M. George, David T. Brown, and Tina Izard. 2014. “Lipid Binding Promotes Oligomerization and Focal Adhesion Activity of Vinculin.” *The Journal of Cell Biology* 207 (5): 643–56.
- Choi, Colin K., Miguel Vicente-Manzanares, Jessica Zareno, Leanna A. Whitmore, Alex Mogilner, and Alan Rick Horwitz. 2008. “Actin and Alpha-Actinin Orchestrate the Assembly and Maturation of Nascent Adhesions in a Myosin II Motor-Independent Manner.” *Nature Cell Biology* 10 (9): 1039–50.
- Chorev, Dror S., Tova Volberg, Ariel Livne, Miriam Eisenstein, Bruno Martins, Zvi Kam, Brigitte M. Jockusch, Ohad Medalia, Michal Sharon, and Benny Geiger. 2018. “Conformational States during Vinculin Unlocking Differentially Regulate Focal Adhesion Properties.” *Scientific Reports* 8 (1): 2693.
- Coll JL, et al. Targeted disruption of vinculin genes in F9 and embryonic stem cells changes cell morphology, adhesion, and locomotion. *Proc Nat Acad Sci U S A.* 1995;92:9161–9165.
- Collet, C., et al., Protein polarization driven by nucleoid exclusion of DnaK(HSP70)-substrate complexes *Nature Communications*, 2018 May 23;9(1):2027.
- Cormier, Anthony, Melody G. Campbell, Saburo Ito, Shenping Wu, Jianlong Lou, James Marks, Jody L. Baron, Stephen L. Nishimura, and Yifan Cheng. 2018. “Cryo-EM

- Structure of the $\alpha\text{v}\beta\text{8}$ Integrin Reveals a Mechanism for Stabilizing Integrin Extension.” *Nature Structural & Molecular Biology* 25 (8): 698–704.
- Deakin NO, Turner CE. Paxillin comes of age. *J Cell Sci.* 2008 Aug 1;121(Pt 15):2435-44.
- Dedden, Dirk, Stephanie Schumacher, Charlotte F. Kelley, Martin Zacharias, Christian Biertümpfel, Reinhard Fässler, and Naoko Mizuno. 2019. “The Architecture of Talin1 Reveals an Autoinhibition Mechanism.” *Cell* 179 (1): 120–31.e13.
- Delorenzi, Mauro, and Terry Speed. 2002. “An HMM Model for Coiled-Coil Domains and a Comparison with PSSM-Based Predictions.” *Bioinformatics* 18 (4): 617–25.
- Dey S, Chakravarty A, Guha Biswas P, De Guzman RN. The type III secretion system needle, tip, and translocon. *Protein Sci.* 2019 Sep;28(9):1582-1593.
- Diez, G., Kollmannsberger, P., Mierke, C.T., Koch, T.M., Vali, H., Fabry, B. and Goldmann, W.H. (2009) Anchorage of vinculin to lipid membranes influences cell mechanical properties. *Biophys. J.* 97, 3105–3112.
- Elosegui-Artola, Alberto, Xavier Trepast, and Pere Roca-Cusachs. 2018. “Control of Mechanotransduction by Molecular Clutch Dynamics.” *Trends in Cell Biology* 28 (5): 356–67.
- Gardel, Margaret L., Ian C. Schneider, Yvonne Aratyn-Schaus, and Clare M. Waterman. 2010. “Mechanical Integration of Actin and Adhesion Dynamics in Cell Migration.” *Annual Review of Cell and Developmental Biology* 26: 315–33.
- Galkin, V.E., Orlova, A., Schroder, G.F. and Egelman, E.H. (2010) Structural polymorphism in F-actin. *Nat. Struct. Mol. Biol.* 17, 1318–1323,
- Gefen, Amit. 2010. *Cellular and Biomolecular Mechanics and Mechanobiology*. Springer Science & Business Media.
- Geiger, Benjamin. 1979. “A 130K Protein from Chicken Gizzard: Its Localization at the Termini of Microfilament Bundles in Cultured Chicken Cells.” *Cell*. [https://doi.org/10.1016/0092-8674\(79\)90368-4](https://doi.org/10.1016/0092-8674(79)90368-4).
- Gielata, Mateusz, Kamila Karpińska, Tomasz Pieczonka, and Agnieszka Kobiela. 2022. “Emerging Roles of the α -Catenin Family Member α -Catulin in Development, Homeostasis and Cancer Progression.” *International Journal of Molecular Sciences* 23 (19). <https://doi.org/10.3390/ijms231911962>.
- Gingras, Alexandre R., Wolfgang H. Ziegler, Ronald Frank, Igor L. Barsukov, Gordon C. K. Roberts, David R. Critchley, and Jonas Emsley. 2005. “Mapping and Consensus Sequence Identification for Multiple Vinculin Binding Sites within the Talin Rod.” *The Journal of Biological Chemistry* 280 (44): 37217–24.
- Gomez, T.M., et al., Filopodial calcium transients promote substrate-dependent growth cone turning. *Science*, 2001. 291(5510): p. 1983-7
- Goult, Benjamin T., Jie Yan, and Martin A. Schwartz. 2018. “Talin as a Mechanosensitive Signaling Hub.” *The Journal of Cell Biology* 217 (11): 3776–84.
- Han, Mitchell K. L., and Johan de Rooij. 2016. “Converging and Unique Mechanisms of Mechanotransduction at Adhesion Sites.” *Trends in Cell Biology* 26 (8): 612–23.
- Horton, Edward R., Adam Byron, Janet A. Askari, Daniel H. J. Ng, Angélique Millon-Frémillon, Joseph Robertson, Ewa J. Koper, et al. 2015. “Definition of a Consensus Integrin Adhesome and Its Dynamics during Adhesion Complex Assembly and Disassembly.” *Nature Cell Biology* 17 (12): 1577–87.
- Hu, W., B. Wehrle-Haller, and V. Vogel, Maturation of filopodia shaft adhesions is upregulated by local cycles of lamellipodia advancements and retractions. *PLoS One*,

2014. 9(9): p. e107097.
- Huang DL, Bax NA, Buckley CD, Weis WI, Dunn AR. Vinculin forms a directionally asymmetric catch bond with F-actin. *Science*. 2017 Aug 18;357(6352):703-706
- Humphries, Jonathan D., Megan R. Chastney, Janet A. Askari, and Martin J. Humphries. 2019. "Signal Transduction via Integrin Adhesion Complexes." *Current Opinion in Cell Biology* 56 (February): 14–21.
- Humphries, Martin J. 2002. "Insights into Integrin-Ligand Binding and Activation from the First Crystal Structure." *Arthritis Research* 4 Suppl 3 (May): S69–78.
- Izard, Tina, Gwyndaf Evans, Robert A. Borgon, Christina L. Rush, Gerard Bricogne, and Philippe R. J. Bois. 2004. "Vinculin Activation by Talin through Helical Bundle Conversion." *Nature* 427 (6970): 171–75.
- Izard T, Tran Van Nhieu G, Bois PR. *Shigella* applies molecular mimicry to subvert vinculin and invade host cells. *J Cell Biol*. 2006 Nov 6;175(3):465-75. doi: 10.1083/jcb.200605091. PMID: 17088427; PMCID: PMC2064523.
- Janssen, M.E., Kim, E., Liu, H., Fujimoto, L.M., Bobkov, A., Volkmann, N. and Hanein, D. (2006) Three-dimensional structure of vinculin bound to actin filaments. *Mol. Cell* 21, 271–281,
- Jansen, Karin A., Dominique M. Donato, Hayri E. Balcioglu, Thomas Schmidt, Erik H. J. Danen, and Gijssje H. Koenderink. 2015. "A Guide to Mechanobiology: Where Biology and Physics Meet." *Biochimica et Biophysica Acta* 1853 (11 Pt B): 3043–52.
- Jaumouille, V., et al., Cytoplasmic targeting of IpaC to the bacterial pole directs polar type III secretion in *Shigella*. *EMBO J*, 2008. 27(2): p. 447-57
- Jumper, John, Richard Evans, Alexander Pritzel, Tim Green, Michael Figurnov, Olaf Ronneberger, Kathryn Tunyasuvunakool, et al. 2021. "Highly Accurate Protein Structure Prediction with AlphaFold." *Nature* 596 (7873): 583–89.
- Kanchanawong, Pakorn, Gleb Shtengel, Ana M. Pasapera, Ericka B. Ramko, Michael W. Davidson, Harald F. Hess, and Clare M. Waterman. 2010. "Nanoscale Architecture of Integrin-Based Cell Adhesions." *Nature* 468 (7323): 580–84.
- Kechagia, Jenny Z., Johanna Ivaska, and Pere Roca-Cusachs. 2019. "Integrins as Biomechanical Sensors of the Microenvironment." *Nature Reviews. Molecular Cell Biology* 20 (8): 457–73.
- Kim, Laura Y., Peter M. Thompson, Hyunna T. Lee, Mihir Pershad, Sharon L. Campbell, and Gregory M. Alushin. 2016. "The Structural Basis of Actin Organization by Vinculin and Metavinculin." *Journal of Molecular Biology* 428 (1): 10–25.
- Kluger, Carleen, Lukas Braun, Steffen M. Sedlak, Diana A. Pippig, Magnus S. Bauer, Ken Miller, Lukas F. Milles, Hermann E. Gaub, and Viola Vogel. 2020. "Different Vinculin Binding Sites Use the Same Mechanism to Regulate Directional Force Transduction." *Biophysical Journal* 118 (6): 1344–56.
- Kotloff KL, Riddle MS, Platts-Mills JA, Pavlinac P, Zaidi AKM. Shigellosis. *Lancet*. 2018 Feb 24;391(10122):801-812.
- Le Clainche C, Dwivedi SP, Didry D, Carlier MF. Vinculin is a dually regulated actin filament barbed end-capping and side-binding protein. *J Biol Chem*. 2010 Jul 23;285(30):23420-32.
- Lee, Gwangrog, Khadar Abdi, Yong Jiang, Peter Michaely, Vann Bennett, and Piotr E. Marszalek. 2006. "Nanospring Behaviour of Ankyrin Repeats." *Nature* 440 (7081): 246–49.

- Lee, Jun Hyuck, Hajeung Park, and Yong Ho Park. 2014. "Molecular Mechanisms of Host Cytoskeletal Rearrangements by *Shigella* Invasins." *International Journal of Molecular Sciences* 15 (10): 18253–66.
- Le, Shimin, Miao Yu, and Jie Yan. 2019. "Direct Single-Molecule Quantification Reveals Unexpectedly High Mechanical Stability of Vinculin-Talin/ α -Catenin Linkages." *Science Advances* 5 (12): eaav2720.
- Lo, Su Hao. 2004. "Tensin." *The International Journal of Biochemistry & Cell Biology* 36 (1): 31–34.
- Mattila, P.K. and P. Lappalainen, Filopodia: molecular architecture and cellular functions. *Nat Rev Mol Cell Biol*, 2008. 9(6): p. 446-54.
- Mattock E, Blocker AJ. How Do the Virulence Factors of *Shigella* Work Together to Cause Disease? *Front Cell Infect Microbiol*. 2017 Mar 24;7:64.
- Milam, L. M. 1985. "Electron Microscopy of Rotary Shadowed Vinculin and Vinculin Complexes." *Journal of Molecular Biology* 184 (3): 543–45.
- Miller, Phillip W., Donald N. Clarke, William I. Weis, Christopher J. Lowe, and W. James Nelson. 2013. "The Evolutionary Origin of Epithelial Cell-Cell Adhesion Mechanisms." *Current Topics in Membranes* 72: 267–311.
- Miller, Phillip W., Sabine Pokutta, Jennyfer M. Mitchell, Jayanth V. Chodaparambil, D. Nathaniel Clarke, W. James Nelson, William I. Weis, and Scott A. Nichols. 2018. "Analysis of a Vinculin Homolog in a Sponge (phylum Porifera) Reveals That Vertebrate-like Cell Adhesions Emerged Early in Animal Evolution." *The Journal of Biological Chemistry* 293 (30): 11674–86.
- Molony, L., and K. Burridge. 1985. "Molecular Shape and Self-Association of Vinculin and Metavinculin." *Journal of Cellular Biochemistry* 29 (1): 31–36.
- Moreno-Layseca, Paulina, Jaroslav Icha, Hellyeh Hamidi, and Johanna Ivaska. 2019. "Integrin Trafficking in Cells and Tissues." *Nature Cell Biology* 21 (2): 122–32.
- Moser, Markus, Kyle R. Legate, Roy Zent, and Reinhard Fässler. 2009. "The Tail of Integrins, Talin, and Kindlins." *Science* 324 (5929): 895–99.
- Murphy, Korinn N., and Amanda J. Brinkworth. 2021. "Manipulation of Focal Adhesion Signaling by Pathogenic Microbes." *International Journal of Molecular Sciences* 22 (3). <https://doi.org/10.3390/ijms22031358>.
- Muthuramalingam M, Whittier SK, Picking WL, Picking WD. The *Shigella* Type III Secretion System: An Overview from Top to Bottom. *Microorganisms*. 2021 Feb 22;9(2):451.
- Niemann HH, Schubert WD, Heinz DW. Adhesins and invasins of pathogenic bacteria: a structural view. *Microbes Infect*. 2004 Jan;6(1):101-12.
- Park, Hajeung, Cesar Valencia-Gallardo, Andrew Sharff, Guy Tran Van Nhieu, and Tina Izard. 2011. "Novel Vinculin Binding Site of the IpaA Invasin of *Shigella*." *The Journal of Biological Chemistry* 286 (26): 23214–21.
- Pedrosa, António T., Korinn N. Murphy, Ana T. Nogueira, Amanda J. Brinkworth, Tristan R. Thwaites, Jesse Aaron, Teng-Leong Chew, and Rey A. Carabeo. 2020. "A Post-Invasion Role for Type III Effector TarP in Modulating the Dynamics and Organization of Host Cell Focal Adhesions." *The Journal of Biological Chemistry* 295 (43): 14763–79.
- Peng, Xiao, Elke S. Nelson, Jessica L. Maiers, and Kris A. DeMali. 2011. "New Insights into Vinculin Function and Regulation." *International Review of Cell and Molecular*

- Biology* 287: 191–231.
- Ribet D, Cossart P. How bacterial pathogens colonize their hosts and invade deeper tissues. *Microbes Infect.* 2015 Mar;17(3):173-83.
- Romero, S., et al., Filopodium retraction is controlled by adhesion to its tip. *J Cell Sci*, 2012. 125(Pt 21): p. 4999-5004.
- Romero, S., et al., ATP-mediated Erk1/2 activation stimulates bacterial capture by filopodia, which precedes *Shigella* invasion of epithelial cells. *Cell Host Microbe*, 2011. 9(6): p. 508-19.
- Rossier, Olivier, Vivien Oceau, Jean-Baptiste Sibarita, Cécile Leduc, Béatrice Tessier, Deepak Nair, Volker Gatterdam, et al. 2012. “Integrins β 1 and β 3 Exhibit Distinct Dynamic Nanoscale Organizations inside Focal Adhesions.” *Nature Cell Biology* 14 (10): 1057–67.
- Sansonetti P. Host-pathogen interactions: the seduction of molecular cross talk. *Gut*. 2002 May;50 Suppl 3(Suppl 3):III2-8.
- Saxena, Mayur, Rishita Changede, James Hone, Haguy Wolfenson, and Michael P. Sheetz. 2017a. “Force-Induced Calpain Cleavage of Talin Is Critical for Growth, Adhesion Development, and Rigidity Sensing.” *Nano Letters* 17 (12): 7242–51. *Nano Letters* 17 (12): 7242–51.
- Schaller, M. D. 2001. “Paxillin: A Focal Adhesion-Associated Adaptor Protein.” *Oncogene* 20 (44): 6459–72.
- Schnupf P, Sansonetti PJ. *Shigella* Pathogenesis: New Insights through Advanced Methodologies. *Microbiol Spectr.* 2019 Mar;7(2). doi: 10.1128/microbiolspec
- Shen, Da-Kang & Blocker, Ariel. (2016). MxiA, MxiC and IpaD Regulate Substrate Selection and Secretion Mode in the T3SS of *Shigella flexneri*. *PLOS ONE*. 11. e0155141. 10.1371/journal.pone.0155141.
- Shen, Kai, Caitlin E. Tolbert, Christophe Guilluy, Vinay S. Swaminathan, Matthew E. Berginski, Keith Burridge, Richard Superfine, and Sharon L. Campbell. 2011. “The Vinculin C-Terminal Hairpin Mediates F-Actin Bundle Formation, Focal Adhesion, and Cell Mechanical Properties.” *The Journal of Biological Chemistry* 286 (52): 45103–15.
- Shibata, Akihiro C. E., Takahiro K. Fujiwara, Limin Chen, Kenichi G. N. Suzuki, Yoshiro Ishikawa, Yuri L. Nemoto, Yoshihiro Miwa, et al. 2012. “Archipelago Architecture of the Focal Adhesion: Membrane Molecules Freely Enter and Exit from the Focal Adhesion Zone.” *Cytoskeleton* 69 (6): 380–92.
- Spiess, Matthias, Pablo Hernandez-Varas, Anna Oddone, Helene Olofsson, Hans Blom, Dominic Waite, John G. Lock, Melike Lakadamyali, and Staffan Strömblad. 2018. “Active and Inactive β 1 Integrins Segregate into Distinct Nanoclusters in Focal Adhesions.” *The Journal of Cell Biology* 217 (6): 1929–40.
- Stec, Dominik L., and Boguslaw Stec. 2022. “Complete Model of Vinculin Suggests the Mechanism of Activation by Helical Super-Bundle Unfurling.” *The Protein Journal* 41 (1): 55–70.
- Stutchbury, Ben, Paul Atherton, Ricky Tsang, De-Yao Wang, and Christoph Ballestrem. 2017. “Distinct Focal Adhesion Protein Modules Control Different Aspects of Mechanotransduction.” *Journal of Cell Science* 130 (9): 1612–24.
- Sun, Li, Jeffrey K. Noel, Herbert Levine, and José N. Onuchic. 2017. “Molecular Simulations Suggest a Force-Dependent Mechanism of Vinculin Activation.”

- Biophysical Journal* 113 (8): 1697–1710.
- Sun, Zhiqi, Mercedes Costell, and Reinhard Fässler. 2019. “Integrin Activation by Talin, Kindlin and Mechanical Forces.” *Nature Cell Biology* 21 (1): 25–31.
- Tapial Martínez, Paula, Pilar López Navajas, and Daniel Lietha. 2020. “FAK Structure and Regulation by Membrane Interactions and Force in Focal Adhesions.” *Biomolecules* 10 (2). <https://doi.org/10.3390/biom10020179>.
- Thompson, Peter M., Caitlin E. Tolbert, and Sharon L. Campbell. 2013. “Vinculin and Metavinculin: Oligomerization and Interactions with F-Actin.” *FEBS Letters* 587 (8): 1220–29.
- Thompson PM, Tolbert CE, Shen K, Kota P, Palmer SM, Plevock KM, Orlova A, Galkin VE, Burrige K, Egelman EH, Dokholyan NV, Superfine R, Campbell SL. Identification of an actin binding surface on vinculin that mediates mechanical cell and focal adhesion properties. *Structure*. 2014 May 6;22(5):697-706
- Tobi, Dror, and Ivet Bahar. 2005. “Structural Changes Involved in Protein Binding Correlate with Intrinsic Motions of Proteins in the Unbound State.” *Proceedings of the National Academy of Sciences of the United States of America* 102 (52): 18908–13.
- Tamiello, Chiara, Antonetta B. C. Buskermolen, Frank P. T. Baaijens, Jos L. V. Broers, and Carlijn V. C. Bouten. 2016. “Heading in the Right Direction: Understanding Cellular Orientation Responses to Complex Biophysical Environments.” *Cellular and Molecular Bioengineering* 9: 12–37.
- Tran Van Nhieu, G., A. Ben-Ze’ev, and P. J. Sansonetti. 1997. “Modulation of Bacterial Entry into Epithelial Cells by Association between Vinculin and the *Shigella* IpaA Invasin.” *The EMBO Journal* 16 (10): 2717–29.
- Tran Van Nhieu G, Izard T. Vinculin binding in its closed conformation by a helix addition mechanism. *EMBO J*. 2007 Oct 31;26(21):4588-96.
- Tran Van Nhieu G, Latour-Lambert P, Enninga J. Modification of phosphoinositides by the *Shigella* effector IpgD during host cell infection. *Front Cell Infect Microbiol*. 2022 Oct 27;12:1012533.
- Turner, C. E. 2000. “Paxillin and Focal Adhesion Signalling.” *Nature Cell Biology* 2 (12): E231–36.
- Valencia-Gallardo, Cesar, Daniel-Isui Aguilar-Salvador, Hamed Khakzad, Benjamin Cocom-Chan, Charles Bou-Nader, Christophe Velours, Yosra Zarrouk, et al. 2022. “*Shigella* IpaA Mediates Actin Bundling through Diffusible Vinculin Oligomers with Activation Imprint.” *bioRxiv*. <https://doi.org/10.1101/2022.11.07.515412>.
- Valencia-Gallardo, Cesar, Charles Bou-Nader, Daniel-Isui Aguilar-Salvador, Nathalie Carayol, Nicole Quenech’Du, Ludovic Pecqueur, Hajeung Park, Marc Fontecave, Tina Izard, and Guy Tran Van Nhieu. 2019. “*Shigella* IpaA Binding to Talin Stimulates Filopodial Capture and Cell Adhesion.” *Cell Reports* 26 (4): 921–32.e6.
- Valencia-Gallardo, Cesar M., Nathalie Carayol, and Guy Tran Van Nhieu. 2015. “Cytoskeletal Mechanics during *Shigella* Invasion and Dissemination in Epithelial Cells.” *Cellular Microbiology* 17 (2): 174–82.
- Varnum-Finney B, Reichardt LF. Vinculin-deficient PC12 cell lines extend unstable lamellipodia and filopodia and have a reduced rate of neurite outgrowth. *J Cell Biol*. 1994;127:1071–1084
- Walker, Janice L., Alaina K. Fournier, and Richard K. Assoian. 2005. “Regulation of

- Growth Factor Signaling and Cell Cycle Progression by Cell Adhesion and Adhesion-Dependent Changes in Cellular Tension.” *Cytokine & Growth Factor Reviews* 16 (4-5): 395–405.
- Walma, David A. Cruz, and Kenneth M. Yamada. 2020. “The Extracellular Matrix in Development.” *Development* 147 (10). <https://doi.org/10.1242/dev.175596>.
- Whitewood, Austin J., Abhimanyu K. Singh, David G. Brown, and Benjamin T. Goult. 2018. “Chlamydial Virulence Factor TarP Mimics Talin to Disrupt the Talin-Vinculin Complex.” *FEBS Letters* 592 (10): 1751–60.
- Winograd-Katz, Sabina E., Reinhard Fässler, Benjamin Geiger, and Kyle R. Legate. 2014. “The Integrin Adhesome: From Genes and Proteins to Human Disease.” *Nature Reviews. Molecular Cell Biology* 15 (4): 273–88.
- Yao M., Goult B.T., Klapholz B., Hu X., Toseland C.P., Guo Y., Cong P., Sheetz M.P., and Yan J.. 2016. The mechanical response of talin. *Nat. Commun.* 7:11966
10.1038/ncomms11966
- Zhao, Xiaofeng, and Jun-Lin Guan. 2011. “Focal Adhesion Kinase and Its Signaling Pathways in Cell Migration and Angiogenesis.” *Advanced Drug Delivery Reviews* 63 (8): 610–15.

V. APPENDIX I : RÉSUMÉ LONG

La vinculine est une protéine associée au renforcement des adhésions dépendantes des intégrines des cellules à la matrice extracellulaire (MEC). Au niveau structurel, la vinculine (117 kDa) est organisée en cinq faisceaux hélicoïdaux (D1-D5). Il a été proposé que la vinculine présente deux états conformationnels différents, à savoir la conformation "fermée" ou auto-inhibée et la conformation "ouverte" ou active. Dans la conformation ouverte, des motifs amphipathiques spécifiques désignés comme sites de liaison de la vinculine ou VBS se lient au domaine D1, tandis que le domaine C-terminal (D5) se lie à la F-actine de manière à former une liaison d'accrochage. La liaison de deux signaux pour promouvoir l'activation de la vinculine est la manière habituelle dont la vinculine est activée dans les cellules. Cependant, la capacité de la vinculine à se lier efficacement à différents partenaires intracellulaires dépend fortement de son organisation structurelle. Des modèles structurels récents et des données biochimiques suggèrent que l'interaction spécifique entre la structure et la fonction de la vinculine dépend de la capacité de la vinculine à répondre à une tension mécanique sur la molécule elle-même et pas seulement de sa capacité de liaison aux VBS ou à des activateurs complémentaires. Cela suggère que des changements conformationnels intermédiaires existent entre les formes actives-inactives, et que les entrées mécaniques peuvent avoir des effets différents sur la capacité de la vinculine à lier d'autres composants cellulaires et régulateurs d'adhésion cellulaire. Ce scénario propose que la vinculine soit à la fois un composant de signalisation et un composant biomécanique au niveau cellulaire.

Dans les cellules en migration, les récepteurs des intégrines peuvent se lier de manière extracellulaire et coupler les forces mécaniques exercées par la matrice extracellulaire (MEC) aux composants intracellulaires. Cette force de traction externe peut être transmise au cytosquelette d'actine par l'intermédiaire des composants associés aux récepteurs d'intégrine qui abritent des sites de liaison à l'actine (SLA) tels que la taline, une protéine allongée étirable (270 kDa) qui expose ses SLA internes lors de la transmission de la tension mécanique des intégrines associées à la MEC à son extrémité N et à la F-actine à son extrémité C. La vinculine peut alors être recrutée sur les VBSs des talines et agir comme un échafaudage de signalisation dans les structures d'adhésion cellulaire, lorsque la tension mécanique augmente sur celles-ci.

Shigella spp. est un pathogène intracellulaire humain qui cible les cellules épithéliales du côlon comme sa niche et est un agent causal de la dysenterie dans le monde entier. Dans le cadre de son processus infectieux, la bactérie injecte une série de protéines effectrices dans le cytoplasme de sa cellule hôte au moyen d'un mécanisme moléculaire en forme d'aiguille appelé système de sécrétion de type 3. Cet assemblage moléculaire est capable d'accéder au cytoplasme de l'hôte. La protéine effectrice IpaA de *Shigella* cible la vinculine au cours du processus infectieux, et est capable d'imiter certains changements de conformation de la vinculine associés aux forces mécaniques exercées sur elle, afin de déclencher l'internalisation de la bactérie. Ce modèle d'activation de la vinculine est désigné comme le modèle non-combinatoire, car la seule présence d'un IpaA est suffisante pour obtenir le même effet. Ce travail est consacré à la caractérisation du rôle des résidus polaires dans les sous-domaines D1 et D2 de la tête de la vinculine, par rapport à leur interaction prédite avec les résidus IpaA-VBS3 de *Shigella*. Des tests biochimiques et de microscopie cellulaire ont été réalisés afin d'évaluer les effets de ces substitutions de résidus dans les domaines D1 et D2 de la tête de la vinculine, suggérant un rôle lors des changements de conformation de la vinculine associés à la tension mécanique pendant la maturation de l'adhésion cellulaire.

L'IpaA de *Shigella* contient trois VBS différents situés dans son domaine C-terminal, et il représente un excellent outil étant donné sa capacité à imiter les propriétés d'événements mécaniquement sensibles (autrement) se produisant dans des cellules soumises à un stress mécanique) *in vitro*, avec une capacité à se lier à des Kd très faibles (de l'ordre du pM) que leurs partenaires VBS endogènes. Il est important de noter que la transfection de cellules avec des IpaA-VBS leur confère la capacité de former une adhésion stable résistant au désassemblage de l'adhésion focale après l'application de molécules relaxantes d'acto-myosine (Y27632). Cependant, une propriété frappante récemment découverte dans ce laboratoire provient de la caractérisation biochimique des vD1D2 et IpaA-VBSs de la vinculine car leur interaction est capable d'induire différents complexes protéine:protéine *in vitro* (C. Valencia-Gallardo et al., 2022). Néanmoins, les mécanismes moléculaires conduisant à la formation de ces complexes et à l'activation de la vinculine par IpaA sont encore manquants.

L'objectif de ce travail est de caractériser les effets *in vitro* et *in vivo* de substitutions d'acides aminés uniques ciblées sur des résidus polaires de la vinculine situés à l'interphase des domaines D1-D2 de la vinculine. Ces résidus et leur interaction peuvent potentiellement affecter la réponse de la molécule aux changements conformationnels mécaniquement dépendants. Comme les modèles basés sur la structure l'ont prédit, les sites de liaison potentiels pour le VBS3 IpaA-VBS123 de *Shigella* sont situés au niveau des domaines D1 et D2 (C. Valencia-Gallardo et al., 2022). De plus, le rôle du domaine D2 dans la réponse mécanique de la vinculine a également été exploré en modifiant l'intégrité du faisceau hélicoïdal de ce domaine dans les résidus d'acides aminés non exposés situés dans l'hélice alpha H4 du D2. L'hélice H4 pourrait contribuer à maintenir l'état conformationnel du faisceau hélicoïdal car une analyse bioinformatique a prédit la présence d'un motif enroulé et bobiné (CC).

La caractérisation biochimique des variantes de la protéine vinculine D1D2 (vD1D2) a montré une réduction de sa capacité à être recrutée par les VBS exposés à l'IpaA. L'analyse sur gels PAGE natifs des différents complexes protéine:protéine a indiqué que les IpaA-VBS peuvent se lier aux variants vD1D2 à des taux de réponse différents.

Au niveau technique, les protéines ont été laissées en interaction en solution pendant 30-40 min (20mM Tris-HCL PH 7.4, 100mM NaCl, 1mM β -Mercaptoethanol) à une concentration de 10 μ M pour D1D2 et de 0 à 10 μ M de AVBS123 maximum dans un volume final de 20 μ l à RT. Ensuite, la solution de protéines a été mélangée avec un tampon de chargement sans SDS et chargée à raison de 10 μ l du volume final (~40 μ l) par puits dans des mini gels PAGE natifs de 1 mm de large, fabriqués par un peigne de 10 puits.

Les complexes protéiques ont été séparés en faisant tourner les gels dans des tampons de PAGE native à 25 mAmp par gel pendant 150 minutes. Une coloration de Commassie a été utilisée pour visualiser les différentes bandes. Normalement, on peut distinguer entre 3 et 4 bandes, mais seules les bandes principales inférieures et supérieures ont été quantifiées pour des raisons de simplicité. L'idée était de comparer la quantité de monomère pouvant être transformée en complexes et le taux de formation d'oligomères par rapport à la protéine D1D2 WT.

Néanmoins, les substitutions de résidus d'acides aminés dans D1 (différent du site de liaison des VBS) ou D2 (résidus de surface ou internes) ont réduit de manière significative sa capacité à former des hétérocomplexes par rapport à la vD1D2wt.

Le phénotype général observé est que les substitutions de résidus n'ont pas modifié de manière significative le taux de dissémination des monomères, mais ont surtout réduit le taux de formation des oligomères, c'est-à-dire les changements conformationnels hypothétiques associés à l'activation de la vinculine dépendant des changements allostériques de D2.

Lorsque ces substitutions ont été transférées à la version pleine longueur de la vinculine (FLV) de la protéine, fusionnée à un rapporteur fluorescent (mCherry), des changements de morphologie au niveau des cellules et de l'adhésion cellulaire ont été observés.

Techniquement, l'analyse a consisté à ensemercer 40K/puits de cellules de fibroblastes endothéliaux de souris sans vinculine (MEF vinc -/-) dans des plaques de 12 puits 24 heures avant la transfection. Des lamelles lavées à l'acide ont été recouvertes de 0,5 ml de fibronectine 20µg/ml et montées dans les plaques avant d'ensemencer les cellules. Des milieux DMEM à haute teneur en glucose (4,5 mg/ml) complétés par du SFB 10% et des acides aminés non essentiels (aucun antibiotique n'a été utilisé). Transfection à l'aide des constructions hFLVmCherry-N1 pour les versions WT et variantes transférées en utilisant le réactif Fugene et en suivant les instructions du vendeur. Les réactions par puits ont utilisé 1,6 µg d'ADN et le réactif Fugene 3X dilué dans le milieu OPTIMEM jusqu'à un volume final de 100 µl/ml. Les lamelles ont été traitées pendant 20 minutes avec du PFA 4%, et traitées pour la microscopie à fluorescence, et montées sur des lames en utilisant le milieu de montage Dako (Dako, Agilent Technologies).

Notamment, les cellules se sont moins étalées et ont formé moins d'adhésions en général, ce qui suggère que leur capacité à intégrer les signaux mécaniques dans les réponses biologiques était déficiente. En même temps, deux variantes, E143K et V367D, ont montré une différence marquée en termes de taille et de forme de leurs adhésions. Alors que le

premier variant (FLVmCherry-E143K) formait des adhésions plus grandes et plus arrondies, le second (FLVmCherry-V367D) formait des structures d'adhésion comparativement plus petites et plus allongées. Cela suggère que ces adhésions pourraient être plus ou moins sensibles à la tension exercée par les fibres du cytosquelette d'actomyosine, associées aux adhésions.

Une analyse fonctionnelle plus poussée serait nécessaire pour comprendre la réponse mécanique de la vinculine dérivée des substitutions d'acides aminés dans les domaines D1 et D2 de la protéine et sa signification biologique en termes de motilité, de survie et de différenciation des cellules.

Par rapport à la liaison VBS-D1 et à la liaison de D5 à la F-actine de la vinculine, nous avons constaté que les résidus D1 et D2 situés sur des sites différents de ces interactions peuvent avoir un impact important sur l'activité de la vinculine. Comme l'ont montré nos essais *in vitro*, les complexes protéiques vinculine:IpaA-VBSs et la formation d'oligomères peuvent être diminués indépendamment de leur capacité de liaison D1:VBS, et cela pourrait être dû à une conformation alternative imposée par les substitutions de résidus dans leur forme apo-protéique vD1D2.

De plus, dans nos expériences de transfection cellulaire, nous avons observé que lors du transfert de ces substitutions dans des variantes protéiques complètes, une réduction de l'étalement cellulaire et une modification de la morphologie des FA ont été observées dans les cellules. Cela pourrait s'expliquer par un rôle sous-estimé de l'organisation du domaine de tête de la vinculine régulant la réponse de la protéine à la tension de traction mécanique, indépendamment de leurs activités de liaison à la VBS ou à l'actine, ce qui soutient l'idée que la vinculine agit comme un composant mécanosensible dans les structures d'adhésion cellulaire.

CONCLUSION GÉNÉRALE ET PERSPECTIVE

La vinculine a surtout été considérée comme une protéine d'échafaudage dans les structures d'adhésion cellulaire. Cependant, la vinculine peut se lier à différentes molécules régulatrices dans les adhésions cellulaires comme les kinases, les phosphatases, les protéines

adaptatrices, les régulateurs d'actine ou les lipides (Bays & DeMali, 2017). Pour ce faire, la vinculine doit changer sa conformation en une forme "active" avec une conformation structurelle insaisissable lorsqu'elle est présente dans les adhésions cellulaires. Comme ces traits structure-fonction sont conservés au cours de l'évolution, différents pathogènes intracellulaires ont coévolué des mécanismes moléculaires pour contourner ces changements structurels dépendants de la mécanique en ciblant la liaison et l'activation de la vinculine par des protéines hébergeant des motifs VBS (Murphy & Brinkworth, 2021), afin de " détourner " les cellules pour former des structures de type adhésion en l'absence de traction mécanique. L'IpaA de *Shigella* a une capacité exceptionnelle d'activer la vinculine sans avoir besoin de signaux supplémentaires et d'induire des changements conformationnels indépendants de la mécanique, par rapport à l'activation impliquant la présence de la liaison VBS et des forces de traction de l'actine sur la protéine. Dans cette étude, nous avons découvert que des substitutions d'acides aminés uniques situées dans les domaines D1 ou D2, mais pas dans les sites impliqués dans la liaison des VBS ou de la F-actine, modifiaient la capacité de la protéine à être recrutée dans les VBS exposés d'IpaA.

De plus, la capacité de la vinculine à répondre correctement aux forces de traction agissant dans l'environnement intracellulaire dans les cellules transfectées avec des variants complets de la vinculine, semble être altérée (en particulier les variants E143K et V367D). Cela réduit la capacité d'étalement des cellules et la morphologie des FA. Dans l'ensemble, la substitution des résidus d'acides aminés dans les domaines D1 et D2 de la vinculine a révélé que l'intégrité du domaine Vh de la protéine est aussi importante que l'interaction de liaison avec la VBS ou la F-actine pour réguler l'activité de la vinculine pendant le processus d'activation mécanique-dépendante. Ces résultats apportent des preuves supplémentaires aux observations précédentes qui considèrent la vinculine comme un mécanosenseur et pas seulement un adaptateur ou un échafaudage protéique.

Deux observations peuvent être approfondies à partir de ce travail, la première correspond à corroborer la présence d'un motif VBS endogène prédit comme étant situé au niveau de l'hélice H1 du domaine D5 de la vinculine, et les implications possibles pour les fonctions de

la vinculine dans la cellule, probablement en ciblant les substitutions de résidus. Le second correspond à la caractérisation des mécanismes moléculaires sous-jacents aux phénotypes observés après altération du domaine "Vh" de la vinculine, plus précisément les variants E143K et V367D de la vinculine. Les phénotypes des AF associés à ces deux variants suggèrent que le premier est incapable de connecter correctement les AF avec les fibres de stress de l'actine, et que le second semble être plus sensible aux forces de traction de l'actine, car il a été observé que le variant D2 C-C présente des adhésions allongées dès les premiers stades de la formation des adhésions.

Traduit avec www.DeepL.com/Translator (version gratuite)